EBM Experimental Biology and Medicine

Volume 251 | Issue 1

Experimental Biology and Medicine

Editor-in-Chief

Nicola Conran
University of Campinas, Brazil

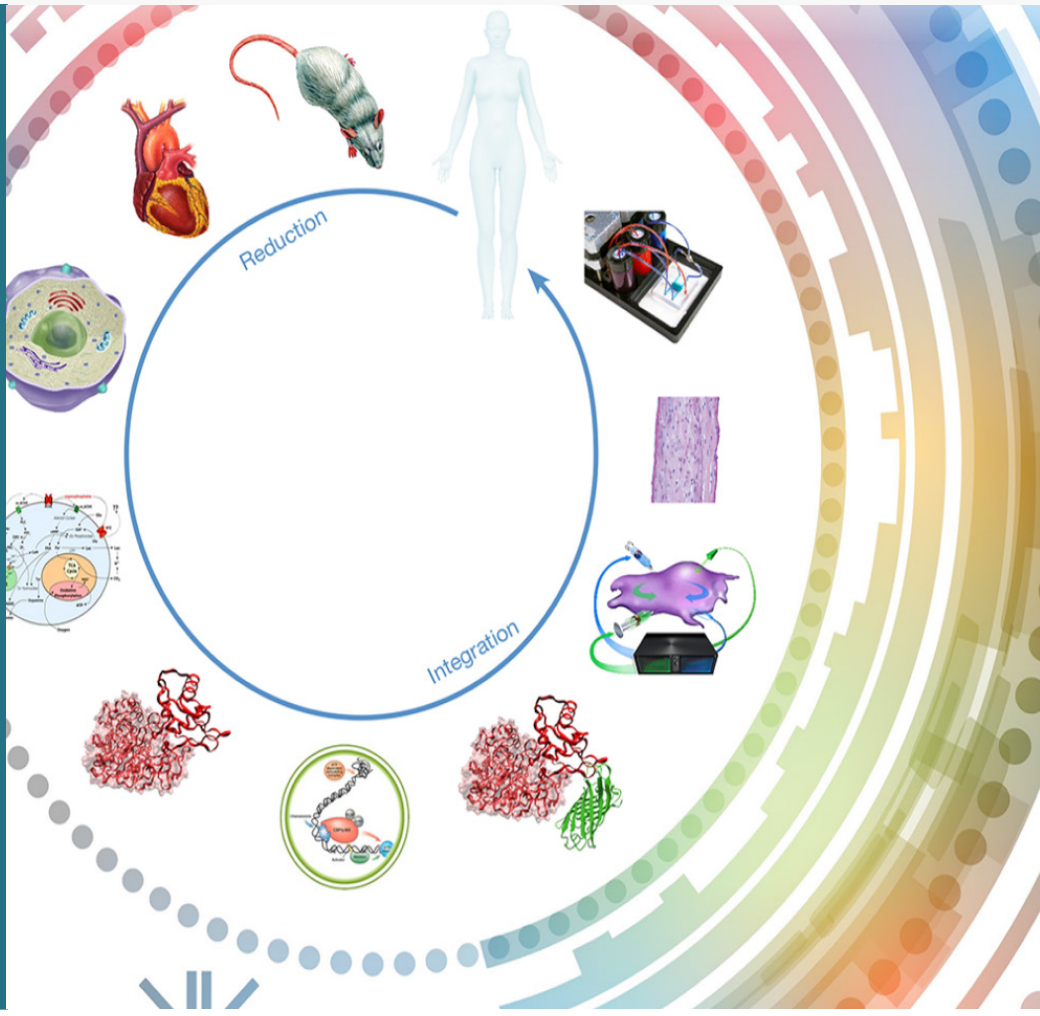

ISBN 978-2-8325-7477-5
DOI 10.3389/978-2-8325-7477-5

frontiers | Publishing Partnerships

Society for Experimental Biology and Medicine
3220 N Street NW, #179
Washington DC 20007, USA
Executive Director – ed@sebm.org

www.sebm.org

EBM Experimental Biology and Medicine

Editorial Board

ISSN 1535-3699
ISBN 978-2-8325-7477-5
DOI 10.3389/978-2-8325-7477-5

Generative AI statement
Any alternative text (Alt text) provided alongside figures in the articles in this ebook has been generated by Frontiers with the support of artificial intelligence and reasonable efforts have been made to ensure accuracy, including review by the authors wherever possible. If you identify any issues, please contact us.

EBM Experimental Biology and Medicine

2026 | Volume 251 | Issue 1 | ISSN 1535-3699

Table of contents

Pharmacology and Toxicology

Population Health

Population Health

EBM Experimental Biology and Medicine

TYPE Original Research
PUBLISHED 03 December 2025
DOI 10.3389/ebm.2025.10808

OPEN ACCESS

*CORRESPONDENCE
Shuling Wang,
wangshulinghappy@163.com
Weihua Yang,
benben0606@139.com
Qianfang Jia,
qianfangjia27@163.com

†These authors have contributed equally to this work and share first authorship

RECEIVED 03 September 2025
REVISED 10 November 2025
ACCEPTED 21 November 2025
PUBLISHED 03 December 2025

CITATION
Wang X, Guo Y, Zha Y, Wang S, Yang W and Jia Q (2025) Mapping microglial mechanisms in Alzheimer's disease: a comprehensive analysis.
Exp. Biol. Med. 250:10808.
doi: 10.3389/ebm.2025.10808

Mapping microglial mechanisms in Alzheimer's disease: a comprehensive analysis

Xiaofang Wang[1†], Yuqing Guo[2†], Yonghan Zha[3], Shuling Wang[2*], Weihua Yang[4*] and Qianfang Jia[5*]

[1]Hebei University of Chinese Medicine, Shijiazhuang, China, [2]Department of Traditional Chinese Medicine, Affiliated Children's Hospital of Jiangnan University, Wuxi Children's Hospital, Wuxi, China, [3]The First Clinical College of Henan Medical University, Xinxiang, China, [4]Shenzhen Eye Hospital, Shenzhen Eye Medical Center, Southern Medical University, Shenzhen, China, [5]Department of Children's Rehabilitation, First Affiliated Hospital of Xinxiang Medical University, Xinxiang, China

Abstract

Microglia, the brain's primary immune cells, play crucial roles in Alzheimer's disease (AD) pathogenesis. However, existing research remains abundant yet fragmented. Therefore, this study aimed to systematically identify hotspots and trends in microglia-related AD research, while providing an in-depth analysis of the underlying mechanisms to advance mechanistic understanding and therapeutic development. To achieve this, articles on microglia in AD were retrieved from the Web of Science Core Collection (WoSCC) database, and bibliometric analysis was performed using the WoSCC platform and CiteSpace 6.3.R1, with a focus on global collaboration, institutional and journal contributions, keyword bursts, and high-impact articles to comprehensively elucidate the underlying mechanisms. In total, 1,043 articles from 67 countries and regions were included.Among them, the United States led with 484 articles and an H-index of 100, followed by China with 276 articles. The University of California system (77 articles) and Harvard University (74 articles) had the highest H-index, both at 41. Journal of Neuroinflammation published the most articles (57 articles). Burst keywords persisting until 2024 included "memory," "NLRP3 inflammasome," and "system." High-impact studies emphasized microglial roles in AD pathology, including Aβ clearance, synaptic pruning, inflammation, metabolism, phenotype shifts, immune memory, and genetic variation. Overall, microglial mechanisms are at the forefront of AD research. The United States leads in both article number and influence, followed by China. The University of California system and Harvard University demonstrate the greatest output and impact. *Journal of Neuroinflammation* is the leading journal. Microglial NLRP3 activation, system-level interactions, and memory impairment have emerged as key research hotspots in AD. Future research will focus on microglial mechanisms and therapeutic targets in AD.

KEYWORDS

microglia, Alzheimer's disease, mechanism, hotspot, trend

Impact statement

Alzheimer's disease (AD) remains one of the most pressing challenges in aging research, with microglia increasingly recognized as central players in disease onset and progression. Despite abundant publications, existing studies are fragmented and lack a systematic overview of global trends and emerging directions. This work fills that gap by providing the first comprehensive bibliometric mapping of microglial research in AD over the past decade. It highlights how microglia contribute to aging-related processes, including inflammation, metabolic shifts, immune memory, and genetic susceptibility, and identifies the key institutions, journals, and research themes driving the field. By integrating this information, the study offers a clearer picture of how microglial biology intersects with aging mechanisms in AD. This perspective not only advances understanding of disease pathology but also helps guide future research toward innovative therapeutic strategies targeting microglial dysfunction in aging-related neurodegeneration.

Introduction

Alzheimer's disease (AD) is a prototypical neurodegenerative disorder, characterized by amyloid-β (Aβ) plaque deposition and abnormal tau phosphorylation [1]. Increasing evidence indicates that AD is accompanied by disrupted neuroimmune homeostasis, with neuroinflammation playing a central role in its pathogenesis [2, 3]. Microglia, the principal immune cells of the central nervous system (CNS), display functional abnormalities in AD. These abnormalities not only sustain chronic neuroinflammation but also impair Aβ clearance, synaptic remodeling, and neuronal survival, thereby positioning microglia as both initiators and amplifiers of AD pathology [4–6].

Mechanistically, neuronal overexpression of cathepsin S activates the CX3CL1–CX3CR1 axis and JAK2–STAT3 signaling, driving microglia toward a pro-inflammatory M1 phenotype and disrupting lysosomal protease balance, which intensifies neuroinflammation and accelerates disease progression [7]. Activated microglia further secrete pro-inflammatory cytokines via the MAPK, PI3K, and JAK/STAT pathways, establishing a positive feedback loop with peripheral immune cells that exacerbates neuronal injury [8]. In addition, microglial upregulation of the complement system under AD conditions induces aberrant phag [9]. Dysregulation of the TREM2/PGRN signaling axis further diminishes microglial capacity to clear Aβ plaques, while TREM2-driven microglial activation independently aggravates synaptic injury [10]. Collectively, these findings highlight microglia as a pathological hub linking Aβ deposition, tau abnormalities, synaptic dysfunction, and neuroinflammation in AD.

Given their central role, microglia have emerged as promising therapeutic targets in AD, with novel strategies including TREM2 agonists [11, 12], anti-inflammatory modulation [13, 14], and gene-editing approaches [15, 16]. However, despite rapid advances, microglia-related AD research remains highly heterogeneous, encompassing diverse mechanisms and intervention strategies. This fragmentation underscores the need for an integrative perspective to clarify research hotspots, developmental trajectories, and translational potential. To this end, the present study performed a bibliometric analysis of publications from the past decade indexed in the Web of Science Core Collection (WoSCC), aiming to map the evolving landscape of microglia-related AD research and to conduct an in-depth analysis of the underlying mechanisms, thereby providing systematic insights that may inform the development of novel therapeutic interventions and their clinical translation.

Materials and methods

The WoSCC serves as a standard dataset for journal impact and institutional performance indicators and has become a key resource in bibliometric research [17, 18]. To systematically identify the related literature, we established a stringent selection strategy. In the WoSCC database, we set the topic as "microglia*" and the additional topic as "Alzheimer*" or "AD", restricting the language to English, the document type to"article," and the publication date range from January 1, 2015 to December 31, 2024, resulting in 2,856 retrieved articles.

All retrieved records were imported into CiteSpace 6.3.R1 software for data processing. Duplicate entries were automatically detected and removed based on DOI, title, author, and publication year. Furthermore, a manual screening procedure was conducted to ensure the quality of the dataset, and the following criteria were applied: (1) documents including conference proceedings, review articles, book chapters, early access, editorial materials, letters, meeting abstracts, corrections, data papers, and retracted publications were excluded by document type; (2) articles were then filtered based on their content to ensure alignment with the target topic—for instance, studies addressing only AD or only microglia were excluded. During the manual screening, a double-blind review mechanism was implemented. Two independent reviewers (XW and YG) screened the records according to the above criteria without access to each other's decisions. Any discrepancies were resolved through discussion or by consultation with a third-party expert adjudicator (QJ). As a result, a total of 1,043 high-quality articles were ultimately included following manual screening. Moreover, CiteSpace was employed for collaboration network analysis (by country/region, institution, and journal) and for burst keywords identification, and the WoSCC analysis system was used to analyze annual and regional article counts. The full literature

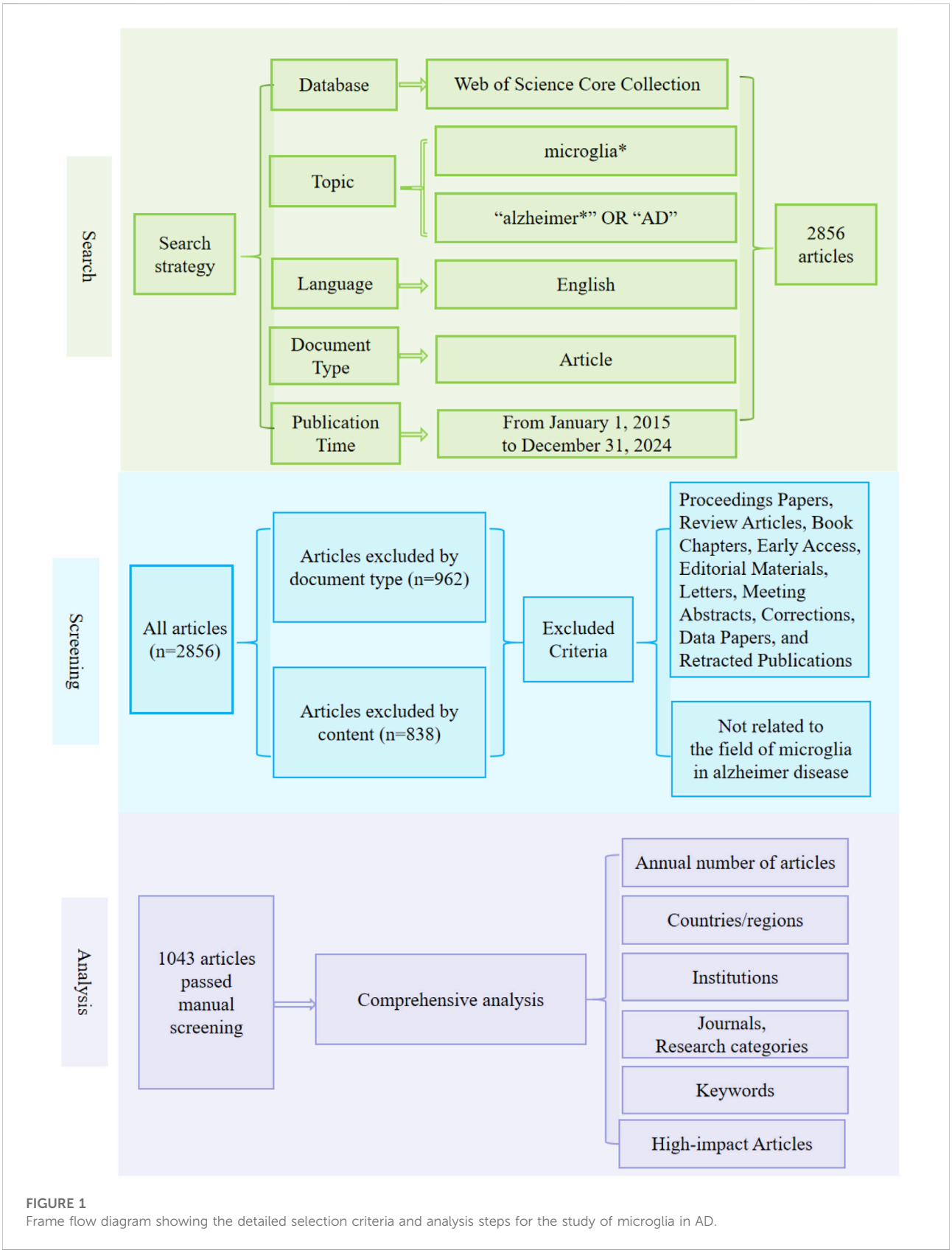

FIGURE 1
Frame flow diagram showing the detailed selection criteria and analysis steps for the study of microglia in AD.

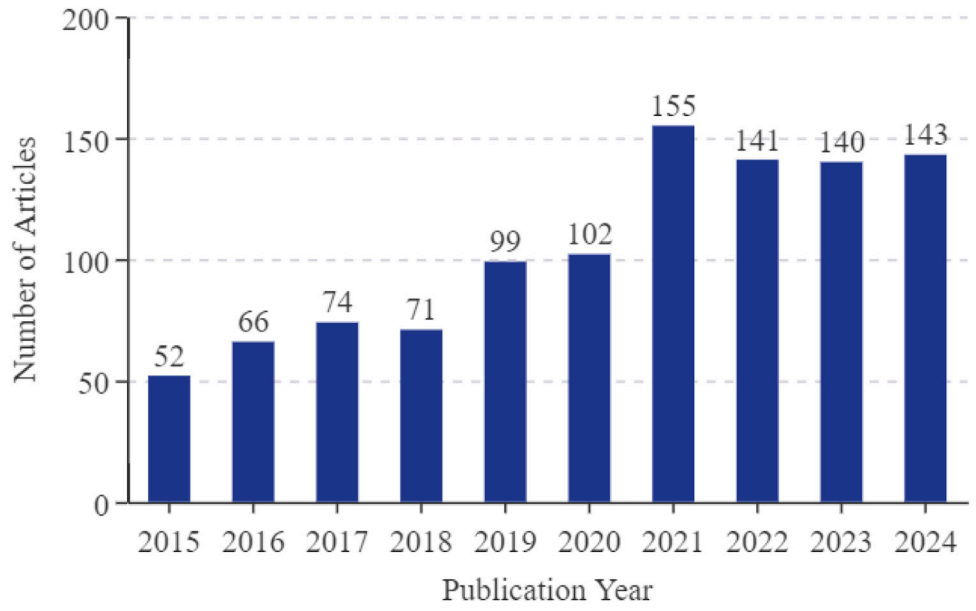

FIGURE 2
Annual number of articles on microglia in AD.

FIGURE 3
Cooperation of countries or regions that contributed to articles on microglia in AD.

TABLE 1 Top 10 countries or regions with articles on microglia in AD.

Rank	Countries or regions	Counts	Centrality	H-index
1	United States	484	0.60	100
2	China	276	0.09	58
3	England	112	0.14	47
4	Germany	112	0.18	53
5	Canada	54	0.02	31
6	Spain	53	0.13	26
7	Japan	53	0.00	29
8	South Korea	46	0.07	22
9	Sweden	42	0.07	21
10	Italy	41	0.13	23

screening process is illustrated in Figure 1. In addition, high-impact articles were subjected to in-depth analysis to better showcase pivotal findings in the field of microglia in AD.

Results

Annual number of articles

Over the past decade, annual articles in the field of microglia in AD have consistently exceeded 50, exhibiting a general increasing trend. Between 2015 and 2020, the number of annual articles rose steadily, from 52 to 102. Beginning in 2021, the number of articles in this field has grown markedly, with an average of more than 140 articles per year from 2021 to 2024. Figure 2 depicts the annual number of articles in this field over the last decade.

Countries or regions

These articles originated from 67 countries and regions. Figure 3 illustrates the collaboration network of countries and regions constructed with the default parameters in CiteSpace. The size of each label and node in Figure 3 is proportional to the number of articles. The largest nodes and labels belonged to the United States (484 articles), China (276), and England (112), indicating their dominant contributions. Connections between nodes indicate collaboration between countries, with more links signifying closer cooperation. Table 1 lists the top 10 countries or regions by number of articles, along with centrality scores (reflecting collaboration intensity) and H-indices (measuring academic impact). The United States ranked first with the highest H-index (100) and also demonstrated the greatest centrality (0.60). China followed with an H-index of 58 but exhibited a lower centrality score of 0.09.

Institutions

Figure 4 presents the institutional collaboration network constructed with CiteSpace's default settings. The size of nodes and labels of each institution in the figure is proportional to its article output, with connections representing collaborations. Table 2 lists details of the top 10 institutions based on article counts. Regarding article output, the University of California System (77 articles), Harvard University (74 articles), and Helmholtz Association (55 articles) hold the top 3 positions. The University of California System and Harvard University shared the highest H-index of 41. Of the top 10 institutions, five are based in the United States, three in Germany, and two in England.

Journals

Table 3 presents the top 10 journals ranked by article number in the research field of microglia in AD. The journals with the highest article counts were *Journal of Neuroinflammation, Journal of Alzheimer's Disease,* and *Glia*, with 57, 41, and 31 articles, respectively, primarily covering Immunology, Neurosciences, and Multidisciplinary Sciences. Among these 10 journals, Molecular Neurodegeneration had the greatest impact, with an impact factor of 14.9.

Keywords

CiteSpace was employed to analyze co-occurring collaborative networks of keywords using the parameters: "Year Per Slice" = 1, "Top N%" = 10.0%, and "Minimum Duration" = 1. Figure 5 highlights the top 10 keywords with the strongest citation bursts, where strength indicates the

FIGURE 4
Cooperation of institutions that contributed to articles on microglia in AD.

TABLE 2 Top 10 Institutions with articles on microglia in AD.

Rank	Institution	Country or regions	Counts	H-index
1	University of California System	United States	77	41
2	Harvard University	United States	74	41
3	Helmholtz Association	Germany	55	35
4	Harvard University Medical Affiliates	United States	55	33
5	University of London	England	52	27
6	German Center for Neurodegenerative Diseases (DZNE)	Germany	48	33
7	University College London	England	45	25
8	Harvard Medical School	United States	41	25
9	Washington University (WUSTL)	United States	37	29
10	University of Munich	Germany	30	24

intensity of the keyword's emergence. The red squares denote the timeline of keyword surges. The keywords that persisted until 2024 include "memory," "NLRP3 inflammasome," and "system."

High-impact publications

Articles with high citation counts represent highly acknowledged research in the field of microglial research in AD and are classified as high-impact articles. Table 4 presents the top 10 articles with the highest citations in this research area. These studies focused on investigating the pathological mechanisms of AD and the functions of microglia, including induction of neurotoxic astrocytes (A1 type) via secretion of inflammatory factors, identification of novel disease-associated microglia (DAM) and their role in Aβ clearance, synaptic pruning mediated by the complement pathway, and regulation of microglial phenotype transformation by the TREM2-APOE pathway. Additionally, microglial metabolic dysfunction, epigenetic reprogramming, and inflammasome involvement, along with the effects of genetic variants on microglial functions, were elucidated.

TABLE 3 Top 10 journals with articles on microglia in AD.

Rank	Citing journals	Research categories	Counts	Journal impact factor 2023
1	*Journal of Neuroinflammation*	Immunology; neurosciences	57	9.0
2	*Journal of Alzheimer's Disease*	Neurosciences	41	3.4
3	*Glia*	Neurosciences	31	5.4
4	*Nature Communications*	Multidisciplinary sciences	30	14.7
5	*International Journal of Molecular Sciences*	Biochemistry and molecular biology; chemistry, multidisciplinary	29	4.9
6	*Molecular Neurodegeneration*	Neurosciences	27	14.9
7	*Brain Behavior and Immunity*	Immunology; neurosciences; psychiatry	23	8.8
8	*Acta Neuropathologica Communications*	Neurosciences	20	6.2
9	*Molecular Neurobiology*	Neurosciences	19	4.6
10	*Neurobiology of Aging*	Geriatrics and gerontology; neurosciences	19	3.7

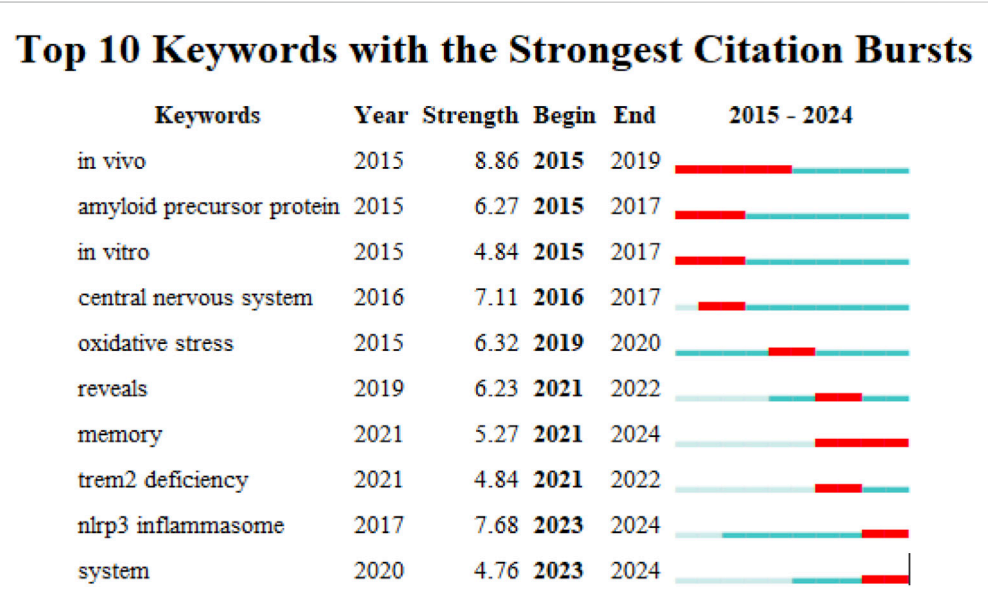

FIGURE 5
Keywords with the strongest citation bursts for publications on microglia in AD.

Discussion

Overall data

AD is a neurodegenerative disease characterized by β-amyloid (Aβ) accumulation and abnormal phosphorylation of tau protein [6]. Moreover, Neuroinflammation has gradually been acknowledged as a pathological factor in AD progression [19, 20]. Microglia, as the central immune regulators in the CNS, undergo dysfunction and abnormal activation, thereby triggering chronic neuroinflammation and exacerbating cognitive impairment through multisystem synaptic damage [21]. The neuroimmune mechanisms mediated by microglia have emerged as a crucial focus in AD research, with notable advancements. This study analyzed articles from the WoSCC database during the last decade to uncover research hotspots and trends related to microglia in AD. Results showed that research on microglia in AD has increased rapidly over the past decade,

TABLE 4 Articles with top 10 citation on microglia in AD.

Rank	Title of article	DOI	Times cited	Interpretation of the findings
1	Neurotoxic reactive astrocytes are induced by activated microglia	10.1038/nature21029	5043	Microglia promote A1-type astrocyte generation via IL-1α, TNF, and C1q. These astrocytes lose neuroprotective function, induce neuronal and oligodendrocyte death, and contribute to multiple neurodegenerative diseases. Blocking A1 formation protects neurons
2	A unique microglia type associated with restricting development of Alzheimer's disease	10.1016/j.cell.2017.05.018	3198	Single-cell transcriptomics revealed disease-associated microglia (DAM). They clear Aβ through a TREM2-dependent two-step activation: Downregulation of homeostatic markers, followed by upregulation of phagocytosis-related genes
3	Complement and microglia mediate early synapse loss in Alzheimer mouse models	10.1126/science.aad8373	2134	C1q attaches to synapses before plaques and triggers microglial CR3-mediated phagocytosis. Blocking complement prevents synaptic injury, showing aberrant complement-driven pruning as a key early AD mechanism
4	The TREM2-APOE pathway drives the transcriptional phenotype of dysfunctional microglia in neurodegenerative diseases	10.1016/j.immuni.2017.08.008	1753	The TREM2-APOE pathway regulates microglial phenotypic shift from homeostasis to neurodegeneration after phagocytosis of apoptotic neurons. Therapeutic targeting restores homeostasis and protects neurons
5	TREM2 Maintains microglial metabolic fitness in Alzheimer's disease	10.1016/j.cell.2017.07.023	805	In AD patients and TREM2-deficient mice, microglia showed defective ATP synthesis and autophagosome accumulation. Dectin-1 activation or creatine supplementation rescued metabolism and reduced neuronal injury
6	Microglia-derived ASC specks cross-seed amyloid-β in Alzheimer's disease	10.1038/nature25158	691	Inflammasome-activated microglia release ASC specks that bind Aβ, promoting aggregation and spread. Blocking ASC suppresses pathology, linking neuroinflammation to Aβ propagation
7	Rare coding variants in PLCG2, ABI3, and TREM2 implicate microglial-mediated innate immunity in Alzheimer's disease	10.1038/ng.3916	657	Genetic study (85,133 participants) identified AD-associated variants: PLCG2-Pro522Arg (protective), ABI3-Ser209Phe and TREM2-Arg62His (risk). These genes form a microglia-centered immune network in AD pathogenesis
8	Human and mouse single-nucleus transcriptomics reveal TREM2-dependent and TREM2-independent cellular responses in Alzheimer's disease	10.1038/s41591-019-0695-9	651	Single-nucleus RNA sequencing revealed both TREM2-dependent microglial activation and unique human-specific responses (oligodendrocyte myelination defects, astrocyte metabolic dysregulation). TREM2 mutations weaken microglial responses
9	Innate immune memory in the brain shapes neurological disease hallmarks	10.1038/s41586-018-0023-4	630	Peripheral inflammation induces long-lasting microglial immune memory (training or tolerance). Training worsens Aβ pathology; tolerance mitigates it. Epigenetic reprogramming underlies this regulation
10	TREM2 binds to apolipoproteins, including APOE and CLU/APOJ, and thereby facilitates uptake of amyloid-beta by microglia	10.1016/j.neuron.2016.06.015	629	TREM2 mediates microglial clearance of lipoprotein–Aβ complexes. AD-associated TREM2 mutations impair this function, linking APOE-CLU-TREM2 risk network to impaired Aβ clearance.of the TREM2-APOE-CLU genetic risk network, and offering new targets for immunometabolic therapy in AD.

with expanding global participation and closer international collaboration. The United States and China remain leading contributors, and high-impact studies are concentrated in top neuroscience institutions such as the University of California system and Harvard University, as well as in specialized journals such as *Journal of Neuroinflammation*.

Acknowledged research findings

High-impact articles have highlighted acknowledged findings regarding microglia in AD, emphasizing their pivotal role in disease pathogenesis. These articles illustrate alterations in microglial function across diverse pathological mechanisms, including Aβ clearance, synaptic pruning, inflammatory response, metabolic regulation, phenotypic transformation, immune memory, and genetic variation.

The pathological effects of microglia in AD involve multiple dimensions: (1) Impaired phagocytic and clearance capacity: Mutations in TREM2 reduce the ability of microglia to phagocytose and eliminate Aβ, resulting in increased Aβ deposition and accelerating pathological progression [22]. Furthermore, inflammasome-activated microglia release ASC specks that bind to Aβ, promoting its aggregation and spread, thereby intensifying amyloid pathology [23]. (2) Synaptic injury and dysregulated pruning: excessive activation of the complement system leads to over-pruning of synapses. C1q binds synapses prior to plaque formation, initiating synaptic pruning via microglial CR3 receptors, which worsens synaptic dysfunction [24]. (3) Neuroinflammation and glial cytotoxicity: microglia release inflammatory factors such as IL-1α, TNF, and C1q, driving the formation of neurotoxic A1 astrocytes that cause neuronal and oligodendroglial loss [25].

Microglia also exhibit intrinsic pathological changes: (1) Disrupted metabolism: under TREM2 deficiency, microglia accumulate autophagosomes and show impaired ATP production due to mitochondrial dysfunction. TREM2 supports microglial function by regulating energy metabolism [26]. (2) Dysregulated phenotypic switching: the TREM2–APOE axis orchestrates the transition from homeostatic to disease-associated microglial phenotypes (e.g., DAM). Mutations disrupt this process and contribute to neurodegeneration [27, 28]. (3) Immune imprinting and epigenetic remodeling: peripheral inflammation triggers microglia to develop prolonged immune memory. While trained immunity exacerbates pathology, immune tolerance mitigates it. Furthermore, epigenetic reprogramming is critically involved in the neuropathology of AD [29]. (4) Genetic influences: AD-associated genetic variants (e.g., TREM2 mutations) impair microglial Aβ clearance and neuroprotection, further worsening disease progression [26, 30, 31].

In conclusion, microglial dysfunction contributes to Aβ accumulation, synaptic degeneration, neuroinflammation, and neuronal loss in AD. These functional and phenotypic impairments are modulated by both genetic and epigenetic factors, as shown in Figure 6. Altogether, these alterations constitute the neuroimmune foundation of AD and underscore microglia as a promising target for therapeutic intervention.

Research hotspots

Analysis of articles from the WoSCC database over the past decade provides insights into research hotspots on microglia in AD. The progression of burst keywords across time highlights transitions of research hotspots in this field. During 2015–2022, burst keywords such as "*in vivo*," "amyloid precursor protein,""*in vitro*,""central nervous system,""oxidative stress,""reveals,"and "TREM2 deficiency" suggested a predominant emphasis on molecular pathology, neurodegeneration, and associated gene defects in early research. In particular, "amyloid precursor protein" is a pivotal molecule implicated in AD, with its aberrant processing leading to β-amyloid (Aβ) deposition and neuronal injury [32]. Integrating "*in vivo*" and "*in vitro*" approaches has offered crucial strategies for uncovering AD's molecular underpinnings [33, 34]. The degenerative changes in the "central nervous system" have emerged as a core focus, especially concerning microglial mechanisms in AD pathogenesis [35, 36]. "Oxidative stress" alters microglial activity and contributes to the aggravation of neurodegeneration in AD [37]. The keyword "reveals" is commonly used in research findings to highlight the validated neurotoxicity of specific molecules (e.g., Aβ) or their efficacy as therapeutic targets [38]. "TREM2 deficiency" contributes significantly to microglial impairment, with TREM2 being essential for phagocytic activity, inflammatory modulation, and homeostatic balance. Moreover, mutations in this gene compromise these functions, promoting Aβ deposition and tau propagation [39, 40].

The keywords persisting until 2024 reflect current research hotspots: "memory," "NLRP3 inflammasome," and "system."

"Memory", as a core component of cognitive function, deteriorates characteristically in neurodegenerative diseases such as AD [41]. Evidence indicates that memory impairment in AD patients is associated not only with Aβ accumulation and tau pathology but also directly with synaptic plasticity deficits caused by microglial dysfunction [42, 43]. Moreover, hippocampal atrophy and functional decline observed in AD are linked to neuroinflammation and synaptic damage driven by abnormal microglial activity [44, 45]. For instance, Li et al. demonstrated that hippocampal microglia regulate cellular communication through CCL and CSF signaling crosstalk, contributing to AD-related cognitive and memory decline [46]. Similarly, Wei Lei et al. showed that increased H3K18 lactylation in aging microglia activates the hippocampal NF-κB pathway, promoting inflammation and exacerbating AD-associated cognitive deficits [47]. Ye et al. observed increased AIM2 levels in microglia of AD mice, and targeted knockout of AIM2 in microglia markedly ameliorates synaptic plasticity disruptions and spatial memory deficits in these mice [48]. These studies suggest that memory impairments in AD patients are closely linked to microglia-driven neuropathological alterations, synaptic dysfunction, and cascades of neuroinflammation. Through modulating neuroinflammation, synaptic plasticity, and multiple other

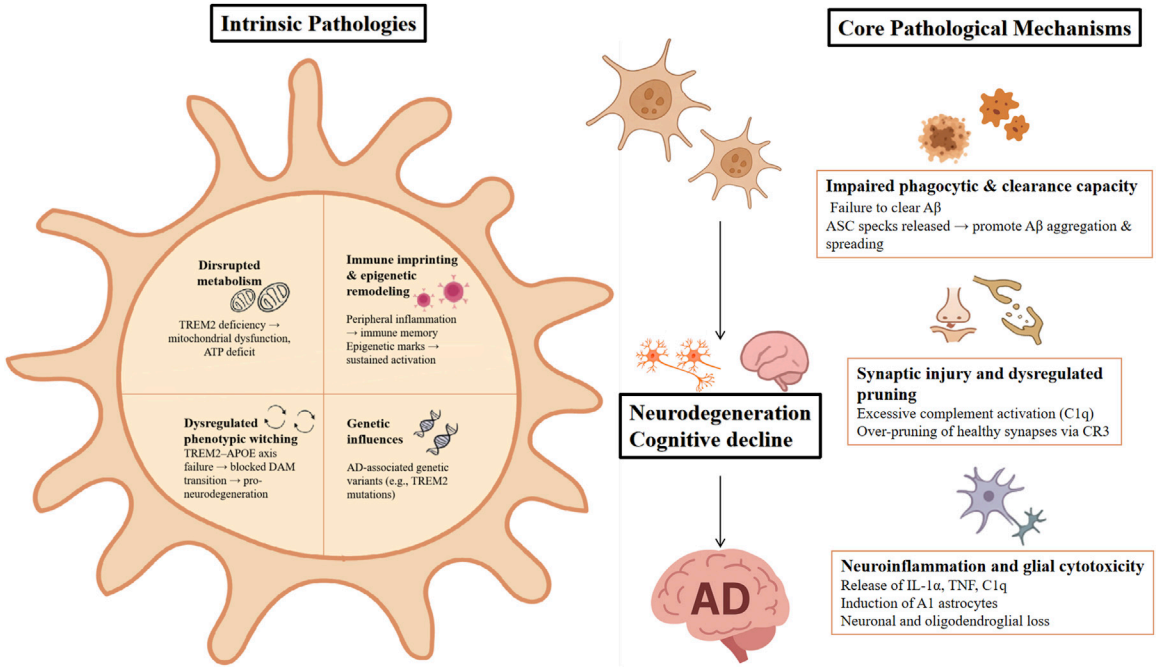

FIGURE 6
Acknowledged Findings on Microglial Dysfunction in AD. Intrinsic microglial alterations in AD include [1] disrupted metabolism (TREM2 deficiency, mitochondrial dysfunction) [2], impaired phenotypic switching (TREM2–APOE axis failure, blocked DAM transition) [3], immune imprinting and epigenetic remodeling (peripheral inflammation, maladaptive epigenetic marks), and [4] genetic influences (TREM2 mutations). These abnormalities drive [1] impaired Aβ clearance (defective phagocytosis, ASC speck–mediated aggregation) [2], synaptic injury and dysregulated pruning (C1q overactivation, CR3-dependent loss of synapses), and [3] neuroinflammation with glial cytotoxicity (release of IL-1α, TNF, C1q; induction of A1 astrocytes; neuronal and oligodendroglial loss). Final outcome involves neurodegeneration and cognitive decline in AD. Abbreviations: AD, Alzheimer's disease; DAM, disease-associated microglia; Aβ, amyloid-β; APOE, apolipoprotein E; CR3, complement receptor 3; IL, interleukin; TNF, tumor necrosis factor.

pathways, microglia are crucial contributors to the development and progression of memory impairments in AD.

"NLRP3 inflammasome", an essential element of immune responses, exerts a prominent role in neuroinflammation driven by microglia. In AD, microglia sense pathogens or danger signals through receptors like TLRs, which trigger activation of NF-κB and the NLRP3 inflammasome. This inflammasome activates caspase-1, cleaves GSDMD to induce pyroptosis, and releases IL-1β and IL-18, further facilitating Aβ plaque propagation, which amplifies inflammation and neuronal injury. The death of neurons activates microglia, forming a vicious feedback loop that accelerates neurodegeneration [49, 50]. According to Zhang et al., abnormal glutamine metabolism in microglia under AD pathology suppresses mitophagy through the AMPK/mTORC1 signaling pathway, resulting in reactive oxygen species (ROS) accumulation and selective activation of the NLRP3 inflammasome. Moreover, inhibition of glutaminase can block this process and improve cognitive impairment in AD [51]. Moonen et al. found distinct cell type-specific patterns of pyroptosis activation in AD brains: microglia showed classical activation of the NLRP3-ASC-caspase-1 pathway, while astrocytes and neurons induced GSDMD cleavage through caspase-8 and caspase-4, respectively [52]. These discoveries reveal that the microglial NLRP3 inflammasome contributes to neurodegeneration via distinct molecular pathways, offering new molecular targets for therapeutic strategies.

The keyword "system" denotes microglia as essential immune cells within the central nervous system, involved in AD progression through multiple critical systems. At the immune system level, Juul-Madsen et al. expanded the understanding of the peripheral-central immune system. Notably, he revealed that the complement receptor system mediates selective phagocytosis and lysosomal clearance of Aβ by peripheral monocytes and central microglia. Consequently, dysfunction in this system could be a key hallmark of the AD prodromal phase [53]. At the metabolic regulation level, Kaji et al. found that defective handling of APOE protein by microglia serves as a trigger for AD pathology. This lysosomal impairment promotes APOE protofibril buildup, which subsequently activates the JAK/STAT signaling pathway, leading to Aβ amyloid formation and plaque deposition, contributing to AD progression [54]. Haney et al. reported that the AD high-risk genotype APOE4/4 promotes lipid droplet accumulation in microglia via ACSL1 mediation, leading to Tau

phosphorylation and neurotoxicity, highlighting lipid metabolic dysregulation as a key mechanism in AD pathogenesis [55]. At the cellular heterogeneity level, Wu et al. applied single-cell sequencing and identified 11 distinct microglial subtypes. Among these, AD-associated subpopulations exhibited significant synaptic dysfunction, revealing the intricate molecular heterogeneity of microglial responses in AD and providing a novel framework for targeted diagnosis and treatment [56]. Moreover, advances in technological intervention systems. Feng et al. developed a CNP-cardiolipin nanosystem that modulates the TLR4/NF-κB pathway to induce microglial polarization toward the M2 phenotype, thereby effectively improving AD pathology [13].

Trends discussion

The growing number of articles on microglia in AD highlights the prominence of this field, with recent emerging burst keywords and high-impact articles signaling shifting trends. This suggests that research focusing on microglia as a breakthrough point for neurodegenerative diseases is likely to become a major future direction. The keywords persisting until 2024- "memory," "NLRP3 inflammasome," and "system"- represent current research hotspots. Future research is expected to further focus on the molecular mechanisms by which microglia regulate neuroinflammation and synaptic plasticity, with particular attention to programmed cell death (such as pyroptosis) mediated by the NLRP3 inflammasome signaling pathway in the pathogenesis of AD. Meanwhile, with the advancement of systems biology, increasing emphasis will be placed on the multi-level interactions of microglia within immune, metabolic, and neural systems, elucidating their pivotal roles in systemic dysregulation associated with neurodegenerative diseases. High-impact studies have already employed cutting-edge technologies such as single-cell transcriptomics, genetic analysis, and single-nucleus RNA sequencing to uncover microglial heterogeneity and their multidimensional roles in AD pathology. These advanced techniques are expected to provide essential methodological support for future research, facilitating deeper exploration of microglial regulatory networks and their potential as therapeutic targets in AD. Overall, future investigations are likely to further elucidate the system-level functions of microglia in neurodegenerative diseases, offering new perspectives for early diagnosis and precision intervention.

Limitations

This study has several limitations that may compromise the comprehensiveness and generalizability of the findings. First, to ensure literature quality, only the WoSCC database was used, which might have led to an incomplete retrieval of relevant studies. Employing multiple databases could offer a broader perspective. Second, the search was restricted to English-language articles, potentially excluding valuable research published in other languages. Third, the document type was limited to article, possibly overlooking important contributions from other formats. Due to time constraints and the focus on emerging hotspots and trends, only articles from the past 10 years were included, which may have resulted in partial coverage of the field. Furthermore, some relevant research findings may not be publicly available in the published literature.

Moreover, the research content of the selected articles presents several limitations. Current studies on the role of microglia in AD largely remain at the basic research stage. Methodologically, most existing studies rely on *in vivo* experiments using animal models (such as transgenic AD mice) and *in vitro* cell line studies, while direct evidence from human subjects remains limited. Although some investigations have examined human tissue samples, these efforts are constrained by small sample sizes and incomplete clinical information. In terms of mechanistic research, several pathological processes have been identified, including NLRP3 inflammasome activation, metabolic reprogramming, and synaptic pruning abnormalities. However, the lack of systematic integration and the methodological heterogeneity across laboratories have resulted in fragmented and sometimes inconsistent findings. Furthermore, most therapeutic interventions targeting microglia are still in the experimental or early clinical research phases, facing technical challenges such as poor blood-brain barrier permeability, limited specificity, and potential adverse effects. Given the substantial heterogeneity of microglia and the individual variability among AD patients, achieving precise and personalized interventions.

Conclusion

This study systematically analyzed microglia-related research in AD over the past decade through bibliometric methods, offering a comprehensive overview of the field's current landscape, emerging hotspots, and future trends, while providing an in-depth analysis of the underlying mechanisms. The results indicate a growing global interest in the mechanisms of microglial involvement in AD since 2021, with the United States and China emerging as the most influential contributors. Leading institutions include the University of California system and Harvard University. *Journal of Neuroinflammation* was the journal with the highest number of articles. Through NLRP3 inflammasome activation, microglia orchestrate neuroinflammatory responses in concert with systemic immune, metabolic, and cellular alterations, contributing to AD's pathology and cognitive deficits—a rapidly expanding area of research interest. High-impact articles concentrate on microglial activation, metabolic

regulation, epigenetic alterations, inflammasome signaling, and genetic variants, offering theoretical insights into disease pathogenesis and guiding therapeutic development. However, an in-depth investigation into the dynamic transitions and regulatory networks of microglia across different AD stages is essential to support early diagnosis and precision therapy, ultimately improving clinical outcomes.

Author contributions

XW, YG, and YZ conceived and designed the analysis, performed the analysis, and wrote the manuscript; SW, WY, and QJ designed the research, acquired the article information, and revised the manuscript. All authors contributed to the article and approved the submitted version.

Data availability

The original contributions presented in the study are included in the article/supplementary material, further inquiries can be directed to the corresponding authors.

Funding

The authors declare that no financial support was received for the research and/or publication of this article.

Conflict of interest

The author(s) declared no potential conflicts of interest with respect to the research, authorship, and/or publication of this article.

Generative AI statement

The authors declare that no Generative AI was used in the creation of this manuscript.

Any alternative text (alt text) provided alongside figures in this article has been generated by Frontiers with the support of artificial intelligence and reasonable efforts have been made to ensure accuracy, including review by the authors wherever possible. If you identify any issues, please contact us.

References

1. Scheltens P, De Strooper B, Kivipelto M, Holstege H, Chételat G, Teunissen CE, et al. Alzheimer's disease. *The Lancet* (2021) **397**(10284):1577–1590. doi:10.1016/S0140-6736(20)32205-4

2. Twarowski B, Herbet M. Inflammatory processes in Alzheimer's disease-pathomechanism, diagnosis and treatment: a review. *Int J Mol Sci* (2023) **24**(7):6518. doi:10.3390/ijms24076518

3. Yeung CHC, Schooling CM. Systemic inflammatory regulators and risk of Alzheimer's disease: a bidirectional mendelian-randomization study. *Int J Epidemiol* (2021) **50**(3):829–840. doi:10.1093/ije/dyaa241

4. Wang S, Mustafa M, Yuede CM, Salazar SV, Kong P, Long H, et al. Anti-human TREM2 induces microglia proliferation and reduces pathology in an Alzheimer's disease model. *J Exp Med* (2020) **217**(9):e20200785. doi:10.1084/jem.20200785

5. Sun N, Victor MB, Park YP, Xiong X, Scannail AN, Leary N, et al. Human microglial state dynamics in Alzheimer's disease progression. *Cell* (2023) **186**(20):4386–403.e29. doi:10.1016/j.cell.2023.08.037

6. Zhao X, Sun J, Xiong L, She L, Li L, Tang H, et al. β-amyloid binds to microglia Dectin-1 to induce inflammatory response in the pathogenesis of Alzheimer's disease. *Int J Biol Sci* (2023) **19**(10):3249–65. doi:10.7150/ijbs.81900

7. Liu PP, Liu XH, Ren MJ, Liu XT, Shi XQ, Li ML, et al. Neuronal cathepsin S increases neuroinflammation and causes cognitive decline via CX3CL1-CX3CR1 axis and JAK2-STAT3 pathway in aging and Alzheimer's disease. *Aging Cell* (2025) **24**(2):e14393. doi:10.1111/acel.14393

8. Zuppe H, Reed E. Common cytokine receptor gamma chain family cytokines activate MAPK, PI3K, and JAK/STAT pathways in microglia to influence Alzheimer's disease. *Front Mol Neurosci* (2024) **17**:1441691. doi:10.3389/fnmol.2024.1441691

9. Cangalaya C, Wegmann S, Sun W, Diez L, Gottfried A, Richter K, et al. Real-time mechanisms of exacerbated synaptic remodeling by microglia in acute models of systemic inflammation and tauopathy. *Brain Behav Immun* (2023) **110**:245–259. doi:10.1016/j.bbi.2023.02.023

10. Lan G, Chen X, Yang J, Sun P, Cai Y, Li A, et al. Microglial reactivity correlates with presynaptic loss independent of β-Amyloid and tau. *Ann Neurol* (2024) **95**(5):917–928. doi:10.1002/ana.26885

11. Schlepckow K, Morenas-Rodríguez E, Hong S, Haass C. Stimulation of TREM2 with agonistic antibodies-an emerging therapeutic option for Alzheimer's disease. *Lancet Neurol* (2023) **22**(11):1048–60. doi:10.1016/S1474-4422(23)00247-8

12. Long H, Simmons A, Mayorga A, Burgess B, Nguyen T, Budda B, et al. Preclinical and first-in-human evaluation of AL002, a novel TREM2 agonistic antibody for Alzheimer's disease. *Alzheimer's Res and Ther* (2024) **16**(1):235. doi:10.1186/s13195-024-01599-1

13. Feng Q, Zhang X, Zhao X, Liu J, Wang Q, Yao Y, et al. Intranasal delivery of pure nanodrug loaded liposomes for Alzheimer's disease treatment by efficiently regulating microglial polarization. *Small* (2024) **20**(50):e2405781. doi:10.1002/smll.202405781

14. Sanjay SJH, Park M, Lee HJ. Cyanidin-3-O-Glucoside regulates the M1/M2 polarization of microglia via PPARγ and Aβ42 phagocytosis through TREM2 in an alzheimer's disease model. *Mol Neurobiol* (2022) **61**(2):1223. doi:10.1007/s12035-023-03877-9

15. Raikwar SP, Thangavel R, Dubova I, Selvakumar GP, Ahmed ME, Kempuraj D, et al. Targeted gene editing of glia maturation factor in microglia: a novel Alzheimer's disease therapeutic target. *Mol Neurobiol* (2019) **56**(1):378–93. doi:10.1007/s12035-018-1068-y

16. Meier S, Larsen ASG, Wanke F, Mercado N, Mei A, Takacs L, et al. An efficient, non-viral arrayed CRISPR screening platform for iPSC-derived myeloid and microglia models. *Stem Cell Rep* (2025) **20**(3):102420. doi:10.1016/j.stemcr.2025.102420

17. Guo M, Gong D, Yang W. In-depth analysis of research hotspots and emerging trends in AI for retinal diseases over the past decade. *Front Med* (2024) **11**:1489139. doi:10.3389/fmed.2024.1489139

18. Jia Q, Wang X, Li X, Xie C, Zhang Q, Mu J, et al. Analysis of research hotspots and trends in pediatric ophthalmopathy based on 10 years of WoSCC literature. *Front Pediatr* (2024) **12**:1405110. doi:10.3389/fped.2024.1405110

19. Xie J, Van Hoecke L, Vandenbroucke RE. The impact of systemic inflammation on Alzheimer's disease pathology. *Front Immunol* (2022) **12**:796867. doi:10.3389/fimmu.2021.796867

20. Guerrero A, De Strooper B, Arancibia-Cárcamo IL. Cellular senescence at the crossroads of inflammation and Alzheimer's disease. *Trends Neurosci* (2021) **44**(9):714–27. doi:10.1016/j.tins.2021.06.007

21. Baligács N, Albertini G, Borrie SC, Serneels L, Pridans C, Balusu S, et al. Homeostatic microglia initially seed and activated microglia later reshape amyloid

plaques in Alzheimer's disease. *Nat Commun* (2024) **15**(1):10634. doi:10.1038/s41467-024-54779-w

22. Yeh FL, Wang Y, Tom I, Gonzalez LC, Sheng M. TREM2 binds to apolipoproteins, including APOE and CLU/APOJ, and thereby facilitates uptake of amyloid-beta by microglia. *Neuron* (2016) **91**(2):328–40. doi:10.1016/j.neuron.2016.06.015

23. Venegas C, Kumar S, Franklin BS, Dierkes T, Brinkschulte R, Tejera D, et al. Microglia-derived ASC specks cross-seed amyloid-β in Alzheimer's disease. *Nature* (2017) **552**(7685):355–61. doi:10.1038/nature25158

24. Hong S, Beja-Glasser VF, Nfonoyim BM, Frouin A, Li S, Ramakrishnan S, et al. Complement and microglia mediate early synapse loss in Alzheimer mouse models. *Science* (2016) **352**(6286):712–6. doi:10.1126/science.aad8373

25. Liddelow SA, Guttenplan KA, Clarke LE, Bennett FC, Bohlen CJ, Schirmer L, et al. Neurotoxic reactive astrocytes are induced by activated microglia. *Nature* (2017) **541**(7638):481–7. doi:10.1038/nature21029

26. Ulland TK, Song WM, Huang SC, Ulrich JD, Sergushichev A, Beatty WL, et al. TREM2 maintains microglial metabolic fitness in Alzheimer's disease. *Cell* (2017) **170**(4):649–63.e13. doi:10.1016/j.cell.2017.07.023

27. Keren-Shaul H, Spinrad A, Weiner A, Matcovitch-Natan O, Dvir-Szternfeld R, Ulland TK, et al. A unique microglia type associated with restricting development of Alzheimer's disease. *Cell* (2017) **169**(7):1276–90.e17. doi:10.1016/j.cell.2017.05.018

28. Krasemann S, Madore C, Cialic R, Baufeld C, Calcagno N, El Fatimy R, et al. The TREM2-APOE pathway drives the transcriptional phenotype of dysfunctional microglia in neurodegenerative diseases. *Immunity* (2017) **47**(3):566–81.e9. doi:10.1016/j.immuni.2017.08.008

29. Wendeln AC, Degenhardt K, Kaurani L, Gertig M, Ulas T, Jain G, et al. Innate immune memory in the brain shapes neurological disease hallmarks. *Nature* (2018) **556**(7701):332–8. doi:10.1038/s41586-018-0023-4

30. Sims R, van der Lee SJ, Naj AC, Bellenguez C, Badarinarayan N, Jakobsdottir J, et al. Rare coding variants in PLCG2, ABI3, and TREM2 implicate microglial-mediated innate immunity in Alzheimer's disease. *Nat Genet* (2017) **49**(9):1373–84. doi:10.1038/ng.3916

31. Zhou Y, Song WM, Andhey PS, Swain A, Levy T, Miller KR, et al. Human and mouse single-nucleus transcriptomics reveal TREM2-dependent and TREM2-independent cellular responses in Alzheimer's disease. *Nat Med* (2020) **26**(1):131–42. doi:10.1038/s41591-019-0695-9

32. Gerrits E, Brouwer N, Kooistra SM, Woodbury ME, Vermeiren Y, Lambourne M, et al. Distinct amyloid-β and tau-associated microglia profiles in Alzheimer's disease. *Acta Neuropathol* (2021) **141**(5):681–96. doi:10.1007/s00401-021-02263-w

33. Zhu M, Liu Y, Chen C, Chen H, Ni W, Song Y, et al. TLR4/Rac1/NLRP3 pathway mediates Amyloid-β-Induced neuroinflammation in Alzheimer's disease. *J Alzheimer's Dis* (2024) **99**(3):911–925. doi:10.3233/JAD-240012

34. Wang D, Liu J, Zhu Q, Wei X, Zhang X, Chen Q, et al. Ouabain ameliorates Alzheimer's disease-associated neuropathology and cognitive impairment in FAD4T mice. *Nutrients* (2024) **16**(20):3558. doi:10.3390/nu16203558

35. Morris GP, Foster CG, Courtney JM, Collins JM, Cashion JM, Brown LS, et al. Microglia directly associate with pericytes in the central nervous system. *Glia* (2023) **71**(8):1847–69. doi:10.1002/glia.24371

36. Chen H, Guo Z, Sun Y, Dai X. The immunometabolic reprogramming of microglia in Alzheimer's disease. *Neurochem Int* (2023) **171**:105614. doi:10.1016/j.neuint.2023.105614

37. Kang YJ, Hyeon SJ, McQuade A, Lim J, Baek SH, Diep YN, et al. Neurotoxic microglial activation via IFNγ-Induced Nrf2 reduction exacerbating Alzheimer's disease. *Adv Sci* (Weinh) (2024) **11**(20):e2304357. doi:10.1002/advs.202304357

38. Xia D, Lianoglou S, Sandmann T, Calvert M, Suh JH, Thomsen E, et al. Novel app knock-in mouse model shows key features of amyloid pathology and reveals profound metabolic dysregulation of microglia. *Mol Neurodegeneration* (2022) **17**(1):41. doi:10.1186/s13024-022-00547-7

39. Lee-Gosselin A, Jury-Garfe N, You Y, Dabin L, Soni D, Dutta S, et al. TREM2-Deficient microglia attenuate Tau spreading *in vivo*. *Cells* (2023) **12**(12):1597. doi:10.3390/cells12121597

40. Stoiljkovic M, Gutierrez KO, Kelley C, Horvath TL, Hajós M. TREM2 deficiency disrupts network oscillations leading to epileptic activity and aggravates Amyloid-β-Related hippocampal pathophysiology in mice. *J Alzheimer's Dis* (2022) **88**(3):837–847. doi:10.3233/JAD-210041

41. Kamatham PT, Shukla R, Khatri DK, Vora LK. Pathogenesis, diagnostics, and therapeutics for Alzheimer's disease: breaking the memory barrier. *Ageing Res Rev* (2024) **101**:102481. doi:10.1016/j.arr.2024.102481

42. Wang W, Li Y, Ma F, Sheng X, Chen K, Zhuo R, et al. Microglial repopulation reverses cognitive and synaptic deficits in an Alzheimer's disease model by restoring BDNF signaling. *Brain Behav Immun* (2023) **113**:275–288. doi:10.1016/j.bbi.2023.07.011

43. Udeochu JC, Amin S, Huang Y, Fan L, Torres ERS, Carling GK, et al. Tau activation of microglial cGAS-IFN reduces MEF2C-mediated cognitive resilience. *Nat Neurosci* (2023) **26**(5):737–750. doi:10.1038/s41593-023-01315-6

44. Falcicchia C, Tozzi F, Gabrielli M, Amoretti S, Masini G, Nardi G, et al. Microglial extracellular vesicles induce Alzheimer's disease-related cortico-hippocampal network dysfunction. *Brain Commun* (2023) **5**(3):fcad170. doi:10.1093/braincomms/fcad170

45. Rao YL, Ganaraja B, Murlimanju BV, Joy T, Krishnamurthy A, Agrawal A. Hippocampus and its involvement in Alzheimer's disease: a review. *3 Biotech* (2022) **12**(2):55. doi:10.1007/s13205-022-03123-4

46. Li H, Ye T, Liu X, Guo R, Yang X, Li Y, et al. The role of signaling crosstalk of microglia in hippocampus on progression of ageing and Alzheimer's disease. *J Pharm Anal* (2023) **13**(7):788–805. doi:10.1016/j.jpha.2023.05.008

47. Wei L, Yang X, Wang J, Wang Z, Wang Q, Ding Y, et al. H3K18 lactylation of senescent microglia potentiates brain aging and Alzheimer's disease through the NFκB signaling pathway. *J Neuroinflammation* (2023) **20**(1):208. doi:10.1186/s12974-023-02879-7

48. Ye L, Hu M, Mao R, Tan Y, Sun M, Jia J, et al. Conditional knockout of AIM2 in microglia ameliorates synaptic plasticity and spatial memory deficits in a mouse model of Alzheimer's disease. *CNS Neurosci Ther* (2024) **30**(6):e14555. doi:10.1111/cns.14555

49. Liu Y, Dai Y, Li Q, Chen C, Chen H, Song Y, et al. Beta-amyloid activates NLRP3 inflammasome via TLR4 in mouse microglia. *Neurosci Lett* (2020) **736**:135279. doi:10.1016/j.neulet.2020.135279

50. Ayyubova G, Madhu LN. Microglial NLRP3 inflammasomes in Alzheimer's disease pathogenesis: from interaction with autophagy/mitophagy to therapeutics. *Mol Neurobiol* (2025) **62**(6):7124–43. doi:10.1007/s12035-025-04758-z

51. Zhang Z, Li M, Li X, Feng Z, Luo G, Wang Y, et al. Glutamine metabolism modulates microglial NLRP3 inflammasome activity through mitophagy in Alzheimer's disease. *J Neuroinflammation* (2024) **21**(1):261. doi:10.1186/s12974-024-03254-w

52. Moonen S, Koper MJ, Van Schoor E, Schaeverbeke JM, Vandenberghe R, von Arnim CAF, et al. Pyroptosis in Alzheimer's disease: cell type-specific activation in microglia, astrocytes and neurons. *Acta Neuropathol* (2023) **145**(2):175–95. doi:10.1007/s00401-022-02528-y

53. Juul-Madsen K, Parbo P, Ismail R, Ovesen PL, Schmidt V, Madsen LS, et al. Amyloid-β aggregates activate peripheral monocytes in mild cognitive impairment. *Nat Commun* (2024) **15**(1):1224. doi:10.1038/s41467-024-45627-y

54. Kaji S, Berghoff SA, Spieth L, Schlaphoff L, Sasmita AO, Vitale S, et al. Apolipoprotein E aggregation in microglia initiates Alzheimer's disease pathology by seeding β-amyloidosis. *Immunity* (2024) **57**(11):2651–68.e12. doi:10.1016/j.immuni.2024.09.014

55. Haney MS, Pálovics R, Munson CN, Long C, Johansson PK, Yip O, et al. APOE4/4 is linked to damaging lipid droplets in Alzheimer's disease microglia. *Nature* (2024) **628**(8006):154–161. doi:10.1038/s41586-024-07185-7

56. Wu X, Liu M, Zhang X, Pan X, Cui X, Jin J, et al. Elucidating microglial heterogeneity and functions in Alzheimer's disease using single-cell analysis and convolutional neural network disease model construction. *Sci Rep* (2024) **14**(1):17271. doi:10.1038/s41598-024-67537-1

EBM Experimental Biology and Medicine

TYPE Original Research
PUBLISHED 06 January 2026
DOI 10.3389/ebm.2025.10766

OPEN ACCESS

*CORRESPONDENCE
Zhike Liang,
eylzk@scut.edu.cn
Shuquan Wei,
eyweishuquan@scut.edu.cn

†These authors have contributed equally to this work and share first authorship

RECEIVED 23 July 2025
REVISED 05 December 2025
ACCEPTED 12 December 2025
PUBLISHED 06 January 2026

CITATION
Zhu F, Mo Z, Lin W, Sun C, Huang X, Ye M, He H, Li Y, Wang K, Zhu J, Lin C, Wei S and Liang Z (2026) LncRNA HOTAIR promotes LPS-induced inflammatory responses by activating the NF-κB pathway.
Exp. Biol. Med. 250:10766.
doi: 10.3389/ebm.2025.10766

LncRNA HOTAIR promotes LPS-induced inflammatory responses by activating the NF-κB pathway

Fengqing Zhu[1†], Zexun Mo[1†], Wuzhou Lin[1†], Cheng Sun[1], Xiaomei Huang[1], Meifeng Ye[1], Hua He[1], Yujun Li[1], Kangwei Wang[2], Juan Zhu[1], Chuwen Lin[3], Shuquan Wei[1*] and Zhike Liang[1*]

[1]Department of Pulmonary and Critical Care Medicine, The Second Affiliated Hospital, School of Medicine, South China University of Technology, Guangzhou, Guangdong, China, [2]Department of Pathology, Guangzhou Red Cross Hospital of Jinan University, Guangzhou, Guangdong, China, [3]Department of Histology and Embryology, School of Medicine, Shenzhen Campus of Sun Yat-Sen University, Sun Yat-Sen University, Shenzhen, Guangdong, China

Abstract

Acute lung injury (ALI) is a disease with an excessive inflammatory response triggered by activating the NF-κB signaling pathway. Our study aims to investigate the role of the long non-coding RNA HOTAIR in ALI-associated hyperinflammation, providing evidence for HOTAIR as a potential therapeutic target for ALI. Here, we examined the contribution of HOTAIR to LPS-induced lung injury using both A549 cell and murine models. LPS stimulation markedly increased HOTAIR expression in A549 cells, accompanied by reduced cell viability and elevated secretion of pro-inflammatory cytokines, including IL-1β, IL-6, and TNF-α. Overexpression of HOTAIR further amplified NF-κB signaling, as indicated by increased phosphorylation of IκBα and p65 and enhanced nuclear translocation of p65, whereas silencing HOTAIR effectively reversed these effects. *In vivo*, knockdown of HOTAIR significantly mitigated LPS-induced lung injury, reduced inflammatory cytokine production, and suppressed NF-κB activation in mice. Our findings reveal the contribution of HOTAIR to NF-κB–driven inflammatory injury in ALI, offering insight into its regulatory role and informing future exploration of targeted therapeutic approaches.

KEYWORDS

acute lung injury, HOTAIR, inflammation, LncRNA, NF-κB pathway

Impact statement

Acute lung injury (ALI) is a life-threatening condition driven by uncontrolled inflammation, yet effective therapeutic targets remain limited. This study identifies the long non-coding RNA HOTAIR as a critical regulator of ALI progression by amplifying NF-κB-mediated hyperinflammation. Using both cellular and animal models, we

demonstrate that HOTAIR is upregulated upon LPS exposure and exacerbates lung injury by enhancing NF-κB activation, leading to excessive cytokine release (IL-1β, IL-6, and TNF-α) and tissue damage. Importantly, silencing HOTAIR attenuates inflammation and lung injury, suggesting its therapeutic potential. Our work advances the field by: Establishing HOTAIR as a novel pro-inflammatory driver in ALI, expanding its known roles beyond cancer and chronic diseases. Unveiling a direct link between HOTAIR and NF-κB activation in LPS-induced lung injury, providing mechanistic insight. Proposing HOTAIR inhibition as a strategy to mitigate A LI, offering a new avenue for clinical intervention. These findings could reshape ALI treatment paradigms by targeting epigenetic regulators like HOTAIR to suppress harmful inflammation.

Introduction

Acute lung injury (ALI) represents a life-threatening pulmonary disorder carrying a significant clinical burden due to its high fatality rates [1, 2]. Bacterial pathogens are key drivers of ALI pathogenesis through LPS-mediated activation of the NF-κB cascade, which orchestrates cytokine storms and subsequent pulmonary tissue destruction [3]. The NF-κB transcription factor complex is composed of five distinct subunits, namely NF-κB1 (p105/p50), NF-κB2 (p100/p52), c-Rel, RelA (p65), and RelB [4]. NF-κB signaling operates through two major branches: the canonical pathway, which is rapidly activated by pro-inflammatory stimuli such as LPS and TNF-α and relies primarily on the p65/p50 heterodimer [5]; and the noncanonical pathway, which involves NF-κB–inducing kinase (NIK)–dependent processing of p100 to p52 and regulates slower immune and developmental processes [6].

Emerging evidence has established long non-coding RNAs (lncRNAs) as critical epigenetic regulators in human pathologies, with notable examples such as GAS5, HULC, NKILA, MALAT1, CASC2, SNHG5, LINC01134, HOTAIR, and PINT demonstrating disease-specific regulatory functions [7–16]. As a well-characterized lncRNA, HOTAIR (HOX transcript antisense intergenic RNA) has emerged as a significant epigenetic regulator in cancer and non-malignant disorders, involving positive feedback loops and compensatory harmful regulation mechanisms [17]. In cancer, HOTAIR contributes to aberrant transcription, chronic inflammation, and treatment resistance via NF-κB–dependent pathways [15, 18–23]. In addition, HOTAIR-NF-κB signaling axis was reported to be involved in aggravating the inflammatory environment of osteoarthritis [24], releasing epithelial-mesenchymal transition (EMT), and airway remodeling during smoke-induced COPD development, and promoting neuronal injury [25–27]. Furthermore, previous studies have shown that HOTAIR activates the NF-κB pathway by promoting p65 phosphorylation, thereby enhancing TNF-α secretion in LPS-stimulated cardiomyocytes from septic mice [28]. Recent studies also link HOTAIR to ALI, demonstrating its roles in regulating epithelial cell autophagy and apoptosis [29], as well as promoting aerobic glycolysis and inflammatory factor secretion through interaction with LIN28 [30]. These findings suggest that HOTAIR contributes to LPS-induced lung epithelial damage and inflammation. However, whether HOTAIR modulates NF-κB signaling in ALI *in vivo* and its broader effects on alveolar epithelial proliferation remain unclear.

This study investigated HOTAIR's role in ALI by employing A549 cells and LPS-injured mice. Our results reveal that HOTAIR drives inflammatory responses via the NF-κB pathway and influences alveolar epithelial proliferation, providing new mechanistic insights and highlighting HOTAIR as a potential therapeutic target in ALI.

Materials and methods

Cells

A549 cells were grown in RPMI-1640 medium (#11875093, Gibco) supplemented with 10% FBS and 1% penicillin-streptomycin (#15140122, Gibco) in an incubator with 5% CO2 at 37 ˚C. To create a model of lung injury inflammation, A549 cells were exposed to 1 μg/mL of LPS (#L2630, Sigma-Aldrich) for 24 h at 37 ˚C, seeded into 6-well plates at a density of 1×10^6 cells/well 24 h before transfection. Transfection was performed using Lipofectamine 2000 reagent (#1168027, Invitrogen) according to the manufacturer's instructions. These cells were harvested for subsequent experiments.

A549 cells were divided into four groups: 1) HOTAIR-overexpression (HOTAIR-OE) group with overexpression of HOTAIR using HOTAIR-pcDNA 3.1 (GenePharma, Shanghai, China); 2) si-HOTAIR group with siRNA specifically targeting HOTAIR for knockdown (GenePharma, Shanghai, China); 3) NC group with pcDNA 3.1 empty vector; 4) si-NC group with siRNA negative control. HOTAIR-OE groups were treated with BAY 11-7082 (10 μM, HY-13453) or an equal volume of DMSO (as control) for 24 h.

Animals

Eight-week-old wild-type C57BL/6 mice (weighing 20–25 g) were maintained at the Sun Yat-sen University Laboratory Animal Center. All animals were cared for, and procedures followed the approved protocols of the Institutional Animal Care and Use Committee of Guangzhou First People's Hospital (K-2021-141-01). An acute lung injury animal model was established with gradient concentrations of 5 mg/kg, 10 mg/kg, and 20 mg/kg LPS, and 5 mg/kg was chosen to

establish the LPS mice model [Supplementary Figure]. Mice were divided into three groups: 1) Ctrl group with PBS treatment in mice with intratracheal injection of 2.5 nmol of siRNA siNC; 2) LPS group with LPS treatment in mice with intratracheal injection of 2.5 nmol of siRNA siNC; 3) si-HOTAIR group with LPS treatment in mice with intratracheal injection of 2.5 nmol of siRNA si-HOTAIR.

After euthanasia, the right middle lobe was ligated and removed for protein extraction, the right lower lobe was collected for RNA analysis, and the right upper lobe was dissected for the lung wet-to-dry ratio measurement. To ensure proper preservation of airway and alveolar architecture, the trachea was then cannulated, and the remaining lung–heart bloc was fixed by intratracheal instillation of 4% paraformaldehyde (PFA). Following inflation fixation, the tissue was immersed in 4% PFA for 24 h, dehydrated, embedded in paraffin, and sectioned at 7 μm.

BALF collection and cell counting

The BALF samples were collected by flushing the lung tissues with 0.8 mL of pre-cooled PBS solution twice, centrifuged at 400 g for 5 min at 4 °C, and the cell pellets were collected. The cell pellets were resuspended with PBS and then cytospun onto slides and subjected to Diff-Quik staining (#G1540, Solarbio). Observations were performed using an optical microscope (Zeiss), followed by photography.

The neutrophils, macrophages, and total cell count were quantified, and the ratio of neutrophils to macrophages was calculated. The cell supernatant was stored at −80 °C for protein quantification and ELISA determination.

Cell proliferation assay

Following a 48-h infection period, A549 single-cell suspensions were plated in 96-well formats with an initial seeding density of 2×10^3 cells/well and digested with trypsin after 24-h incubations. Each group of cells had three replicates. Cell proliferation was assessed using the MTS assay (#G3580, Promega) at 0, 24, 48, and 72 h. The OD absorbance at 490 nm was measured using a microplate absorbance reader.

RNA extraction and RT-qPCR

Total RNA isolation from cellular or tissue specimens was performed with RNA pure Tissue & Cell Kit (#CW0584, Cwbio), followed by reverse transcription of 1 μg RNA template using PrimeScript RT reagent (#R333, Vazyme), incubate at 50 °C for 15 min and then briefly incubate at 85 °C for 5 s. Quantitative reverse transcription PCR (qRT-PCR) analyses were conducted on the QuantStudio platform (Applied Biosystems) using Vazyme SYBR Mix (#Q712), targeting HOTAIR along with key inflammatory mediators (IL-1β, IL-6, TNF-α) and the NF-κB pathway component NFKB1A (primer sequences in Supplementary Material). The amplification data were quantified using the $2^{-\Delta\Delta CT}$ method, with the housekeeping gene GAPDH as the normalization control.

ELISA

Protein lysates were prepared from cellular/tissue specimens using RIPA buffer containing phosphatase and protease inhibitors (#1005, #P1081, Beyotime), followed by quantitative protein assessment with the Thermo Scientific Pierce™ BCA assay system (#23225) for precise concentration determination. ELISA assay kit (#H0109c, #H0149c, #H6156, Elabscience) was used to detect the following biomarkers: The absorbance at 450 nm (A450) was recorded using a microplate reader.

Western blotting

Electrophoretic separation of protein lysates was conducted using SDS-PAGE, followed by transfer onto PVDF membranes (Merck Millipore #ISEQ00010). Membranes underwent blocking in 5% BSA/TBS (1h, RT) with subsequent TBST washes, then were probed overnight at 4 °C with phospho-specific and total antibodies against key NF-κB pathway components: p-IκBα (#340776), IκBα (#R23322), p-p65 (#310013), p65 (#380172) (all 1:1000, Zen-bioscience). Detection was achieved through 2 h incubation with HRP-conjugated secondary antibodies (Thermo Scientific, 1:10,000). The bands were visualized using SuperSignal West Femto (#34094, Thermo Scientific) and quantified with a chemiluminescence system (Bio-Rad) and ImageJ.

Immunofluorescence

A549 cells were seeded onto coverslips (#801010, NEST Biotechnology), fixed with 4% PFA for 15 min, washed with PBS, and permeabilized with 0.5% Triton X-100 for 10 min. After blocking with 5% goat serum/0.1% Triton X-100/PBS for 1 hour, samples were incubated overnight at 4 °C with rabbit anti-p65 NF-κB (1:50; #710048, Ebioscience). Cells were then incubated with donkey anti-rabbit Alexa Fluor 488 secondary antibody (1:1000; #ab150073, Abcam) for 1 hour and dyed with DAPI (#D9542, Sigma-Aldrich) for 5 min. Imaging was performed by a fluorescence microscope (magnification ×400; Zeiss Axio Observer 7).

Lung Wet-to-dry ratio

The Lung Wet-to-dry ratio was determined using the right upper lobe. The right upper lung lobe was excised and rinsed with PBS, and wet weight (WW) was then determined using an analytical balance (accuracy: 0.1 mg). Tissues were then dried in a 60 °C oven for 48–72 h until completely dried (defined as <2% weight variation between 24-h intervals) to determine dry weight (DW). The wet-to-dry ratio was calculated as (WW/DW) × 100%.

H&E staining

Lung specimens underwent standardized histoprocessing with 4% PFA immersion fixation, followed by graded ethanol dehydration series (70%–100%) and paraffin infiltration for optimal structural preservation. Samples were then sectioned into seven μm-thick slices, the slices were deparaffinized, rehydrated, stained with hematoxylin, rinsed, and counterstained with eosin for 1 min. After dehydration and clearing in xylene, slides were mounted with neutral resin. Observation using a light microscope (Zesis) and photographing were performed using a Digital Pathology Slide Scanner (KFBIO).

Histopathological assessment of lung injury was performed using a semi-quantitative scoring system adapted from Gustavo et.al [31]. Lung sections were evaluated independently by two blinded investigators based on the following criteria: (1) alveolar wall thickening, (2) interstitial or intra-alveolar inflammatory cell infiltration, (3) alveolar edema, (4) hemorrhage, and (5) hyaline membrane formation. Each parameter was scored on a scale of 0–4 (0 = absent, 1 = minimal, 2 = mild, 3 = moderate, 4 = severe). The total lung injury score was calculated as the sum of these individual components.

Statistical analysis

All statistical computations were performed using GraphPad Prism 9.4.0, with quantitative results expressed as mean ± SD. For comparisons between two groups, Student's t-test was used. For multigroup comparisons, one-way ANOVA was applied, followed by Bonferroni *post hoc* adjustments. A significance threshold of $p < 0.05$ considered statistically significant for all experimental conditions.

Results

LPS inhibits proliferation, promotes inflammation, and HOTAIR expression

A549 cells were treated with LPS to examine its effects on the cells. Cell proliferation was inhibited at 24 h, 48 h, and 72 h after LPS stimulation, compared to the control group (Figure 1A). The levels of mRNA and proteins of pro-inflammatory cytokines IL1B, IL6, and TNF-α were significantly increased in response to LPS stimulation (Figures 1B,C). Furthermore, a notable elevation in the expression of HOTAIR was observed in the group treated with LPS (Figure 1D).

HOTAIR promotes the inflammatory responses

HOTAIR levels were manipulated in A549 cells, which were then subjected to LPS administration to investigate the role of HOTAIR in ALI. HOTAIR was successfully overexpressed in the HOTAIR OE group, while effective knockdown of HOTAIR was observed in the si-HOTAIR group (Figure 1E). Following LPS treatment, A549 cells overexpressing HOTAIR exhibited significantly lower proliferation levels than the NC group, whereas si-HOTAIR-transfected cells showed significantly higher proliferation than the si-NC group (Figure 1F). Without LPS stimulation, qPCR analysis showed that the mRNA levels of pro-inflammatory cytokines (IL-1β, IL-6, and TNF-α) remained unchanged in both HOTAIR-overexpressing and si-HOTAIR groups (Figure 1G), indicating that HOTAIR alone does not significantly activate NF-κB signaling. Under LPS stimulation, however, HOTAIR-overexpressing cells displayed marked upregulation of IL-1β, IL-6, and TNF-α, whereas these cytokines were significantly downregulated in si-HOTAIR cells at both mRNA and protein levels (Figures 1H,I). Notably, co-treatment with BAY 11-7082 significantly reversed these effects (Figure 1J), reducing the mRNA levels of pro-inflammatory cytokines (IL-1β, IL-6, and TNF-α) comparable to HOTAIR OE group. This suggests that HOTAIR primarily modulates NF-κB–mediated inflammatory responses in the presence of inflammatory stimuli such as LPS.

HOTAIR activates the NF-κB pathway

The NF-κB pathway plays a key role in mediating cell inflammatory response to injury, and HOTAIR has been shown to regulate the NF-κB pathway in osteoarthritis 20. To investigate the molecular mechanisms underlying HOTAIR regulation of inflammation in ALI, we examined whether HOTAIR regulated the NF-κB pathway in this condition. Upon HOTAIR overexpression, the ratios of p-IκBα/IκBα and p-p65/p65 were significantly increased, suggesting activation of the NF-κB pathway (Figures 2A,B). Consistently, upon HOTAIR silencing, the ratios were decreased, suggesting inactivation of the NF-κB pathway (Figures 2A,B). The canonical NF-κB signaling

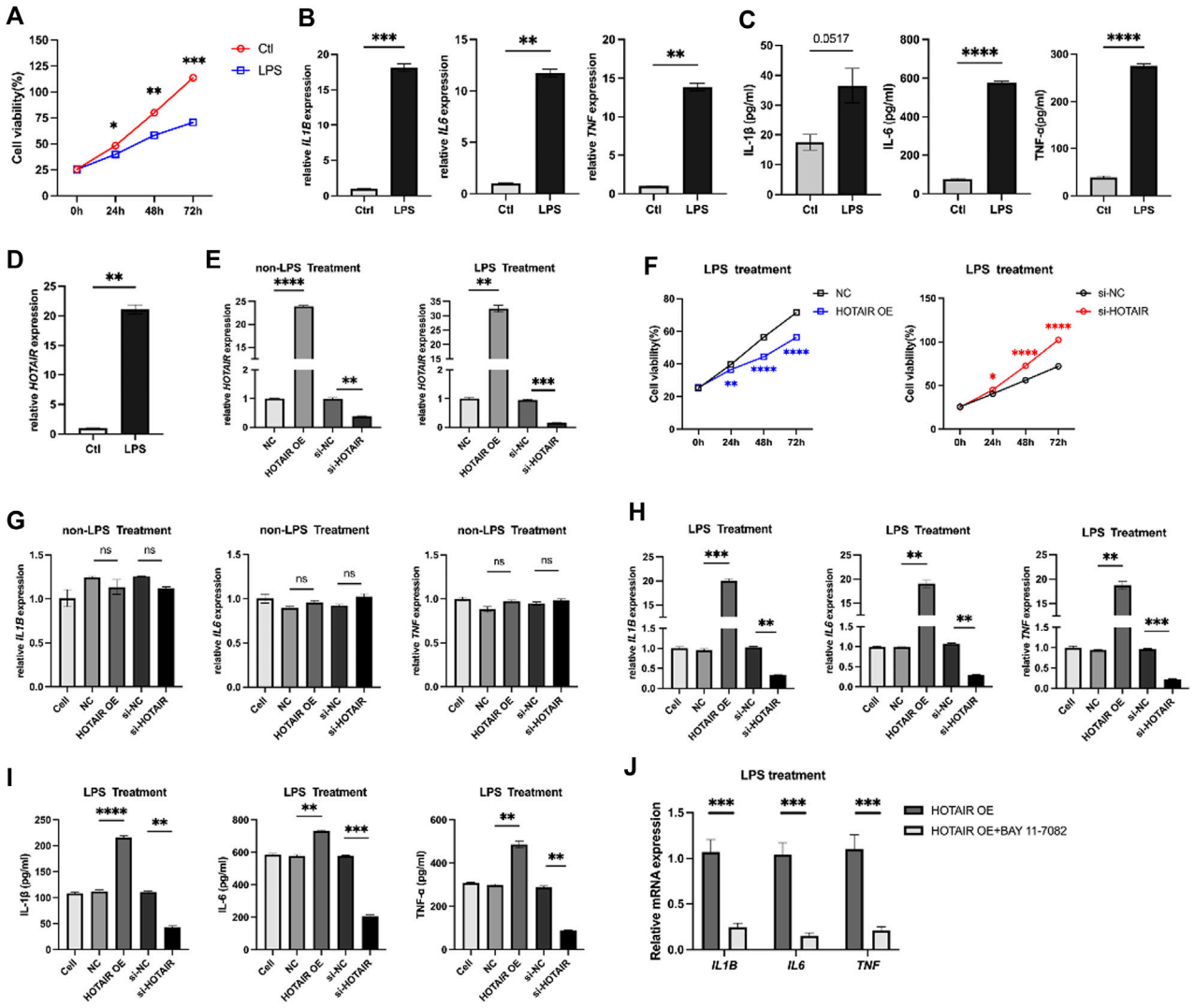

FIGURE 1
LPS treatment inhibits proliferation, promotes inflammation, and HOTAIR expression in A549 cells. **(A)** MTS assay for cell proliferation in control and LPS treatment A549 cells. **(B)** qPCR for the relative mRNA expression level of *IL1B*, *IL6*, and *TNF* in control and LPS treatment A549 cells, normalized to GAPDH. **(C)** ELISA for inflammatory cytokines, including IL-1β, IL-6, and TNF-α production in control and LPS treatment A549 cells. **(D)** qPCR for the relative mRNA expression level of *HOTAIR* in control and LPS treatment A549 cells, normalized to GAPDH. n = 3. **(E)** qPCR for the relative mRNA expression level of *HOTAIR* in A549 cells after transfection with NC, HOTAIR OE, si-NC, and si-HOTAIR and treatment with/without LPS, normalized to GAPDH. **(F)** MTS assay for cell proliferation in LPS-induced A549 cells after transfection with NC and HOTAIR OE (left), as well as si-NC and si-HOTAIR (right). **(G)** qPCR for the relative mRNA expression level of *IL1B*, *IL6*, and *TNF* in non-LPS treatment A549 cells after transfection with NC, HOTAIR OE, si-NC, and si-HOTAIR, normalized to GAPDH. **(H)** qPCR for the relative mRNA expression level of *IL1B*, *IL6*, and *TNF* in LPS induced treatment A549 cells after transfection with NC, HOTAIR OE, si-NC, and si-HOTAIR, normalized to GAPDH. **(I)** ELISA for inflammatory cytokines production, including IL-1β, IL-6, and TNF-α, in LPS treatment A549 cells after transfection with NC, HOTAIR OE, si-NC, and si-HOTAIR. **(J)** qPCR for the relative mRNA expression level of *IL1B*, *IL6*, and *TNF* in LPS induced treatment A549 cells after transfection with HOTAIR OE, with or with out Bay 11-7082, normalized to GAPDH. n = 3. $p < 0.05$ (*); $p < 0.01$ (**); $p < 0.001$ (***); and $p < 0.0001$ (****).

cascade culminates in p65 nuclear localization. Following LPS stimulation, nuclear localization of p65 protein was enhanced in HOTAIR-overexpressing cells, and consistently, it was decreased in HOTAIR-silenced cells (Figures 2C,D). These results suggested that HOTAIR regulates the inflammation in ALI by positively regulating the NF-κB pathway.

HOTAIR promotes LPS-induced lung injury *in vivo*

LPS treatment significantly upregulated the expression of HOTAIR in a dose-dependent manner, indicating a potential role of HOTAIR in the inflammatory response triggered by LPS

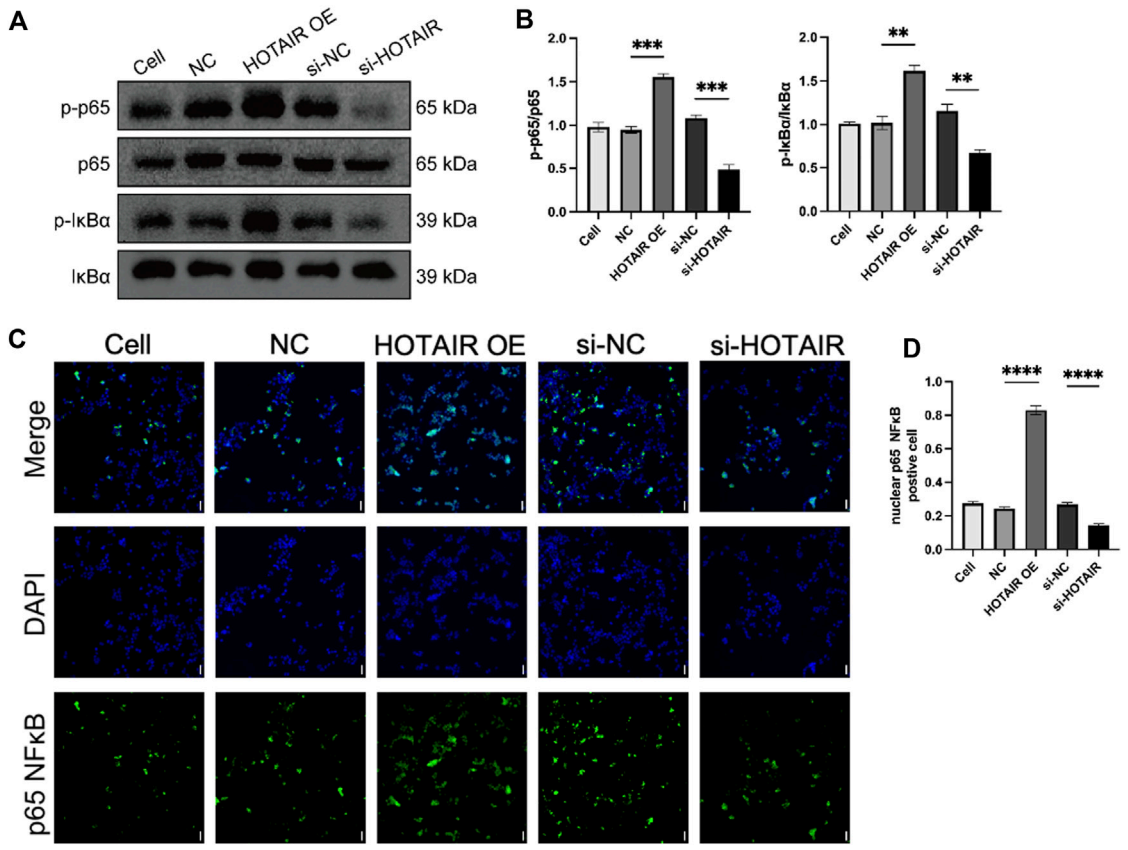

FIGURE 2
HOTAIR activates the NF-κB pathway by promoting the nuclear translocation of p65 in LPS-induced A549. **(A)** p-IκBα, IκBα, p-p65 NF-κB, and p65 NF-κB protein expression was detected using western blot in LPS treatment A549 cells after transfection with NC, HOTAIR OE, si-NC, and si-HOTAIR. **(B)** Ratio of p-IκBα/IκBα and p-p65 NF-κB and p-p65 NF-κB/NF-κB in LPS treatment A549 cells after transfection with NC, HOTAIR OE, si-NC, and si-HOTAIR. **(C)** Immunofluorescence (IF) for p65 NF-κB in LPS treatment A549 cells after transfection with NC, HOTAIR OE, si-NC, and si-HOTAIR. Scale bar, 50 μm. **(D)** Quantifying nuclear p65 NF-κB positive cells in LPS treatment A549 cells after transfection with NC, HOTAIR OE, si-NC, and si-HOTAIR. n = 3. $p < 0.01$ (**); $p < 0.001$ (***); and $p < 0.0001$ (****).

(Suppleymentary Figure). To investigate the role of HOTAIR in ALI *in vivo*, we generated HOTAIR-knockdown mice by injection of siRNA si-HOTAIR and stimulated the mice with LPS (Figure 3A). At 24 h post-LPS stimulation, compared to the Ctrl group, the LPS group exhibited significant weight loss and increased lung wet-to-dry ratio (Figure 3B). The si-HOTAIR group also showed weight loss (Figure 3B). On the other hand, the lung wet-to-dry ratio of the si-HOTAIR group was significantly lower than that of the LPS group, and was comparable to that of the Ctrl group (Figure 3C). Histopathological analysis showed minimal lymphocyte and plasma cell infiltration without notable inflammatory response and intact pulmonary architecture in the Ctrl group (Figure 3D, left panel). In contrast, the LPS group exhibited a marked increase in inflammatory cell infiltration, especially neutrophils and macrophages, with localized inflammatory foci; moreover, fluid infiltration was observed in the alveoli, with bronchial wall swelling and obvious interstitial edema, and some alveolar walls became thinner or ruptured, and the integrity of the bronchi and alveoli was compromised (Figure 3D, middle panel). In the si-HOTAIR group, inflammatory cells were mainly concentrated in localized areas with reduced fluid accumulation in the alveolar cavity and mild interstitial edema, and the alveolar wall cells were relatively orderly arranged. The overall degree of inflammation and tissue damage was alleviated compared with the LPS group, but still more pronounced than the control group (Figure 3D, right panel). These results suggested that HOTAIR promotes LPS-induced lung injury *in vivo* (Figures 3D,E).

HOTAIR promotes LPS-induced inflammation through regulating the NF-κB pathway *in vivo*

Following LPS stimulation, the total protein levels in bronchoalveolar lavage fluid (BALF) of mice were elevated,

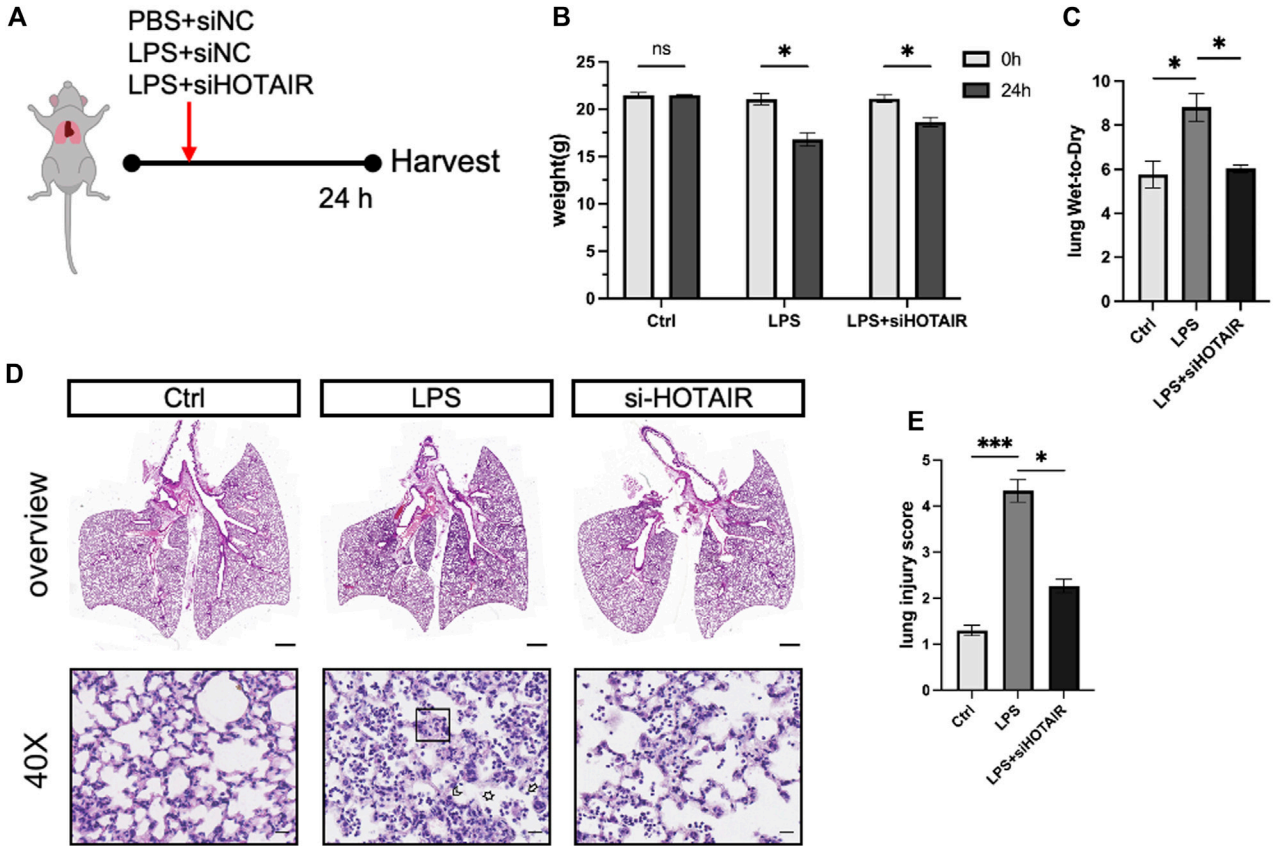

FIGURE 3
HOTAIR promotes LPS-induced ALI *in vivo*. **(A)** Mice were oropharyngeally administered LPS to simulate ALI, with PBS as the control. si-HOTAIR was co-administered with LPS/PBS simultaneously. After 24 h, mice were euthanized, and lung tissues were harvested. The mice were grouped into PBS + si-NC (Ctrl), LPS + si-NC (LPS), and LPS + si-HOTAIR. **(B)** The body weight (g) at 0 and 24 h of mice in the Ctrl, LPS, and LPS + siHOTAIR groups. **(C)** The lung wet-to-dry ratio (lung W/D) of mice in the Ctrl, LPS, and LPS + siHOTAIR groups. **(D)** Representative histology images of H&E staining from mice in the Ctrl, LPS, and LPS + siHOTAIR groups. Scale bars, 20 μm. Arrowheads: Neutrophils located within the alveolar space or interstitium, indicate alveolar and interstitial inflammation. Box area: alveolar wall thickening and edema. Asterisks: proteinaceous debris filling the airspaces. **(E)** Semi-quantification of lung injury score in the Ctrl, LPS, and LPS + siHOTAIR groups. n = 3 per group; scale bars(black), 50 μm. Ns, not significant; $p < 0.05$ (*); and $p < 0.0001$ (****).

which was attenuated in HOTAIR-knockdown mice (Figure 4A). Elevated protein content in BALF reflects enhanced vascular permeability and disruption of the alveolar–capillary barrier, a characteristic pathological feature of ALI. Concurrently, LPS stimulation induced macrophage and neutrophil accumulation in BALF. However, because neutrophils expanded more dramatically, the proportional representation of macrophages appeared reduced. Compared to the LPS group, HOTAIR knockdown showed a mild decrease in macrophage and neutrophil counts, consistent with an attenuated inflammatory response (Figures 4B,C).Further analysis of pro-inflammatory cytokines, including IL-1β, IL-6, and TNF-α, revealed that, while LPS stimulation markedly elevated the protein levels of these cytokines, HOTAIR silencing significantly attenuated this elevation (Figure 4D). Although no statistically significant differences were detected, the mRNA levels of these cytokines exhibited trends similar to protein levels (Figure 4E). Hence, the LPS-induced inflammation was attenuated by HOTAIR silencing.

Next, we investigated the molecular mechanisms by examining the NF-κB signaling pathway *in vivo*. In the mouse lung, LPS stimulation upregulated Nfkb1, a core transcriptional target of the NF-κB pathway, but this upregulation was diminished by HOTAIR silencing (Figure 4F). Furthermore, LPS treatment elevated the ratio of p-p65/p65 and p-IκBα/IκBα, suggesting activation of NF-κB signaling (Figure 4G). Importantly, HOTAIR silencing significantly attenuated the elevation in the ratio of p-p65/p65 and p-IκBα/IκBα, suggesting a compromised NF-κB pathway (Figure 4G). Therefore, LPS-induced activation in the NF-κB pathway was impaired by HOTAIR silencing *in vivo*.

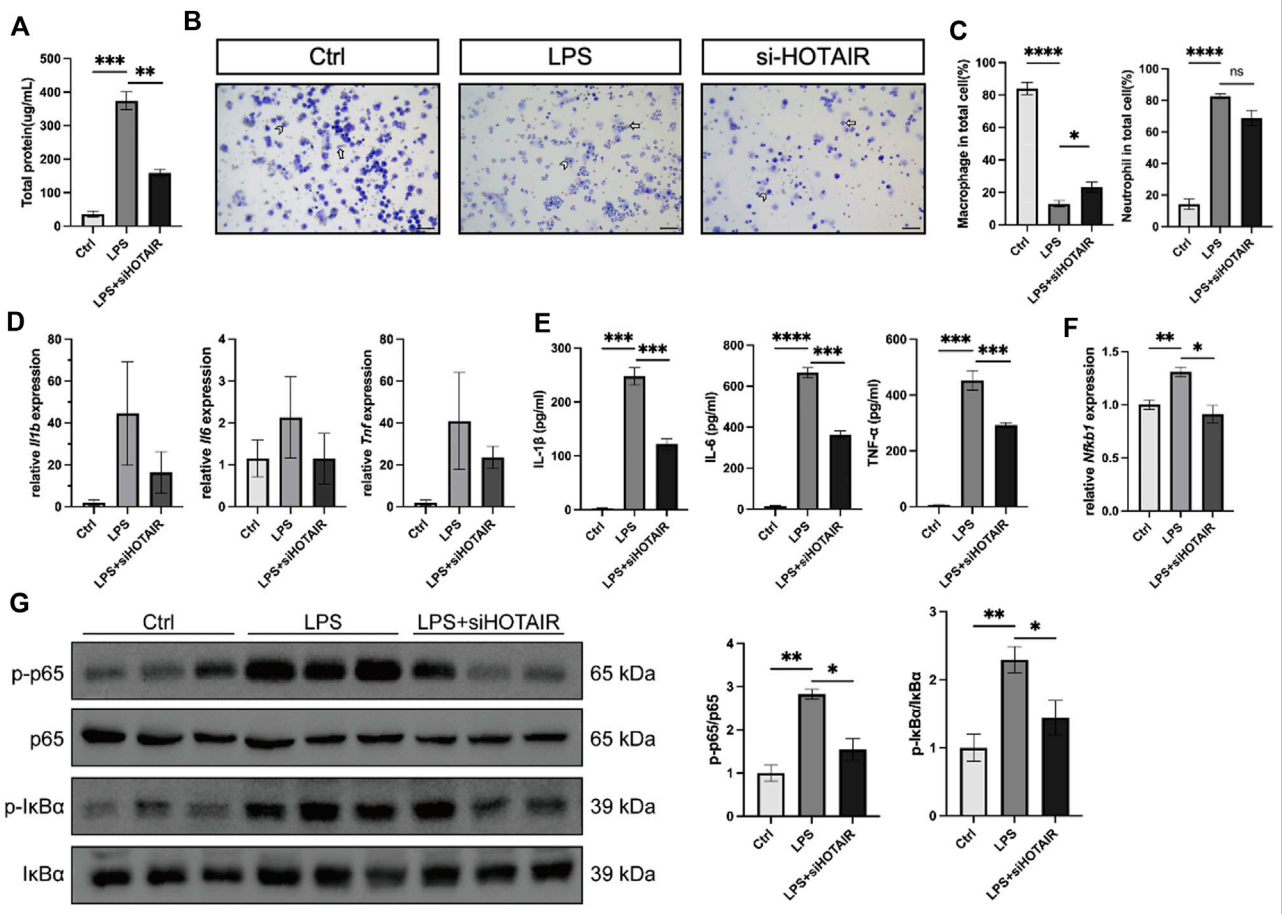

FIGURE 4
HOTAIR promotes LPS-induced inflammation and promotes LPS-induced inflammation *in vivo*. **(A)** Total protein levels in bronchoalveolar lavage fluid (BALF) from mice after LPS stimulation. n = 3. **(B)** BALF cells from mice in the Ctrl, LPS, and LPS + siHOTAIR groups were cytospun on slides and subjected to Diff-Quik staining. Macrophages and neutrophils were identified based on morphological criteria. Representative images of Diff-Quik staining, Short arrow, macrophage; long arrow, neutrophil. Scale bar, 50 μm. **(C)** Quantification of macrophages and neutrophils as a percentage of total cells in the BALF of mice in the Ctrl, LPS, and LPS + siHOTAIR groups. **(D)** qPCR for the relative mRNA expression level of *Il1b*, *Il6*, and *Tnf* from mice in the Ctrl, LPS, and LPS + siHOTAIR groups, normalized to GAPDH. **(E)** qPCR for the relative mRNA expression level of *Nfkb1* from mice in the Ctrl, LPS, and LPS + siHOTAIR groups, normalized to GAPDH. **(F)** p-IκBα, IκBα, p-p65 NF-κB, and p65 NF-κB protein expression was detected using western blot from mice in the Ctrl, LPS, and LPS + siHOTAIR groups. **(G)** Ratio of p-IκBα/IκBα and p-p65 NF-κB/NF-κB from mice in the Ctrl, LPS, and LPS + siHOTAIR groups. n = 3 per group; $p < 0.05$ (*); $p < 0.01$ (**); $p < 0.001$ (***); and $p < 0.0001$ (****).

Discussion

Our study confirmed that HOTAIR activated the NF-κB pathway through key proteins, including p50, p-p65/p65, and p-IκBα/IκBα, in both *in vitro* and *in vivo* models of LPS-induced ALI. This activation leads to the massive recruitment of inflammatory cells, including macrophages and neutrophils, triggers the secretion of pro-inflammatory cytokines, and results in pulmonary tissue damage characterized by inflammatory cell infiltration, tissue edema, and other pathological manifestations.

Serving as the primary driver of inflammatory pathogenesis in LPS-challenged ALI, the NF-κB cascade executes its regulatory dominance through a canonical molecular sequence: IκBα phosphorylation-triggered proteolytic breakdown liberates sequestered p65 subunits for nuclear accumulation, thereby activating transcription of pro-inflammatory mediators [4]. We observed that HOTAIR knockdown could reduce the accumulation of p-IκB and p-p65 induced by LPS stimulation and prevent p65 nuclear translocation, suggesting that HOTAIR knockdown could attenuate severe lung inflammation caused by LPS. Excessive lung inflammation with abnormal macrophage activation is known to be characteristic of ALI. Studies have demonstrated that alveolar macrophages (AMs) increase substantially in

BALF following lung injury or inflammation [32, 33]. Interferon drives AM differentiation into M1 macrophages in LPS-induced ALI through recognition receptors such as TLRs, secreting cytokines such as IL-1β, IL-6, IL-18, IL-12, and iNOS, which contribute to the clearance of bacteria and endotoxins, promote the recruitment and infiltration of neutrophils and M1 AM, thereby exacerbating the inflammatory response [34]. Previous studies indicate that HOTAIR regulates NF-κB activation by modulating IκBα degradation in LPS-stimulated macrophages [35]. Whole-transcriptome RNA sequencing analysis identified a series of long non-coding RNAs, including HOTAIR, with potential regulatory functions in cytokine expression and inflammatory responses in macrophages and revealed that HOTAIR exhibits an expression pattern similar to that of pro-inflammatory cytokines following LPS stimulation [36]. In our study, we found that HOTAIR knockdown significantly reduced the expression of macrophages and neutrophils, accompanied by significant reductions in the expression levels of TNF-α, IL-1β, and IL-6, suggesting that HOTAIR knockdown can effectively inhibit the recruitment of macrophages and neutrophils, reducing the expression of pro-inflammatory factors. However, the effect of HOTAIR on macrophage polarization needs to be further confirmed.

ALI is characterized not only by inflammatory cell infiltration but also by epithelial barrier dysfunction. Alveolar type 1 (AT1) cells, a key part of the alveolar-capillary barrier, cover >95% of the gas exchange surface [37]. AT1 cells contain E-NaC, responsible for the bulk of transepithelial Na(+) transport. They may be interfered with under hypoxia or inflammation, triggering fluid retention within the alveolar space and a poor prognosis [38, 39]. Our findings demonstrate that HOTAIR can reverse severe damage to alveolar epithelial cells in LPS-induced ALI in mice, reducing the severity of pulmonary edema, though the direct impact on AT1/AT2 regeneration requires further validation using primary cell cultures or organoid models.

Alveolar type II (AT2) cells exhibit stem-like properties, enabling self-renewal, mobilization, and transdifferentiation into AT1 lineages via an epithelial regeneration program reconstructing alveolar architecture [40]. Our findings demonstrate that HOTAIR knockdown enhances the proliferation of A549 cells in a time-dependent manner, suggesting its potential role in promoting alveolar epithelial regeneration and facilitating lung tissue repair. The main signaling pathways that may promote the proliferation and differentiation of AT2 cells include the Wnt/β-catenin pathway and the YAP/TAZ pathway [41]. The Wnt/β-catenin and YAP/TAZ signaling axes emerge as core regulators of AT2 cell fate determination, orchestrating alveolar regeneration through progenitor cell activation. Notably, HOTAIR exhibits pan-pathological regulatory capacities, driving oncogenic phenotypes in epithelial malignancies (including esophageal/gastric/colorectal carcinomas), modulating vascular calcification in cardiovascular pathologies, governing cartilage homeostasis in degenerative joint diseases, and rewiring placental signaling cascades in hypertensive gestational disorders—predominantly via Wnt/β-catenin-dependent mechanisms [42–48]. Based on these findings, we hypothesize that HOTAIR may mediate the proliferation of AT2 cells in ALI via the Wnt/β-catenin signaling pathway, which requires further confirmation.

Taken together, our findings reveal that HOTAIR amplifies acute inflammatory responses and worsens lung injury largely through NF-κB–dependent mechanisms. HOTAIR silencing mitigated cytokine production, inflammatory cell infiltration, vascular leakage, and tissue destruction, highlighting its potential as a therapeutic target for modulating dysregulated inflammation in ALI. However, it should be noted that the A549 cell system and the single-hit LPS mouse model mainly reflect endotoxin-induced acute injury and do not fully reproduce the clinical heterogeneity of ALI/ARDS, which may arise from bacterial pneumonia, sepsis, aspiration, trauma, or mixed etiologies. Future studies employing clinically relevant models, patient-derived cells, or translational cohorts will be crucial to validate our observations and to further elucidate the therapeutic potential of targeting HOTAIR in diverse ALI/ARDS settings.

Author contributions

FZ: Conceptualization, Investigation and Writing – original draft; ZM: Investigation and Writing – original draft; WL: Investigation and Writing – original draft; CS: Investigation; XH: Investigation; MY: Investigation; HH: Investigation; YL: Investigation; KW: Investigation; JZ: Investigation; CL: Writing – review and editing; SW: Conceptualization, Funding acquisition and Writing – review and editing; ZL: Conceptualization, Funding acquisition and Writing – review and editing. All authors contributed to the article and approved the submitted version.

Data availability

The raw data supporting the conclusions of this article will be made available by the authors, without undue reservation.

Ethics statement

The animal study was approved by the Ethics Committee of Guangzhou First People's Hospital (protocol code K-2021-141-01; approval date: 19 October 2021). All procedures were

conducted in accordance with institutional guidelines and local legislation.

Funding

The author(s) declared that financial support was received for this work and/or its publication. This research was funded by the Science and Technology Program of Guangzhou, grant number #2024A03J0960 to SW and #202201020299 to ZL.

Conflict of interest

The author(s) declared no potential conflicts of interest with respect to the research, authorship, and/or publication of this article.

Generative AI statement

The author(s) declared that generative AI was not used in the creation of this manuscript.

Any alternative text (alt text) provided alongside figures in this article has been generated by Frontiers with the support of artificial intelligence and reasonable efforts have been made to ensure accuracy, including review by the authors wherever possible. If you identify any issues, please contact us.

Supplementary material

The Supplementary Material for this article can be found online at: https://www.ebm-journal.org/articles/10.3389/ebm.2025.10766/full#supplementary-material

References

1. McNicholas BA, Rooney GM, Laffey JG. Lessons to learn from epidemiologic studies in ARDS. *Curr Opin Crit Care* (2018) **24**(1):41–8. doi:10.1097/MCC.0000000000000473

2. Zheng L, Su J, Zhang Z, Jiang L, Wei J, Xu X, et al. Salidroside regulates inflammatory pathway of alveolar macrophages by influencing the secretion of miRNA-146a exosomes by lung epithelial cells. *Sci Rep* (2020) **10**(1):20750. doi:10.1038/s41598-020-77448-6

3. Huang Q, Le Y, Li S, Bian Y. Signaling pathways and potential therapeutic targets in acute respiratory distress syndrome (ARDS). *Respir Res* (2024) **25**(1):30. doi:10.1186/s12931-024-02678-5

4. Alharbi KS, Fuloria NK, Fuloria S, Rahman SB, Al-Malki WH, Javed Shaikh MA, et al. Nuclear factor-kappa B and its role in inflammatory lung disease. *Chem Biol Interact* (2021) **345**:109568. doi:10.1016/j.cbi.2021.109568

5. Liu T, Zhang L, Joo D, Sun SC. NF-κB signaling in inflammation. *Signal Transduct Target Ther* (2017) **2**:17023. doi:10.1038/sigtrans.2017.23

6. Sun SC. The non-canonical NF-κB pathway in immunity and inflammation. *Nat Rev Immunol* (2017) **17**(9):545–58. doi:10.1038/nri.2017.52

7. Zheng Z, Pupwe G, Takehiro K, Yu G, Zhan M, Xu B. The function and mechanisms of action of non-coding RNAs in prostatic diseases. *Cell Invest* (2025) **1**(2):100021. doi:10.1016/j.clnves.2025.100021

8. Filippova EA, Fridman MV, Burdennyy AM, Loginov VI, Pronina IV, Lukina SS, et al. Long noncoding RNA GAS5 in breast cancer: epigenetic mechanisms and biological functions. *Int J Mol Sci* (2021) **22**(13):6810. doi:10.3390/ijms22136810

9. Liu S, Huttad L, He G, He W, Liu C, Cai D, et al. Long noncoding RNA HULC regulates the NF-κB pathway and represents a promising prognostic biomarker in liver cancer. *Cancer Med* (2023) **12**(4):5124–36. doi:10.1002/cam4.5263

10. Huang D, Chen J, Yang L, Ouyang Q, Li J, Lao L, et al. NKILA lncRNA promotes tumor immune evasion by sensitizing T cells to activation-induced cell death. *Nat Immunol* (2018) **19**(10):1112–25. doi:10.1038/s41590-018-0207-y

11. Shi Z, Zheng Z, Lin X, Ma H. Long noncoding RNA MALAT1 regulates the progression of atherosclerosis by miR-330-5p/NF-κB signal pathway. *J Cardiovasc Pharmacol* (2021) **78**(2):235–46. doi:10.1097/FJC.0000000000001061

12. Zhao L, Zhang Y, Zhang Y. Long noncoding RNA CASC2 regulates hepatocellular carcinoma cell oncogenesis through miR-362-5p/Nf-κB axis. *J Cell Physiol* (2018) **233**(10):6661–70. doi:10.1002/jcp.26446

13. Kang S, Ou C, Yan A, Zhu K, Xue R, Zhang Y, et al. Long noncoding RNA SNHG5 induces the NF-κB pathway by regulating miR-181c-5p/CBX4 axis to promote the progression of non-small cell lung cancer. *Arch Bronconeumol* (2023) **59**(1):10–8. doi:10.1016/j.arbres.2022.07.001

14. Zhou Z, Zhu Y, Gao G, Zhang Y. Long noncoding RNA SNHG16 targets miR-146a-5p/CCL5 to regulate LPS-Induced WI-38 cell apoptosis and inflammation in acute pneumonia. *Life Sci* (2019) **228**:189–97. doi:10.1016/j.lfs.2019.05.008

15. Wang J, Liu X, Li P, Wang J, Shu Y, Zhong X, et al. Long noncoding RNA HOTAIR regulates the stemness of breast cancer cells via activation of the NF-κB signaling pathway. *J Biol Chem* (2022) **298**(12):102630. doi:10.1016/j.jbc.2022.102630

16. Ye M, Wang C, Zhu J, Chen M, Wang S, Li M, et al. An NF-κB-responsive long noncoding RNA, PINT, regulates TNF-α gene transcription by scaffolding p65 and EZH2. *FASEB J.* (2021) **35**(9):e21667. doi:10.1096/fj.202002263R

17. Gupta SC, Awasthee N, Rai V, Chava S, Gunda V, Challagundla KB. Long non-coding RNAs and nuclear factor-κB crosstalk in cancer and other human diseases. *Biochim Biophys Acta Rev Cancer* (2020) **1873**(1):188316. doi:10.1016/j.bbcan.2019.188316

18. Zeng C. Advances in cancer treatment: the role of new technologies and research. *Cell Invest* (2025) **1**(1):100001. doi:10.1016/j.clnves.2024.100001

19. Wang Y, Yi K, Liu X, Tan Y, Jin W, Li Y, et al. HOTAIR Up-Regulation activates NF-κB to induce immunoescape in gliomas. *Front Immunol* (2021) **12**:785463. doi:10.3389/fimmu.2021.785463

20. Zhang Z, Fan B, Liu F, Song N, Peng Y, Ma W, et al. HOX transcript antisense RNA is elevated in gastric carcinogenesis and regulated by the NF-κB pathway. *J Cell Biochem* (2019) **120**(6):10548–55. doi:10.1002/jcb.28340

21. Hu CY, Su BH, Lee YC, Wang CT, Yang ML, Shen WT, et al. Interruption of the long non-coding RNA HOTAIR signaling axis ameliorates chemotherapy-induced cachexia in bladder cancer. *J Biomed Sci* (2022) **29**(1):104. doi:10.1186/s12929-022-00887-y

22. Li P, Zhang X, Wang L, Du L, Yang Y, Liu T, et al. lncRNA HOTAIR contributes to 5FU resistance through suppressing miR-218 and activating NF-κB/TS signaling in colorectal cancer. *Mol Ther Nucleic Acids* (2017) **8**:356–69. doi:10.1016/j.omtn.2017.07.007

23. Özeş AR, Miller DF, Özeş ON, Fang F, Liu Y, Matei D, et al. NF-κB-HOTAIR axis links DNA damage response, chemoresistance and cellular senescence in ovarian cancer. *Oncogene* (2016) **35**(41):5350–61. doi:10.1038/onc.2016.75

24. Hu K, Wen H, Song T, Che Z, Song Y, Song M. Deciphering the role of LncRNAs in osteoarthritis: inflammatory pathways unveiled. *J Inflamm Res* (2024) **17**:6563–81. doi:10.2147/JIR.S489682

25. Xia H, Xue J, Xu H, Lin M, Shi M, Sun Q, et al. Andrographolide antagonizes the cigarette smoke-induced epithelial-mesenchymal transition and pulmonary dysfunction through anti-inflammatory inhibiting HOTAIR. *Toxicology* (2019) **422**:84–94. doi:10.1016/j.tox.2019.05.009

26. Zhao J, Li H, Chang N. LncRNA HOTAIR promotes MPP+-induced neuronal injury in Parkinson's disease by regulating the miR-874-5p/ATG10 axis. *EXCLI J.* (2020) **19**:1141–53. doi:10.17179/excli2020-2286

27. Spreafico M, Grillo B, Rusconi F, Battaglioli E, Venturin M. Multiple layers of CDK5R1 regulation in alzheimer's disease implicate long non-coding RNAs. *Int J Mol Sci* (2018) **19**(7):2022. doi:10.3390/ijms19072022

28. Wu H, Liu J, Li W, Liu G, Li Z. LncRNA-HOTAIR promotes TNF-α production in cardiomyocytes of LPS-induced sepsis mice by activating NF-κB pathway. *Biochem Biophys Res Commun* (2016) **471**(1):240–6. doi:10.1016/j.bbrc.2016.01.117

29. Li Y, Liang Z, He H, Huang X, Mo Z, Tan J, et al. The lncRNA HOTAIR regulates autophagy and affects lipopolysaccharide-induced acute lung injury through the miR-17-5p/ATG2/ATG7/ATG16 axis. *J Cell Mol Med* (2021) **25**(16):8062–73. doi:10.1111/jcmm.16737

30. Xie J, Zheng Z, Wang B, Zhang J, Jiang J, Wu F, et al. LncRNA HOTAIR promotes aerobic glycolysis by recruiting Lin28 to induce inflammation and apoptosis in acute lung injury. *RNA Biol* (2025) **22**(1):1–12. doi:10.1080/15476286.2025.2475255

31. Matute-Bello G, Downey G, Moore BB, Groshong SD, Matthay MA, Slutsky AS, et al. An official American thoracic society workshop report: features and measurements of experimental acute lung injury in animals. *Am J Respir Cell Mol Biol* (2011) **44**(5):725–38. doi:10.1165/rcmb.2009-0210ST

32. Aggarwal NR, King LS, D'Alessio FR. Diverse macrophage populations mediate acute lung inflammation and resolution. *Am J Physiol Lung Cell Mol Physiol* (2014) **306**(8):L709–725. doi:10.1152/ajplung.00341.2013

33. Chen X, Tang J, Shuai W, Meng J, Feng J, Han Z. Macrophage polarization and its role in the pathogenesis of acute lung injury/acute respiratory distress syndrome. *Inflamm Res* (2020) **69**(9):883–95. doi:10.1007/s00011-020-01378-2

34. Wu D, Pan P, Su X, Zhang L, Qin Q, Tan H, et al. Interferon regulatory Factor-1 mediates alveolar macrophage pyroptosis during LPS-induced acute lung injury in mice. *Shock* (2016) **46**(3):329–38. doi:10.1097/SHK.0000000000000595

35. Obaid M, Udden SMN, Deb P, Shihabeddin N, Zaki MH, Mandal SS. LncRNA HOTAIR regulates lipopolysaccharide-induced cytokine expression and inflammatory response in macrophages. *Sci Rep* (2018) **8**(1):15670. doi:10.1038/s41598-018-33722-2

36. Chini A, Guha P, Malladi VS, Guo Z, Mandal SS. Novel long non-coding RNAs associated with inflammation and macrophage activation in human. *Sci Rep* (2023) **13**(1):4036. doi:10.1038/s41598-023-30568-1

37. Yang J, Hernandez BJ, Martinez Alanis D, Narvaez del Pilar O, Vila-Ellis L, Akiyama H, et al. The development and plasticity of alveolar type 1 cells. *Development* (2016) **143**(1):54–65. doi:10.1242/dev.130005

38. Johnson MD, Widdicombe JH, Allen L, Barbry P, Dobbs LG. Alveolar epithelial type I cells contain transport proteins and transport sodium, supporting an active role for type I cells in regulation of lung liquid homeostasis. *Proc Natl Acad Sci U S A* (2002) **99**(4):1966–71. doi:10.1073/pnas.042689399

39. Johnson MD, Bao HF, Helms MN, Chen XJ, Tigue Z, Jain L, et al. Functional ion channels in pulmonary alveolar type I cells support a role for type I cells in lung ion transport. *Proc Natl Acad Sci U S A* (2006) **103**(13):4964–9. doi:10.1073/pnas.0600855103

40. Olsen CO, Isakson BE, Seedorf GJ, Lubman RL, Boitano S. Extracellular matrix-driven alveolar epithelial cell differentiation *in vitro*. *Exp Lung Res* (2005) **31**(5):461–82. doi:10.1080/01902140590918830

41. Aspal M, Zemans RL. Mechanisms of ATII-to-ATI cell differentiation during lung regeneration. *Int J Mol Sci* (2020) **21**(9):3188. doi:10.3390/ijms21093188

42. Ge XS, Ma HJ, Zheng XH, Ruan HL, Liao XY, Xue WQ, et al. HOTAIR, a prognostic factor in esophageal squamous cell carcinoma, inhibits WIF-1 expression and activates wnt pathway. *Cancer Sci* (2013) **104**(12):1675–82. doi:10.1111/cas.12296

43. Cheng C, Qin Y, Zhi Q, Wang J, Qin C. Knockdown of long non-coding RNA HOTAIR inhibits cisplatin resistance of gastric cancer cells through inhibiting the PI3K/Akt and Wnt/β-catenin signaling pathways by up-regulating miR-34a. *Int J Biol Macromol* (2018) **107**(Pt B):2620–9. doi:10.1016/j.ijbiomac.2017.10.154

44. Xiao Z, Qu Z, Chen Z, Fang Z, Zhou K, Huang Z, et al. LncRNA HOTAIR is a prognostic biomarker for the proliferation and chemoresistance of colorectal cancer via MiR-203a-3p-Mediated Wnt/ß-Catenin signaling pathway. *Cell Physiol Biochem* (2018) **46**(3):1275–85. doi:10.1159/000489110

45. Han B, Peng X, Cheng D, Zhu Y, Du J, Li J, et al. Delphinidin suppresses breast carcinogenesis through the HOTAIR/microRNA-34a axis. *Cancer Sci* (2019) **110**(10):3089–97. doi:10.1111/cas.14133

46. Carrion K, Dyo J, Patel V, Sasik R, Mohamed SA, Hardiman G, et al. The long non-coding HOTAIR is modulated by cyclic stretch and WNT/β-CATENIN in human aortic valve cells and is a novel repressor of calcification genes. *PLoS One* (2014) **9**(5):e96577. doi:10.1371/journal.pone.0096577

47. Hu J, Wang Z, Shan Y, Pan Y, Ma J, Jia L. Long non-coding RNA HOTAIR promotes osteoarthritis progression via miR-17-5p/FUT2/β-catenin axis. *Cell Death Dis.* (2018) **9**(7):711. doi:10.1038/s41419-018-0746-z

48. Song X, Luo X, Gao Q, Wang Y, Gao Q, Long W. Dysregulation of LncRNAs in placenta and pathogenesis of preeclampsia. *Curr Drug Targets* (2017) **18**(10):1165–70. doi:10.2174/1389450118666170404160000

EBM Experimental Biology and Medicine

TYPE Review
PUBLISHED 19 December 2025
DOI 10.3389/ebm.2025.10841

OPEN ACCESS

*CORRESPONDENCE
Size Chen,
chensize@gdpu.edu.cn

RECEIVED 27 September 2025
REVISED 19 November 2025
ACCEPTED 09 December 2025
PUBLISHED 19 December 2025

CITATION
Xiang Y, Dong J, Shao L and Chen S (2025) Chimeric antigen receptor natural killer cell therapy for solid tumors: mechanisms, clinical progress, and strategies to overcome the tumor microenvironment.
Exp. Biol. Med. 250:10841.
doi: 10.3389/ebm.2025.10841

Chimeric antigen receptor natural killer cell therapy for solid tumors: mechanisms, clinical progress, and strategies to overcome the tumor microenvironment

Yu Xiang[1,2,3,4,5], Jiayi Dong[1,2,3,4], Lijuan Shao[1,2,3,4,5] and Size Chen[1,2,3,4,5]*

[1]Department of Immuno-Oncology, The First Affiliated Hospital of Guangdong Pharmaceutical University, Guangdong Pharmaceutical University, Guangzhou, China, [2]Guangdong Provincial Engineering Research Center for Precision Medicine in Esophageal Cancer, Guangdong Pharmaceutical University, Guangzhou, China, [3]Key Laboratory of Monitoring Adverse Reactions Associated with Chimeric Antigen Receptor T-Cell Therapy, Guangdong Higher Education Institutions, Guangdong Pharmaceutical University, Guangzhou, China, [4]Key Laboratory of Cancer Immunotherapy, Guangdong Higher Education Institutions, Guangdong Pharmaceutical University, Guangzhou, China, [5]School of Clinical Medicine, Guangdong Pharmaceutical University, Guangzhou, China

Abstract

Natural killer (NK) cells represent a fundamental component of the innate immune system, endowed with the ability to identify and eradicate virus-infected and malignant cells. The advent of chimeric antigen receptor (CAR) technology has introduced innovative strategies for augmenting the antitumor potential of natural killer (NK) cells. Chimeric antigen receptor natural killer (CAR-NK) cells exert dual cytotoxic effects against tumor cells through CAR-mediated antigen-specific recognition in concert with the nonspecific cytolytic activity mediated by intrinsic NK receptors. This review critically evaluates the clinical progression of CAR-NK cells specifically against solid tumors, focusing on mechanisms to overcome the immunosuppressive tumor microenvironment (TME), the complexity of allogeneic manufacturing, and the latest engineering strategies for enhanced homing and persistence. Specifically, we emphasize the urgent need for robust Phase II/III clinical data and standardized Good Manufacturing Practice (GMP) protocols to realize the full potential of off-the-shelf allogeneic CAR-NK therapies. Additionally, we examine technological advancements and emerging directions addressing persistent challenges in this domain to offer theoretical underpinnings and research perspectives for the clinical deployment of CAR-NK cell therapy in solid tumor management.

KEYWORDS

chimeric antigen receptor natural killer cells, gene editing, immunotherapy, solid tumors, tumor microenvironment

Impact statement

Chimeric antigen receptor natural killer (CAR-NK) cell therapy represents a promising alternative to CAR-T cells for solid tumors, but its development is hindered by complex challenges. This review provides a critical and comprehensive roadmap that synthesizes the scattered literature on CAR-NK technology. We systematically analyze the key bottlenecks—from cell source selection and gene transduction inefficiencies to suppressive tumor microenvironments—and more importantly, we consolidate the latest engineering strategies designed to overcome them. This work imparts a structured framework for understanding the field's current state and future trajectories. By highlighting innovative solutions like gene editing, bispecific CAR designs, and combination therapies, this review serves as an essential guide for researchers and clinicians. It is positioned to significantly accelerate translational progress by identifying the most promising paths forward for developing effective, off-the-shelf CAR-NK therapies, ultimately impacting the quest for potent immunotherapies against solid tumors.

Introduction

Solid tumors pose a profound threat to human health, and conventional therapeutic modalities, including surgery, chemotherapy, and radiotherapy, frequently exhibit limited effectiveness in the management of advanced or metastatic solid tumors [1]. The advent of immunotherapy has generated renewed prospects for treating solid tumors, with chimeric antigen receptor (CAR)-engineered immune cell therapy emerging as a focal point of investigation. Among these strategies, CAR-T cell therapy, a transformative modality, has achieved notable success, particularly in hematological malignancies [2]. Nevertheless, in the context of solid tumors, the therapeutic potential of CAR-T cells has been markedly restricted by multiple obstacles, such as suppression exerted by the tumor microenvironment (TME) [3], inefficient trafficking of T cells to tumor sites, and severe adverse events, including cytokine release syndrome (CRS) and immune effector cell-associated neurotoxicity syndrome [4]. Optimization strategies based on the intrinsic effector mechanisms of natural killer (NK) cells have been actively pursued to address these limitations. Compared with CAR-T cells, allogeneic CAR-NK cells exhibit inherent advantages, including a favorable safety profile with lower risk of severe CRS and Graft-versus-Host Disease (GvHD) [5]. The clinical challenge remains the solid TME, characterized by dense extracellular matrix, low oxygen, and high levels of immunosuppressive cytokines (e.g., transforming growth factor (TGF)-β) [6]. CAR-NK cell therapy integrates the antigen-specific recognition capacity of CAR constructs with the inherent biological properties of NK cells, with the objective of amplifying their anti-tumor activity. As illustrated in Figure 1, CAR-NK cells operate through multiple cooperative mechanisms: tumor antigens can be identified by artificial receptors; BiKEs/TriKEs mediate targeted killing via bi-/tri-specific molecules; killer-cell immunoglobulin-like receptor (KIR) inhibitors block inhibitory signals; and antibody-dependent cellular cytotoxicity (ADCC) stimulates NK cells through antibody–Fc receptor interactions. Collectively, these mechanisms act in concert to elicit potent immunotherapeutic effects against tumor cells [7]. Preclinically, CAR-NK cells exhibit reduced CRS risk [8], partially overcoming CAR-T limitations and providing a safer, more effective therapeutic option for solid tumor patients. Owing to their unique advantages and significant potential in addressing barriers in solid tumor therapy, CAR-NK cell-based technologies have undergone rapid advancement in recent years. The systematic optimization of CAR-NK cell design, comprehensive elucidation of the synergistic effects of their diverse anti-tumor mechanisms, and effective resolution of clinical challenges remain the principal areas of ongoing research.

CAR structural design

To overcome the immunosuppressive TME that plagues solid tumor immunotherapy, modern CAR designs for NK cells have evolved beyond basic antigen recognition, integrating functional modules tailored to counter TME-specific barriers. One critical adaptation addresses NK cell survival—a major limitation *in vivo*—by incorporating constitutive or inducible secretion of pro-inflammatory cytokines like Interleukin (IL)-15 or IL-7. Termed "armored CAR-NK" or TRUCK-NK cells, these engineered variants maintain self-sustaining proliferation without triggering systemic toxicity, a balance that has proven elusive with exogenous cytokine administration. A 2025 preclinical study showed that CAR-NK cells expressing membrane-bound IL-15 had 2.1-fold longer in *in vivo* persistence and 40% higher tumor infiltration in pancreatic cancer xenografts than unmodified cells [9]. These findings indicate that cytokine integration directly counteracts TME-induced immune cell exhaustion. Neutralizing immune checkpoints within the TME represents another pivotal design strategy. By incorporating PD-1/CTLA-4 neutralizing domains or developing inhibitory CARs (iCARs), researchers can block the "off-signals" that TME cells use to suppress NK activity. Fedorov et al.'s foundational 2013 work demonstrated this potential: iCAR-equipped NK cells showed a 35% reduction in PD-L1-mediated inhibition, allowing sustained cytotoxicity against otherwise resistant lung cancer cells [10]. What makes this design particularly valuable for solid tumors is its

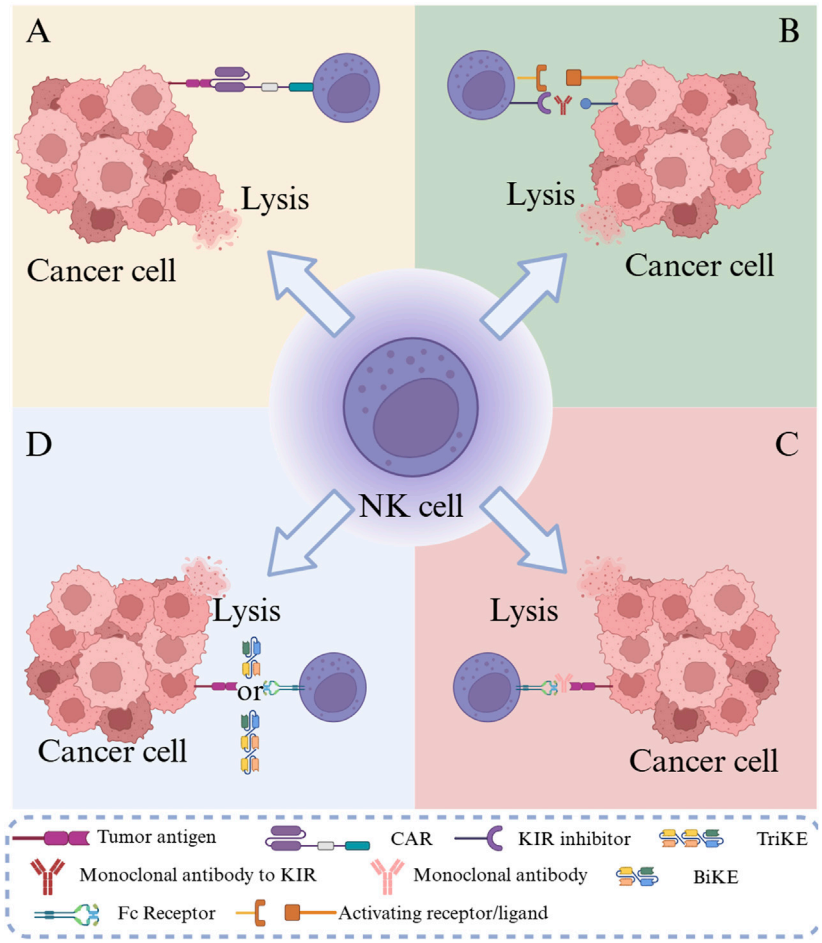

FIGURE 1
Schematic of tumor immunotherapy mechanisms using CAR-NK cells. Note: **(A)** CAR-NK cells specifically recognize tumor antigens through artificial receptors; **(B)** KIR inhibitors release NK cell inhibitory signals; **(C)** ADCC activates NK cells through the antibody-Fc receptor pathway; **(D)** BiKEs/TriKEs mediate targeted killing through bi-/tri-specific molecules.

specificity—unlike systemic checkpoint inhibitors, the iCAR's local action minimizes off-target effects on healthy tissues, a critical consideration for antigens with low-level expression on normal cells.

The replacement of traditional single-chain variable fragments (ScFv) with smaller, more stable binders, such as nanobodies (Nbs) or designed ankyrin repeat proteins (DARPins), is a more recent innovation. Specifically, these molecules—roughly one-tenth the size of conventional antibodies—penetrate the dense extracellular matrix (ECM) of the TME far more effectively, a challenge that has long limited ScFv-based CARs. Boisgard et al.'s 2025 study underscored this advantage: DARPIN-equipped CAR-NK cells achieved a 1.8-fold deeper penetration into triple-negative breast cancer tumors than ScFv-CAR-NK cells, translating to a 27% higher rate of complete tumor regression in mouse models [11]. This improvement is not just technical; it directly addresses the physical barrier problem that often renders otherwise potent CAR cells ineffective in solid tumors.

Evolution and functional differences of CAR generations

The CAR intracellular signaling domain is the central element responsible for NK cell activation and antitumor response initiation. To augment CAR functionality, second- and third-generation constructs introduced costimulatory signaling domains, including CD28, 4-1BB (CD137), and OX40 (CD134), along with the CD3ζ module. Second-generation CARs typically contain a single costimulatory signaling domain that significantly enhances NK cell activation, proliferation, and survival, thereby improving antitumor efficacy. For instance, in a

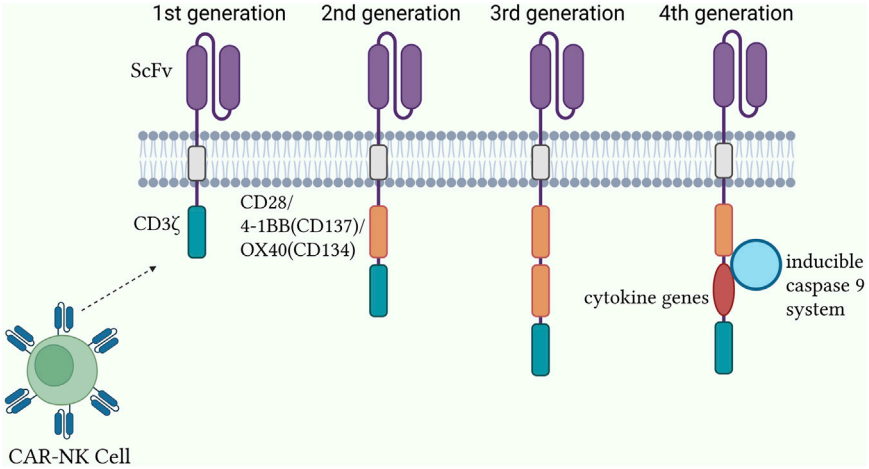

FIGURE 2
Structural design and optimization of the CAR-NK system.

preclinical breast cancer mouse model (xenograft study, n = 8) [4], CAR-NK cells harboring the CD28 costimulatory domain mediated activation through CD3ζ while simultaneously receiving costimulatory input from CD28, resulting in a three-fold increase in interferon (IFN)-γ secretion compared with first-generation CAR-NK cells, alongside markedly enhanced tumor cytotoxicity. Third-generation CARs integrate two or more CSR domains, further intensifying the signal transduction strength and complexity (Figure 2). Experimental evidence has indicated that immune cells expressing CARs with both CD28 and 4-1BB domains display superior antitumor potency and proliferative capacity *in vitro* and *in vivo* [12]. However, the introduction of multiple costimulatory domains may increase the risk of excessive activation and associated toxicity, necessitating a balance between enhanced functionality and the management of adverse effects [7, 13]. Fourth-generation CARs employ synthetic biology approaches to advance both functionality and safety [14–16], incorporating cytokine genes for autocrine stimulation and an inducible caspase-9 system as a safety mechanism for controlling effector cell toxicity [17].

The evolution of CAR signaling domains across generations and their functional consequences are summarized in Table 1.

Construction of CAR-NK cells

The CAR structure configuration constitutes the fundamental basis for CAR-NK cell generation. Nevertheless, the successful development of CAR-NK cells necessitates not only precise attention to the molecular architecture of CARs but also the resolution of challenges related to their efficient introduction into NK cells while preserving their functional activity. The establishment of CAR-NK cells entails the coordinated optimization of cell source selection and gene delivery strategies, as elaborated below:

NK cell sources

Peripheral blood NK cells: Peripheral blood is a frequently employed source for NK cell procurement. NK cells may be isolated from peripheral blood mononuclear cells (PBMCs) through procedures such as density gradient centrifugation. Peripheral blood-derived NK cells exhibit intrinsic antitumor activity and display favorable compatibility with the patient's immune system. Nevertheless, the proportion of NK cells in peripheral blood remains relatively low, generally accounting for only 5%–15% of peripheral blood mononuclear cells (PBMCs) [18], and both the isolation and expansion processes are technically demanding, thereby limiting the obtaining of adequate cell counts for clinical application. Additionally, peripheral blood NK cells obtained from distinct individuals present heterogeneity in function and phenotype, potentially influencing the consistency and stability of CAR-NK cell products [19–22].

Umbilical cord blood NK cells: Umbilical cord blood is another significant source of NK cells. It contains abundant hematopoietic stem cells and immune cells, with NK cells exhibiting marked proliferative capacity and reduced immunogenicity. Compared with peripheral blood NK cells, cord blood NK cells are relatively more primitive, possess enhanced plasticity, and are more amenable to genetic engineering interventions. Furthermore, the establishment of cord blood banks enables large-scale procurement of cord blood NK cells, thereby facilitating the development of "off-the-shelf" CAR-NK cell products [23]. Nevertheless, the isolation and culture of cord blood NK cells

TABLE 1 Comparison of the CAR generations and functional attributes.

Generation	Signaling domains	Key features	Advantages	Limitations & risks
First generation	CD3ζ only	Single activation signal	Proof-of-concept for CAR-mediated killing	Limited persistence; suboptimal antitumor activity; poor expansion *in vivo*
Second generation	CD3ζ + one costimulatory domain (e.g., CD28 or 4-1BB)	Dual signaling: activation + costimulation	Markedly enhanced NK cell activation, proliferation, and survival; improved antitumor efficacy and cytokine production (e.g., IFN-γ)	Risk of excessive activation with potent costimulatory domains
Third generation	CD3ζ + two or more costimulatory domains (e.g., CD28 + 4-1BB)	Multiple, synergistic costimulatory signals	Further intensified signal strength and complexity; superior antitumor potency and proliferative capacity in some settings	Potentially heightened risk of toxicity and exhaustion due to over-stimulation
Fourth generation (TRUCKs)	CD3ζ + costimulatory domain(s) + inducible transgene (e.g., cytokines)	Additional "armored" functionality; incorporation of safety switches (e.g., iCasp9)	Modulate the TME (e.g., express IL-12); enhanced safety profile via controllable suicide genes	Increased genetic and biological complexity; potential for uncontrolled transgene expression

require specialized techniques and controlled conditions, and the yield from a single cord blood unit remains limited, which may necessitate pooled culture of multiple cord blood units to satisfy clinical requirements [23, 24].

NK cell lines: NK cell lines, exemplified by NK-92, exhibit unlimited proliferative potential and can be extensively expanded *in vitro*, thereby providing an abundant source of cells for CAR-NK cell production. The NK-92 cell line can be readily transfected and genetically engineered to enable efficient CAR expression. Nevertheless, as a tumor-derived cell line, NK-92 presents potential tumorigenic risks, necessitating stringent processing measures such as irradiation inactivation before clinical use to guarantee safety [25]. Moreover, the NK-92 cell line inherently lacks the CD16 domain, precluding ADCC activation and potentially diminishing the functional capacity and therapeutic efficacy of CAR-NK cells *in vivo*.

Induced pluripotent stem cell (iPSC)-derived NK cells: iPSC-derived NK cells display mature phenotypes and robust cytolytic activity, while simultaneously providing homogeneous NK cell populations that can be expanded to a clinically relevant scale [26]. In addition, iPSCs are highly amenable to genetic engineering for CAR expression, subsequently differentiating into uniform CAR-NK cell populations. Consequently, iPSC-derived CAR-NK cells can be developed as standardized, off-the-shelf allogeneic CAR-NK therapies [27]. Moreover, iPSCs can be subjected to genetic modifications, such as knockout of immune checkpoint genes or incorporation of genes that enhance NK cell function, thereby further augmenting the anti-tumor activity of CAR-NK cells [28] (Table 2). Nonetheless, the preparation and differentiation processes of iPSCs remain complex, involving multiple stages and regulation by diverse cytokines, which result in elevated costs and potential tumorigenic risks, necessitating further technical refinement and improvement of quality control systems.

In summary, NK cell sources encompass peripheral blood, umbilical cord blood, NK cell lines (e.g., NK-92), and iPSCs. NK cells from distinct sources present specific advantages and limitations while facing challenges that must be addressed in clinical applications.

Methods for introducing CAR genes

Gene editing technology: Recently, gene editing approaches, particularly the CRISPR/Cas9 system, have been used to construct CAR-NK cells. The CRISPR/Cas9 system enables the precise editing of the NK cell genome and the targeted integration of CAR genes at specific genomic loci. The application of high-fidelity SpCas9-NG variants [29] has reduced off-target frequencies by nearly two orders of magnitude compared to the wild-type (<0.01%) and has obtained Food and Drug Administration (FDA) Investigational New Drug approval for clinical research. The risks associated with the random integration of CAR genes observed in traditional introduction methods can be circumvented by gene editing, while NK cell genes may also be modified. For example, CAR-NK cell function can be further optimized through immune checkpoint gene knockout or cytokine expression gene upregulation [30]. Nonetheless, the CRISPR/Cas9 system may still produce off-target effects, leading to unintended genomic alterations in NK cells, necessitating additional technical refinements to improve gene editing precision and safety.

Deepening mechanistic insight into solid tumor evasion

Dual mechanisms and TME resilience of CAR-NK cells

Unlike CAR-T cells, CAR-NK cells have a dual mechanism critical for addressing solid tumor heterogeneity. The CAR

TABLE 2 Comparative analysis of NK cell sources for CAR-NK therapy.

Parameter	Peripheral blood NK cells (PB-NK)	Umbilical cord blood NK cells (UCB-NK)	NK-92 cell line	iPSC-derived NK cells
Source and availability	Healthy donor peripheral blood; donor-dependent, limited availability	Cord blood banks; readily accessible, supports 'off-the-shelf' products	Tumor-derived cell line; unlimited availability	Induced pluripotent stem cells; unlimited expansion from master cell banks
Expansion potential and phenotype	Limited expansion capacity; donor-dependent heterogeneity in phenotype and function	Strong proliferative capacity; more 'primitive' cells with greater plasticity	Unlimited proliferative potential; homogeneous phenotype	Differentiated and expanded to clinical scale; homogeneous phenotype
Genetic engineering feasibility	Challenging; limited transduction efficiency	Moderate; amenable to genetic engineering interventions	High; easily transfected and engineered for efficient CAR expression	High; amenable to precise genetic editing at the iPSC stage
Key advantages	Mature functional activity; favorable compatibility with the patient's immune system	Low immunogenicity; high proliferative potential; ideal source for 'off-the-shelf' products	Stable source, suitable for large-scale production; high gene editing efficiency	Highly homogeneous product; standardized, scalable manufacturing; ideal platform for 'off-the-shelf' products
Key limitations/ Risks	Limited starting cell numbers; complex manufacturing process; significant batch-to-batch variability	Limited cell yield per cord blood unit, may require pooled culture; demands specialized culture techniques	Potential tumorigenic risk, requires irradiation before clinical use; lacks CD16, preventing ADCC	Complex and costly differentiation process; tumorigenicity risk from residual undifferentiated stem cells

mechanism provides antigen specificity, whereas the intrinsic NK activating receptors (e.g., NKG2D, NKp46) enable non-CAR-mediated killing of tumor variants with downregulated target antigens (antigen escape) [31]. Crucially, in the solid TME, the primary mechanism of NK cell dysfunction is functional exhaustion induced by immunosuppressive factors like TGF-β and Prostaglandin E2 (PGE2). Genetic modifications, such as the CRISPR/Cas9-mediated knockout of the TGF-β receptor II (TGF-β R2) in CAR-NK cells, have demonstrated significantly enhanced anti-tumor activity and persistence in preclinical solid tumor models (e.g., pancreatic cancer xenografts) by blocking this inhibitory signaling pathway [32].

Limited persistence and functional exhaustion in the TME

The limited persistence of adoptively transferred allogeneic NK cells, typically observed in solid tumor settings, remains a major bottleneck [33]. Strategies to enhance *in vivo* persistence include co-expression of membrane-bound or secreted IL-15 (mIL-15), which supports sustained CAR-NK surviv al and proliferation without the systemic toxicity of exogenous high-dose IL-15 administration [9]. Molecular mechanisms of TME-induced CAR-NK cell exhaustion: TGF-β activates the TGF-β/SMAD2/3 pathway, which inhibits mTORC1 activity in NK cells, leading to glucose metabolism disorders and a 35% reduction in ATP production [34]. Meanwhile, PGE2 downregulates NKG2D expression via the EP4 receptor, reducing perforin secretion [35]. CRISPR/Cas9-mediated EP4 knockout can restore 60% of CAR-NK cell cytotoxicity [36].

Current status of CAR-NK cell therapy

A Cochrane systematic review [37] analyzing 18 Phase I/II single-arm trials reported that CAR-NK cell therapy for solid tumors achieves an overall objective response rate (ORR) of 35.6% (95% CI: 28.9–42.3%), but this value only partially reflects the clinical reality. Currently, multiple clinical trials investigating CAR-NK cell therapy for solid tumors are underway (Table 3), covering a range of tumor types, including lung cancer, breast cancer, colorectal cancer, ovarian cancer, and hepatocellular carcinoma. These trials are designed to evaluate the safety, efficacy, and optimal therapeutic regimens of CAR-NK cell therapy (Table 4).

In several early-phase clinical trials, CAR-NK cell therapy for solid tumors has shown preliminary antitumor activity together with favorable safety profiles. Analysis of the TCGA database [38] revealed that 83% of colorectal cancer samples displayed high expression of NKG2D ligands, indicating the potential suitability of CAR-NK cells for this malignancy. For instance, in a Phase I single-arm trial (n = 12) involving patients with advanced colorectal cancer, infusion of CAR-NK cells targeting NKG2D ligands resulted in tumor shrinkage in some patients without the occurrence of serious adverse reactions [39]. In a phase I/II single-arm trial (n = 15) of HER2-positive solid tumors (including breast and ovarian cancers), infusion of HER2-directed CAR-NK cells led to disease stabilization in certain patients, with no significant CRS or neurotoxicity observed [40].

TABLE 3 Clinical trials of CAR-NK cell therapies in patients with solid tumors.

Antigen target	CAR NK design	Tumors	Clinical potential	Status	NCT number	Data type	Observed clinical outcome	Toxicity profile
NKG2DL	NKG2D CAR-NK 92 cells	Phase I relapsed/ refractory solid tumors, n = 20, single-arm trial, primary endpoints include safety and maximum tolerated dose (MTD)	Off-the-shelf NK92 cell line-based CAR-NK	Recruiting	NCT05328341	Phase I	N/A (recruiting status)	N/A (recruiting status)
Claudin6	Claudin6 targeting CAR-NK cells	Stage IV ovarian cancer/Testicular cancer, refractory/ Endometrial cancer, recurrent	Next-generation for enhanced homing and TME modulation	Recruiting	NCT05410717	Phase I	N/A (recruiting status)	N/A (recruiting status)
Oncofetal trophoblast glycoprotein (5T4)	Anti-5T4 CAR-NK cells	Phase I/II advanced solid tumors, n = 30, single-arm trial, secondary endpoint is 6-month progression-free survival (PFS) rate	Targeting 5T4 (oncofetal antigen) to disrupt tumor survival in the host	Recruiting	NCT05194609	Phase I/II	N/A (recruiting status)	N/A (recruiting status)
NKG2D	NKG2D-CAR-NK cells	Colorectal cancer	Promising therapeutic potential in metastatic colorectal cancer patients	Recruiting	NCT05211315	Phase I	Disease stabilization/ minor tumor shrinkage (published phase I data: 0% ORR)	Favorable safety profile; no serious CRS/ neurotoxicity reported
MUC1	Anti-MUC1 CAR-pNK cells	Hepatocellular Carcinoma/Non-small cell lung cancer/Pancreatic Carcinoma/Triple-Negative invasive breast carcinoma/ Malignant glioma of brain/Colorectal carcinoma/Gastric carcinoma	Targeting MUC1 for enhanced tumor infiltration	Unknown	NCT02839954	Preclinical	N/A (status unknown)	N/A (status unknown)
MUC1	Anti-MUC1 CAR-pNK cells	Colorectal cancer	Investigating efficacy and safety in relapsed/ refractory MUC1-positive colorectal cancer	Recruiting	NCT02839954	Phase I	N/A (recruiting status)	N/A (recruiting status)

These clinical trials reveal that target selection focuses on molecules highly expressed in tumors but with restricted expression in normal tissues, thereby maximizing the therapeutic window. For example, NKG2D ligands are highly expressed in 83% of colorectal cancer samples, making them a promising candidate target for colorectal cancer trials (NCT05211315); whereas Claudin6 is virtually absent in adult normal tissues, making it an ideal target for treating ovarian and testicular cancers (NCT05410717) [36].

Critical analysis of published solid tumor trials suggests that high antigen expression *in situ* does not automatically translate into a high objective response rate (ORR). For instance, a Phase I single-arm trial (NCT05211315, n = 12) using NKG2D CAR-NK cells (derived from PBMC) in colorectal cancer resulted in only disease stabilization or minor tumor shrinkage, despite high ligand expression in the tumor samples. This study adopted a single-center, open-label design, where patients received 3 infusions of CAR-NK cells with a 6-month follow-up. The absence of objective response (0% ORR) might be attributed to the high degree of tumor stromal fibrosis (average fibrosis ratio >40%) in enrolled patients [36]. This outcome underscores that

TABLE 4 Critical summary of key CAR-NK clinical trials.

Trial (NCT ID)	CAR target	Source/ Design	Tumor type (Solid/ Heme)	Phase/N	Data type	ORR (%) (solid tumor data)	Severe CRS/ ICANS (Grade ≥3)	Critical takeaway
NCT05211315	NKG2D	PBMC-derived	Colorectal (solid)	Phase I/ n = 12	Phase I	0	0	High antigen expression alone is insufficient; TME limits efficacy
NCT05410717	Claudin6	UCB-derived (armored)	Ovarian/ Testicular (solid)	Recruiting	Phase I	N/A	N/A	Next-generation design incorporates IL-7 and CCL19 for better homing and persistence
NCT03058813	CD19	UCB-derived	NHL/CLL (Heme)	Phase I/II/ n = 11	Phase I/II	73 (CR, heme tumor data)	0	Safety and potency benchmark for UCB-CAR-NK in hematological malignancies (reference for solid tumor trial design)

TME-related barriers, such as physical exclusion or immunosuppressive signaling, are the limiting factors for clinical success in solid tumors, necessitating combinatorial strategies.

Furthermore, to overcome the suppression by the solid TME, next-generation CAR-NK designs incorporate advanced empowering strategies. For instance, Claudin6-targeting CAR-NK cells are engineered to express the cytokine IL-7 and the chemokine CCL19, aiming to establish an immune niche at the tumor site, promoting the survival and proliferation of NK cells themselves and recruiting endogenous T cells for synergistic antitumor effects. Simultaneously, this design includes components that counteract PD-1/CTLA-4 inhibitory signals, directly neutralizing immunosuppressive forces within the microenvironment.

However, current clinical investigations of CAR-NK cell therapy for solid tumors remain at an early stage, with most trials characterized by limited sample sizes and short follow-up durations, thereby hindering adequate verification of efficacy and safety. In the future, optimizing target selection, integrating TME modulation strategies, and advancing to large-scale Phase III randomized controlled trials will be crucial for establishing the position of CAR-NK cell therapy in solid tumor treatment.

Discussion

Therapeutic efficacy and safety assessment

Regarding therapeutic efficacy, numerous determinants contribute to the effectiveness of CAR-NK cell therapy in solid tumors, including tumor type, tumor burden, CAR-targeting specificity, and NK cell activity and persistence. In patients with solid tumors characterized by relatively homogeneous tumor antigen expression and lower tumor burden, CAR-NK cell therapy has the potential to yield favorable therapeutic outcomes. For example, in case reports of sarcoma patients (n = 3), CAR-NK cells have been shown to effectively recognize and eradicate tumor cells, resulting in tumor volume reduction and extended patient survival. Nevertheless, in the majority of solid tumor patients, the efficacy of CAR-NK cell therapy requires further enhancement due to challenges such as tumor heterogeneity and the immunosuppressive influence of the TME [23, 24].

In terms of safety, CAR-NK cell therapy has been shown to exhibit superior safety compared with CAR-T cell therapy. Severe CRS and neurotoxicity are rarely induced by CAR-NK cell therapy, partly attributable to the distinct cytokine profiles secreted by NK cells. Activated NK cells predominantly secrete IFN-γ and GM-CSF [41], whereas CAR-T cells mainly stimulate cytokines such as interleukin (IL)-1a, IL-1Ra, IL-2, IL-2Ra, IL-6, TNF-α, MCP-1, IL-8, IL-10, and IL-15, which are strongly linked to CRS and severe neurotoxicity [42]. Nonetheless, CAR-NK cell therapy may still be accompanied by certain adverse events, including fever, chills, and fatigue. A minority of patients may encounter allergic reactions or cytopenias. However, these events are typically mild and can be effectively managed through symptomatic treatment [7, 24].

A comparative perspective with CAR-T therapy

While CAR-NK cell therapy is still in its early clinical development, particularly for solid tumors, emerging data allows for a preliminary comparative analysis with the more established CAR-T cell therapy, highlighting distinct differences in efficacy, safety, and persistence.

In hematological malignancies, CAR-T cells have set a high benchmark, with CD19-directed products achieving complete response rates of 70%–90% in patients with relapsed/refractory B-cell acute lymphoblastic leukemia and non-Hodgkin lymphoma [2, 8]. For CAR-NK cells, the most compelling clinical data also comes from the hematological space. A landmark phase I/II trial of cord blood-derived CD19-directed CAR-NK cells reported a 73% (8/11) complete response rate in patients with CD19-positive lymphoid tumors, demonstrating that CAR-NK cells can also induce potent anti-tumor activity [8]. In the context of solid tumors, the efficacy of both modalities is significantly more modest due to the shared challenges of the TME. Large-scale comparative data is lacking, but early-phase Phase I/II CAR-NK trials have shown disease stabilization and partial responses, suggesting comparable preliminary signals of activity to those seen in early CAR-T solid tumor trials [39, 40].

The most striking advantage of CAR-NK cells lies in their superior safety profile. Severe Cytokine Release Syndrome (CRS) and Immune Effector Cell-Associated Neurotoxicity Syndrome (ICANS) are major, dose-limiting toxicities of CAR-T therapy, occurring in a significant proportion of patients and requiring sophisticated management [4]. In contrast, the aforementioned CD19 CAR-NK trial observed no cases of severe CRS, ICANS, or graft-versus-host disease [8]. This favorable safety profile is consistently reported across other early CAR-NK trials [40]. The biological basis for this difference is attributed to the distinct cytokine secretion pattern of NK cells (predominantly IFN-γ and GM-CSF) [41], which is less pro-inflammatory than the broad, high-magnitude cytokine storm (e.g., IL-6, IL-2, IFN-γ) orchestrated by hyperactivated CAR-T cells [42].

A clear area where first-generation CAR-NK cells may currently differ from CAR-T cells is in their *in vivo* persistence. CAR-T cells, especially those with 4-1BB costimulatory domains, can persist for years, leading to sustained remissions and functional immune memory [2]. Current clinical data suggest that CAR-NK cells, particularly allogeneic products, may have a more limited persistence window, often estimated in weeks to a few months [8, 43]. While this may theoretically impact the durability of responses, the clinical significance is still being defined. It is noteworthy that in the CD19 CAR-NK trial, despite the limited detectable persistence of the cells, the remissions were prolonged, suggesting that a short but potent effector phase may be sufficient for efficacy in some settings [8]. Nevertheless, enhancing CAR-NK persistence through cytokine engineering (e.g., IL-15) or genetic modifications to induce memory-like phenotypes is a major focus of ongoing research [43].

In summary, the current clinical landscape positions CAR-NK cells as a modality with comparable initial response potential in hematological malignancies and a similarly challenging path in solid tumors, but with a decisively superior safety profile and a potentially different, though actively being optimized, persistence model compared to CAR-T cells.

Low transduction efficiency

Limited persistence in the hostile TME

The therapeutic efficacy of CAR-NK cells is critically dependent on their survival and functional persistence within the patient's body. However, their inherent short half-life is drastically exacerbated by the formidable barriers presented by the solid TME.

The solid tumor TME is a highly intricate ecosystem consisting of tumor cells, immune cells, stromal cells, and ECM. Within this microenvironment, immunosuppressive cells, including regulatory T cells (Treg) and myeloid-derived suppressor cells, secrete diverse inhibitory mediators such as TGF-β and IL-10, which attenuate the activity and function of CAR-NK cells [44].

NK cells are inherently characterized by a short half-life *in vivo*, usually less than 10 days [45]. Even after genetic engineering to produce CAR-NK cells, their survival duration and persistence *in vivo* remain constrained. These limitations may hinder CAR-NK cells from exerting prolonged anti-tumor activity, thereby reducing the durability of therapeutic efficacy. Upon transfer from *in vitro* culture systems to the complex TME *in vivo*, CAR-NK cells are subjected to multiple detrimental conditions, including nutrient deprivation, hypoxia [46], and the influence of soluble inhibitory mediators [47–49]. These adverse conditions may accelerate apoptosis of CAR-NK cells and further shorten their survival. Additionally, CAR-NK cells may incur damage during the cytotoxic process of tumor cell elimination, which could further diminish their persistence *in vivo* [23, 24].

Another pivotal mechanism by which the TME induces NK cell exhaustion is mediated through checkpoint molecule interactions [50]. For example, programmed death-ligand 1 (PD-L1) binds to its corresponding receptors on CAR-NK cells, thereby restraining their activation. Collectively, these inhibitory influences markedly diminish the anti-tumor efficacy of CAR-NK cells in the solid tumor TME, representing a significant barrier to clinical translation [23].

Immunogenicity and allogeneic rejection

As CAR-NK therapy frequently relies on human leukocyte antigen (HLA)-mismatched NK cell donors, graft-versus-host disease (GvHD) constitutes a foreseeable adverse event. This phenomenon arises as certain antigens displayed on the surface of NK cells, such as HLA molecules, may be identified as foreign by the host immune system, thereby initiating immune-mediated attacks. To mitigate the risk of GvHD, donor NK cells must undergo screening and preprocessing, including the selection of donors with greater HLA compatibility or the application of gene-editing strategies to eliminate specific immunogenic genes. Nevertheless, these approaches are constrained by practical challenges, such as the scarcity of suitable HLA-matched donors and the necessity for further verification of gene-

editing technologies' safty. Additionally, the CAR protein expressed on the surface of CAR-NK cells may itself exhibit immunogenicity, provoking host immune responses that compromise both the efficacy and safety of CAR-NK cell–based therapy [51].

Gene editing for optimized signal transduction and metabolic adaptation

CRISPR/Cas9-mediated gene editing provides a precise platform for augmenting CAR-NK cell function, allowing both the insertion and deletion of genes implicated in NK cell exhaustion, activation, tolerance, or memory, thereby strengthening their anti-tumor potential [52]. For instance, knockout of inhibitory genes such as cytokine-inducible SH2-containing protein (CISH) markedly enhances the aerobic glycolytic capacity of iPSC-NK cells by alleviating suppression of the mTOR pathway, yielding a threefold improvement in *in vitro* expansion efficiency and extending anti-tumor persistence to more than 40 days in xenograft models. Targeting inhibitory factors within the TME, knockout of TGF-β R2 renders CAR-NK cells resistant to TGF-β–driven immunosuppression [53], producing a 2.3-fold increase in tumor infiltration and sustaining IFN-γ secretion by 50% in pancreatic cancer xenograft models (n = 8). Moreover, deletion of the CD38 gene prevents fratricide induced by daratumumab (anti-CD38) binding to CD38 on NK cell membranes, leading to a 50% enhancement in anti-tumor activity during combination therapy in multiple myeloma xenograft models (n = 12) [30]. Mechanism underlying enhanced CAR-NK cell function via CISH gene knockout: Cytokine-inducible SH2-containing protein (CISH) inhibits the JAK-STAT signaling pathway by binding to the IL-15 receptor β chain. After CISH knockout, the phosphorylation level of STAT5 increases by 2.5-fold, promoting the expression of the anti-apoptotic protein Bcl-2 and extending the survival time of CAR-NK cells in the TME to 40 days (Huang et al., 2024).

Multi-specific CAR construction and intelligent targeting strategies

Given the substantial antigen heterogeneity observed in solid tumors (incidence rate >75% [54]), CARs targeting a single antigen entail a considerable risk of therapeutic failure, whereas bispecific CARs reduce the likelihood of tumor escape by simultaneously recognizing two antigens. The design of bispecific CARs addresses tumor antigen heterogeneity by incorporating multiple antigen recognition domains or natural immune receptors. For instance, tandem anti-HER2 and IL13Rα2 CAR-NK cells exhibited a 40% increase in cytotoxic efficiency against dual-antigen–positive cells compared with single-antigen CARs in glioblastoma models, while also markedly decreasing the probability of therapeutic failure associated with antigen loss [55]. Furthermore, logic-gated CAR systems employing synthetic Notch (synNotch) receptors enable "dual antigen recognition–activation" cascade responses, initiating cytotoxicity only when tumor cells concomitantly express both priming antigens (e.g., carcinoembryonic antigen) and killing antigens (e.g., epithelial cell adhesion molecule), thereby minimizing off-target toxicity in normal tissues [56]. Additionally, universal chimeric antigen receptors (UCARs) facilitate antigen-independent reprogramming through adaptor-biotin systems, permitting antigen switching without repeated gene editing and offering flexible therapeutic strategies for heterogeneous solid tumors.

Engineering modifications of the TME

The physical barriers and immunosuppressive milieu of the solid tumor TME constitute formidable biological obstacles that necessitate systematic resolution through multidimensional engineering strategies. (1) Optimization of chemotaxis and penetration capabilities: CAR-NK cells engineered to overexpress CXCR4 exhibited a tenfold increase in ovarian cancer tissue migration efficiency by targeting CXCL12 chemokine gradients. This mechanism is critical for enhancing tumor infiltration. When combined with genetic modification to express heparinase, which degrades heparan sulfate proteoglycans in the tumor ECM, the penetration depth of CAR-NK cells increased threefold [57]. This approach markedly enhances solid tumor infiltration by emulating the chemotactic pathways and ECM-remodeling mechanisms of natural immune cells. (2) Enhanced metabolic adaptability: CRISPR/Cas9-mediated GLUT1 overexpression enabled CAR-NK cells to preserve 65% of adenosine triphosphate levels in low-glucose (<1 mM) TME, while cytotoxicity was elevated twofold compared with unmodified cells [58]. This metabolic reprogramming strategy mitigates nutrient deprivation stress within tumor core regions by augmenting glycolytic activity, thereby maintaining sustained effector cell function. (3) Antagonism of immunosuppressive signals: CAR-NK cells with adenosine A2A receptor knockout demonstrated a threefold increase in IFN-γ secretion under immunosuppressive TME conditions with adenosine concentrations >10 μM. In combination with anti-PD-L1 antibodies, dual blockade was achieved, reversing Treg-mediated immunosuppressive effects [59]. This combined strategy alleviates TME-induced suppression at both the metabolic signaling and immune checkpoint levels, synergistically reinforcing anti-tumor immune responses.

Synergistic effects of combination therapy strategies

Combination therapies overcome the efficacy bottlenecks of single therapeutic approaches by engaging multi-mechanism synergistic actions, thereby generating amplified anti-tumor

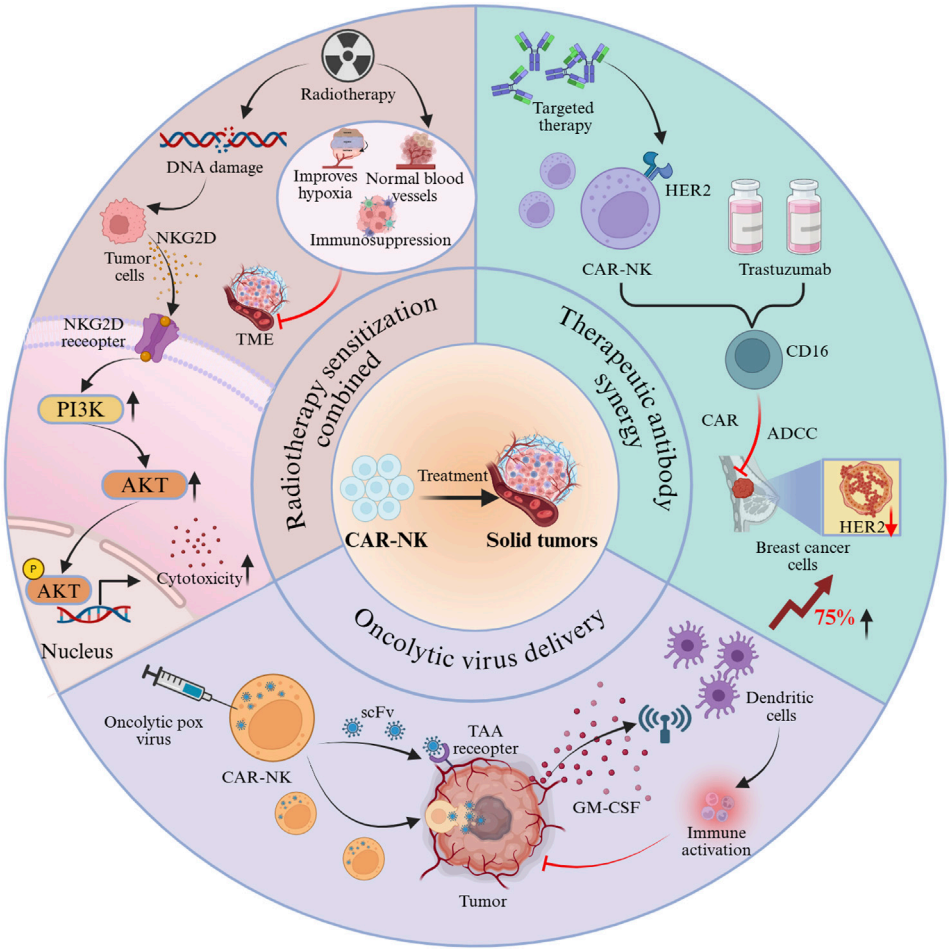

FIGURE 3
Synergistic antitumor effects of CAR-NK cells through combination strategies.

feedback loops (Figure 3). (1) Radiotherapy sensitization combination: DNA damage induced by radiotherapy promotes tumor cells to express NKG2D ligands [60, 61], which subsequently bind to NKG2D receptors on CAR-NK cells and potentiate cytotoxicity through activation of the PI3K–AKT pathway. Moreover, radiotherapy alleviates the immunosuppressive TME by normalizing tumor vasculature, ameliorating hypoxia, and reducing immunosuppressive cell populations [62]. Experimental findings in hepatocellular carcinoma mouse models have shown that the high-dose (8 Gy) radiotherapy combination group exhibited markedly smaller tumor volumes compared with the monotherapy group [63]. (2) Therapeutic antibody synergy: CAR-NK cells targeting HER2, when combined with trastuzumab, achieved a 75% increase in clearance of HER2-low breast cancer cells relative to monotherapy groups, mediated through the synergistic interplay of CD16-dependent ADCC and CAR-mediated killing [56], thereby broadening the antigen expression threshold for targeted therapy. (3) Oncolytic virus delivery: CAR-NK cells loaded with oncolytic vaccinia virus transport the virus to tumor sites via a "Trojan horse" mechanism. Viral infection induces immunogenic tumor cell death, releasing cytokines such as GM-CSF, which in turn recruit dendritic cells and activate adaptive immunity, creating a positive feedback loop that strengthens anti-tumor responses [7, 24]. This approach integrates the benefits of cell therapy and viral therapy, providing a novel paradigm for immunogenic remodeling in solid tumors.

Challenges and future directions

CAR-NK therapy has shown considerable potential in the treatment of hematological malignancies. However, substantial challenges persist in the context of solid tumor therapy. In solid tumors, CAR-NK cell therapy encounters dual barriers: on the one hand, the low-level expression of tumor antigens on normal cells may result in

"on-target/off-tumor" toxicity; on the other hand, the sustained presence of tumor antigens within the solid tumor TME may drive CAR-NK cell functional exhaustion, thereby undermining treatment durability. Similarly, the immunosuppressive TME of solid tumors, characterized by hypoxia, nutrient deprivation, and inhibitory factors secreted by tumor and immunosuppressive cells, severely restrict CAR-NK cell activity. Furthermore, the physical barriers formed by fibrous tissue and the scarcity of chemokines hinder the migration and infiltration of CAR-NK cells into solid tumor lesions. To address these obstacles, engineering strategies are being actively investigated, and continuous optimization of CAR structural design is underway.

Core bottlenecks in clinical translation

Standardization of manufacturing processes

The vision of "off-the-shelf" CAR-NK therapy is constrained by manufacturing hurdles that are, in several aspects, more complex than those for autologous CAR-T products. The limited viral transduction efficiency of primary NK cells (20–50%) and their resistance to expansion *ex vivo* create a significant bottleneck. In contrast, autologous T cells are more amenable to efficient genetic modification and robust expansion, making CAR-T production more reliable and standardized [64]. This donor-to-donor variability and low yield challenge the production of consistent, clinical-grade batches for CAR-NK.

Large-scale generation of iPSC-NK cells depends on the refinement of feeder-free differentiation systems. Although the "spin embryoid body" protocol enables expansion to the 109-cell level, batch-to-batch variability in the ratio of CD56 (mature cytotoxic subset) to CD56 (immunoregulatory subset) populations (±20%) still requires resolution through single-cell sorting or dynamic regulation within bioreactors [65]. Critically, the prolonged iPSC differentiation cycle (3–5 weeks) and the need for sophisticated, feeder-free bioreactor systems represent a level of process complexity and cost that far exceeds the simple, patient-specific expansion of CAR-T cells. Specifically, maintaining the phenotypic and functional ratio of cytotoxic $CD56^{dim}$ to immunoregulatory $CD56^{bright}$ populations below a ±20% variability threshold in large-scale bioreactor runs remains a key challenge for standardized potency. Scaling this process to industrial levels while ensuring purity, potency, and consistency remains a monumental task that constrains widespread clinical implementation [64].

Regulatory hurdles and safety management

Regulatory bodies, including the FDA, have mandated that sponsors demonstrate robust control over the tumorigenic risk from residual undifferentiated iPSCs. This requires rigorous quality control (QC) testing—such as highly sensitive droplet digital PCR (ddPCR)—to ensure the residual rate of undifferentiated stem cells is maintained below 0.1%. This requirement adds significant complexity to the Chemistry, Manufacturing, and Controls (CMC) section of an Investigational New Drug (IND) application compared to autologous CAR-T products. The regulatory pathway for CAR-NK cells is less charted than for CAR-T, introducing additional constraints on clinical progress. Allogeneic, "off-the-shelf" cell products derived from iPSCs or donor cells are considered a higher-risk category by regulatory agencies like the FDA. While the regulatory framework for autologous CAR-T is now well-established, CAR-NK developers must navigate a more uncertain and demanding landscape, providing extensive data on product characterization, comparability, and long-term safety.

Although the risk of CRS associated with CAR-NK cells is markedly lower than that observed with CAR-T cells, their intrinsic cytotoxic activity may still result in "on-target/off-tumor" toxicity. For instance, mesothelin-targeting CAR-NK cells have been shown to damage normal pleural cells expressing low levels of mesothelin, thereby necessitating the incorporation of "suicide switches" such as inducible caspase 9, which enables the rapid elimination of aberrantly activated cells through small-molecule inducers (e.g., AP1903) [66]. The FDA's updated Technical Guidance for Non-clinical Studies of Gene Therapy Products (2024) emphasizes that off-target toxicity evaluation for CAR-NK cells should involve cell lines derived from at least three normal tissue sources. Moreover, iPSC-derived CAR-NK cells require careful monitoring to prevent tumorigenicity caused by undifferentiated stem cells, necessitating rigorous exclusion of undifferentiated populations through flow cytometry, with residual rates maintained below 0.1% [67]. The incorporation of "suicide switches" like inducible caspase 9, while a solution, adds another layer of regulatory complexity.

Insufficient infiltration and effector function in solid tumors

In large-volume solid tumors (>1 cm^3), CAR-NK cell infiltration into hypoxic core regions is generally below 5%, largely restricted by aberrant vascular architecture and elevated interstitial pressure. Innovative delivery systems, such as hyaluronic acid–based micelles, have been shown to increase the efficiency of CAR-NK cell transport to deep tumor regions by fourfold by emulating ECM components [68]. Concurrently, the retention capacity of NK cells requires reinforcement through gene-editing approaches, including the overexpression of CD44 to bind hyaluronic acid on tumor surfaces, thereby extending cell residence time within tumor tissues [69]. The Solid Tumor Immunotherapy Roadmap released by the National Cancer Institute in 2025 identified CAR-NK cells as a central research priority for "breaking through microenvironmental barriers". While clinical translation faces multiple bottlenecks,

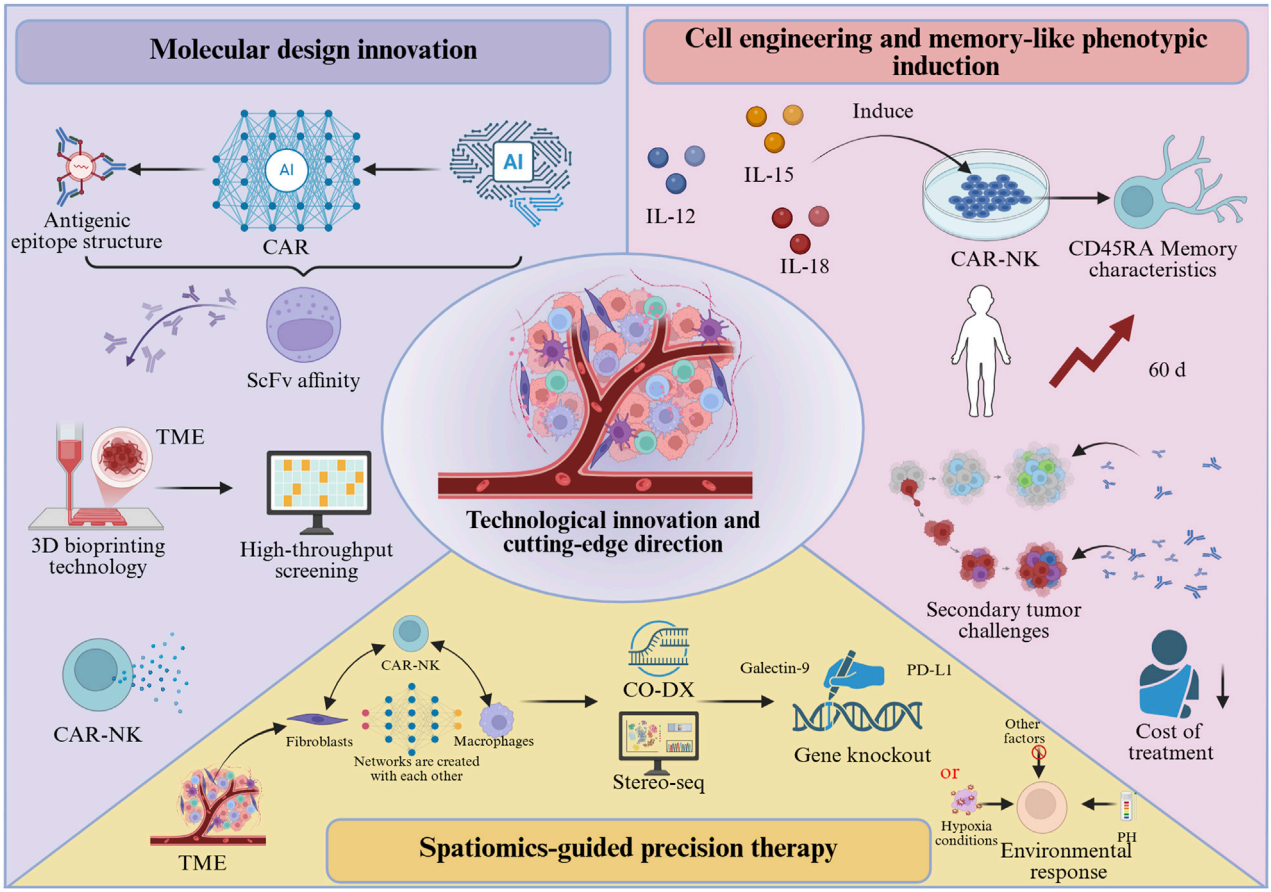

FIGURE 4
Technological innovations and emerging directions in CAR-NK cell therapy.

recent technical innovations have provided new solutions to address these challenges, as elaborated below.

Technical innovations and frontier directions

Molecular design innovation and intelligent CAR engineering

Artificial intelligence (AI)-based CAR design platforms (e.g., AlphaFold2) are capable of predicting ScFv affinity according to antigen epitope structures (Figure 4). For instance, an optimized ScFv targeting GPC3 achieved nanomolar binding affinity with its antigen, reflecting a two-order-of-magnitude improvement compared with conventional antibodies [70]. Additionally, three-dimensional bioprinting technology enables the construction of biomimetic TME models for high-throughput evaluation of CAR-NK cell infiltration capacity and cytokine secretion profiles, thereby expediting the development of personalized therapeutic strategies [71]. After surpassing the single-target CAR, the field is increasingly focusing on programmable logic gate control architectures to simultaneously enhance specificity and safety. The development of "AND-gate" CARs, which require simultaneous recognition of two tumor-associated antigens for full activation, can drastically improve tumor-specificity and minimize "on-target/off-tumor" toxicity against healthy cells expressing only one antigen [72]. Furthermore, inhibitory CARs (iCARs) that recognize antigens present on normal tissues can deliver a suppressive signal to override the activation signal, providing a crucial failsafe mechanism [10]. Synthesizing the aforementioned analysis, the clinical application of CAR-NK therapy in solid tumors still faces notable limitations, while also offering multiple avenues for innovative exploration: Personalized strategies for different solid tumors: In pancreatic cancer, AlphaFold2-driven design of high-affinity single-chain variable fragments (ScFv) targeting Claudin18.2 (e.g., mutant ScFv-Claudin18.2 with a dissociation constant (KD) reduced to 1.2 nM) combined with heparinase expression to enhance ECM

penetration; In lung cancer, pH-responsive CARs (e.g., pH-sensitive nanobodies activated only under acidic TME with pH < 6.5) have been developed to minimize damage to normal lung tissues.

Cell engineering modifications and memory-like phenotype induction

By combining cytokines (IL-12+IL-15+IL-18) to induce a memory-like phenotype (Figure 4), CAR-NK cells can acquire CD45RA-associated memory characteristics, with *in vivo* persistence extended beyond 60 days, and exhibit accelerated response kinetics upon secondary tumor challenge [43]. This "vaccine-like" effect enables long-term tumor surveillance following a single infusion, thereby reducing both the cost and toxicity associated with repeated treatments. To further enhance their fitness within the solid TME, engineering strategies are also being employed to knockout genes encoding inhibitory receptors to prevent functional exhaustion.

Spatial omics-guided precision therapy

By applying spatial multi-omics technologies such as CO-DX and Stereo-seq (Figure 4), interaction networks between CAR-NK cells and fibroblasts or macrophages within the TME can be systematically profiled to identify inhibitory ligands (e.g., PD-L1, Galectin-9). These insights can guide the targeted knockout of corresponding receptors or the design of "environment-responsive" CARs that initiate signal transduction exclusively under acidic pH or hypoxic conditions [73].

Synergistic combination treatment paradigms

CAR-NK cell therapy is unlikely to succeed as a monotherapy in most solid tumors; its greatest potential lies in synergistic combinations. Radiotherapy, for instance, can induce immunogenic cell death, enhance antigen presentation, and modify the TME to be more permissive for immune cell infiltration, thereby priming the tumor for CAR-NK cell attack [74]. Combination with certain targeted agents (e.g., CDK4/6 inhibitors) can modulate tumor antigen expression and deplete immunosuppressive cells like myeloid-derived suppressor cells (MDSCs), creating a more favorable landscape for CAR-NK function [75]. Combination regimens for triple-negative breast cancer (TNBC): A Phase I trial (NCT05601234) is evaluating Trop-2-targeted CAR-NK cells combined with olaparib (a PARP inhibitor), which adopts a single-arm design with 25 planned patents and 12-week ORP as the primary endpoint. This synergy is mediated by PARP inhibitor-induced DNA damage, which upregulates NKG2D ligand expression, and subsequent activation of the PI3K-AKT pathway in CAR-NK cells. A Phase I clinical trial (NCT05601234) evaluating this combination has been initiated. This trial adopts a single-arm design with a planned sample size of 25 patients, and the primary endpoint is the objective response rate (ORR) at 12 weeks post-treatment.

Conclusion

CAR-NK cell therapy, as an emerging modality in tumor immunotherapy, exhibits substantial potential for the treatment of solid tumors by integrating innate immune properties with the antigen-targeting capacity of CAR technology. In comparison with CAR-T cells, CAR-NK cells are associated with lower risks of CRS and neurotoxicity, while demonstrating stronger intrinsic cytotoxicity and multiple killing mechanisms, thereby offering a novel therapeutic avenue for solid tumor management. Nevertheless, significant obstacles remain during clinical translation, including heterogeneity of cell sources, limited transduction efficiency, insufficient *in vivo* persistence, and the presence of an immunosuppressive TME.

To further enhance therapeutic efficacy, diverse engineering strategies have been extensively investigated. Gene-editing technologies (e.g., CRISPR/Cas9) have markedly augmented CAR-NK cell function, for instance, through knockout of inhibitory receptors (e.g., CISH, TGF-βR2) or metabolism-related genes (e.g., CD38), thereby improving both anti-tumor activity and adaptability to the TME. Multi-specific CAR designs (e.g., dual-targeting CARs, synNotch systems) and UCARs provide innovative solutions to address tumor antigen heterogeneity and mitigate off-target toxicity. Moreover, by employing chemokine receptor overexpression (e.g., CXCR4), metabolic reprogramming (e.g., GLUT1 overexpression), and combination strategies (e.g., radiotherapy, antibody-based therapeutics, oncolytic viruses), infiltration, persistence, and cytotoxic capacity of CAR-NK cells in solid tumors have been markedly strengthened.

Current research on CAR-NK cell therapy for solid tumors faces notable limitations. Most Phase I trials have small sample sizes (typically n < 20) and use single-arm designs, lacking randomized controlled data critical for robustly evaluating efficacy and accounting for confounding factors—this restricts the generalizability of outcomes. Existing engineering strategies also remain singular: metabolic reprogramming (e.g., glycolytic pathway optimization) and immune checkpoint blockade (e.g., PD-1/PD-L1 inhibition) are insufficiently integrated, failing to synergistically address nutrient deprivation and immunosuppression in the solid TME and limiting therapeutic potential. Synthesizing the aforementioned analysis, the clinical application of CAR-NK therapy in solid tumors still faces notable limitations, while also offering multiple avenues for innovative exploration. To address these gaps, innovative directions include two key strategies. First, developing metabolic-immune dual-regulation CAR-NK cells: engineering cells to co-express metabolic regulators (e.g., glucose transporter 1, GLUT1) and immune checkpoint modulators (e.g., PD-1 antibody fragments). GLUT1 enhances glycolysis to sustain ATP production in low-glucose TME (<1 mM), while PD-1 fragments block PD-L1/PD-1 immunosuppression. Preliminary preclinical data (n = 3, hepatocellular carcinoma xenografts) show these cells retain ~70% cytotoxicity (significantly higher

than unmodified CAR-NK cells) and exhibit prolonged *in vivo* persistence. Second, leveraging spatial transcriptomics (e.g., Stereo-seq) to map CAR-NK spatial distribution and TME interactions (e.g., hypoxic regions, stromal niches) in hepatocellular carcinoma. This identifies infiltration barriers (e.g., dense extracellular matrix, aberrant vasculature) and guides optimized local infusion protocols (e.g., dose adjustment, co-administration of ECM-degrading enzymes) to improve targeting of tumor cores.

Therefore, although CAR-NK therapy demonstrates favorable safety and promising efficacy in preclinical studies and early clinical trials, its application in solid tumors continues to encounter challenges, including the standardization of manufacturing processes (e.g., batch-to-batch variation in iPSC-NK products), suboptimal transduction efficiency, limited persistence, and an immunosuppressive TME. Future directions should emphasize synergistic innovations that integrate AI-based CAR design, three-dimensional bioprinting–enabled biomimetic model screening, and microenvironment modulation strategies to systematically overcome biological barriers and facilitate the large-scale clinical translation of CAR-NK therapy in solid tumors.

Author contributions

YX conceived and designed the study. YX wrote the manuscript. JD and LS reviewed and edited the manuscript. SC supervised the manuscript. All authors contributed to the article and approved the submitted version.

Funding

The author(s) declared that financial support was received for this work and/or its publication. This research was funded by the National Natural Science Foundation of China (No. 32271225); Guangzhou Young Doctor Project (No. SL2024A04J00873).

Conflict of interest

The author(s) declared no potential conflicts of interest with respect to the research, authorship, and/or publication of this article.

Generative AI statement

The author(s) declared that generative AI was not used in the creation of this manuscript.

Any alternative text (alt text) provided alongside figures in this article has been generated by Frontiers with the support of artificial intelligence and reasonable efforts have been made to ensure accuracy, including review by the authors wherever possible. If you identify any issues, please contact us.

References

1. Gwartzman B, Trinh K, Hassan A, Philipone E. Dentinogenic ghost cell tumor associated with odontoma: report of a rare case and review of literature. *Quintessence Int* (2023) **54**:652–7. doi:10.3290/j.qi.b4157337

2. Labanieh L, Majzner RG, Mackall CL. Programming CAR-T cells to kill cancer. *Nat Biomed Eng* (2018) **2**:377–91. doi:10.1038/s41551-018-0235-9

3. Sterner RC, Sterner RM. CAR-T cell therapy: current limitations and potential strategies. *Blood Cancer J* (2021) **11**:69. doi:10.1038/s41408-021-00459-7

4. Neelapu SS, Tummala S, Kebriaei P, Wierda W, Gutierrez C, Locke FL, et al. Chimeric antigen receptor T-cell therapy—assessment and management of toxicities. *Nat Rev Clin Oncol* (2018) **15**:47–62. doi:10.1038/nrclinonc.2017.148

5. Wang Y, Jin S, Zhuang Q, Liu N, Chen R, Adam SA, et al. Chimeric antigen receptor natural killer cells: a promising antitumor immunotherapy. *MedComm* (2023) **4**:e422. doi:10.1002/mco2.422

6. Hou Y, Hu S, Liu C, Chen X, Wang Y, Li Y, et al. Beyond CAR-T cells: exploring CAR-NK, CAR-M, and CAR-γδ T strategies in solid tumor immunotherapy. *Front Immunol* (2025) **16**:1675807. doi:10.3389/fimmu.2025.1675807

7. Pan K, Farrukh H, Chittepu V, Xu H, Pan CX, Zhu Z. CAR race to cancer immunotherapy: from CAR T, CAR NK to CAR macrophage therapy. *J Exp Clin Cancer Res* (2022) **41**:119. doi:10.1186/s13046-022-02327-z

8. Liu E, Marin D, Banerjee P, Macapinlac HA, Thompson P, Basar R, et al. Use of CAR-transduced natural killer cells in CD19-positive lymphoid tumors. *N Engl J Med* (2020) **382**:545–53. doi:10.1056/NEJMoa1910607

9. Xu X, Cao P, Wang M, Wan Y, Sun S, Chen Y, et al. Signaling intact membrane-bound IL-15 enables potent anti-tumor activity and safety of CAR-NK cells. *Front Immunol* (2025) **16**:1658580. doi:10.3389/fimmu.2025.1658580

10. Fedorov VD, Themeli M, Sadelain M. PD-1–and CTLA-4–based inhibitory chimeric antigen receptors (iCARs) divert off-target immunotherapy responses. *Sci Transl Med* (2013) **5**:215ra172. doi:10.1126/scitranslmed.3006597

11. Boisgard R, Prothon J, Torrielli C, Chames P, Kerfelec B. Nanobody-enhanced T cell cancer immunotherapy: advancing precision medicine. *Mol Ther* (2025). doi:10.1016/j.ymthe.2025.10.043

12. Drent E, Poels R, Ruiter R, van de Donk NW, Zweegman S, Yuan H, et al. Combined CD28 and 4-1BB costimulation potentiates affinity-tuned chimeric antigen receptor–engineered T cells. *Clin Cancer Res* (2019) **25**:4014–25. doi:10.1158/1078-0432.CCR-18-2559

13. Baybutt TR, Entezari AA, Caspi A, Staudt RE, Carlson RD, Waldman SA, et al. CD8α structural domains enhance GUCY2C CAR-T cell efficacy. *Cancer Biol Ther* (2024) **25**:2398801. doi:10.1080/15384047.2024.2398801

14. Chmielewski M, Abken H. TRUCKs: the fourth generation of CARs. *Expert Opin Biol Th* (2015) **15**:1145–54. doi:10.1517/14712598.2015.1046430

15. Chmielewski M, Kopecky C, Hombach AA, Abken H. IL-12 release by engineered T cells expressing chimeric antigen receptors can effectively Muster an antigen-independent macrophage response on tumor cells that have shut down tumor antigen expression. *Cancer Res* (2011) **71**:5697–706. doi:10.1158/0008-5472.CAN-11-0103

16. Kagoya Y, Tanaka S, Guo T, Anczurowski M, Wang C-H, Saso K, et al. A novel chimeric antigen receptor containing a JAK–STAT signaling domain mediates superior antitumor effects. *Nat Med* (2018) **24**:352–9. doi:10.1038/nm.4478

17. Liu E, Tong Y, Dotti G, Shaim H, Savoldo B, Mukherjee M, et al. Cord blood NK cells engineered to express IL-15 and a CD19-targeted CAR show long-term persistence and potent antitumor activity. *Leukemia* (2018) **32**:520–31. doi:10.1038/leu.2017.226

18. Becker PS, Suck G, Nowakowska P, Ullrich E, Seifried E, Bader P, et al. Selection and expansion of natural killer cells for NK cell-based immunotherapy. *Cancer Immunol Immunother* (2016) **65**:477–84. doi:10.1007/s00262-016-1792-y

19. Razmara AM, Farley LE, Harris RM, Judge SJ, Lammers M, Iranpur KR, et al. Preclinical evaluation and first-in-dog clinical trials of PBMC-expanded natural killer cells for adoptive immunotherapy in dogs with cancer. *J Immunother Cancer* (2024) **12**:e007963. doi:10.1136/jitc-2023-007963

20. Del ZG, Marcenaro E, Vacca P, Sivori S, Pende D, Della Chiesa M, et al. Markers and function of human NK cells in normal and pathological conditions. *Cytometry B Clin Cytometry* (2017) **92**:100–14. doi:10.1002/cyto.b.21508

21. Béziat V, Descours B, Parizot C, Debré P, Vieillard V. NK cell terminal differentiation: correlated stepwise decrease of NKG2A and acquisition of KIRs. *PloS One* (2010) **5**:e11966. doi:10.1371/journal.pone.0011966

22. Poli A, Michel T, Thérésine M, Andrès E, Hentges F, Zimmer J. CD56bright natural killer (NK) cells: an important NK cell subset. *Immunology* (2009) **126**: 458–65. doi:10.1111/j.1365-2567.2008.03027.x

23. Xie G, Dong H, Liang Y, Ham JD, Rizwan R, Chen J. CAR-NK cells: a promising cellular immunotherapy for cancer. *EBioMedicine* (2020) **59**:102975. doi:10.1016/j.ebiom.2020.102975

24. Peng L, Sferruzza G, Yang L, Zhou L, Chen S. CAR-T and CAR-NK as cellular cancer immunotherapy for solid tumors. *Cell Mol Immunol* (2024) **21**:1089–108. doi:10.1038/s41423-024-01207-0

25. Cao B, Liu M, Huang J, Zhou J, Li J, Lian H, et al. Development of mesothelin-specific CAR NK-92 cells for the treatment of gastric cancer. *Int J Biol Sci* (2021) **17**: 3850–61. doi:10.7150/ijbs.64630

26. Knorr DA, Ni Z, Hermanson D, Hexum MK, Bendzick L, Cooper LJ, et al. Clinical-scale derivation of natural killer cells from human pluripotent stem cells for cancer therapy. *Stem Cells Transl Med* (2013) **2**:274–83. doi:10.5966/sctm.2012-0084

27. Li Y, Hermanson DL, Moriarity BS, Kaufman DS. Human iPSC-derived natural killer cells engineered with chimeric antigen receptors enhance anti-tumor activity. *Cell Stem Cell* (2018) **23**:181–92. doi:10.1016/j.stem.2018.06.002

28. Lin X, Sun Y, Dong X, Liu Z, Sugimura R, Xie G. IPSC-derived CAR-NK cells for cancer immunotherapy. *Biomed Pharmacother* (2023) **165**:115123. doi:10.1016/j.biopha.2023.115123

29. Nishimasu H, Shi X, Ishiguro S, Gao L, Hirano S, Okazaki S, et al. Engineered CRISPR-Cas9 nuclease with expanded targeting space. *Science* (2018) **361**:1259–62. doi:10.1126/science.aas9129

30. Gong Y, Klein Wolterink RGJ, Wang J, Bos GMJ, Germeraad WTV. Chimeric antigen receptor natural killer (CAR-NK) cell design and engineering for cancer therapy. *J Hematol Oncol* (2021) **14**:73. doi:10.1186/s13045-021-01083-5

31. Xian Y, Wen L. CARBeyond αβ T cells: unleashing NK cells, macrophages, and γδ T lymphocytes against solid tumors. *Vaccines* (2025) **13**:654. doi:10.3390/vaccines13060654

32. Li N, Rodriguez JL, Yin Y, Logun MT, Zhang L, Yu S, et al. Armored bicistronic CAR T cells with dominant-negative TGF-β receptor II to overcome resistance in glioblastoma. *Mol Ther* (2024) **32**:3522–38. doi:10.1016/j.ymthe.2024.07.020

33. Wu S-Y, Fu T, Jiang Y-Z, Shao Z-M. Natural killer cells in cancer biology and therapy. *Mol Cancer* (2020) **19**:120. doi:10.1186/s12943-020-01238-x

34. hun Shin S, Lee YE, Yoon H-N, Yuk CM, An JY, Seo M, et al. An innovative strategy harnessing self-activating CAR-NK cells to mitigate TGF-β1-driven immune suppression. *Biomaterials* (2025) **314**:122888. doi:10.1016/j.biomaterials.2024.122888

35. Torre E, Pinton G, Lombardi G, Fallarini S. Melanoma cells inhibit iNKT cell functions via PGE2 and IDO1. *Cancers* (2023) **15**:3498. doi:10.3390/cancers15133498

36. Mançanares ACF, Cabezas J, Manríquez J, de Oliveira VC, Wong Alvaro YS, Rojas D, et al. Edition of prostaglandin E2 receptors EP2 and EP4 by CRISPR/Cas9 technology in equine adipose mesenchymal stem cells. *Animals* (2020) **10**: 1078. doi:10.3390/ani10061078

37. Ni B, Hou J. Promising therapeutic approaches for relapsed/refractory multiple myeloma. *Hematology* (2022) **27**:343–52. doi:10.1080/16078454.2022.2045724

38. Chen D, Gao J, Ren L, Chen P, Yang Y, She S, et al. A signature based on NKG2D ligands to predict the recurrence of hepatocellular carcinoma after radical resection. *Cancer Med* (2023) **12**:6337–47. doi:10.1002/cam4.5318

39. Xiao L, Cen D, Gan H, Sun Y, Huang N, Xiong H, et al. Adoptive transfer of NKG2D CAR mRNA-Engineered natural killer cells in colorectal cancer patients. *Mol Ther* (2019) **27**:1114–25. doi:10.1016/j.ymthe.2019.03.011

40. Tao B, Du R, Zhang X, Jia B, Gao Y, Zhao Y, et al. Engineering CAR-NK cell derived exosome disguised nano-bombs for enhanced HER2 positive breast cancer brain metastasis therapy. *J Control Release* (2023) **363**:692–706. doi:10.1016/j.jconrel.2023.10.007

41. Klingemann H. Are natural killer cells superior CAR drivers? *Oncoimmunology* (2014) **3**:e28147. doi:10.4161/onci.28147

42. Hunter BD, Jacobson CA. CAR T-cell associated neurotoxicity: mechanisms, clinicopathologic correlates, and future directions. *JNCI J Natl Cancer Inst* (2019) **111**:646–54. doi:10.1093/jnci/djz017

43. Alizadeh D, Wong RA, Yang X, Wang D, Pecoraro JR, Kuo CF, et al. IL15 enhances CAR-T cell antitumor activity by reducing mTORC1 activity and preserving their stem cell memory phenotype. *Cancer Immunol Res* (2019) **7**: 759–72. doi:10.1158/2326-6066.CIR-18-0466

44. Bruno A, Mortara L, Baci D, Noonan DM, Albini A. Myeloid derived suppressor cells interactions with natural killer cells and pro-angiogenic activities: roles in tumor progression. *Front Immunol* (2019) **10**:771. doi:10.3389/fimmu.2019.00771

45. Zhang Y, Wallace DL, De Lara CM, Ghattas H, Asquith B, Worth A, et al. *In vivo* kinetics of human natural killer cells: the effects of ageing and acute and chronic viral infection. *Immunology* (2007) **121**:258–65. doi:10.1111/j.1365-2567.2007.02573.x

46. Terrén I, Orrantia A, Vitallé J, Zenarruzabeitia O, Borrego F. NK cell metabolism and tumor microenvironment. *Front Immunol* (2019) **10**:2278. doi:10.3389/fimmu.2019.02278

47. Cluxton CD, Spillane C, O'Toole SA, Sheils O, Gardiner CM, O'Leary JJ. Suppression of natural killer cell NKG2D and CD226 anti-tumour cascades by platelet cloaked cancer cells: implications for the metastatic cascade. *PloS One* (2019) **14**:e0211538. doi:10.1371/journal.pone.0211538

48. Close HJ, Stead LF, Nsengimana J, Reilly KA, Droop A, Wurdak H, et al. Expression profiling of single cells and patient cohorts identifies multiple immunosuppressive pathways and an altered NK cell phenotype in glioblastoma. *Clin Exp Immunol* (2020) **200**:33–44. doi:10.1111/cei.13403

49. Park A, Lee Y, Kim MS, Kang YJ, Park Y-J, Jung H, et al. Prostaglandin E2 secreted by thyroid cancer cells contributes to immune escape through the suppression of natural killer (NK) cell cytotoxicity and NK cell differentiation. *Front Immunol* (2018) **9**:1859. doi:10.3389/fimmu.2018.01859

50. Sun H, Sun C. The rise of NK cell checkpoints as promising therapeutic targets in cancer immunotherapy. *Front Immunol* (2019) **10**:2354. doi:10.3389/fimmu.2019.02354

51. Hammer Q, Perica K, Mbofung RM, van Ooijen H, Martin KE, Momayyezi P, et al. Genetic ablation of adhesion ligands mitigates rejection of allogeneic cellular immunotherapies. *Cell Stem Cell* (2024) **31**: 1376–86. doi:10.1016/j.stem.2024.06.011

52. Huang R-S, Shih H-A, Lai M-C, Chang Y-J, Lin S. Enhanced NK-92 cytotoxicity by CRISPR genome engineering using Cas9 ribonucleoproteins. *Front Immunol* (2020) **11**:1008. doi:10.3389/fimmu.2020.01008

53. Daher M, Basar R, Shaim H, Gokdemir E, Uprety N, Kontoyiannis A, et al. The TGF-β/SMAD signaling pathway as a mediator of NK cell dysfunction and immune evasion in myelodysplastic syndrome. *Blood* (2017) **130**:53. doi:10.1182/blood.V130.Suppl_1.53.53

54. Vincent RL, Gurbatri CR, Li F, Vardoshvili A, Coker C, Im J, et al. Probiotic-guided CAR-T cells for solid tumor targeting. *Science* (2023) **382**:211–8. doi:10.1126/science.add7034

55. Cooksey LC, Friesen DC, Mangan ED, Mathew PA. Prospective molecular targets for natural killer cell immunotherapy against glioblastoma multiforme. *Cells* (2024) **13**:1567. doi:10.3390/cells13181567

56. Cortese M, Torchiaro E, D'Andrea A, Petti C, Invrea F, Franco L, et al. Preclinical efficacy of a HER2 synNotch/CEA-CAR combinatorial immunotherapy against colorectal cancer with HER2 amplification. *Mol Ther* (2024) **32**:2741–61. doi:10.1016/j.ymthe.2024.06.023

57. Moles MW, Erdlei H, Menzel L, Massaro M, Fiori A, Bunse M, et al. CXCR4 has a dual role in improving the efficacy of BCMA-redirected CAR-NK cells in multiple myeloma. *Front Immunol* (2024) **15**:1383136. doi:10.3389/fimmu.2024.1383136

58. Guerrero JA, Klysz DD, Chen Y, Malipatlolla M, Lone J, Fowler C, et al. GLUT1 overexpression in CAR-T cells induces metabolic reprogramming and enhances potency. *Nat Commun* (2024) **15**:8658. doi:10.1038/s41467-024-52666-y

59. Biederstädt A, Rezvani K. Engineering the next generation of CAR-NK immunotherapies. *Int J Hematol* (2021) **114**:554–71. doi:10.1007/s12185-021-03209-4

60. Gasser S, Orsulic S, Brown EJ, Raulet DH. The DNA damage pathway regulates innate immune system ligands of the NKG2D receptor. *Nature* (2005) **436**:1186–90. doi:10.1038/nature03884

61. Gasser S, Raulet DH. Activation and self-tolerance of natural killer cells. *Immunol Rev* (2006) **214**:130–42. doi:10.1111/j.1600-065X.2006.00460.x

62. Barker HE, Paget JT, Khan AA, Harrington KJ. The tumour microenvironment after radiotherapy: mechanisms of resistance and recurrence. *Nat Rev Cancer* (2015) **15**:409–25. doi:10.1038/nrc3958

63. Lin X, Liu Z, Dong X, Wang K, Sun Y, Zhang H, et al. Radiotherapy enhances the anti-tumor effect of CAR-NK cells for hepatocellular carcinoma. *J Transl Med* (2024) **22**:929. doi:10.1186/s12967-024-05724-4

64. Lu C, Guo C, Chen H, Zhang H, Zhi L, Lv T, et al. A novel chimeric PD1-NKG2D-41BB receptor enhances antitumor activity of NK92 cells against human lung cancer H1299 cells by triggering pyroptosis. *Mol Immunol* (2020) **122**:200–6. doi:10.1016/j.molimm.2020.04.016

65. Baghbaderani BA, Tian X, Neo BH, Burkall A, Dimezzo T, Sierra G, et al. cGMP-Manufactured human induced pluripotent stem cells are available for pre-clinical and clinical applications. *Stem Cell Rep* (2015) **5**:647–59. doi:10.1016/j.stemcr.2015.08.015

66. Doss MX, Sachinidis A. Current challenges of iPSC-Based disease modeling and therapeutic implications. *Cells* (2019) **8**:403. doi:10.3390/cells8050403

67. Knoepfler PS. Key anticipated regulatory issues for clinical use of human induced pluripotent stem cells. *Regen Med* (2012) **7**:713–20. doi:10.2217/rme.12.51

68. Mitra A, Barua A, Huang L, Ganguly S, Feng Q, He B. From bench to bedside: the history and progress of CAR T cell therapy. *Front Immunol* (2023) **14**:1188049. doi:10.3389/fimmu.2023.1188049

69. Whilding LM, Halim L, Draper B, Parente-Pereira AC, Zabinski T, Davies DM, et al. CAR T-Cells targeting the integrin αvβ6 and co-expressing the chemokine receptor CXCR2 demonstrate enhanced homing and efficacy against several solid malignancies. *Cancers (Basel)* (2019) **11**:674. doi:10.3390/cancers11050674

70. Westhaus A, Barba-Sarasua E, Chen Y, Hsu K, Scott S, Knight M, et al. Tailoring capsid-directed evolution technology for improved AAV-mediated CAR-T generation. *Mol Ther* (2025) **33**:2801–18. doi:10.1016/j.ymthe.2024.12.012

71. Wang Z, McWilliams-Koeppen HP, Reza H, Ostberg JR, Chen W, Wang X, et al. 3D-organoid culture supports differentiation of human CAR(+) iPSCs into highly functional CAR T cells. *Cell Stem Cell* (2022) **29**:515–27. doi:10.1016/j.stem.2022.02.009

72. Roybal KT, Rupp LJ, Morsut L, Walker WJ, McNally KA, Park JS, et al. Precision tumor recognition by T cells with combinatorial antigen-sensing circuits. *Cell* (2016) **164**:770–9. doi:10.1016/j.cell.2016.01.011

73. Ou Z, Lin S, Qiu J, Ding W, Ren P, Chen D, et al. Single-nucleus RNA sequencing and spatial transcriptomics reveal the immunological microenvironment of cervical squamous cell carcinoma. *Adv Sci* (2022) **9**:e2203040. doi:10.1002/advs.202203040

74. Zheng W, Ling S, Cao Y, Shao C, Sun X. Combined use of NK cells and radiotherapy in the treatment of solid tumors. *Front Immunol* (2024) **14**:1306534. doi:10.3389/fimmu.2023.1306534

75. Deng J, Wang ES, Jenkins RW, Li S, Dries R, Yates K, et al. CDK4/6 inhibition augments antitumor immunity by enhancing T-cell activation. *Cancer Discov* (2018) **8**:216–33. doi:10.1158/2159-8290.CD-17-0915

EBM Experimental Biology and Medicine

TYPE Review
PUBLISHED 07 January 2026
DOI 10.3389/ebm.2025.10781

OPEN ACCESS

*CORRESPONDENCE
Yajun Chen,
104762933@qq.com
Xianpeng Dai,
2003020003@usc.edu.cn

RECEIVED 02 August 2025
REVISED 29 October 2025
ACCEPTED 04 December 2025
PUBLISHED 07 January 2026

CITATION
Lyu X, Liu Q, Shi J, Chen Y and Dai X (2026) Neutrophil extracellular traps: emerging drivers and therapeutic targets in abdominal aortic aneurysm pathogenesis.
Exp. Biol. Med. 250:10781.
doi: 10.3389/ebm.2025.10781

Neutrophil extracellular traps: emerging drivers and therapeutic targets in abdominal aortic aneurysm pathogenesis

Xinyi Lyu[1], Qi Liu[1], Jiahao Shi[1], Yajun Chen[2]* and Xianpeng Dai[1]*

[1]Department of Vascular Surgery, The Second Affiliated Hospital, Hengyang Medical School, University of South China, Hengyang, China, [2]Department of Endocrinology and Metabolism, The Second Affiliated Hospital, Hengyang Medical School, University of South China, Hengyang, China

Abstract

Abdominal aortic aneurysm (AAA) is a life-threatening condition with no effective pharmacological treatments, underscoring the critical need to identify novel therapeutic targets. Emerging translational and clinical evidence implicates neutrophil extracellular traps (NETs) as potential drivers of AAA pathogenesis. This review systematically delineates the mechanisms by which NETs contribute to aortic wall degradation, focusing on their direct cytotoxicity to vascular smooth muscle cells (VSMCs), induction of VSMC phenotypic switching and ferroptosis, amplification of inflammatory cascades, and propagation of thromboinflammation. Key mediators include PAD4, IL-1β, PI3Kγ, neutrophil elastase, myeloperoxidase, and mitochondrial DNA. NET components (citrullinated histone H3, cell-free DNA, neutrophil elastase) serve as promising diagnostic and prognostic biomarkers. Preclinical studies highlight the efficacy of NET-targeting strategies, including inhibiting NET formation, degrading existing NETs, neutralizing cytotoxic components, and modulating downstream pathways (e.g., with ferroptosis inhibitors). Nanotechnology platforms enhance site-specific delivery of these agents. By integrating the research background with its practical implications, we conclude that targeting NETs represents a promising paradigm shift. Despite translational challenges, this approach offers a rational framework for developing the first pharmacotherapies aimed at stabilizing AAA and addressing a major unmet clinical need.

KEYWORDS

neutrophil extracellular traps, abdominal aortic aneurysm, pathogenesis, therapeutic targets, biomarkers

Impact statement

This review establishes neutrophil extracellular traps (NETs) as central drivers of abdominal aortic aneurysm (AAA) progression, a life-threatening condition lacking effective drug therapies. It synthesizes groundbreaking evidence showing how NETs actively degrade the aortic wall by killing vascular muscle cells, amplifying inflammation, and promoting blood clots within the aneurysm. Crucially, we identify NET components (e.g., citrullinated histone H3) as novel diagnostic and prognostic biomarkers linked to aneurysm growth and rupture risk. Furthermore, the work highlights promising NET-targeting therapeutic strategies—including inhibitors of NET formation, degraders of existing NETs, and microbiome modulators—that significantly reduce AAA progression in preclinical models. By defining NETs as fundamental mediators and actionable targets, this review provides a transformative framework for developing the first pharmacological interventions to stabilize AAA, addressing a major unmet clinical need.

Introduction

Abdominal aortic aneurysm (AAA), a potentially life-threatening dilation of the infrarenal aorta, characterized by progressive inflammatory infiltration, extracellular matrix degradation, and vascular smooth muscle cell (VSMC) depletion [1–3]. With no effective pharmacotherapies available, rupture carries a high mortality rate [4–6]. Inflammation is a recognized cornerstone of AAA pathogenesis, which operates within a complex interplay of genetic predisposition, biomechanical stress, metabolic disease, and environmental factors such as smoking, and involves innate and adaptive immune cells [7–9]. Traditionally viewed as first responders, neutrophils contribute to host defense beyond phagocytosis via a distinct process known as Neutrophil extracellular trap (NET) formation, or NETosis [10–12]. NETs, released by neutrophils, are web-like structures composed of decondensed chromatin decorated with cytotoxic granular proteins such as myeloperoxidase (MPO), neutrophil elastase (NE), and citrullinated histone H3 (CitH3), which function to ensnare pathogens [13–15]. Emerging translational and clinical evidence implicates neutrophil extracellular traps (NETs) as potential driver of AAA progression. It is important to note, however, that while these associations are compelling, the causal role of NETs in human AAA pathogenesis is still being delineated, with much of the mechanistic insight derived from preclinical models. Components of NETs, such as CitH3, cell-free DNA (cfDNA), and NE, are significantly elevated in both the plasma and tissues of AAA patients, and these elevations correlate with aneurysm size, growth rate, and severity [16–18]. Histologically, NETs localize within the aortic wall and intraluminal thrombus (ILT), where they mediate multifaceted damage [19, 20].

This review synthesizes evidence establishing NETs as fundamental drivers of AAA pathogenesis. It will specifically examine the molecular and cellular mechanisms by which NETs cause ECM degradation, induce VSMC death (apoptosis, ferroptosis) and phenotypic switching, amplify inflammation (cytokine cascades, pDC activation), and drive metabolic/epigenetic dysregulation. Systemic factors (gut dysbiosis, thromboinflammation) amplifying NETosis are explored. The translational potential of NET components as biomarkers and emerging NET-targeting therapeutic strategies are critically evaluated. Finally, challenges in translating these discoveries to meet the unmet clinical need in AAA management are addressed.

Categorization and mechanisms of NETosis

NETosis can be classified by stimulus (microbial vs. sterile), cellular outcome (lytic/suicidal vs. vital), and molecular pathway (NADPH oxidase-dependent vs. -independent). In the context of AAA, sterile inflammation-induced and thromboinflammatory NETosis are particularly relevant, driven by DAMPs, cytokines, and platelet-neutrophil interactions. A detailed summary of NETosis classifications is provided in Supplementary Table S1.

Pathological mechanisms of NETosis in AAA

NETosis is a central driver of AAA pathogenesis. Its detrimental effects unfold through distinct but interconnected mechanisms, categorized as follows (Table 1).

Molecular triggers of NETosis

Key molecular mediators of NETosis in AAA include interleukin-1β (IL-1β). IL-1β induces ceramide synthase 6-mediated synthesis of C16-ceramide, thereby promoting the nuclear changes essential for NET formation [21]. Oxidized low-density lipoprotein (oxLDL) is another potent inducer of NETosis [22], mechanistically linking dyslipidemia to vascular inflammation in AAA. Additionally, in human AAA tissue PDK isoenzymes are upregulated, which drives a metabolic shift characterized by increased lactate production and phosphorylated PDH levels [23]. Crucially, experimental inhibition of PDK not only reduces NETosis but also attenuates AAA pathogenesis in *in vivo* and *in vitro* models, confirming its significant role [23].

Cellular damage by NET components

NETs, which are composed of chromatin filaments complexes with cytotoxic proteins such as NE, MPO, and CitH3 [20, 24, 25],

TABLE 1 Pathological mechanisms of NETosis in AAA.

Category	Key elements	Pathological effects in AAA	Experimental evidences
Molecular triggers	IL-1β: induces ceramide synthase 6 → C16-ceramide → nuclear changes → NETosis	Promotes neutrophil activation and NET release, driving initial inflammation and wall damage	Il1b KO mice show reduced AAA [21]
	oxLDL: Potent NETosis inducer	Links dyslipidemia to vascular inflammation and NET-driven injury	Plasma oxPL/apoB levels correlate with citH3 levels in AAA patients [22]
	PDK isoenzymes: upregulated in AAA → increases lactate/p-PDH → metabolic shift	Drives NETosis and vascular inflammation	DCA (PDK inhibitor) reduces NETosis in mouse models [23]
Cellular damage	NET components (NE, MPO, CitH3): Direct proteolytic attack on ECM (elastin, collagen)	Elastin degradation, ECM fragmentation → loss of structural integrity	NETs increase MMP-2/9 activity [24]; NE/MPO directly degrade elastin [20, 25]
	VSMC phenotypic switching: NETs suppress Hippo-YAP pathway → increases synthetic/pro-inflammatory VSMCs	VSMC loss of contractility → impaired repair; increases inflammation	*Padi4* or *Yap* knockout (KO) prevents VSMC transformation [26]
	VSMC ferroptosis: NETs deplete mitochondrial glutathione (reduces SLC25A11) + inhibit PI3K/AKT → iron-dependent death	Massive VSMC loss → wall thinning, rupture risk	Ferroptosis inhibitors reduce AAA in mouse models [27, 28]
Systemic drivers	Gut dysbiosis: reduces *Ruminococcus intestinalis* → reduces butyrate	Increases neutrophil infiltration → increases NOX2-dependent NETosis → aortic dilation	Butyrate supplementation or *Ruminococcus intestinalis* gavage attenuates AAA [29]
	Thromboinflammation: NETs → activate pDCs → increases type I IFNs → increases inflammation	Sustained inflammation, macrophage activation, and ECM degradation	pDC depletion or type I IFN blockade attenuates AAA [20]
	PAD4: Mediates histone citrullination → chromatin decondensation → NETosis	Essential for NET formation; drives VSMC apoptosis and ECM damage	PAD4 inhibitors or KO reduces VSMC apoptosis and AAA rupture [18, 30, 31]
	PI3Kγ: Activates non-canonical pyroptosis → NETosis	Amplifies neutrophil-driven inflammation and wall injury	PI3Kγ inhibition reduces NETs in AAA models [32]
Thrombus interface	NET Reservoir: ILT accumulates high levels of citH3, NE, MPO, and cfDNA.	Creates hyper-inflammatory/proteolytic niche → recruits neutrophils → perpetuates NETosis	Thrombus contains 30× more citH3 than wall, CXCL1/CXCL8 recruit neutrophils [10, 19]
	pDC activation: ILT-concentrated NETs → robust pDC activation → increases type I IFNs	Amplifies vascular inflammation and ECM breakdown	pDCs activated by NETs in ILT [20]

Key Abbreviations: citH3, Citrullinated Histone H3; DCA, Dichloroacetate; ECM, Extracellular Matrix; IFN, Interferon; IL-1β: Interleukin-1 beta; ILT, Intraluminal Thrombus; MMP, Matrix Metalloproteinase; MPO, Myeloperoxidase; NE, Neutrophil Elastase; NETosis, Neutrophil Extracellular Trap formation; oxLDL, oxidized low-density lipoprotein; PAD4, Peptidyl Arginine Deiminase 4; pDC, plasmacytoid Dendritic Cell; PDK, Pyruvate Dehydrogenase Kinase; PI3K/AKT, Phosphoinositide 3-kinase/Protein Kinase B; PI3Kγ, Phosphoinositide 3-Kinase gamma; SLC25A11, Mitochondrial Glutamate Carrier; VSMC, Vascular Smooth Muscle Cell.

directly inflict damage upon the vascular wall. Beyond direct injury, NETs significantly exacerbate vascular pathology by inducing phenotypic switching and dysfunction in VSMCs [33]. Specifically, neutrophil elastase (NE), a key component of NETs, has been identified as a direct mediator that suppresses the Hippo-YAP signaling pathway, promoting the transition of VSMCs towards a synthetic, pro-inflammatory phenotype. This shift is associated with distinct histone modifications—enrichment of H3K4me3 and reduction of H3K27me3—at the promoters of contractile apparatus genes [26].

Notably, NETs are potent inducers of VSMC ferroptosis, an iron-dependent form of regulated cell death [27]. Mechanistically, the proteolytic activity of NET-associated NE contributes to the degradation of the mitochondrial glutamate carrier SLC25A11, leading to glutathione depletion and compromising cellular antioxidant defenses [27]. Concurrently, NETs inhibit the pro-survival PI3K/AKT signaling pathway, which downregulates the expression of the central anti-ferroptotic regulator, glutathione peroxidase 4 (GPX4), thereby synergistically enhancing VSMC susceptibility to ferroptosis [28].

Systemic drivers amplifying NETosis

Gut microbiome dysregulation

Alterations in the gut microbiota composition (dysbiosis), particularly a reduced abundance of *Ruminococcus intestinalis*, contribute significantly to AAA pathogenesis by influencing NETosis. This dysbiosis diminishes microbial production of the short-chain fatty acid butyrate. Butyrate deficiency, in turn, promotes neutrophil infiltration into the aortic wall and enhances NOX2-dependent NET formation, potentially through mechanisms involving the inhibition of histone deacetylases (HDAC) activity and subsequent suppression of pro-inflammatory signaling pathways, ultimately accelerating aortic dilation [29].

Thromboinflammation and feed-forward loops

NETosis actively fuels a pro-thrombotic environment within the aneurysm sac. NET components, notably cfDNA and CitH3, stimulate plasmacytoid dendritic cells (pDCs). Activated pDCs produce type I interferons (IFNs), which sustain vascular inflammation and promote macrophage activation. Furthermore, NETs facilitate the development of intraluminal thrombus. Critically, this thrombus acts as a reservoir for NET components and associated proteases, creating a potent pro-inflammatory and proteolytic microenvironment. This niche further recruits neutrophils, perpetuating NETosis and driving continuous wall degradation. Critically, the presence of thrombus significantly enhances the efficacy of NETosis inhibitors in reducing AAA progression in experimental models, highlighting the centrality of this thromboinflammatory cycle [20, 23].

Epigenetic and transcriptional regulation

Key molecular regulators underpin NETosis in AAA. PAD4-mediated histone citrullination is an essential step for chromatin decondensation during NET formation. Pharmacological inhibition or genetic deletion of PAD4 markedly reduces NET generation, attenuates VSMC apoptosis, and decreases AAA rupture incidence [18, 30, 31]. Additionally, phosphoinositide-3-kinase γ (PI3Kγ) signaling promotes NETosis by activating non-canonical pyroptosis pathways dependent on cAMP/PKA signaling [32].

The thrombus interface: a critical hub in AAA pathogenesis

NETs actively promote the formation of ILT within AAA. Once established, the ILT functions as a dynamic repository, accumulating high concentrations of NET-derived components, such as DNA, CitH3, NE, MPO, and various proteases [10, 34]. This thrombotic niche fosters a potent pro-inflammatory microenvironment. Through the release of neutrophil-attracting chemokines, such as CXCL1 and CXCL8, the ILT recruits additional neutrophils to the site [19, 35]. This sustained neutrophil influx perpetuates NETosis and drives continuous degradation of the vascular wall. Notably, the ILT concentrates NET components to extraordinary levels. For instance, CitH3 accumulates within the thrombus at concentrations up to 30-fold higher than those found in the adjacent aortic wall [13, 18]. This concentrated reservoir serves as a potent platform for activating pDCs, stimulating robust type I IFN production, and thereby amplifying vascular inflammation [36].

The central role of the ILT in driving NETosis-dependent pathology is underscored by the differential efficacy of NETosis inhibitors. Pharmacological agents targeting NET formation, such as PAD4 inhibitors, demonstrate significantly enhanced efficacy in attenuating AAA progression in experimental models possessing an ILT [27, 31]. These highlight the ILT not merely as a pathological feature, but as a crucial therapeutic target within the NETosis-amplifying cascade of AAA.

NETs as biomarkers in AAA

NET components exhibit compelling potential as clinical biomarkers across the entire AAA disease continuum. Their emerging diagnostic and prognostic utility, supported by recurrent evidence in the literature, is systematically summarized below.

Circulating NET components serve as diagnostic and prognostic biomarkers

Consistently elevated levels of specific NET components are detected in the plasma/serum of AAA patients compared with healthy controls and patients with other vascular pathologies, such as peripheral artery disease (PAD). These biomarkers demonstrate significant diagnostic and prognostic utility.

CitH3

A highly specific NETosis marker with significantly increased concentrations in AAA plasma and tissue—particularly within the ILT. It demonstrates diagnostic potential (AUC ≈0.705), predicts short-term AAA progression (e.g., 6-month growth), and decreases markedly following successful surgical repair, highlighting its value for postoperative monitoring [10, 16–18, 31, 37].

cfDNA

As the structural DNA backbone of NETs, plasma cfDNA levels are substantially elevated in AAA patients. These elevations correlate strongly with established markers of neutrophil activation and NET formation, highlighting the central role of neutrophil dysregulation and NETosis in AAA progression and positioning cfDNA as a potential biomarker reflecting this key pathological pathway [10, 13, 16–18, 30, 37].

MPO & NE

These granular proteins, embedded within NET structures, are elevated in AAA plasma and tissue. They co-localize with NETs and correlate with both disease presence and activity, positioning them not only as specific markers of NET burden but also as potential indicators of disease severity and future risk [7, 10, 17, 20, 31, 37].

Oxidized DNA

Reflecting NETosis-associated oxidative stress. Specific methodologies (e.g., immunoprecipitation followed by qPCR) enable differentiation between oxidized nuclear and

mitochondrial DNA in plasma. Studies show that AAA patients exhibit trends toward increased oxidized mitochondrial DNA and enrichment of mitochondrial DNA within the oxidized fraction, suggesting a potential link between NETosis and specific organellar damage pathways [16].

Multiplex biomarker panels

Combinations of CitH3, cfDNA, MPO, and potentially oxidized phospholipids on apolipoprotein B-100 (oxPL/apoB) demonstrate enhanced diagnostic accuracy and progression risk stratification over single-marker approaches [17, 18, 30].

Association with disease severity and progression

Circulating levels of key NET biomarkers—including CitH3, cfDNA, MPO, and NE—show strong correlations with established AAA risk factors and adverse clinical outcomes. Specifically, these biomarkers demonstrate significant associations with both AAA maximum diameter and annual expansion rate [16–18, 30, 37]. It is worth noting that Eilenberg et al. reported that elevated CitH3 levels are a predictive indicator for accelerated AAA growth [18].

NET components are consistently found at significantly higher concentrations within the AAA wall tissue and, in particular, are localized within the ILT [18–21, 26, 31, 37]. Furthermore, advances in molecular profiling, utilizing machine learning and multi-omics analyses, have identified distinct NET-related gene expression signatures (e.g., involving *DUSP26, FCN1, MTHFD2, GPRC5C, SEMA4A, CCR7*). These signatures hold considerable diagnostic potential as novel tools for predicting the likelihood and trajectory of AAA progression [33].

Link to pathogenic mechanisms and comorbidities

Circulating NET biomarker levels serve as indicators of key pathological processes underlying AAA development and progression.

Inflammation

NET biomarker concentrations exhibit strong correlations with both general systemic inflammatory markers and specific cytokines (e.g., IL-1β, IL-6) known to be critically involved in AAA pathogenesis [4, 7, 21]. This underscores the integral role of NETs within the inflammatory cascade driving AAA.

Oxidative stress

The significant correlation observed between oxPL/apoB (a biomarker reflecting oxidized phospholipids on apolipoprotein B-100 particles) and CitH3 suggests that oxidized lipids actively promote NETosis within the AAA milieu [17]. This process may constitute a significant mechanism contributing to disease progression.

VSMC dysfunction

NETs directly contribute to AAA wall weakening by inducing detrimental changes in VSMCs, including phenotypic switching, apoptosis, senescence, and ferroptosis. Consequently, elevated NET biomarker levels may indirectly reflect the extent of this crucial VSMC damage [21, 26–28].

Gut microbiome dysbiosis

Alterations in the gut microbiota composition associated with AAA, such as reduced abundance of *Roseburia intestinalis*, have been linked to enhanced NET formation. Therefore, specific NET biomarker profiles may potentially reflect these underlying dysbiotic states [29].

Potential for monitoring therapeutic interventions

NET-derived biomarkers demonstrate significant promise as tools for monitoring responses to therapeutic interventions in AAA. Pharmacological strategies targeting NETosis—including PAD4 inhibitors (e.g., YW3-56), DNase1, resolvin D1, and PDK inhibitors (e.g., dichloroacetate, DCA)—consistently attenuate AAA progression in preclinical models. This therapeutic efficacy is paralleled by a measurable reduction in circulating NET biomarker levels, such as CitH3, cfDNA, and NE [5, 18, 19, 21, 23, 28, 31, 38]. Clinically, CitH3 levels decrease significantly following successful surgical AAA repair, underscoring their potential utility in tracking post-interventional outcomes [18]. Furthermore, emerging NET-targeting nanomedicine approaches (e.g., GlycoRNA nanoparticle-delivered siMT1 [GlycoRNA-NP-siMT1], lactoferrin-coated calcium dipicolinate nanoparticles [LaCD NP]) effectively reduce disease progression in preclinical AAA models [5, 38]. In these studies, the concomitant reduction in NET biomarkers serves as a critical quantitative readout for assessing treatment efficacy.

Despite these promising diagnostic and prognostic associations, the clinical translation of NET-derived biomarkers faces several challenges. Circulating levels of markers such as CitH3, cfDNA, MPO, and NE show marked heterogeneity across studies, influenced by variations in sample processing, detection methodologies, and patient cohort characteristics. The lack of standardized, validated assays and universally accepted clinical cut-off values currently prevents their routine application in clinical decision-making. Therefore, large-scale, multi-center prospective studies are crucial to harmonize detection protocols and definitively establish the utility of these biomarkers for risk stratification and monitoring therapeutic responses.

Imaging biomarkers

Beyond circulating molecular biomarkers, emerging molecular imaging techniques offer the potential for direct, non-invasive visualization of NETosis *in vivo*. A promising approach utilizes anti-Ly6G antibody-conjugated superparamagnetic iron oxide nanoparticles (Ly6G-SPIONs) in conjunction with Magnetic Particle Imaging (MPI). This combined platform enables highly sensitive detection and quantification of neutrophil infiltration specifically within AAA lesions in murine models. Critically, the MPI signal intensity correlates strongly with AAA severity and exhibits a significant decrease following pharmacological inhibition of NETosis, demonstrating its utility as a dynamic imaging biomarker for disease activity and therapeutic response [37].

Therapeutic targeting of NETs in AAA

NETs have been established as key pathogenic drivers of AAA progression, orchestrating vascular inflammation, VSMC death, extracellular matrix degradation, and maladaptive vascular remodeling. These processes collectively weaken the aortic wall, ultimately driving aneurysm expansion and rupture risk. Therefore, pharmacologically targeting NET formation or activity has emerged as a promising therapeutic approach to mitigate AAA pathogenesis, as summarized in Table 2.

PAD4 inhibition

PAD4 catalyzes histone citrullination, a critical step in NET formation [39, 40]. Consequently, PAD4 represents a pivotal therapeutic target for NET-driven pathologies like AAA. Both genetic ablation of *Padi4* and pharmacological inhibition with compounds such as Cl-amidine or YW3-56 significantly suppress NET release in preclinical AAA models. This suppression translates to substantial therapeutic benefits, including attenuated AAA formation and rupture risk, alongside preserved VSMCs contractility [4, 18, 19, 26, 31]. Importantly, plasma levels of citrullinated CitH3, a direct product of PAD4 activity and a specific NET biomarker, correlate with both AAA presence and aneurysm growth rate. Furthermore, CitH3 levels decrease significantly following successful surgical AAA repair. These findings not only highlight the utility of CitH3 as a sensitive biomarker for disease activity and therapeutic response but also provide compelling clinical validation for PAD4 as a viable therapeutic target in AAA [18].

Targeting specific NET components

Metallothionein 1 (MT1) is significantly upregulated within human and murine AAA lesions, where it actively promotes NET formation [5]. To counteract this, glycoRNA-conjugated nanoparticles delivering MT1-targeting siRNA (GlycoRNA-NP-siMT1) achieve site-specific delivery to aneurysmal tissue. This nanotherapeutic platform effectively suppresses NET generation, pathological vascular remodeling, and aortic dilation through dual mechanisms: competitively inhibiting neutrophil infiltration while directly silencing pathogenic MT1 expression within inflammatory cells [5]. Parallel strategies target the proteolytic cascade centered on dipeptidyl peptidase I (DPPI/Cathepsin C), which activates NE and PR3 to drive NET release. Genetic deficiency in either DPPI or its downstream effectors confers protection against experimental AAA, confirming their non-redundant role in NET-driven pathogenesis [20]. Crucially, NE executes dual functions in this process—facilitating NET chromatin decondensation through histone degradation while independently contributing to extracellular matrix destruction within the aortic wall [5, 20].

Immunometabolic reprogramming

Targeting the dysregulated PDK/pyruvate dehydrogenase (PDK/PDH) axis through inhibition of PDK—using either DCA or PDK1-targeting siRNA—is a potent immunometabolic intervention for AAA. This metabolic reprogramming effectively suppresses NET release and reduces pathological neutrophil infiltration into the aortic wall. Concurrently, it preserves the contractile phenotype of SMCs and prevents elastin degradation. Collectively, these mechanisms attenuate AAA progression by approximately 58%, as evidenced by significant reduction in aortic dilation in preclinical models [23].

PI3Kγ pathway inhibition

PI3Kγ functions as an upstream regulator of NET formation in AAA, driving this process through a noncanonical pyroptosis pathway dependent on cAMP/PKA signaling activation. Pharmacological inhibition of PI3Kγ significantly reduces NETosis, attenuates inflammatory cell infiltration within the aortic wall, decreases pro-inflammatory cytokine production, and ultimately ameliorates key AAA pathological features including vascular remodeling and aneurysm expansion in preclinical models [32].

Resolvin D1 (RvD1)

RvD1, a specialized pro-resolving lipid mediator derived from docosahexaenoic acid (DHA), potently suppresses NET formation by inhibiting ceramide synthase 6 (CerS6)-dependent C16-ceramide biosynthesis. This molecular intervention significantly reduces key NET components including CitH3 and NE.

TABLE 2 Therapeutic targeting of NETs in AAA.

Therapeutic strategy	Molecular target	Intervention	Mechanism	Experimental outcomes	References
PAD4 inhibition	PAD4	Genetic deletion of *Padi4*; pharmacological inhibitors (e.g., Cl-amidine, YW3-56)	Inhibits histone citrullination and NET formation	Reduces NET release; reduces AAA formation/rupture; increases SMC contractility; reduces plasma citH3 (biomarker)	[4, 18, 19, 26, 31]
Targeting NET components	MT1	GlycoRNA-NP-siMT1 nanoparticles	Coated NPs deliver MT1 siRNA to AAA site. Competitively inhibits neutrophil infiltration & suppresses MT1 expression, inhibiting NET formation	Reduces NET formation; reduces pathological remodeling; reduces aortic dilation	[5]
	DPPI/NE/PR3	Genetic deficiency; pharmacological inhibition	DPPI activates NE/PR3, crucial for NET release. NE degrades DNA during NETosis	Protects against AAA development	[20]
Immunometabolic reprogramming	PDK	DCA; PDK1-siRNA	Corrects the skewed PDK/PDH axis metabolism	Reduces NET release; reduces neutrophil infiltration; increases SMC contractile phenotype; prevents elastin breakdown; reduces AAA formation (~58%)	[23]
PI3Kγ pathway inhibition	PI3Kγ	PI3Kγ inhibitors	Acts upstream to promote NET formation through noncanonical pyroptosis (cAMP/PKA-dependent)	Reduces NETosis; reduces aortic wall inflammation; ameliorates AAA	[32]
Pro-resolving mediators	CerS6/C16-ceramide	RvD1	Inhibits CerS6/C16-ceramide synthesis, reducing NETosis	Reduces NETosis (reduces CitH3, reduces NE); reduces AAA formation (elastase & Ang II models); reduces inflammation (e.g., IL-1β); reduces MMP activity	[19]
Anti-inflammatory nanotherapies	General neutrophil inflammation/ NETosis	LaCD nanoparticles	Intrinsically anti-inflammatory NPs accumulate in aneurysmal aorta, inhibiting neutrophil-mediated inflammation and NETosis	Reduces NET formation; suppresses NET-driven inflammation & pathological remodeling; reduces AAA	[38]
Targeting NET-induced SMC pathologies	mitoGSH depletion/ ferroptosis	Ferrostatin-1; prevent mitoGSH depletion	NETs induce SMC ferroptosis via reduces mitoGSH (destabilizing SLC25A11)	Protects against AAA	[27]
	SLC25A11/ ferroptosis	MSC-EVs	Reduce NET release and inhibit NET-induced SMC ferroptosis	Alleviates AAA	[28]
	Hippo-YAP pathway/ H3K4me3/ H3K27me3	Potential target implied	NETs promote synthetic/ proinflammatory SMC phenotypes via inhibiting Hippo-YAP and modulating histone marks (H3K4me3/ H3K27me3) at gene promoters		[26]
Microbiome modulation	Gut dysbiosis/ Butyrate levels	*Roseburia intestinalis* supplementation; butyrate	Corrects dysbiosis, increases butyrate. Reduces NOX2-dependent NETosis	Reduces neutrophil infiltration; reduces NETosis; reduces inflammation; reduces SMC phenotypic switching; reduces AAA	[29]

Key Abbreviations: AAA, Abdominal Aortic Aneurysm; Ang II, Angiotensin II; cAMP, Cyclic Adenosine Monophosphate; CerS6, Ceramide Synthase 6; citH3, Citrullinated Histone H3; DCA, Dichloroacetate; DPPI, Dipeptidyl Peptidase I; EVs, Extracellular Vesicles; Hippo-YAP, Hippo pathway and Yes-Associated Protein; IL-1β, Interleukin-1 beta; mitoGSH, Mitochondrial Glutathione; MMP, Matrix Metalloproteinase; MSC, Mesenchymal Stem Cell; MT1, Metallothionein 1; NE, Neutrophil Elastase; NETs, Neutrophil Extracellular Traps; NOX2, NADPH Oxidase 2; NP, Nanoparticle; PAD4, Peptidyl Arginine Deiminase 4; PDH, Pyruvate Dehydrogenase; PDK, Pyruvate Dehydrogenase Kinase; PI3Kγ, Phosphoinositide 3-Kinase gamma; PKA, Protein Kinase A; PR3, Proteinase 3; RvD1, Resolvin D1; siRNA, small interfering RNA; SLC25A11, Mitochondrial Glutamate Carrier; SMC, Smooth Muscle Cell.

Therapeutic administration of RvD1 attenuates AAA progression in both elastase-perfusion and angiotensin II (Ang II)-induced murine models. The protective effects are mediated through substantial reductions in pro-inflammatory cytokines (e.g., IL-1β) and matrix metalloproteinase (MMP-2/MMP-9) activity, collectively preserving vascular structural integrity [19].

Anti-inflammatory nanotherapies

Engineered nanoparticles with inherent anti-inflammatory properties, exemplified by lactoferrin-coated calcium dipicolinate nanoparticles (LaCD NPs), demonstrate targeted biodistribution to aneurysmal aortic tissue. This nanotherapeutics effectively suppresses neutrophil-mediated inflammation through inhibition of NLRP3 inflammasome activation and subsequent IL-1β release. Crucially, they potently attenuate NETosis, thereby interrupting the self-perpetuating cycle of NET-driven inflammation. This dual-action mechanism significantly reduces pro-inflammatory cytokine cascades and pathological vascular remodeling, establishing LaCD NPs as promising targeted therapeutics for abdominal aortic aneurysm intervention [38].

Targeting NET-Induced SMC pathologies

NETs drive SMC ferroptosis by destabilizing the mitochondrial glutamate carrier SLC25A11, resulting in depletion of mitochondrial glutathione (mitoGSH). This metabolic disruption compromises cellular redox homeostasis and promotes iron-dependent cell death. Therapeutic prevention of mitoGSH depletion or pharmacological inhibition of ferroptosis pathways—using specific inhibitors such as ferrostatin-1—confers significant protection against AAA development in preclinical models [27]. Additionally, mesenchymal stem cell-derived extracellular vesicles (MSC-EVs) represent a complementary approach, as they simultaneously suppress NET release and directly inhibit NET-induced SMC ferroptosis, thereby attenuating AAA progression [28]. Beyond ferroptosis, NETs additionally promote pathological SMC phenotypic switching toward synthetic and proinflammatory states. This transition is mechanistically linked to NET-mediated inhibition of the Hippo-YAP signaling pathway and epigenetic dysregulation through altered histone methylation marks (specifically reduced H3K4me3 and elevated H3K27me3) at promoters of contractile apparatus genes [26].

Microbiome modulation

Gut dysbiosis represents a significant pathogenic contributor to AAA development, characterized by depletion of *Roseburia intestinalis* and reduced butyrate production. Therapeutic restoration of microbial homeostasis through *Roseburia intestinalis* supplementation or direct butyrate administration effectively suppresses neutrophil infiltration into the aortic wall, inhibits NOX2-dependent NETosis, attenuates pro-inflammatory cytokine cascades, and prevents pathological SMC phenotypic switching. These coordinated mechanisms collectively reduce aortic dilation by >50% in preclinical models, demonstrating the therapeutic potential of microbiome modulation in AAA management [29].

Discussion

The clinical translation of NET-targeting therapies faces significant hurdles. Current preclinical models—particularly acute angiotensin II infusion in mice which induces AAA over weeks—fail to adequately recapitulate the slow, smoldering inflammation that characterizes human AAA progression over years or decades [41–43]. Further complicating translation, the therapeutic efficacy of many NET inhibitors is thrombus-dependent, necessitating validation in models that faithfully mimic human disease progression timelines.

Therapeutic specificity and safety remain paramount. Furthermore, the therapeutic suppression of NETosis raises legitimate concerns regarding the impairment of innate antimicrobial defense. Systemic inhibition of neutrophil function, for instance via PAD4 blockade or DNase administration, could potentially increase susceptibility to infections. Therefore, achieving cell- and context-specificity—for example, through localized delivery systems such as nanoparticles or the development of inhibitors targeting disease-specific NET components—is paramount to maximizing safety. Patient stratification based on infection risk and immunocompetence will also be a crucial consideration for future clinical application. While PAD4 inhibitors show promise due to functional redundancy in host immunity, targeting downstream effectors (e.g., SMC ferroptosis pathways) may offer superior safety profiles.

NET heterogeneity—driven by stimulus-specific activation, disease stage, and anatomically distinct microenvironments—demands precision interventions tailored to individual pathological contexts [44–46]. Validation of NET biomarkers (e.g., CitH3, cfDNA) through large-scale longitudinal clinical studies is imperative for robust diagnostic and prognostic applications. Spatially resolved multi-omics approaches combined with advanced molecular imaging (e.g., Ly6G-NP-MPI) will enable comprehensive mapping of NET spatiotemporal dynamics within AAA microenvironments.

Future success will require: (1) Combinatorial strategies concurrently targeting NETs and complementary pathogenic pathways (e.g., MMPs, cytokine networks, renin-angiotensin

signaling), (2) Prioritization of interventions for established aneurysms rather than prevention-only paradigms, and (3) Identification of NET-driven patient endotypes (e.g., high-CitH3 phenotypes, rapid progressors) to enable personalized therapeutic stratification.

The promising preclinical data now necessitate a decisive transition to clinical validation. Future success is contingent upon initiating early-phase human trials to evaluate the safety, tolerability, and bioactivity of NET-inhibiting agents. These studies should prioritize patient populations with a high unmet need, such as those with rapidly expanding aneurysms, and utilize the emerging NET-related biomarkers (e.g., plasma CitH3) for patient enrichment and pharmacodynamic assessment.

Summary

NETs are emerging as key regulators within the multifactorial network of AAA pathogenesis, integrating neutrophil activation with SMC death, ECM degradation, inflammation, thrombosis, and metabolic reprogramming. Their consistent detection in human AAA tissues and circulation, coupled with strong correlations to disease severity and expansion, underscores their clinical relevance. Preclinical strategies targeting NET formation, degradation, and their downstream effects demonstrate robust efficacy in attenuating AAA progression, with nanotechnology offering promising avenues for enhanced site-specific delivery.

Despite this promise, translating these findings necessitates focused future efforts. First, the clinical utility of NET-derived biomarkers requires validation in large-scale, longitudinal cohorts to establish standardized thresholds for risk stratification. Second, the refinement of targeted delivery systems is crucial to maximize therapeutic efficacy while minimizing systemic impact on host defense. Third, combination therapies concurrently targeting NETs and complementary pathways (e.g., MMPs, renin-angiotensin system) should be explored to achieve synergistic effects in established aneurysms. Finally, identifying NET-driven patient endotypes will be essential for personalizing therapeutic interventions. By addressing these priorities, NETosis inhibition can evolve from a compelling preclinical concept into a viable clinical strategy for stabilizing AAA.

Author contributions

All authors listed have made a substantial, direct, and intellectual contribution to the work and approved it for publication.

Funding

The author(s) declared that financial support was received for this work and/or its publication. This work was supported by Natural Science Foundation of Hunan Province (2025JJ81010, 2024JJ9387), and Postgraduate Scientific Research Innovation Project of Hunan Province (CX20240849).

Conflict of interest

The author(s) declared no potential conflicts of interest with respect to the research, authorship, and/or publication of this article.

Generative AI statement

The author(s) declared that generative AI was not used in the creation of this manuscript.

Any alternative text (alt text) provided alongside figures in this article has been generated by Frontiers with the support of artificial intelligence and reasonable efforts have been made to ensure accuracy, including review by the authors wherever possible. If you identify any issues, please contact us.

Supplementary material

The Supplementary Material for this article can be found online at: https://www.ebm-journal.org/articles/10.3389/ebm.2025.10781/full#supplementary-material

References

1. Gong W, Tian Y, Li L. T cells in abdominal aortic aneurysm: immunomodulation and clinical application. *Front Immunology* (2023) **14**: 1240132. doi:10.3389/fimmu.2023.1240132

2. Bi C, Liu B, Gao P, Wang C, Fang S, Huo Z, et al. RAGE deficiency ameliorates abdominal aortic aneurysm progression. *Inflamm Research* (2025) **74**:63. doi:10.1007/s00011-025-02027-2

3. Domagala D, Data K, Szyller H, Farzaneh M, Mozdziak P, Wozniak S, et al. Cellular, molecular and clinical aspects of aortic aneurysm-vascular physiology and pathophysiology. *Cells* (2024) **13**:274. doi:10.3390/cells13030274

4. Yang WT, Li FD, Zheng YH, Wang L. Myeloid cells in abdominal aortic aneurysm. *Curr Atheroscler Rep* (2025) **27**:57. doi:10.1007/s11883-025-01302-1

5. Zhang Z, Ling T, Ding Q, Zhu F, Cheng X, Li X, et al. GlycoRNA-rich, neutrophil membrane-coated, siMT1-loaded nanoparticles mitigate abdominal aortic aneurysm progression by inhibiting the formation of neutrophil extracellular traps. *Mater Today Bio* (2025) **31**:101630. doi:10.1016/j.mtbio.2025.101630

6. Sidik AI, Al-Ariki MK, Shafii AI, Hossain ML, Najneen F, Ak G, et al. Advances in imaging and diagnosis of abdominal aortic aneurysm: a shift in clinical practice. *Cureus* (2025) **17**:e81321. doi:10.7759/cureus.81321

7. Yuan Z, Lu Y, Wei J, Wu J, Yang J, Cai Z. Abdominal aortic aneurysm: roles of inflammatory cells. *Front Immunology* (2020) **11**:609161. doi:10.3389/fimmu.2020.609161

8. Schrottmaier WC, Mussbacher M, Salzmann M, Assinger A. Platelet-leukocyte interplay during vascular disease. *Atherosclerosis* (2020) **307**:109–20. doi:10.1016/j.atherosclerosis.2020.04.018

9. Dale MA, Ruhlman MK, Baxter BT. Inflammatory cell phenotypes in AAAs: their role and potential as targets for therapy. *Arteriosclerosis, Thrombosis, Vascular Biology* (2015) **35**:1746–55. doi:10.1161/ATVBAHA.115.305269

10. Plana E, Oto J, Medina P, Fernandez-Pardo A, Miralles M. Novel contributions of neutrophils in the pathogenesis of abdominal aortic aneurysm, the role of neutrophil extracellular traps: a systematic review. *Thromb Research* (2020) **194**:200–08. doi:10.1016/j.thromres.2020.07.039

11. Liu Q, Chen R, Zhang Z, Sha Z, Wu H. Mechanisms and immune crosstalk of neutrophil extracellular traps in response to infection. *mBio* (2025) **16**:e0018925. doi:10.1128/mbio.00189-25

12. Li Y, Cao Z, Liu J, Qiang R, Wang J, Lyu W. Current perspectives and trends of neutrophil extracellular traps in organ fibrosis: a bibliometric and visualization study. *Front Immunology* (2025) **16**:1508909. doi:10.3389/fimmu.2025.1508909

13. Pisareva E, Mihalovicova L, Pastor B, Kudriavtsev A, Mirandola A, Mazard T, et al. Neutrophil extracellular traps have auto-catabolic activity and produce mononucleosome-associated circulating DNA. *Genome Med* (2022) **14**:135. doi:10.1186/s13073-022-01125-8

14. Guliyeva V, Demirkan FG, Bektas E, Deniz R, Emrence Z, Akgun O, et al. NETs in the spotlight: exploring NETosis markers for tracking disease activity in IgA vasculitis. *Rheumatology* (2025) **64**:5509–17. doi:10.1093/rheumatology/keaf272

15. Jin Y, Dong X, Zhong W, Xu C, Lin S, Peng Y, et al. ATF3 restoration as a potential strategy in managing ulcerative colitis: implications from Sishen pill research. *Phytomedicine* (2025) **142**:156814. doi:10.1016/j.phymed.2025.156814

16. Hayden H, Klopf J, Ibrahim N, Knobl V, Sotir A, Mekis R, et al. Quantitation of oxidized nuclear and mitochondrial DNA in plasma samples of patients with abdominal aortic aneurysm. *Free Radical Biology and Medicine* (2023) **206**:94–105. doi:10.1016/j.freeradbiomed.2023.06.014

17. Brandau A, Ibrahim N, Klopf J, Hayden H, Ozsvar-Kozma M, Afonyushkin T, et al. Association of lipoproteins with neutrophil extracellular traps in patients with abdominal aortic aneurysm. *Biomedicines* (2022) **10**:217. doi:10.3390/biomedicines10020217

18. Eilenberg W, Zagrapan B, Bleichert S, Ibrahim N, Knobl V, Brandau A, et al. Histone citrullination as a novel biomarker and target to inhibit progression of abdominal aortic aneurysms. *Translational Research* (2021) **233**:32–46. doi:10.1016/j.trsl.2021.02.003

19. Spinosa M, Su G, Salmon MD, Lu G, Cullen JM, Fashandi AZ, et al. Resolvin D1 decreases abdominal aortic aneurysm formation by inhibiting NETosis in a mouse model. *J Vascular Surgery* (2018) **68**:93S–03. doi:10.1016/j.jvs.2018.05.253

20. Yan H, Zhou HF, Akk A, Hu Y, Springer LE, Ennis TL, et al. Neutrophil proteases promote experimental abdominal aortic aneurysm via extracellular trap release and plasmacytoid dendritic cell activation. *Arteriosclerosis, Thrombosis, Vascular Biology* (2016) **36**:1660–69. doi:10.1161/ATVBAHA.116.307786

21. Meher AK, Spinosa M, Davis JP, Pope N, Laubach VE, Su G, et al. Novel role of IL (Interleukin)-1beta in neutrophil extracellular trap formation and abdominal aortic aneurysms. *Arteriosclerosis, Thrombosis, Vascular Biology* (2018) **38**:843–53. doi:10.1161/ATVBAHA.117.309897

22. Mozzini C, Garbin U, Stranieri C, Salandini G, Pesce G, Fratta Pasini AM, et al. Nuclear factor kappa B in patients with a history of unstable angina: case re-opened. *Intern Emergency Medicine* (2018) **13**:699–07. doi:10.1007/s11739-018-1885-z

23. Griepke S, Grentzmann A, Tripodi GL, Hansen J, Fonseca MP, Nilsson MD, et al. Targeting the PDK/PDH axis modulates neutrophil and smooth muscle cell pathological responses and prevents abdominal aortic aneurysm formation. *Cardiovasc Research* (2025) **121**:1269–81. doi:10.1093/cvr/cvaf032

24. da Silva RF, Baptista D, Roth A, Miteva K, Burger F, Vuilleumier N, et al. Anti-apolipoprotein A-1 IgG influences neutrophil extracellular trap content at distinct regions of human carotid plaques. *Int Journal Molecular Sciences* (2020) **21**:7721. doi:10.3390/ijms21207721

25. Kopytek M, Kolasa-Trela R, Zabczyk M, Undas A, Natorska J. NETosis is associated with the severity of aortic stenosis: links with inflammation. *Int Journal Cardiology* (2019) **286**:121–26. doi:10.1016/j.ijcard.2019.03.047

26. Yang S, Chen L, Wang Z, Chen J, Ni Q, Guo X, et al. Neutrophil extracellular traps induce abdominal aortic aneurysm formation by promoting the synthetic and proinflammatory smooth muscle cell phenotype via Hippo-YAP pathway. *Translational Research* (2023) **255**:85–6. doi:10.1016/j.trsl.2022.11.010

27. Qi Y, Chen L, Ding S, Shen X, Wang Z, Qi H, et al. Neutrophil extracellular trap-induced ferroptosis promotes abdominal aortic aneurysm formation via SLC25A11-mediated depletion of mitochondrial glutathione. *Free Radical Biology and Medicine* (2024) **221**:215–24. doi:10.1016/j.freeradbiomed.2024.05.036

28. Chen L, Liu Y, Wang Z, Zhang L, Xu Y, Li Y, et al. Mesenchymal stem cell-derived extracellular vesicles protect against abdominal aortic aneurysm formation by inhibiting NET-induced ferroptosis. *Exp and Molecular Medicine* (2023) **55**:939–51. doi:10.1038/s12276-023-00986-2

29. Tian Z, Zhang Y, Zheng Z, Zhang M, Zhang T, Jin J, et al. Gut microbiome dysbiosis contributes to abdominal aortic aneurysm by promoting neutrophil extracellular trap formation. *Cell Host and Microbe* (2022) **30**:1450–63 e8. doi:10.1016/j.chom.2022.09.004

30. Nana P, Dakis K, Brodis A, Spanos K, Kouvelos G. Circulating biomarkers for the prediction of abdominal aortic aneurysm growth. *J Clinical Medicine* (2021) **10**:1718. doi:10.3390/jcm10081718

31. Wei M, Wang X, Song Y, Zhu D, Qi D, Jiao S, et al. Inhibition of peptidyl arginine deiminase 4-Dependent neutrophil extracellular trap formation reduces angiotensin II-Induced abdominal aortic aneurysm rupture in mice. *Front Cardiovascular Medicine* (2021) **8**:676612. doi:10.3389/fcvm.2021.676612

32. Xiong Y, Liu S, Liu Y, Zhao J, Sun J, Li Y, et al. PI3Kgamma promotes neutrophil extracellular trap formation by noncanonical pyroptosis in abdominal aortic aneurysm. *JCI Insight* (2024) **9**:e183237. doi:10.1172/jci.insight.183237

33. Wu C, Ren Y, Li Y, Cui Y, Zhang L, Zhang P, et al. Identification and experimental validation of NETosis-Mediated abdominal aortic aneurysm gene signature using multi-omics, machine learning, and Mendelian randomization. *J Chemical Information Modeling* (2025) **65**:3771–88. doi:10.1021/acs.jcim.4c02318

34. Ibrahim N, Bleichert S, Klopf J, Kurzreiter G, Hayden H, Knobl V, et al. Reducing abdominal aortic aneurysm progression by blocking neutrophil extracellular traps depends on thrombus formation. *JACC Basic Translational Science* (2024) **9**:342–60. doi:10.1016/j.jacbts.2023.11.003

35. Houard X, Touat Z, Ollivier V, Louedec L, Philippe M, Sebbag U, et al. Mediators of neutrophil recruitment in human abdominal aortic aneurysms. *Cardiovasc Research* (2009) **82**:532–41. doi:10.1093/cvr/cvp048

36. Cervantes-Luevano KE, Caronni N, Castiello MC, Fontana E, Piperno GM, Naseem A, et al. Neutrophils drive type I interferon production and autoantibodies in patients with Wiskott-Aldrich syndrome. *The J Allergy Clinical Immunology* (2018) **142**:1605–17 e4. doi:10.1016/j.jaci.2017.11.063

37. Wang H, Zhang R, Jia X, Gao S, Gao T, Fan K, et al. Highly sensitive magnetic particle imaging of abdominal aortic aneurysm NETosis with anti-Ly6G iron oxide nanoparticles. *Cell Death Discovery* (2024) **10**:395. doi:10.1038/s41420-024-02156-3

38. Hu K, Zhong L, Lin W, Zhao G, Pu W, Feng Z, et al. Pathogenesis-guided rational engineering of nanotherapies for the targeted treatment of abdominal aortic aneurysm by inhibiting neutrophilic inflammation. *ACS Nano* (2024) **18**:6650–72. doi:10.1021/acsnano.4c00120

39. Kinsella RL, Sur Chowdhury C, Smirnov A, Mreyoud Y, Kimmey JM, Esaulova E, et al. ATG5 suppresses type I IFN-dependent neutrophil effector functions during *Mycobacterium tuberculosis* infection in mice. *Nat Microbiology* (2025) **10**:1323–39. doi:10.1038/s41564-025-01988-8

40. Dinc R, Ardic N. Inhibition of neutrophil extracellular traps: a potential therapeutic strategy for hemorrhagic stroke. *J Integrative Neuroscience* (2025) **24**:26357. doi:10.31083/JIN26357

41. Wang Q, Ding Y, Song P, Zhu H, Okon I, Ding YN, et al. Tryptophan-derived 3-Hydroxyanthranilic acid contributes to angiotensin II-Induced abdominal aortic aneurysm formation in mice *in vivo*. *Circulation* (2017) **136**:2271–83. doi:10.1161/CIRCULATIONAHA.117.030972

42. Golledge J, Lu HS, Curci JA. Small AAAs: recommendations for rodent model research for the identification of novel therapeutics. *Arteriosclerosis, Thrombosis, Vascular Biology* (2024) **44**:1467–73. doi:10.1161/ATVBAHA.124.320823

43. Phillips EH, Lorch AH, Durkes AC, Goergen CJ. Early pathological characterization of murine dissecting abdominal aortic aneurysms. *APL Bioengineering* (2018) **2**:046106. doi:10.1063/1.5053708

44. Collins MS, Imbrogno MA, Kopras EJ, Howard JA, Zhang N, Kramer EL, et al. Heterogeneity in neutrophil extracellular traps from healthy human subjects. *Int Journal Molecular Sciences* (2023) **25**:525. doi:10.3390/ijms25010525

45. Nakazawa D, Masuda S, Nishibata Y, Watanabe-Kusunoki K, Tomaru U, Ishizu A. Neutrophils and NETs in kidney disease. *Nat Reviews Nephrol* (2025) **21**:383–98. doi:10.1038/s41581-025-00944-3

46. Hidalgo A, Libby P, Soehnlein O, Aramburu IV, Papayannopoulos V, Silvestre-Roig C. Neutrophil extracellular traps: from physiology to pathology. *Cardiovasc Research* (2022) **118**:2737–53. doi:10.1093/cvr/cvab329

EBM Experimental Biology and Medicine

TYPE Original Research
PUBLISHED 12 December 2025
DOI 10.3389/ebm.2025.10749

OPEN ACCESS

*CORRESPONDENCE
Hua Yue,
yuehua10288@outlook.com,
yuehua1028@sina.com

RECEIVED 14 July 2025
REVISED 08 October 2025
ACCEPTED 20 November 2025
PUBLISHED 12 December 2025

CITATION
Liu Y, Hussain SA and Yue H (2025) Protective effects of berberine-loaded chitosan/solid lipid nanoparticles in streptozotocin-induced gestational diabetes mellitus rats.
Exp. Biol. Med. 250:10749.
doi: 10.3389/ebm.2025.10749

Protective effects of berberine-loaded chitosan/solid lipid nanoparticles in streptozotocin-induced gestational diabetes mellitus rats

Yu Liu[1], Shaik Althaf Hussain[2] and Hua Yue [1]*

[1]Department of Obstetrics and Gynecology, XD Group Hospital, Xi'an, China, [2]Department of Zoology, College of Science, King Saud University, Riyadh, Saudi Arabia

Abstract

Berberine, known as an antioxidant agent, can improve glycemic indices in animal models of diabetes; however, it is clinically limited by poor bioavailability. Nanoparticles show the desirable capacity as delivery platforms for improving the bioavailability of medicinal agents. Here, we aimed to enhance the bioavailability and therapeutic impacts of berberine in streptozotocin (STZ)-induced gestational diabetes mellitus (GDM) rats by its encapsulation into the chitosan-coated solid lipid nanoparticles (SLNs) formulation. Berberine-loaded chitosan/SLN nanoparticles were formulated by the solvent-injection approach followed by a homogenization operation. The particle size, surface charge, and polydispersity index, as well as encapsulation efficiency percent (EE%), *in vitro* stability and berberine release, and *in vivo* pharmacokinetics were studied. Glycemic indices, such as fasting glucose and insulin, oral glucose tolerance, insulin tolerance, and homeostasis model of insulin resistance (HOMA-IR) scores, as well as the activity level of liver antioxidant and pro-oxidant enzymes, were evaluated in STZ-induced GDM rats. The particle size of berberine-loaded chitosan/SLN formulation was detected in the nano-range with high stability and high EE% as well as a sustained-release profile. Berberine nanoparticle treatment could provide a significantly higher oral bioavailability of berberine in experimental rats. Berberine nanoparticles remarkably reversed the altered glycemic indices, body weight, and pro-oxidant/antioxidant balance in STZ-induced GDM rats, with significantly higher effects than free berberine. In conclusion, chitosan-coated SLN nanoparticles firmly enhanced the therapeutic impacts of berberine on STZ-induced GDM, suggesting chitosan-coated SLN nanoparticles as an efficient oral delivery system for enhancing the bioavailability of berberine and, thus, improving its pharmacological impacts.

KEYWORDS

berberine, chitosan, gestational diabetes mellitus, rat, solid lipid nanoparticle

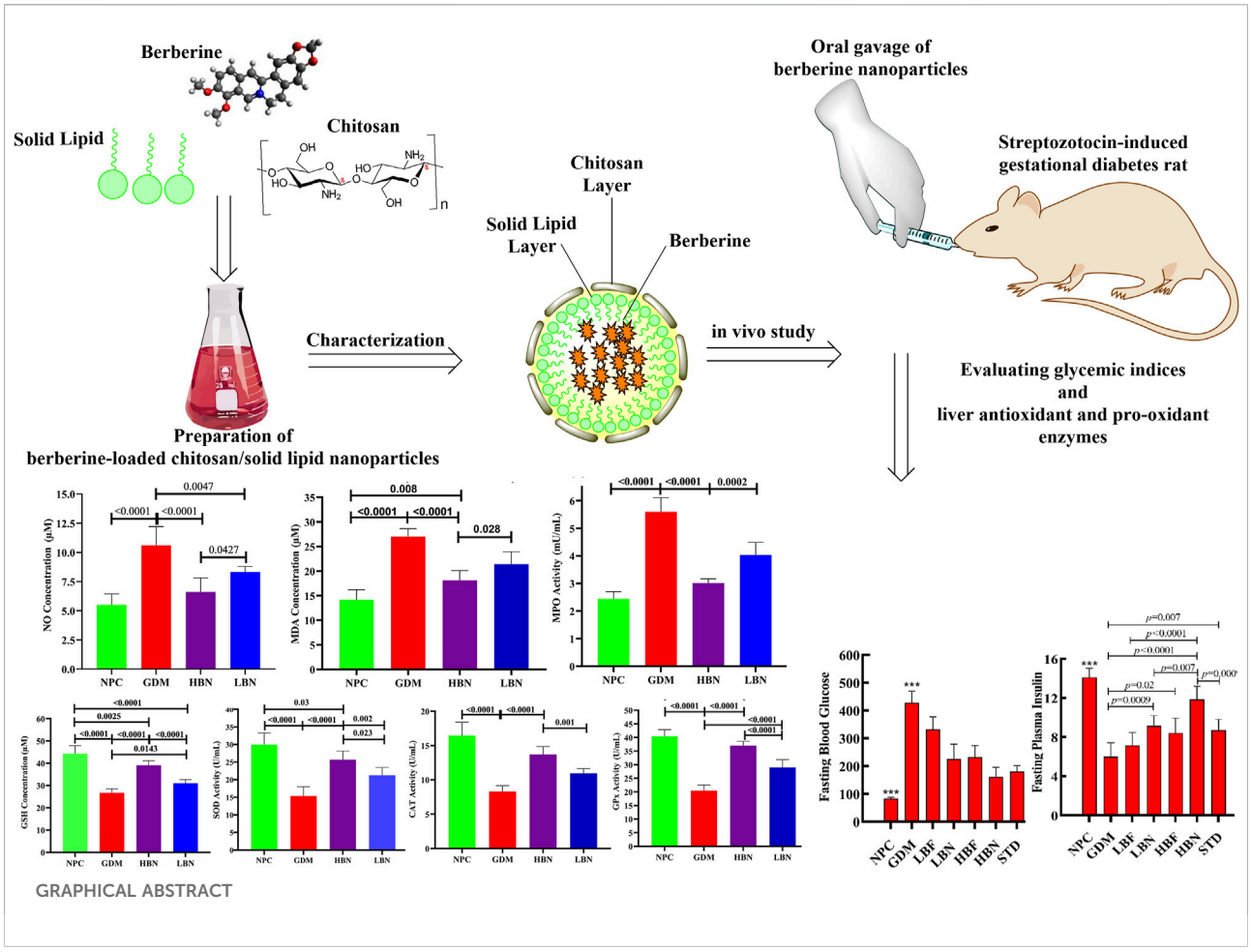

Impact statement

Chitosan-coated SLN nanoparticles provide an efficient oral delivery system to enhance oral bioavailability of berberine and, thus, improve its pharmacological impacts.

Introduction

Diabetes Mellitus is a chronic metabolic disease manifested via increased concentration of blood glucose through impaired glucose, protein, and lipid metabolism due to insulin deficiency, which can result from impaired production of insulin by the pancreas gland's Langerhans beta cells and/or result from insulin resistance by unresponsiveness of the body's cells to insulin. It is a leading cause of morbidity and mortality, particularly in pregnant women, termed gestational diabetes mellitus (GDM). GDM shows various degrees of glucose intolerance in pregnant women, leading to chronic hyperglycemia that causes long-term injuries, including the development of pre-eclampsia, gestational hypertension, liver damage, and kidney damage. The pathological feature of GDM, like type 2 diabetes mellitus (T2DM), is correlated with both defective insulin secretion and insulin resistance. Notably, normal pregnancy requires elevated glucose production and decreased insulin sensitivity to provide the energy required for the fetus; thus, there is an association between pregnancy and the progression of maternal insulin resistance [1]. During pregnancy, insulin resistance occurs because of the secretion of placental hormones that antagonize insulin. Therefore, during pregnancy, the body needs a high demand for insulin, which increases the load on the pancreatic β-cells, leading to β-cells exhaustion and consequently reduced insulin production [2]. Of note, oxidative stress, an imbalance between the body's antioxidant defense mechanisms and the generation of free radicals, is an important contributor to the development and pathogenesis of GDM during pregnancy. The increased level of glucose during the GDM condition leads to increased formation of highly toxic oxygen and hydroxyl free radicals through glucose metabolism, such as glucose auto-oxidation, metabolism of methylglyoxal formation, and oxidative phosphorylation [3]. Using antidiabetic drugs (mainly metformin) orally or insulin injection is the main

treatment in GDM. However, such treatments are expensive, and long-term use of antidiabetic medications can cause serious adverse impacts on the various organs. In addition, although the insulin therapy can control the blood glucose, it has no therapeutic impact on the function of β-cells and the insulin resistance [4]. On the other hand, targeting oxidative stress may inhibit the GDM-related pathogenesis, suggesting antioxidant agents as potential protective treatment against diabetes complications by reducing free radicals.

Berberine, as a plant-derived medicinal compound, is the major active ingredient detected in the stem, bark, roots, and rhizome of many plants, including barberry (Berberis vulgaris), tree turmeric (Berberis aristata), Oregon grape (Berberis aquifolium), Coptis (Coptis chinensis), and goldenseal (Hydrastis canadensis) [5]. Berberine is mainly known for its antioxidant property, through which it exerts protective impacts on various diseases in preclinical and clinical settings, such as diabetes, cancer, infection, and cardiovascular diseases [6–15]. An increasing body of research has recently shown that berberine can exert effective hypoglycemic activity and, thereby, provide an improving effect on diabetic complications, including diabetic cardiomyopathy, diabetic neuropathy, diabetic nephropathy, diabetic encephalopathy, as well as GDM [11, 16–22]. Interestingly, berberine is found to have a hypoglycemic impact similar to rosiglitazone and metformin in patients with T2DM [23, 24]. Several meta-analyses of clinical trials in T2DM patients revealed that berberine has good safety and a low incidence of total adverse events, and berberine administered alone or in combination with oral hypoglycemic drugs is effective in the treatment of T2DM patients and firmly regulates postprandial blood glucose, fasting blood glucose, and HbA1c [11, 18–20]. Several preclinical investigations have recently shown potential of berberine in the GDM treatment, where it was found to improve glucose tolerance, insulin response, body and fetal weight, placental weight, as well as the number of dead and absorptive fetuses in the experimental models of GDM [21, 25–28]. *B*erberine has been found to exert the glucose-lowering impact by multiple mechanisms, such as elevating glucose uptake, inhibiting gluconeogenesis, enhancing glycolysis, improving insulin secretion and insulin response, and suppressing the action of important enzymes involved in the carbohydrate digestion in the digestive tract (such as α-glucosidase and α-amylase), and improving the anti-oxidant and anti-inflammatory responses [18, 29, 30]. Although berberine has shown a wide range of therapeutic benefits, its oral use is clinically limited because of poor aqueous solubility and intestinal absorption, rapid metabolism by the first-pass effect in the liver and intestine, as well as short biological half-life, which cause low blood concentrations and poor bioavailability. In addition, berberine at high doses causes gastrointestinal side effects, such as cramping and stomach upset, because of its low intestinal absorption and long-term administration [31–33]. Therefore, manufacturing a delivery system to provide a sustained release of berberine is required to improve its bioavailability by reducing the dissolution rate in the gastric environment and increasing the residence time in the intestinal mucus.

Solid lipid nanoparticles (SLNs) have been used as a delivery system to enhance the bioavailability and therapeutic efficiency of natural compounds [34]. In recent years, SLNs have received a significant considerable attention because of their interesting advantages, such as low toxicity and immunogenicity, increasing solubility and bioavailability of both hydrophobic and hydrophilic drugs, triggering pharmacological property of drugs, protecting the drugs against digestive enzymes, having excellent biodegradability and biocompatibility, as well as providing an easy and low-price formulation [35]. The important criteria impacting the *in vivo* efficacy of the oral drug delivery formulations are their integrity and stability in gastrointestinal media. Despite a high stability against digestive enzymes, the low stability of SLNs in the stomach's acidic pH limits their clinical utilization. For resolving this issue, coating of SLNs by the biopolymers, such as chitosan, with a significant resistance to the acidic media and a high mucoadhesive property, has been employed [36]. Chitosan is a chitin-derived cationic polysaccharide that, under acidic pH, is protonated and strongly binds to the negatively charged SLNs, thereby providing a stable delivery system with the ability to sustainably release an encapsulated drug [37]. Further, when chitosan is coated on the nanoparticle surface, it can improve the absorption of encapsulated drugs via a mucosal surface [38]. Therefore, formulating SLNs with chitosan can protect them against the acidic gastrointestinal medium and enhance their transmucosal delivery, consequently increasing the effective concentration of encapsulated drugs at the absorption site. Of note, chitosan-coated SLN nanoparticles have been found to remarkably improve the oral bioavailability of numerous encapsulated drugs *in vivo* by elevating residence time at mucosa due to their enhanced mucoadhesive property [37, 39–41]. Here, we aimed to bring together biological properties of SLNs and chitosan to manufacture a nanoparticle-based carrier system for oral delivery of berberine, and to determine ameliorating impact of the prepared berberine-loaded nanoparticles on glycemic indices and prooxidant/antioxidant balance in streptozotocin (STZ)-induced GDM rats.

Materials and methods

Manufacturing berberine-loaded chitosan/SLN nanoparticles

Berberine-loaded chitosan/SLN nanoformulation was prepared using a previously described solvent-injection

method [42] followed by a high-pressure homogenization process [43]. Briefly, berberine (50 mg) and the solid lipid Witepsol 85E (40 mg) were dissolved at 75 °C in 1 mL of a mixed solution (acetone and ethanol in an equal ratio (1:1 v/v)) until a homogenous dispersion appeared. To construct berberine-loaded chitosan-coated SLN nanoparticles, prepared solid lipid/berberine mix was injected into hot double-distilled water (75 °C) containing chitosan (0.5 mg/mL) and a stabilizing surfactant (Pluronic, 2.5 mg/mL). The prepared solution was emulsified by high agitation (25,000 rpm for 4 min at 70 °C) and then homogenized at the same temperature through employing nine homogenization cycles at 750 bars by a high-pressure homogenizer. Immediately after homogenization, the obtained suspension was cooled in an ice-water bath to keep the structure of berberine-loaded chitosan/SLN nanoparticles stable. Finally, the prepared nanoformulation was filtered by a 400 nm filter and then freeze-dried.

Characterization of the manufactured berberine nano-formulation

Physiochemical analysis

Physicochemical indexes of the constructed nanoformulation were studied by measuring the particle size (Z-average diameter), zeta potential (surface charge), and polydispersity index (PDI) by a dynamic light scattering instrument (Zetasizer, UK) at 25 °C.

Encapsulation efficiency

To measure the amount of berberine entrapment in the chitosan-coated SLN nano-formulation, the encapsulation efficiency (EE) percentage was evaluated by determining the unloaded (free) berberine concentration through the centrifugal ultrafiltration method, followed by the high-performance liquid chromatography (HPLC) technique. To isolate free berberine, the berberine-loaded SLN/chitosan nano-formulation was centrifuged for 30 min at 23,000 rpm and 4 °C. Afterward, the free berberine amount in the liquid supernatant was determined via HPLC on a Shimadzu system (CBM 20A) equipped with a C18 reverse-phase column (4.6 mm × 25 cm) and a multi-channel UV–VIS detector. To determine the concentration of berberine in the test samples, the HPLC standard curve was made based on the standard solutions containing known concentrations of berberine. Eventually, the nanoparticle EE (%) was determined from the amount of entrapped berberine to the primary loaded berberine. The entrapped concentration of berberine was measured by subtracting berberine amount detected by HPLC from the initially added amount of berberine. The following equation was used to calculate EE (%) [44]: EE (%) = $(C_0 - C)/C_0 \times 100\%$, where C_0 is the amount of berberine primary loaded into nano-formulation, and C is the amount of free berberine.

In vitro stability

The stability of berberine-loaded chitosan/SLN nanoparticles was determined within the simulated gastric fluid (SGF, pH 1.5) and simulated intestinal fluid (SIF, pH 6.8). Nanoparticles were loaded into the SGF and SIF, and then incubated at 37 °C for 2 and 6 h, respectively. Such time intervals were used in accordance with the predicted homing times in the intestine and stomach. Particle size and EE% were evaluated during these time periods.

The SGF medium was prepared by dissolving 2 g/L of sodium chloride NaCl and 3.2 g/L pepsin in deionized water and then adjusting the pH to 1.5 ± 0.2 with 1 M hydrochloric acid (HCl). The SIF medium was prepared by dissolving 6.8 g/L of potassium phosphate monobasic (KH2PO4), 10 g/L of sodium dodecyl sulfate (SDS), and 8400 U/L of 8400 U/L in deionized water and then pH adjusted to 6.8 ± 0.2 with 1 N sodium hydroxide (NaOH) solution [45].

In vitro drug release

In vitro drug release was performed in the SGF and SIF media to simulate the physiological status through oral use. Berberine-loaded chitosan/SLN nanoparticles were incubated at 37 °C through constant shaking (100 rpm) with the SGF or SIF in micro-centrifuge tubes, individually. Nanoparticles were separated through ultrafiltration-centrifugation by Millipore tubes (MWCO = 5 kDa). Eventually, the filtered nanoparticle formulation was analyzed to determine the concentration of berberine by the previously explained HPLC method [46]. The cumulative release calculation method involved determining the percentage of berberine released over time from the nanoformulation, using the following formula [47]:

$$\text{Cumulative percentage release (\%)} = \frac{\text{Volume of sample withdrawn (ml)}}{\text{Bath volume (v)}} \times P\,(t-1) + Pt$$

Where Pt = percentage release at time "t" and P (t – 1) = percentage release previous to "t."

In vivo pharmacokinetic study

Berberine-loaded chitosan/SLN nanoparticles and free berberine were gavaged (50 mg/kg) in two groups (n = 10 rats per group) of female Wistar-Albino rats. Tail vein blood samples were collected and moved into K_3EDTA tubes at the following times: 0.5, 1, 2, 4, 8, 12, 18, and 24-h after dosing. The plasma was then separated from the blood samples by centrifuging at 3000 rpm for 8 min at 4 °C, and stored in 1.5 mL tubes at −20 °C. Pharmacokinetic parameters, including the area under the berberine plasma versus time curve (AUC), the maximum plasma concentration of berberine after oral administration (C_{max}), and the time to maximum plasma concentration of berberine (T_{max}), were measured via HPLC analysis of plasma samples [48].

Gestational rats

Forty-nine female (180 ± 10 g) and seven male (230 ± 10 g) Wistar-Albino rats (8–10 weeks old) were obtained from the laboratory animal research center of the College of Science, King Saud University, Saudi Arabia. All animal experiments were performed in full accordance with the Animal Welfare instructions approved by the Institutional Ethics Committee and Research Advisory Committee of the King Saud University, Saudi Arabia (No.: A2025000127). All animals were housed in a specific pathogen-free environment in positive pressure rooms at a constant temperature of 22 ± 2 °C and relative humidity of 50–70% with a standard 12/12-h day-night cycle and fed a standard rodent diet and water *ad libitum*. Every possible attempt or action was taken to achieve the lowest suffering. The animals were kept in the laboratory for 1 week to acclimate to the conditions. After acclimatization, vaginal smears were carried out every day to determine the rats' oestrous cycle, and female rats in the oestrous stage were allowed to mate with male rats by housing them at a 1:1 ratio in individual cages. The next morning, pregnancy in female rats was confirmed by the appearance of sperm in the vagina or by a copulatory plug observed using a microscope, and this day was marked as gestational day (GD) 0 [49].

Induction of gestational diabetes mellitus

After pregnancy confirmation (GD0), a single dose (50 mg/kg) of streptozotocin (STZ; Sigma–Aldrich) was intraperitoneally injected in the overnight fasted pregnant rats to induce GDM [50]. A group of pregnant rats were intraperitoneally injected with citrate buffer lacking STZ, termed the non-diabetic group. On the fourth day after STZ adminstration, fasting blood glucose (FBG) levels were quantified through the tail incision method with the glucometer (Roche Diagnostic), and pregnant rats suffering blood glucose concentrations more than 180 mg/dL were considered as GDM rats and subjected to further studies. Blood was collected in serum-free tubes through retro-orbital sinus bleeding.

Experimental design

The experimental study was carried out in seven groups, consisting of seven pregnant rats in each group, allocated by a blinded randomization. Normal Pregnant Control (NPC) group: non-diabetic pregnant rats orally gavaged with SLN/chitosan nanoparticles. Gestational Diabetes Mellitus (GDM) group: GDM rats orally gavaged with SLN/chitosan nanoparticles. LBN group: GDM rats orally gavaged with a Low dose of Berberine Nanoparticles (25 mg/kg/day, LBN). HBN group: GDM rats orally gavaged with a High dose of Berberine Nanoparticles (50 mg/kg/day, HBN). LBF group; GDM rats orally gavaged with a Low dose of Free-Berberine (25 mg/kg/day, LBF). HBF group: GDM rats orally gavaged with a High dose of Free-Berberine (50 mg/kg/day, HBF). Standard (STD) group: GDM rats orally gavaged by metformin (200 mg/kg/day). Berberine-loaded SLN/chitosan nanoformulation was administered to rats by oral gavage once per day from GD4 to GD18. Treatment doses and sample size were used in accordance with already published studies [51–55]. At the final day of the study, the rats were euthanized via intraperitoneal (i.p.) administration of thiopental sodium (30 mg/kg) [56, 57], and the liver tissue was isolated and stored at low temperature (−80 °C) for further experiments.

Body weight, fasting glucose and insulin, and HOMA-IR

Body weight, as well as the blood glucose level and the serum insulin concentration, were assayed on GD0, GD4, and GD18 after overnight fasting. The body weight of rats was measured by a top loader balance (Thermo Fisher Scientific, Inc.). The FBG level was quantified through the tail incision method with the glucometer (Roche Diagnostics). To measure the fasting insulin levels, the blood samples were obtained from the orbital venous plexus, and plasma samples were isolated by centrifugation at 12,000 rpm for 10 min at 4 °C. The level of fasting insulin was quantified in plasma samples by a rat insulin enzyme-linked immunosorbent assay (ELISA) kit (Termo Scientific). To estimate insulin resistance, the Homeostasis Model of Insulin Resistance (HOMA-IR) was measured by the following formula: HOMA-IR = (Fasting glucose × Fasting insulin)/405. The two main pathophysiological mechanisms of HOMA-IR are insulin resistance and pancreatic cell dysfunction due to insulin resistance [58].

Oral glucose tolerance test

The oral glucose tolerance test (OGTT) was employed to evaluate glucose tolerance in overnight fasted rats orally given glucose (2 g/kg) 2 weeks after treatment (G18). In brief, glucose solution was orally administered, and the blood level of glucose was detected before and 30, 60, 90, and 120 min after glucose gavage [59]. Data were analyzed as the integrated area under the curve for glucose ($AUC_{glucose}$) and calculated by the trapezoid rule by GraphPad Prism version 9.

Insulin tolerance test

The insulin tolerance test (ITT) was carried out to evaluate insulin response, reflecting a value of peripheral usage of the blood glucose. After 2 weeks of treatment (G19), insulin (0.8 U/kg, i.p.) was injected to overnight fasted rats. The blood level of glucose was assessed before insulin administration (0 min) and at 30, 60, 90, and 120 min following insulin administration [60]. Results were expressed as $AUC_{glucose}$.

TABLE 1 *In vitro* stability of berberine-loaded chitosan/SLN nanoparticles in SGF and SIF media.

Medium	Particle size (nm)			Encapsulation efficiency (%)		
	Pre-incubation	Post-incubation	*p*-value	Pre-incubation	Post-incubation	*p*-value
SGF (pH 1.5)	295 ± 12	267.4 ± 15	0.06	88.2 ± 2.4	63.9 ± 8	0.054
SIF (pH 6.8)	295 ± 12	279.5 ± 19	0.2	88.2 ± 2.4	72.7 ± 6	0.07

Hepatic oxidative stress

At the end of the study, the liver tissue was isolated and homogenized at 4 °C in the saline solution (50 mM potassium phosphate, pH 7.0, containing 1 mM EDTA) and centrifuged at 10,000 *g* for 15 min at 4 °C. Afterward, the upper layer of the centrifuged solution was collected for assaying the hepatic status of oxidative stress parameters including super oxide dismutase (SOD; as an antioxidant catalyzing degradation of superoxide radicals into hydrogen peroxide (H_2O_2) and O_2, catalase (CAT; as an antioxidant catalyzing degradation of H_2O_2 into H_2O and O_2), glutathione (GSH; as an antioxidant scavenging ROS), glutathione peroxidase (GPx; as an antioxidant using GSH as a cofactor to convert hydrogen peroxide and organic hydroperoxides to water and alcohol), malonaldehyde (MDA; as a biomarker of oxidative stress indicating lipid peroxidation), myeloperoxidase (MPO; as an oxidative stress biomarker reflecting liver injury), and nitric oxide (NO; as a biomarker of oxidative stress indicating liver injury), by commercial kits (Cayman Chemical Company, USA) according to the manufacturer's protocols.

Statistical analysis

The normality testing (Shapiro-Wilk and Kolmogorov-Smirnov) showed the normal distribution of data and, thus, data were expressed as the mean ± standard deviation (SD). The between-groups significant differences were determined by the unpaired t-test or one-way ANOVA and Tukey-Kramer post-hoc multiple comparison tests (GraphPad Prism software, version 9, San Diego, CA). Data with $p < 0.05$ were statistically considered significant. Data were analyzed by a blinded approach.

Results

Physicochemical properties of berberine nanoparticles

The particle size analysis of Berberine-loaded chitosan/SLN nanoparticles showed a considerably narrow particle size and a notably narrow distribution width, verifying a significant dispersion quality. The prepared nanoparticles exhibited average size, surface charge, and PDI of 295 ± 12 nm, +38 ± 1.1 mV, and 0.19 ± 0.09, respectively. Of note, the PDI values < 0.3 confirm a narrow distribution of mean diameter [61]. The surface charge values allow for the prediction of the storage stability of nanoparticles; there are repulsive forces between charged particles, which prevent particle contact and agglomeration. Consequently, charged particles exhibit lower aggregation than neutral particles. The positive surface charge of Berberine-loaded SLN/chitosan nanoparticles is due to the presence of the protonated amino groups in chitosan polymer, which is suitable for obtaining a stable formulation. Additionally, the positive surface charge also confirmed surface coating of the SLN layer by the chitosan polymer. Further, EE% of berberine by chitosan-coated SLN nanoparticles was found to be 88.2 ± 2.4%, and a final lipid-to-drug ratio of 1:0.9.

In vitro stability of berberine nanoparticles

The stability of berberine-loaded chitosan/SLN nanoparticles was evaluated in SGF and SIF media, *in vitro*. As stated in Table 1, the prepared nanoparticles showed a notable stability in SGF and SIF. It can be attributed to the protective effect of multilayer coatings by SLN and chitosan; the SLN component protects nanoparticles against gastrointestinal digestive enzymes, and chitosan can protect the particle stability and integrity against acidic pH. Therefore, SLN and chitosan layers can protect nanoparticles from a harsh gastrointestinal environment, ensuring the robustness and stability of the prepared nanoformulation.

In vitro drug release of berberine nanoparticles

The *in vitro* release experiment was carried out in SIF (pH 6.8) and SGF (pH 1.5) media simulating *in vivo* physiological status. Figure 1A shows the profile of berberine release from chitosan-coated SLN nanoparticles in SIF and SGF media. Notably, berberine loaded in chitosan/SLN

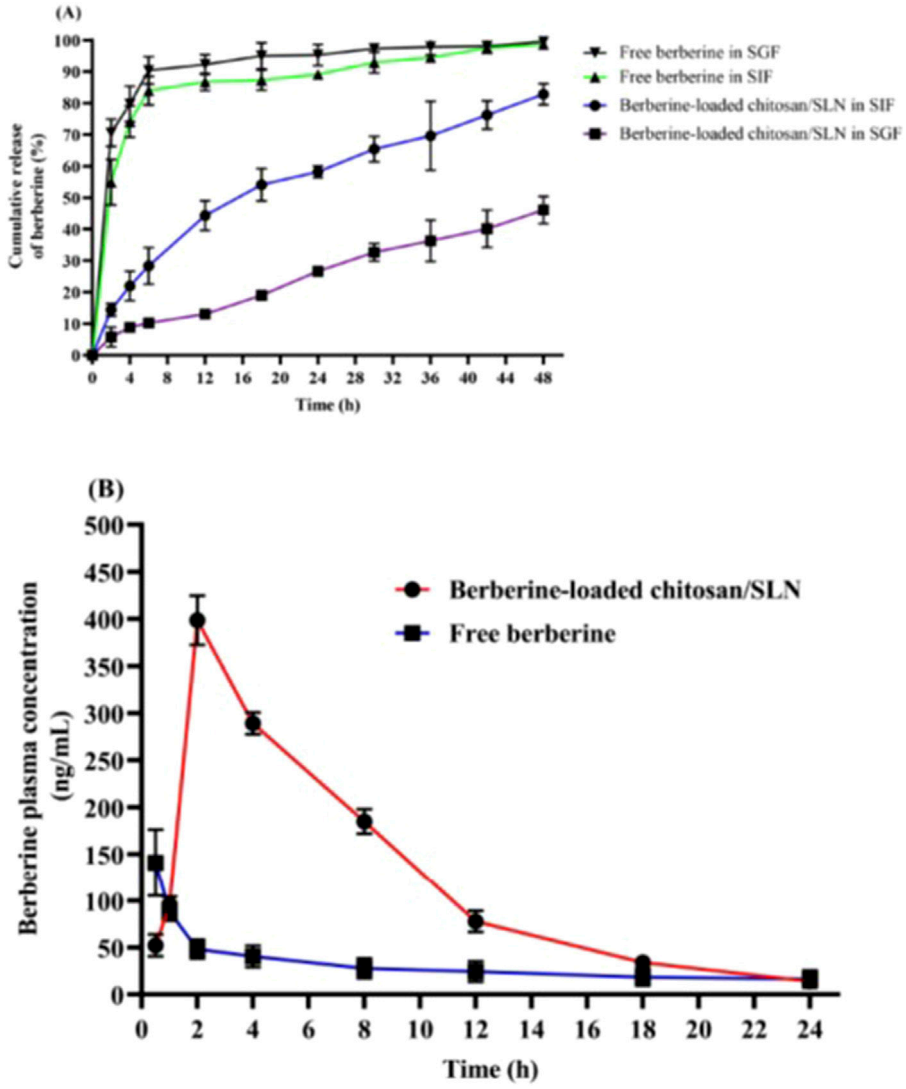

FIGURE 1
(A) *In vitro* release profiles of free berberine and Berberine-loaded chitosan/SLN nanoparticles in simulated gastric fluid (SGF, pH 1.5) and simulated intestinal fluid (SIF, pH 6.8) media. The data are represented as the mean ± SD (n = 3). **(B)** The plasma profile of berberine versus time after oral gavage of free berberine and Berberine-loaded chitosan/SLN nanoparticles in rats. The data are represented as the mean ± SD (n = 10).

nanoparticles demonstrated a much slower cumulative release than free-berberine, suggesting the effective protective effect of nanoparticles on berberine against the gastrointestinal harsh acidic environment. The release rates of berberine from chitosan/SLNs nanoparticles were found to be 82.9% ± 3.3 and 46.1% ± 4.3 after 48 h in SIF and SGF media, respectively. The release profile of berberine showed a biphasic pattern during 48 h, including an initiating phase by an early burst release pattern and a late phase by a sustained release pattern. The presence of chitosan is suitable for much slower release rates [62]. Slow releases of Berberine-loaded chitosan/SLN nanoparticles in the SIF and SGF fluids suggest that an adequately high concentration of berberine can be absorbed via the small intestine. Therefore, chitosan/SLN nanoparticles are able to endow a long-acting and effective carrier system for enhancing the intestinal absorption of orally administered berberine.

In vivo pharmacokinetic study

Figure 1B shows increased blood levels of berberine 24 h after oral gavage of berberine-loaded chitosan/SLN nanoparticles. Pharmacokinetic values of Berberine-loaded chitosan/SLN

TABLE 2 Pharmacokinetic parameters of berberine-loaded chitosan/SLN nanoparticles and free berberine in rats after a single oral dose administration.

Parameter	Unit	Berberine nanoparticles	Free berberine	*p*-value
Dose	mg/kg	50	50	
C_{max}	ng/mL	399 ± 26	141 ± 35	<0.0001
T_{max}	h	2	0.5	
AUC	ng/h/mL	2,926 ± 75	692 ± 74	<0.0001
BA_R	-	-	2.8-fold	

AUC, area under the berberine plasma concentration-time curve; BA_R, the relative bioavailability of oral administration of berberine-loaded chitosan/SLN nanoparticles compared with the pure berberine suspension; C_{max}, the maximum plasma concentration of berberine after oral administration; T_{max}, the time to maximum plasma concentration of berberine.

nanoparticles detected in the treated rats are summarized in Table 2. The T_{max} and C_{max} of Berberine-loaded chitosan/SLN nanoparticles were found to be 2 h and 399 ± 26 ng/mL, respectively, whereas significantly lower T_{max} (0.5 h) and C_{max} (141 ± 35 ng/mL) were detected with free berberine. A higher AUC was achieved with Berberine-loaded chitosan/SLN nanoparticles (2,926 ± 75 ng/h/mL) as compared with free berberine (692 ± 74 ng/h/mL). Of note, relative bioavailability exhibited a 2.8-fold increase in the berberine nanoparticle group when compared with the free berberine group. The delayed T_{max} in the berberine nanoparticle group confirmed the sustained berberine release *in vivo*, which is consistent with the *in vitro* release profile results.

Berberine nanoparticles inhibit body weight reduction in the GDM rats

The body weight reduction is a major diabetic complication, and is known as an important parameter to estimate diabetes. The body weight of rats before pregnancy (GD0) and after 2 weeks of treatment (GD18) was measured (Figure 2A). The body weight showed no significant difference between all groups of rats before pregnancy at GD0. All group rats showed significant body weight elevation ($p < 0.0001$) at GD18 compared to the initial body weight at GD0. The GDM rats demonstrated a significant body weight reduction ($p < 0.0001$) compared to the NPC group and treatment groups at GD18. GDM rats treated with the low and high doses of berberine nano-formulations (LBN and HBN groups) and of free-berberine (LBF and HBF) demonstrated a significant dose-dependent body weight elevation ($p < 0.0001$) by (65.7 ± 3.6 g and 79.6 ± 4.6 g) and (40.3 ± 3.3 g and 42.6 ± 3.3 g), respectively, compared with the GDM group at GD18. Of note, the body weight showed no significant ($p = 0.7$) difference between the HBN group (295 ± 10.5 g) and the metformin-treated (STD) group (301.6 ± 11 g) at GD18. In addition, there was a significant ($p = 0.01$), but low difference (19 ± 4.6 g) between the body weight of the HBN group (295 ± 10.5 g) and the NPC group (314 ± 6 g) at GD18.

Berberine nanoparticles improve fasting glucose and insulin in the GDM rats

The changes in the FBG levels are shown in Figure 2B. Four days after STZ injection (GD4), the FBG assessing showed that STZ-injected pregnant rats subjected to a remarkable ($p < 0.0001$) hyperglycemia (482 ± 63 mg/dL) at GD4 as compared with the NPC group (83 ± 5 mg/dL), verifying STZ-induced GDM. The FBG concentration was remarkably elevated in the GDM group at GD18 as compared with the NPC group ($p < 0.0001$). However, the FBG level in the LBN (225 ± 54 mg/dL), HBN (161 ± 35 mg/dL), LBF (332 ± 45 mg/dL), and HBF (232 ± 42 mg/dL) groups was remarkably reduced by 203 ± 26 mg/dL ($p < 0.0001$), 267 ± 20 mg/dL ($p < 0.0001$), 95 ± 23 mg/dL ($p = 0.007$), and 195 ± 22 mg/dL ($p < 0.0001$), respectively, as compared with the GMD group at GD18.

The level of fasting plasma insulin was significantly improved in the GDM rats treated with berberine nano-formulation and free-berberine at GD18 (Figure 2C). The fasting insulin level in the NPC group remained stable at GD0, GD4, and GD18, and it was significantly ($p < 0.0001$) decreased in the GDM group at GD4 and GD18 by 6.5 ± 0.7 U/mL and 8.2 ± 0.7 U/mL, respectively, as compared with the NPC group. Of note, the level of fasting insulin in the LBN (9.2 ± 1 U/mL), HBN (11.8 ± 1.3 U/mL), and HBF (8.5 ± 1.5 U/mL) groups was significantly increased by 3.14 ± 0.67 U/mL ($p = 0.0009$), 5.9 ± 0.7 U/mL ($p < 0.0001$), and 2.5 ± 0.8 U/mL ($p = 0.02$), respectively, at GD18 as compared with the GMD group (6.0 ± 1.4 U/mL). Fasting level of insulin (7.1 ± 1.3 U/mL) was non-significantly increased by 1.14 ± 0.7 U/mL ($p = 0.47$) in the LBF group at GD18 as compared with the GMD group.

As shown in Figure 2D, the HOMA-IR score was significantly elevated by 2-fold ($p = 0.002$) and 1.2-fold ($p = 0.007$) in the GDM group at GD4 and GD18, respectively, as compared with the NPC group, whereas it was reduced significantly in the HBN group by 0.38-fold ($p = 0.04$) and non-significantly in the LBN, LBF, and HBF groups by 0.2-fold ($p = 0.4$), 0.07-fold ($p = 0.1$), and 0.26-fold ($p = 0.17$), respectively, at GD18 as compared with the GMD group. Furthermore, treatment with the high-dose berberine nano-formulation could improve the FBG, fasting plasma insulin, and

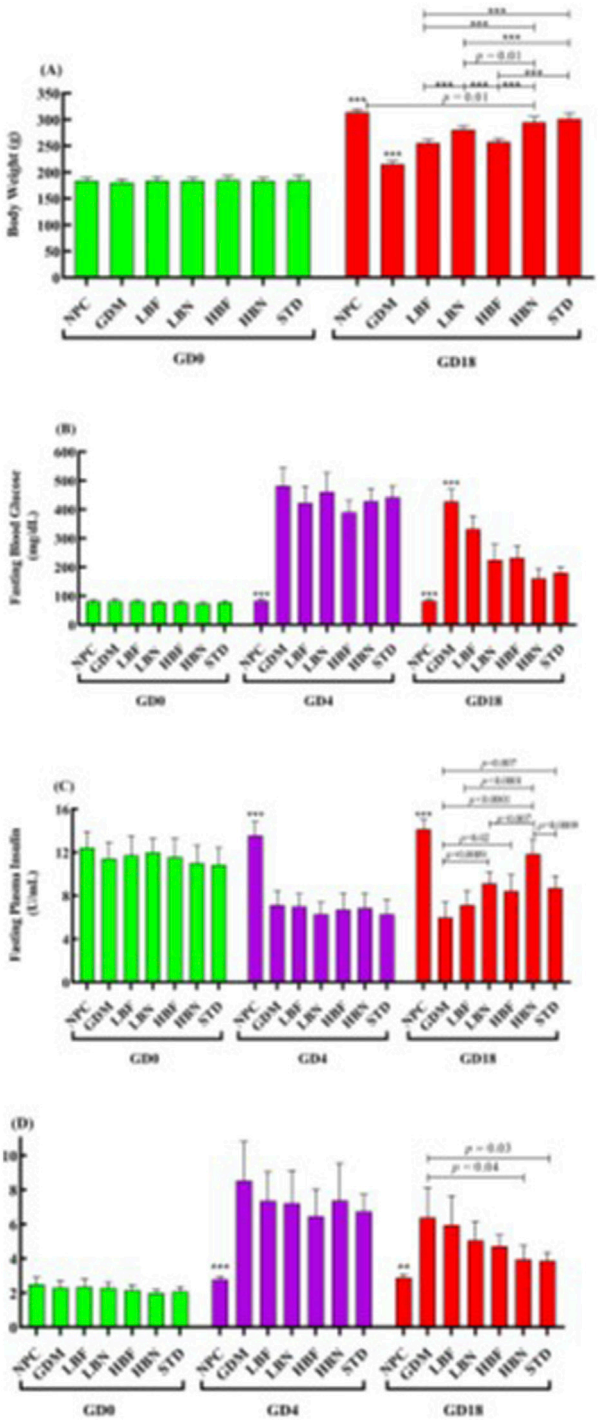

FIGURE 2
Body weight of rats before pregnancy (GD0) and after 2 weeks treatment (GD18) in the normal pregnant control (NPC) group, gestational diabetes mellitus (GDM) group, GDM rats received a low dose of berberine nanoparticles (the LBN group, 25 mg/kg/day), GDM rats received a high dose of berberine nanoparticles (the HBN group, 50 mg/kg/day), GDM rats received a low dose of free-berberine (the LBF group, 25 mg/kg/day), GDM rats received a high dose of free-berberine (the HBF group, (*Continued*)

FIGURE 2 (Continued)
50 mg/kg/day), and the standard (STD) group including GDM rats received metformin (200 mg/kg/day) **(A)**. Levels of fasting blood glucose **(B)** and fasting plasma insulin **(C)** in NPC, GDM, LBN, HBN, LBF, HBF, and STD groups at GD0, 4 days after STZ injection (GD4), and GD18 **(D)**. The scores of Homeostasis Model of Insulin Resistance (HOMA-IR) in the NPC, GDM, LBN, HBN, LBF, HBF, and STD groups at GD0, GD4, and GD18. Data are represented as the mean ± SD (n = 7). ** and *** indicate $p < 0.001$ and $p < 0.0001$, respectively, for the NPC group or the GDM group when compared with other groups.

HOMA-IR score in the HBN group close to those in the STD group treated with metformin.

Berberine nanoparticles improve glucose tolerance in the GDM rats

To determine glucose tolerance in the treated GDM rats, an OGTT over 120 min was carried out after 2 weeks of treatment (GD18). 30 min after oral gavage of glucose, a remarkable elevation in the level of blood glucose was detected in the GDM rats compared with NPC rats, indicating a significantly impaired tolerance to exogenously administered glucose. Glucose tolerance ability was remarkably enhanced in the treated GDM rats compared to the untreated GDM rats. A significant reduction in glucose levels was detected after 30 min toward baseline at time 120 in the treated GDM rats (LBN and HBN groups), whereas a consistently high concentration of glucose was found during 30–120 min in the GDM rats. In addition, the blood level of glucose slowly decreased after 30 min in the LBF and HBF groups; however, it did not reach the baseline level at 120 min (Figure 3A).

$AUC_{glucose}$ scores over 120 min of treated GDM rats and GDM rats were remarkably ($p < 0.0001$) higher than NPC rats. Notably, analyzing $AUC_{glucose}$ scores indicated that blood levels of glucose in the different groups of treated GDM rats, including the LBN, HBN, LBF, and HBF groups, were significantly ($p < 0.0001$) reduced up to 37%, 42%, 24%, and 30%, respectively, compared with the GDM group. As the positive control, metformin reduced AUC values up to 57% in the STD group (Figure 3B).

Berberine nanoparticles improve insulin response in the GDM rats

To evaluate insulin response in the treated GDM rats, the insulin challenge (0.8 U/kg, i.p.) was conducted at GD19. The blood glucose levels and $AUC_{glucose}$ were significantly ($p < 0.0001$) higher at various time points after the insulin injection in the GDM group compared with the NPC group, showing a

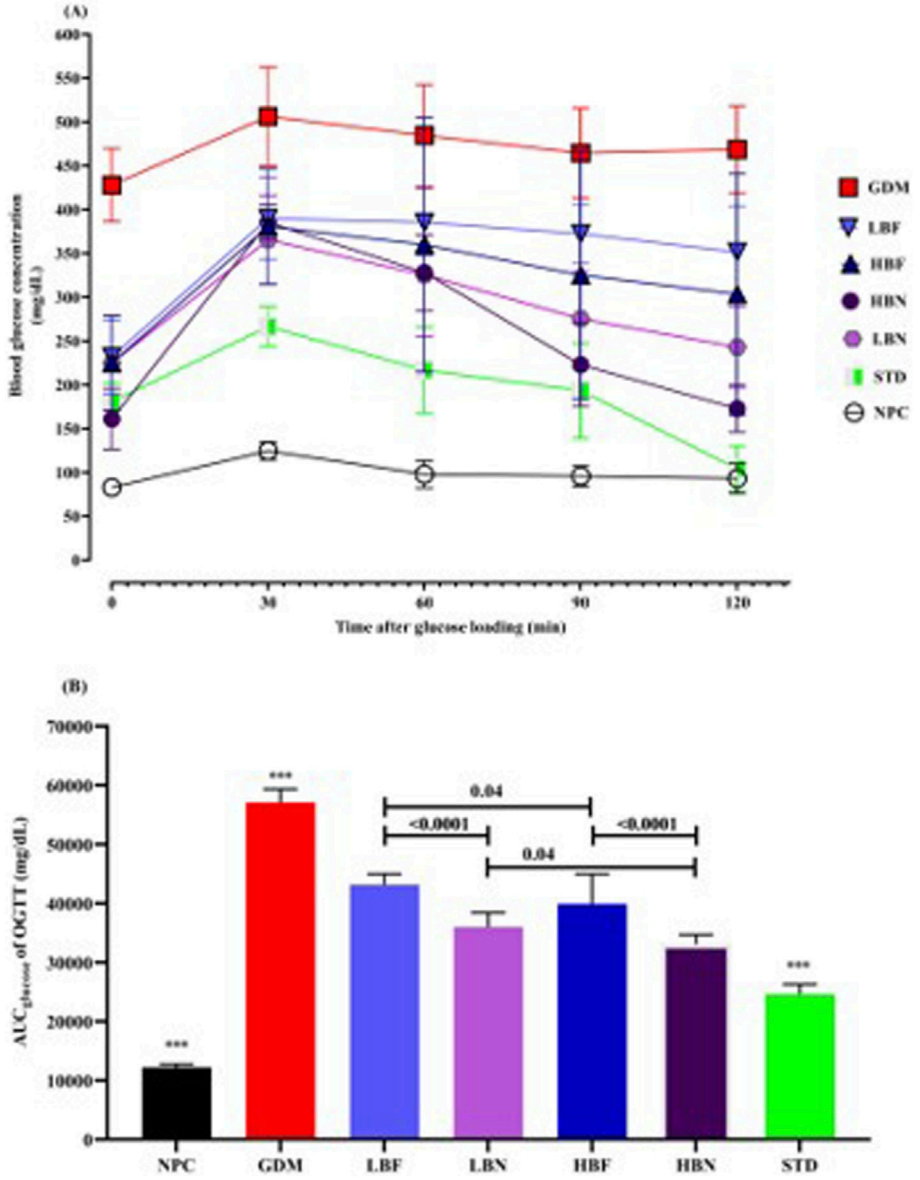

FIGURE 3
Oral glucose tolerance test **(A)** and corresponding areas under the glucose curve ($AUC_{glucose}$) **(B)** over 120 min after the oral glucose was fed in the NPC, GDM, LBN, HBN, LBF, HBF, and STD groups at GD18. Data are represented as the mean ± SD (n = 7). *** indicates $p < 0.0001$ for NPC group, GDM group, or STD group when compared with treatment groups.

remarkably impaired insulin response in the GDM rats. The insulin response ability was significantly enhanced in the treated GDM rats compared to GDM rats. The blood levels of glucose and $AUC_{glucose}$ were lower during ITT in treated GDM rats than in GDM rats (Figure 4). As compared to the GDM group, $AUC_{glucose}$ values in different groups of treated GDM rats, including the LBN, HBN, LBF, and HBF groups, demonstrated significant ($p < 0.0001$) reduction by 52%, 66%, 25%, and 44%, respectively. In addition, $AUC_{glucose}$ values were found to be significantly decreased by 73% ($p < 0.0001$) in the STD group treated with metformin, when compared with the GDM group (Figure 4B).

Berberine nanoparticles improve the hepatic antioxidant capacity in the GDM rats

To determine the impact of berberine nanoparticles on the antioxidant status in GDM rats, the concentration of GSH and the

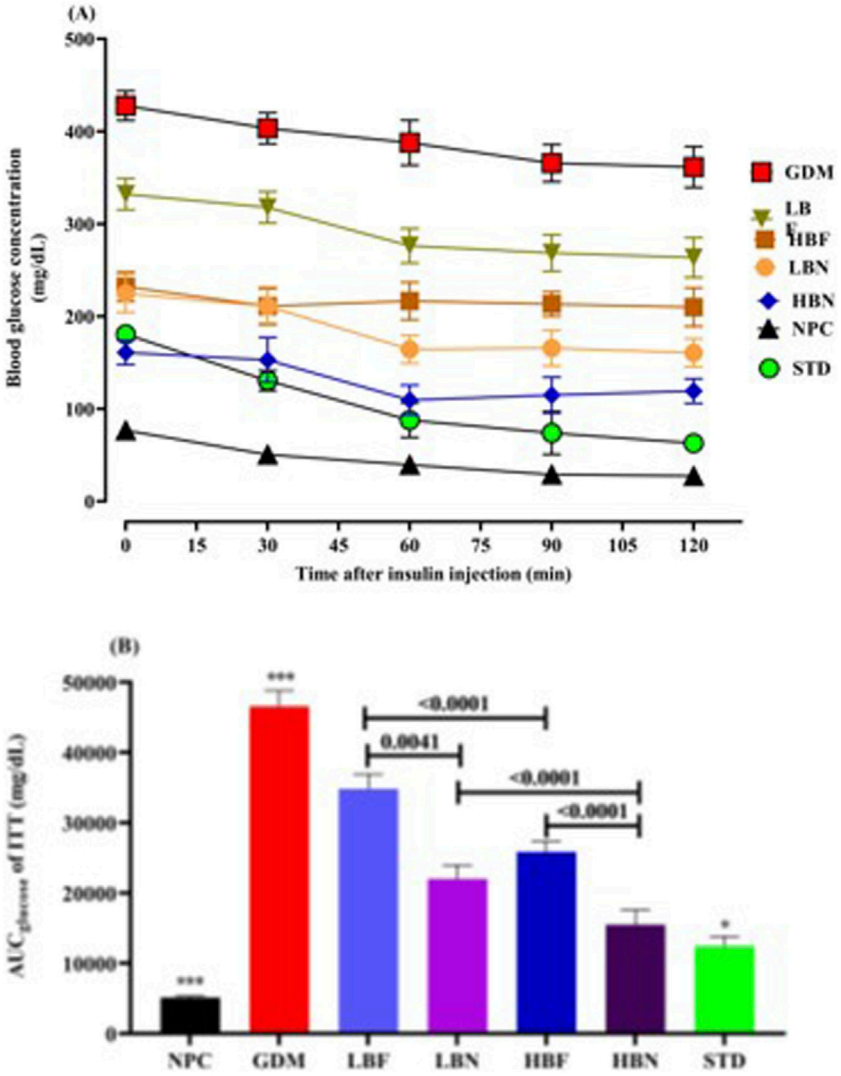

FIGURE 4
The Insulin tolerance test **(A)** and corresponding areas under the glucose curve ($AUC_{glucose}$) **(B)** over 120 min after the insulin injection in the NPC, GDM, LBN, HBN, LBF, HBF, and STD groups at GD18. Data are represented as the mean ± SD (n = 7). *** indicates $p < 0.0001$ for NPC group or GDM group when compared with treatment groups. * indicates $p < 0.03$ for the STD group when compared with the treatment groups.

activity of antioxidant enzymes GPx, CAT, and SOD were measured in hepatic tissues at the end of the study. As demonstrated in the Figure 5, the level of GSH (26.72 ± 1.86 μM) and the activity of SOD (15.35 ± 3.3 U/mL), CAT (6.93 ± 0.84 U/mL), and GPx (20.43 ± 2.1 U/mL) were significantly decreased by – 38-fold ($p < 0.0001$), – 0.47-fold ($p < 0.0001$), – 0.51-fold ($p < 0.0001$), and – 0.49-fold ($p < 0.0001$), respectively, in the GDM group compared with those (44.34 ± 3.57 μM, 30.01 ± 2.64 U/mL, 16.47 ± 1.92 U/mL, and 40.41 ± 2.49, respectively) in the NPC group. However, when the GDM rats were treated with the high and low doses of berberine nano-formulations (HBN and LBN groups), decreased values of GSH, SOD, CAT, and GPx were significantly and dose-dependently elevated by (0.46-fold ($p < 0.0001$) and 0.16-fold ($p = 0.01$)), (0.67-fold ($p < 0.0001$) and 0.38-fold ($p = 0.002$)), (0.65-fold ($p < 0.0001$) and 0.32-fold ($p = 0.003$)), and (0.81-fold ($p < 0.0001$) and 0.42-fold ($p < 0.0001$)), respectively, in comparison with the GDM group. Additionally, a low but significant difference was found between the mean values of antioxidant parameters in treatment (HBN and LBN) groups and the NPC group.

Berberine nanoparticles ameliorate the hepatic pro-oxidant load in the GDM rats

To further evaluate the effect of the high and low doses of berberine nanoformulations on oxidative stress, the

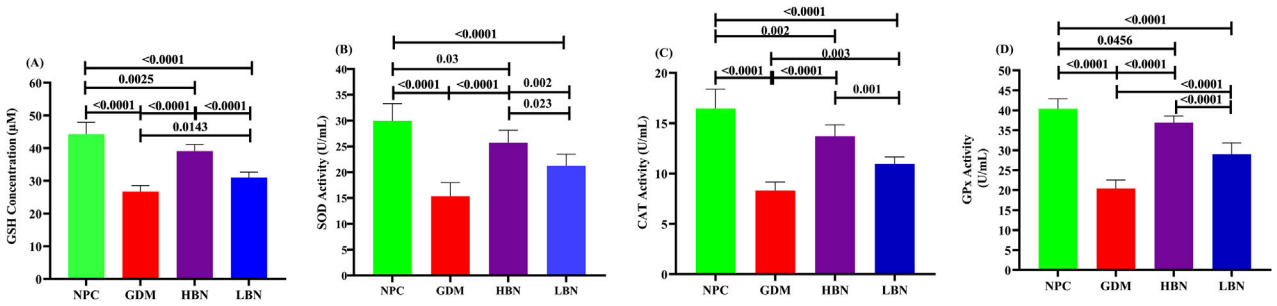

FIGURE 5
The level of GSH **(A)** and the activity of antioxidant enzymes, including SOD **(B)**, CAT **(C)**, and GPx **(D)** in the NPC, GDM, LBN, and HBN groups at GD18. Data are represented as the mean ± SD (n = 7).

concentrations of NO and MDA, as well as the activity of pro-oxidant enzyme MPO, were measured in the liver tissue at GD19. As shown in Figure 6, the levels of NO (10.61 ± 1.61 μM) and MDA (27.01 ± 1.6 μM) as well as the activity of MPO (5.6 ± 0.51 mU/mL) were significantly increased by 0.92-fold ($p < 0.0001$), 0.9-fold ($p < 0.0001$), 1.3-fold ($p < 0.0001$), and – 0.49-fold ($p < 0.0001$), respectively, in the GDM group compared with those (5.52 ± 0.9 μM, 14.2 ± 2 μM, and 2.44 ± 0.26 mU/mL, respectively) in the NPC group. However, when the GDM rats were treated with the high and low doses of berberine nano-formulations, the increased values of NO, MDA, and MPA were significantly and dose-dependently reduced by (– 0.38-fold ($p < 0.0001$) and – 0.21-fold ($p = 0.004$)), (– 0.33-fold ($p < 0.0001$) and – 0.2-fold ($p = 0.0002$)), and (– 0.46-fold ($p < 0.0001$) and – 0.28-fold ($p < 0.0001$)), in the HBN and LBN groups, respectively, in comparison with the GDM group. Additionally, a significant but low difference ($p < 0.05$) were detected between mean values of pro-oxidant parameters in the treatment (HBN and LBN) groups and the NPC group.

Discussion

The results from our study indicate that entrapment in chitosan-coated SLN nanoparticles can significantly improve the bioavailability and hypoglycemic effects of berberine in STZ-provoked GDM rats.

Berberine's ameliorative impacts on the glycemic indices in diabetes mellitus have been well-documented by various preclinical [63–66] and clinical studies [67–71]. There is also growing preclinical evidence indicating the potential of berberine in the GDM treatment. Yang et al. showed that oral gavage of berberine (25, 50, and 100 mg/kg/day from the day before pregnancy till 21st day of pregnancy) could dose-dependently improve body and fetal weight, placental weight, glucose tolerance, and insulin response in the STZ-induced GDM rats [25]. Consistently, Li et al. showed that orally administrated berberine (100 mg/kg/day, gavaged from the 7th to 20th day of pregnancy) could significantly improve maternal insulin response and body weight, placental and fetal weight, as well as the number of dead and absorptive fetuses in the high fat diet-induced GDM rats compared with the GDM rats without berberine treatment [26]. Similarly, other preclinical studies also reported the anti-diabetic impacts of berberine in GDM [21, 27, 28]. However, the poor hydrophilicity and bioavailability of berberine limit therapeutic efficiency after oral administration. Of note, berberine has to be repeatedly used at high doses (0.9–1.5 g/day) once prescribed to patients with diabetes [23]. Though berberine at high doses effectively ameliorates hyperglycemia, it leads to considerable gastrointestinal adverse impacts that limit its clinical use. Thus, improving the oral bioavailability of berberine not only elevates its anti-hyperglycemic impact but also decreases gastrointestinal adverse impacts. To improve berberine bioavailability, numerous investigations have developed berberine nanoformulations and showed their improved effectiveness for treating various diseases, such as diabetes [72, 73]. Based on our current knowledge, there is no published report showing the potential of berberine nanoformulations in GDM treatment. Here, we first studied the anti-hyperglycemic effects of berberine-loaded chitosan/SLN nanoparticles in the STZ-induced GDM rats. STZ induces a diabetes model identified by pancreatic β-cells' damage, causing insulin deficiency and consequent hyperglycemia and body weight reduction [74]. We found a significantly increased blood glucose concentration and body weight loss in STZ-administered pregnant rats (GDM group), when compared with normal pregnant rats (NPC group). Two weeks' daily oral gavage of free-berberine (50 and 100 mg/kg/day) could dose-dependently reverse the STZ-induced insulin deficiency, hyperglycemia, and body weight loss in the GDM rats, which were consistent with the above-mentioned studies [21, 25–28]. Of note, we indicated that the ameliorating effects of berberine on glycemic indices and body

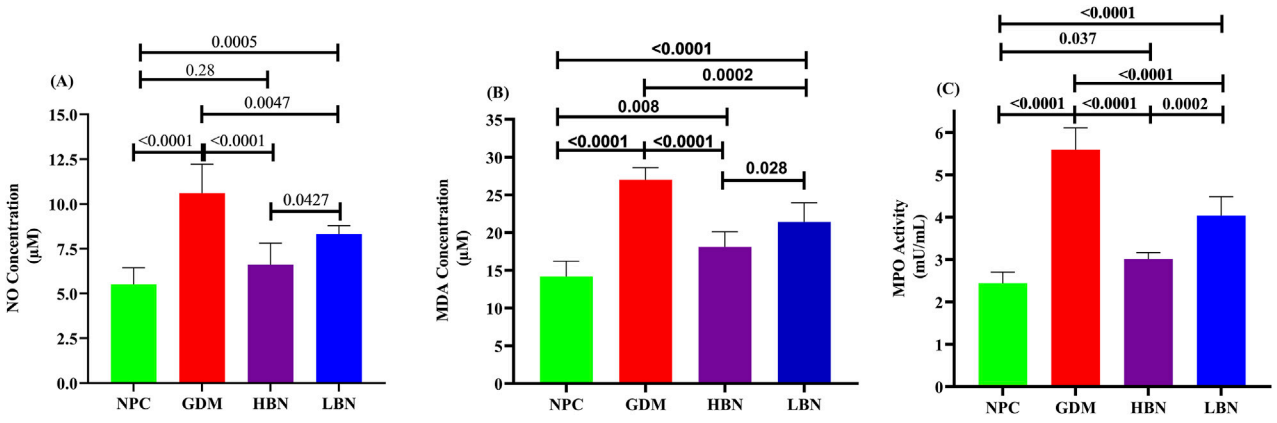

FIGURE 6
The liver levels of NO **(A)** and MDA **(B)**, as well as the activity of pro-oxidant enzyme MPO **(C)** in the NPC, GDM, LBN, and HBN groups at GD18. Data are represented as the mean ± SD (n = 7).

weight loss were significantly improved when encapsulated in chitosan-coated SLN nanoparticles. The low (25 mg/kg/day) and high (50 mg/kg/day) doses of berberine nanoparticles were found to significantly increase the reduction of FBG levels by 2.1-fold and 1.4-fold in the GDM rats, respectively, when compared with the equal doses of free-berberine. As shown by OGTT analysis, reduction of the blood glucose levels at the given times after glucose challenge in free-berberine- and berberine nanoparticle-treated GDM rats showed a 0.54-fold and 0.4-fold higher glucose tolerance in the GDM rats treated by the low and high doses of berberine nanoparticles, respectively, than those treated by free-berberine. The present findings are similar to other studies showing the enhanced efficacy of other berberine nanoformulations in reducing the elevated levels of FBG in STZ-induced diabetic rodents [75, 76]. Such a reduction of blood glucose levels might be attributed to elevated peripheral utilization of glucose. Our results from evaluating fasting insulin suggest that this can be due to the inducing effect of berberine on insulin secretion by pancreatic cells. Notably, the level of fasting plasma insulin was remarkably reduced in the untreated STZ-induced GDM rats compared with NPC rats, showing impaired insulin secretion. Interestingly, berberine nanoparticle-treated GDM rats demonstrated a significant elevation in fasting insulin levels, where a 2.75-fold and 2.4-fold elevation in fasting insulin was found in GDM rats treated by berberine nanoparticles at the low and high doses, respectively, in comparison with those treated by free berberine. However, low-dose free berberine showed no significant elevation in fasting insulin levels in GDM rats, whereas the high-dose could exert a significant improving effect. Mechanistically, berberine can enhance peripheral usage of glucose, at least in part, through promoting insulin production via pancreatic cells. Zhou et al. reported that berberine can significantly elevate islet area, the number of β-cells, the insulin secretion, and the ratio of pancreas to body weight in diabetic rats [77]. Leng et al. found that berberine dose-dependently induces insulin secretion in HIT-T15 cells and mouse islets [78]. Consistently, Wang et al. showed that berberine causes an insulinotropic effect in rat islets [79]. It has also been found that berberine can inhibit β-cell apoptosis and induce insulin release [80, 81]. Mechanistically, berberine has been shown to induce insulin secretion by elevating the levels of the incretin hormone glucagon-like peptide-1 (GLP-1) that participates in the survival of pancreatic cells. GLP-1, by activating adenylate cyclase that converts ATP into cyclic adenosine monophosphate (cAMP), triggers the epac protein and PKA signaling, leading to an elevation in the intracellular level of Ca^{2+}. This promotes the translocation and secretion of insulin granules [82–85].

Besides increasing insulin secretion, results from the ITT's insulin challenge and *the* HOMA-IR scores suggest that berberine might increase peripheral glucose uptake in STZ-induced GDM rats through enhancing the sensitivity/response of the body's cells to the insulin effect. Notably, ITT assessment revealed that, after insulin administration, untreated GDM rats were unable to significantly reduce the blood glucose, indicating that GDM rats suffered from a peripheral response deficiency to insulin and thus were unable to utilize exogenously injected insulin to drop the increased levels of blood glucose. However, free berberine and berberine nanoparticles remarkably decreased blood glucose in GDM rats after insulin injection, while 1.1-fold and 0.5-fold reductions were detected in GDM rats that received berberine nanoparticles at low and high doses, respectively, in comparison with those treated by free berberine. Supporting this, the HOMA-IR scores revealed that insulin resistance was significantly reduced by 2.85-fold and 1.5-fold in GDM rats

treated with the low and high doses of berberine nanoparticles, respectively, when compared with free-berberine, further verifying an improved response of the body's cells to the insulin effect in the berberine nanoparticle-treated GDM rats.

During the insulin resistance condition, there is a dysregulation in the insulin response signaling pathway, the Protein Kinase B (Akt)/Phosphoinositide 3-kinase (PI3K)/Insulin receptor substrate 1 (IRS-1). In improving insulin resistance, mechanistically, berberine can induce insulin response by activating Akt through promoting the 5′-adenosine monophosphate-activated protein kinase (AMPK) signaling as an energy-sensing pathway that is activated/inactivated in accordance with the cellular AMP/ATP ratio [82, 86, 87]. Berberine induces AMPK by promoting phosphorylation of Thr172 on the α subunit of AMPK [88–90], as well as by elevating the ratio of cellular AMP/ATP through suppressing the generation of the mitochondrial ATP [91, 92]. Berberine by AMPK can activate Akt that induces the expression and translocation of glucose transporter type-4 (GLUT4) to the cellular membrane, thus, glucose can be uptaken and utilized by the cell, causing increased glucose uptake and usage by insulin-resistant cells [82].

Furthermore, weight reduction is the main property of human T2DM and STZ-induced diabetes because of degradation of structural proteins and muscle injury, as well as worsened lipolysis and increased lipid peroxidation, which are complications of insulin deficiency [93]. Here, we found that berberine nanoformulation and free berberine treatment could significantly inhibit the body weight reduction in the STZ-induced GDM rats, where a 1.6-fold and 1.9-fold elevation of the body weight was found in the GDM rats treated by low and high doses of berberine nanoparticles, respectively, when compared with those treated by the equal doses of free berberine. Similarly, Yang et al. reported the preventive impact of berberine against body weight loss in the STZ-induced GDM rats [25].

Increased oxidative stress, resulting from an imbalance of free radicals producing and scavenging, is another common characteristic in the diabetes onset and development [94–96]. The results of the present investigation showed that berberine nanoparticles can significantly enhance hepatic antioxidant capacity in the STZ-induced GDM rats through increasing the concentration of GSH and the activity of antioxidant enzymes GPx, CAT, and SOD. Further, berberine nanoparticles could significantly reverse the increased levels of NO and MDA, as well as the enhanced activity of pro-oxidant enzyme MPO in STZ-induced GDM rats. Of note, the difference between the berberine nanoparticle-treated GDM rats (HBN/LBN groups) and the NPC rats was found to be small but sufficient. Mechanistically, berberine has been found to upregulate uncoupling protein 2 (UCP2) as a mitochondrial inner membrane protein that has a significantly negative association with ROS generation and oxidative stress [82].

The better protection against diabetes in STZ-induced GDM rats by berberine-loaded chitosan/SLN nanoparticle treatment than free berberine treatment can be attributed to a higher oral bioavailability of berberine achieved by chitosan-coated SLN formulation. After entrapment in chitosan/SLN nanoparticles, berberine showed an elevated level of the plasma peak, a postponed peak time, and an increased AUC in rats, confirming an improved oral bioavailability of berberine. The improved bioavailability of berberine can be attributed to the physicochemical features of berberine-loaded chitosan/SLN nanoparticles, as discussed in the following. The *in vitro* stability and drug release assessment demonstrated that berberine nanoparticles are stable in the SGF condition and show a sustained release profile in the SIF condition. Further, the chitosan moiety provides a hydrophilic surface layer that enables nanoparticles to form strong hydrogen bonds to the intestinal mucosal surface and, thus, enhances the mucoadhesion. The supporting investigations reported the enhanced intestinal uptake of compounds entrapped in chitosan-coated SLN nanoparticles, which was found to be attributed to hydrophilic and ionic interactions [37, 39]. These nanoparticles also showed a positive surface charge that causes an easy attachment to the intestinal cell membrane with the negative charge, leading to an enhanced uptake by intestinal cells [97]. Moreover, particle size can directly influence the cellular uptake of nanoparticles [98]. Berberine-loaded chitosan/SLN nanoparticles demonstrated a nanosize that facilitates an efficient cellular uptake. A phenomenon known as membrane wrapping, which demonstrates how a membrane may enclose a molecule, can explain the size-dependent uptake of nanoparticles. The nano size of berberine-loaded chitosan/SLN particles is also suitable for invisibility in the reticuloendothelial system and long-term circulation in the bloodstream [98, 99].

Conclusion

We synthesized chitosan-coated SLN nanoparticles to deliver berberine and evaluate their antidiabetic impacts in STZ-provoked GDM rats. The stable and nano-sized particle, high EE%, good *in vivo* stability, and sustained berberine release features are shown by berberine-loaded chitosan/SLN nanoparticles. Compared with free berberine treatment, berberine nanoparticle treatment could provide a significantly higher oral bioavailability of berberine in experimental rats. Chitosan-coated SLN nanoparticles can significantly enhance the protective effect of berberine against hyperglycemia in the STZ-induced GDM rats. Notably, the improved bioavailability of berberine-loaded chitosan/SLN

nanoparticles is a possible reason supporting the improved therapeutic impact of berberine in the STZ-induced GDM rats. In conclusion, chitosan-coated SLN nanoparticles provide a suitable delivery system to enhance the oral bioavailability of berberine and, thus, improve its pharmacological impacts.

Author contributions

All authors listed have made a substantial, direct, and intellectual contribution to the work and approved it for publication.

Data availability

The data used to support the findings of this study are available from the corresponding author upon request.

Ethics statement

The animal study was approved by Zhinanzhen Biology Ethics Committee, No.: A2025000127. The study was conducted in accordance with the local legislation and institutional requirements.

Funding

The authors declare that financial support was received for the research and/or publication of this article. The authors would like to acknowledge the funding from the Ongoing Research Funding Program, (ORF-2026-371), King Saud University, Riyadh, Saudi Arabia.

Conflict of interest

The author(s) declared no potential conflicts of interest with respect to the research, authorship, and/or publication of this article.

Generative AI statement

The authors declare that no Generative AI was used in the creation of this manuscript.

Any alternative text (alt text) provided alongside figures in this article has been generated by Frontiers with the support of artificial intelligence and reasonable efforts have been made to ensure accuracy, including review by the authors wherever possible. If you identify any issues, please contact us.

References

1. Lee J, Lee NK, Moon JH. Gestational diabetes mellitus: mechanisms underlying maternal and fetal complications. *Endocrinol Metab* (2025) **40**:10–25. doi:10.3803/enm.2024.2264

2. Quintanilla Rodriguez BS, Vadakekut ES, Mahdy H. *Gestational diabetes*. Treasure Island (FL): StatPearls Publishing (2024).

3. Ruiz-Martínez ML, Gómez-Díaz RA, Valdez González AL, Ángeles Mejía S, Mondragón González R, Díaz Flores M, et al. Association of oxidative stress markers with incident hyperglycemia in gestational diabetes mellitus in an educational intervention. *Nutrients* (2025) **17**:680. doi:10.3390/nu17040680

4. American Diabetes Association. 2. Classification and diagnosis of diabetes: standards of medical care in Diabetes-2018. *Diabetes Care* (2018) **41**:S13–s27. doi:10.2337/dc18-s002

5. Bobade PS, Ganorkar SB, Baviskar PN, Patil NB, Shinde DB, Shirkhedkar AA, et al. Pharmaceutical analysis of berberine: an update. *Separation and Purif Rev* (2024) **54**:1–10. doi:10.1080/15422119.2024.2423403

6. Shen P, Jiao Y, Miao L, Chen J, Momtazi-Borojeni AA. Immunomodulatory effects of berberine on the inflamed joint reveal new therapeutic targets for rheumatoid arthritis management. *J Cell Mol Med* (2020) **24**:12234–45. doi:10.1111/jcmm.15803

7. Fatahian A, Haftcheshmeh SM, Azhdari S, Farshchi HK, Nikfar B, Momtazi-Borojeni AA. Promising anti-atherosclerotic effect of berberine: evidence from *in vitro*, and clinical studies. *Rev Physiol Biochem Pharmacol* (2020) **178**:83–110. doi:10.1007/112_2020_42

8. Ayati SH, Fazeli B, Momtazi-Borojeni AA, Cicero AF, Pirro M, Sahebkar A. Regulatory effects of berberine on microRNome in cancer and other conditions. *Crit Reviews Oncology/hematology* (2017) **116**:147–58. doi:10.1016/j.critrevonc.2017.05.008

9. Mortazavi H, Nikfar B, Esmaeili S-A, Rafieenia F, Saburi E, Chaichian S, et al. Potential cytotoxic and anti-metastatic effects of berberine on gynaecological cancers with drug-associated resistance. *Eur Journal Medicinal Chemistry* (2020) **187**:111951. doi:10.1016/j.ejmech.2019.111951

10. Mohammadian Haftcheshmeh S, Momtazi-Borojeni AA. Berberine as a promising natural compound for the treatment of periodontal disease: a focus on anti-inflammatory properties. *J Cell Mol Med* (2021) **25**:11333–7. doi:10.1111/jcmm.17019

11. Lan J, Zhao Y, Dong F, Yan Z, Zheng W, Fan J, et al. Meta-analysis of the effect and safety of berberine in the treatment of type 2 diabetes mellitus, hyperlipemia and hypertension. *J Ethnopharmacology* (2015) **161**:69–81. doi:10.1016/j.jep.2014.09.049

12. Ma X, Chen Z, Wang L, Wang G, Wang Z, Dong X, et al. The pathogenesis of diabetes mellitus by oxidative stress and inflammation: its inhibition by berberine. *Front Pharmacol* (2018) **9**:782. doi:10.3389/fphar.2018.00782

13. Ehteshamfar SM, Akhbari M, Afshari JT, Seyedi M, Nikfar B, Shapouri-Moghaddam A, et al. Anti-inflammatory and immune-modulatory impacts of berberine on activation of autoreactive T cells in autoimmune inflammation. *J Cellular Molecular Medicine* (2020) **24**:13573–88. doi:10.1111/jcmm.16049

14. Mo C, Wang L, Zhang J, Numazawa S, Tang H, Tang X, et al. The crosstalk between Nrf2 and AMPK signal pathways is important for the anti-inflammatory effect of berberine in LPS-stimulated macrophages and endotoxin-shocked mice. *Antioxid and Redox Signaling* (2014) **20**:574–88. doi:10.1089/ars.2012.5116

15. Haftcheshmeh SM, Abedi M, Mashayekhi K, Mousavi MJ, Navashenaq JG, Mohammadi A, et al. Berberine as a natural modulator of inflammatory signaling pathways in the immune system: focus on NF-κB, JAK/STAT, and MAPK signaling pathways. *Phytotherapy Res* (2022) **36**:1216–30. doi:10.1002/ptr.7407

16. Chen Q-M, Xie MZ. Studies on the hypoglycemic effect of Coptis chinensis and berberine. *Yao Xue Xue Bao= Acta Pharmaceutica Sinica* (1986) **21**:401–6.

17. Ni YX. Therapeutic effect of berberine on 60 patients with type II diabetes mellitus and experimental research. *Zhong Xi Yi Jie He Za Zhi= Chin J Mod Dev Traditional Med* (1988) **8**:711–3.

18. Xie W, Su F, Wang G, Peng Z, Xu Y, Zhang Y, et al. Glucose-lowering effect of berberine on type 2 diabetes: a systematic review and meta-analysis. *Front Pharmacol* (2022) **13**:4734. doi:10.3389/fphar.2022.1015045

19. Liang Y, Xu X, Yin M, Zhang Y, Huang L, Chen R, et al. Effects of berberine on blood glucose in patients with type 2 diabetes mellitus: a systematic literature review and a meta-analysis. *Endocr Journal* (2019) **66**:51–63. doi:10.1507/endocrj.ej18-0109

20. Wei X-c, Zhu L-q, Wang C-g. Efficacy and safety of berberine in patients with type 2 diabetes mellitus: a meta-analysis. *Chin Herbal Medicines* (2015) **7**:344–53. doi:10.1016/s1674-6384(15)60063-6

21. Cole LK, Zhang M, Chen L, Sparagna GC, Vandel M, Xiang B, et al. Supplemental berberine in a high-fat diet reduces adiposity and cardiac dysfunction in offspring of mouse dams with gestational diabetes mellitus. *The J Nutr* (2021) **151**:892–901. doi:10.1093/jn/nxaa408

22. Cole LK, Sparagna GC, Vandel M, Xiang B, Dolinsky VW, Hatch GM. Berberine elevates cardiolipin in heart of offspring from mouse dams with high fat diet-induced gestational diabetes mellitus. *Scientific Rep* (2021) **11**:15770. doi:10.1038/s41598-021-95353-4

23. Yin J, Xing H, Ye J. Efficacy of berberine in patients with type 2 diabetes mellitus. *Metabolism* (2008) **57**:712–7. doi:10.1016/j.metabol.2008.01.013

24. Zhang H, Wei J, Xue R, Wu J-D, Zhao W, Wang Z-Z, et al. Berberine lowers blood glucose in type 2 diabetes mellitus patients through increasing insulin receptor expression. *Metabolism* (2010) **59**:285–92. doi:10.1016/j.metabol.2009.07.029

25. Yang X, Yang C, Lu W. Berberine suppresses gestational diabetes in streptozotocin-induced diabetes mellitus rats by suppression of inflammatory mediators. *Indian J Pharm Education Res* (2023) **57**:423–31. doi:10.5530/ijper.57.2.53

26. Li A, Lin C, Xie F, Jin M, Lin F. Berberine ameliorates insulin resistance by inhibiting IKK/NF-κB, JNK, and IRS-1/AKT signaling pathway in liver of gestational diabetes mellitus rats. *Metab Syndr Relat Disord* (2022) **20**:480–8. doi:10.1089/met.2022.0017

27. Feng LIN, Jie WU, Xiao W, Yin-ping H, Jing Z. Experimental study of berberine improving insulin resistance in gestational diabetes mellitus rat model and its possible mechanisms. *Chinese Journal of General Practice* (2019) **17**:1647–51. doi:10.16766/j.cnki.issn.1674-4152.001019

28. Wang Y, Gong W, Lv S, Qu H, He Y. Berberine improves insulin resistance in adipocyte models by regulating the methylation of hypoxia-inducible factor-3α. *Biosci Rep* (2019) **39**:BSR20192059. doi:10.1042/bsr20192059

29. Han Y, Xiang Y, Shi Y, Tang X, Pan L, Gao J, et al. Pharmacokinetics and pharmacological activities of berberine in diabetes mellitus treatment. *Evid Based Complement Altern Med* (2021) **2021**:1–15. doi:10.1155/2021/9987097

30. Xu X, Yi H, Wu J, Kuang T, Zhang J, Li Q, et al. Therapeutic effect of berberine on metabolic diseases: both pharmacological data and clinical evidence. *Biomed and Pharmacother* (2021) **133**:110984. doi:10.1016/j.biopha.2020.110984

31. Hua W, Ding L, Chen Y, Gong B, He J, Xu G. Determination of berberine in human plasma by liquid chromatography–electrospray ionization–mass spectrometry. *J Pharmaceutical Biomedical Analysis* (2007) **44**:931–7. doi:10.1016/j.jpba.2007.03.022

32. Zuo F, Nakamura N, Akao T, Hattori M. Pharmacokinetics of berberine and its main metabolites in conventional and pseudo germ-free rats determined by liquid chromatography/Ion trap mass spectrometry. *Drug Metab Disposition* (2006) **34**:2064–72. doi:10.1124/dmd.106.011361

33. Liu Y-T, Hao H-P, Xie H-G, Lai L, Wang Q, Liu C-X, et al. Extensive intestinal first-pass elimination and predominant hepatic distribution of berberine explain its low plasma levels in rats. *Drug Metab Disposition* (2010) **38**:1779–84. doi:10.1124/dmd.110.033936

34. Liu C-S, Zheng Y-R, Zhang Y-F, Long X-Y. Research progress on berberine with a special focus on its oral bioavailability. *Fitoterapia* (2016) **109**:274–82. doi:10.1016/j.fitote.2016.02.001

35. Chen C, Fan T, Jin Y, Zhou Z, Yang Y, Zhu X, et al. Orally delivered salmon calcitonin-loaded solid lipid nanoparticles prepared by micelle–double emulsion method *via* the combined use of different solid lipids. *Nanomedicine* (2013) **8**:1085–100. doi:10.2217/nnm.12.141

36. George M, Abraham TE. Polyionic hydrocolloids for the intestinal delivery of protein drugs: alginate and chitosan—a review. *J Controlled Release* (2006) **114**:1–14. doi:10.1016/j.jconrel.2006.04.017

37. Luo Y, Teng Z, Li Y, Wang Q. Solid lipid nanoparticles for oral drug delivery: Chitosan coating improves stability, controlled delivery, mucoadhesion and cellular uptake. *Carbohydr Polymers* (2015) **122**:221–9. doi:10.1016/j.carbpol.2014.12.084

38. Sogias IA, Williams AC, Khutoryanskiy VV. Why is chitosan mucoadhesive? *Biomacromolecules* (2008) **9**:1837–42. doi:10.1021/bm800276d

39. Fonte P, Nogueira T, Gehm C, Ferreira D, Sarmento B. Chitosan-coated solid lipid nanoparticles enhance the oral absorption of insulin. *Drug Deliv Translational Res* (2011) **1**:299–308. doi:10.1007/s13346-011-0023-5

40. Nair R, Kumar AC, Priya VK, Yadav CM, Raju PY. Formulation and evaluation of chitosan solid lipid nanoparticles of carbamazepine. *Lipids Health Disease* (2012) **11**:1–8. doi:10.1186/1476-511x-11-72

41. Ridolfi DM, Marcato PD, Justo GZ, Cordi L, Machado D, Durán N. Chitosan-solid lipid nanoparticles as carriers for topical delivery of tretinoin. *Colloids Surf B: Biointerfaces* (2012) **93**:36–40. doi:10.1016/j.colsurfb.2011.11.051

42. Hu F-Q, Jiang S-P, Du Y-Z, Yuan H, Ye Y-Q, Zeng S. Preparation and characterization of stearic acid nanostructured lipid carriers by solvent diffusion method in an aqueous system. *Colloids Surf B: Biointerfaces* (2005) **45**:167–73. doi:10.1016/j.colsurfb.2005.08.005

43. Sarmento B, Mazzaglia D, Bonferoni MC, Neto AP, do Céu Monteiro M, Seabra V. Effect of chitosan coating in overcoming the phagocytosis of insulin loaded solid lipid nanoparticles by mononuclear phagocyte system. *Carbohydr Polymers* (2011) **84**:919–25. doi:10.1016/j.carbpol.2010.12.042

44. Ahmaditabar P, Momtazi-Borojeni AA, Rezayan AH, Mahmoodi M, Sahebkar A, Mellat M. Enhanced entrapment and improved *in vitro* controlled release of n-acetyl cysteine in hybrid PLGA/lecithin nanoparticles prepared using a nanoprecipitation/self-assembly method. *J Cellular Biochemistry* (2017) **118**:4203–9. doi:10.1002/jcb.26070

45. Pan XM, Li J, Gan R, Hu XN. Preparation and *in vitro* evaluation of enteric-coated tablets of rosiglitazone sodium. *Saudi Pharm J* (2015) **23**:581–6. doi:10.1016/j.jsps.2015.02.018

46. Anal AK, Stevens WF. Chitosan–alginate multilayer beads for controlled release of ampicillin. *Int Journal Pharmaceutics* (2005) **290**:45–54. doi:10.1016/j.ijpharm.2004.11.015

47. Chandrasekaran AR, Jia CY, Theng CS, Muniandy T, Muralidharan S, Dhanaraj SA. *Invitro* studies and evaluation of metformin marketed tablets-Malaysia. *J Applied Pharmaceutical Science* (2011) 214–7.

48. Khalil NM, do Nascimento TCF, Casa DM, Dalmolin LF, de Mattos AC, Hoss I, et al. Pharmacokinetics of curcumin-loaded PLGA and PLGA–PEG blend nanoparticles after oral administration in rats. *Colloids Surf B: Biointerfaces* (2013) **101**:353–60. doi:10.1016/j.colsurfb.2012.06.024

49. Sun B, Yan H, Li C, Yin L, Li F, Zhou L, et al. Beneficial effects of walnut (Juglans regia L.) oil-derived polyunsaturated fatty acid prevents a prooxidant status and hyperlipidemia in pregnant rats with diabetes. *Nutr and Metabolism* (2020) **17**:1–11. doi:10.1186/s12986-020-00514-3

50. Veerapur V, Pratap V, Thippeswamy B, Marietta P, Bansal P, Kulkarni P, et al. Polyphenolic enriched extract of Cassia glauca Lamk, improves streptozotocin-induced type-1 diabetes linked with partial insulin resistance in rats. *J Ethnopharmacology* (2017) **198**:489–98. doi:10.1016/j.jep.2017.01.025

51. Wang W, Zha G, Zou J-j, Wang X, Li C-n, Wu X-j. Berberine attenuates cigarette smoke extract-induced airway inflammation in mice: involvement of TGF-β1/Smads signaling pathway. *Curr Medical Science* (2019) **39**:748–53. doi:10.1007/s11596-019-2101-8

52. Zhou Y, Liu S-q, Peng H, Yu L, He B, Zhao Q. *In vivo* anti-apoptosis activity of novel berberine-loaded chitosan nanoparticles effectively ameliorates osteoarthritis. *Int Immunopharmacology* (2015) **28**:34–43. doi:10.1016/j.intimp.2015.05.014

53. Wu S-J, Don T-M, Lin C-W, Mi F-L. Delivery of berberine using chitosan/fucoidan-taurine conjugate nanoparticles for treatment of defective intestinal epithelial tight junction barrier. *Mar Drugs* (2014) **12**:5677–97. doi:10.3390/md12115677

54. Xue M, Zhang L, Yang M-x, Zhang W, Li X-m, Ou Z-m, et al. Berberine-loaded solid lipid nanoparticles are concentrated in the liver and ameliorate hepatosteatosis in db/db mice. *Int Journal Nanomedicine* (2015) **10**:5049–57. doi:10.2147/ijn.s84565

55. Xue M, Yang M-x, Zhang W, Li X-m, Gao D-h, Ou Z-m, et al. Characterization, pharmacokinetics, and hypoglycemic effect of berberine loaded solid lipid nanoparticles. *Int J Nanomedicine* (2013) **8**:4677. doi:10.2147/ijn.s51262

56. Close B, Banister K, Baumans V, Bernoth E-M, Bromage N, Bunyan J, et al. Recommendations for euthanasia of experimental animals: part 2. *Lab Animals* (1997) **31**:1–32. doi:10.1258/002367797780600297

57. Close B, Banister K, Baumans V, Bernoth E-M, Bromage N, Bunyan J, et al. Recommendations for euthanasia of experimental animals: part 1. *Lab Animals* (1996) **30**:293–316. doi:10.1258/002367796780739871

58. Siahaan JM, Illyas S, Lindarto D, Nainggolan M. The effect of ethanol and ethyl acetate fraction of chayote fruit (Sechium edule jacq. swartz) on the oxidative stress and insulin resistance of male white rat model type 2 diabetes mellitus. *Open Access Macedonian J Med Sci* (2020) **8**:962–9. doi:10.3889/oamjms.2020.4517

59. Ibrahim MA, Habila JD, Koorbanally NA, Islam MS. Butanol fraction of Parkia biglobosa (Jacq.) G. Don leaves enhance pancreatic β-cell functions, stimulates insulin secretion and ameliorates other type 2 diabetes-associated complications in rats. *J Ethnopharmacology* (2016) **183**:103–11. doi:10.1016/j.jep.2016.02.018

60. Kunasegaran T, Mustafa MR, Murugan DD, Achike FI. The bioflavonoid quercetin synergises with PPAR-γ agonist pioglitazone in reducing angiotensin-II contractile effect in fructose-streptozotocin induced diabetic rats. *Biochimie* (2016) **125**:131–9. doi:10.1016/j.biochi.2016.03.008

61. Luo Y, Zhang Y, Pan K, Critzer F, Davidson PM, Zhong Q. Self-emulsification of alkaline-dissolved clove bud oil by whey protein, gum arabic, lecithin, and their

combinations. *J Agricultural Food Chemistry* (2014) **62**:4417–24. doi:10.1021/jf500698k

62. Ganesan P, Ramalingam P, Karthivashan G, Ko YT, Choi D-K. Recent developments in solid lipid nanoparticle and surface-modified solid lipid nanoparticle delivery systems for oral delivery of phyto-bioactive compounds in various chronic diseases. *Int Journal Nanomedicine* (2018) **13**:1569–83. doi:10.2147/ijn.s155593

63. Shiri S, Gharanjig K, Heidari H, Tahghighi A. Plant sources containing berberine with potential of control type 2 diabetes mellitus: a brief literature review. *Funct Food Sci* (2024) **4**:466–78. doi:10.31989/ffs.v4i12.1461

64. Askari VR, Khosravi K, Baradaran Rahimi V, Garzoli S. A mechanistic review on how berberine use combats diabetes and related complications: molecular, cellular, and metabolic effects. *Pharmaceuticals* (2023) **17**(7):7. doi:10.3390/ph17010007

65. Araj-Khodaei M, Ayati MH, Azizi Zeinalhajlou A, Novinbahador T, Yousefi M, Shiri M, et al. Berberine-induced glucagon-like peptide-1 and its mechanism for controlling type 2 diabetes mellitus: a comprehensive pathway review. *Arch Physiol Biochem* (2024) **130**:678–85. doi:10.1080/13813455.2023.2258559

66. Shrivastava S, Sharma A, Saxena N, Bhamra R, Kumar S. Addressing the preventive and therapeutic perspective of berberine against diabetes. *Heliyon* (2023) **9**:e21233. doi:10.1016/j.heliyon.2023.e21233

67. Miao R, Zhang B, Zhou D, Kang M, Tian J, Zhao L, et al. Clinical efficacy of curcumin, resveratrol, silymarin, and berberine on Cardio-Metabolic risk factors among patients with type 2 diabetes mellitus: a systemic review and bayesian network meta-analysis. *Phytotherapy Research: PTR* (2025). doi:10.1002/ptr.8431

68. Guo J, Chen H, Zhang X, Lou W, Zhang P, Qiu Y, et al. The effect of berberine on metabolic profiles in type 2 diabetic patients: a systematic review and meta-analysis of randomized controlled trials. *Oxidative Med Cell Longevity* (2021) **2021**: 2074610. doi:10.1155/2021/2074610

69. Wang J, Bi C, Xi H, Wei F. Effects of administering berberine alone or in combination on type 2 diabetes mellitus: a systematic review and meta-analysis. *Front Pharmacol* (2024) **15**:1455534. doi:10.3389/fphar.2024.1455534

70. Mansour A, Sajjadi-Jazi SM, Gerami H, Khorasanian AS, Moalemzadeh B, Karimi S, et al. The efficacy and safety of berberine in combination with cinnamon supplementation in patients with type 2 diabetes: a randomized clinical trial. *Eur J Nutr* (2025) **64**:102. doi:10.1007/s00394-025-03618-9

71. Ji L, Ma J, Ma Y, Cheng Z, Gan S, Yuan G, et al. Berberine ursodeoxycholate for the treatment of type 2 diabetes: a randomized clinical trial. *JAMA Netw Open* (2025) **8**:e2462185–e85. doi:10.1001/jamanetworkopen.2024.62185

72. Chaudhari S, Dalabehera M, Subudhi RN, Dua K, Kaur M, Paudel KR, et al. From nature to nanotech: unlocking berberine's therapeutic approaches. *J Drug Deliv Sci Technology* (2025) **108**:106924. doi:10.1016/j.jddst.2025.106924

73. Khan MJ, Hafeez A, Siddiqui MA. Nanocarrier based delivery of berberine: a critical review on pharmaceutical and preclinical characteristics of the bioactive. *Curr Pharm Biotechnol* (2023) **24**:1449–64. doi:10.2174/1389201024666230112141330

74. Wu J, Yan LJ. Streptozotocin-induced type 1 diabetes in rodents as a model for studying mitochondrial mechanisms of diabetic β cell glucotoxicity. *Diabetes Metab Syndr Obes Targets Ther* (2015) **8**:181. doi:10.2147/dmso.s82272

75. Khalaf YH, Dawood Y, Khashan AA. Green biosynthesis of berberine-mediated silver nanorods: their protective and antidiabetic effects in streptozotocin-induced diabetic rats. *Results Chem* (2023) **5**:100722. doi:10.1016/j.rechem.2022.100722

76. Wang Z, Wu J, Zhou Q, Wang Y, Chen T. Berberine nanosuspension enhances hypoglycemic efficacy on streptozotocin induced diabetic C57BL/6 mice. *Evidence-Based Complement Altern Med* (2015) **2015**:239749. doi:10.1155/2015/239749

77. Zhou J, Zhou S, Tang J, Zhang K, Guang L, Huang Y, et al. Protective effect of berberine on beta cells in streptozotocin-and high-carbohydrate/high-fat diet-induced diabetic rats. *Eur J Pharmacol* (2009) **606**:262–8. doi:10.1016/j.ejphar.2008.12.056

78. Leng S-h, Lu F-E, Xu L-j. Therapeutic effects of berberine in impaired glucose tolerance rats and its influence on insulin secretion. *Acta Pharmacologica Sinica* (2004) **25**:496–502.

79. Wang Z-Q, Lu F-E, Leng S-H, Fang X-S, Chen G, Wang Z-S, et al. Facilitating effects of berberine on rat pancreatic islets through modulating hepatic nuclear factor 4 alpha expression and glucokinase activity. *World J Gastroenterol* (2008) **14**: 6004. doi:10.3748/wjg.14.6004

80. Gao N, Zhao TY, Li XJ. The protective effect of berberine on β-cell lipoapoptosis. *J Endocrinological Invest* (2011) **34**:124–30. doi:10.1007/bf03347042

81. Li M, Shen Y, Wang Q, Zhou X. MiR-204-5p promotes apoptosis and inhibits migration of osteosarcoma via targeting EBF2. *Biochimie* (2019) **158**:224–32. doi:10.1016/j.biochi.2018.12.003

82. Chang W, Chen L, Hatch GM. Berberine as a therapy for type 2 diabetes and its complications: from mechanism of action to clinical studies. *Biochem Cell Biol* (2015) **93**:479–86. doi:10.1139/bcb-2014-0107

83. Lu S-S, Yu Y-L, Zhu H-J, Liu X-D, Liu L, Liu Y-W, et al. Berberine promotes glucagon-like peptide-1 (7-36) amide secretion in streptozotocin-induced diabetic rats. *J Endocrinol* (2009) **200**:159–65. doi:10.1677/joe-08-0419

84. Tengholm A, Gylfe E. cAMP signalling in insulin and glucagon secretion. *Diabetes Obesity Metabolism* (2017) **19**:42–53. doi:10.1111/dom.12993

85. Yu Y, Liu L, Wang X, Liu X, Liu X, Xie L, et al. Modulation of glucagon-like peptide-1 release by berberine: *in vivo* and *in vitro* studies. *Biochem Pharmacology* (2010) **79**:1000–6. doi:10.1016/j.bcp.2009.11.017

86. Hardie DG. AMP-activated protein kinase: a master switch in glucose and lipid metabolism. *Rev Endocr Metab Disord* (2004) **5**:119–25. doi:10.1023/b:remd.0000021433.63915.bb

87. Kahn BB, Alquier T, Carling D, Hardie DG. AMP-activated protein kinase: ancient energy gauge provides clues to modern understanding of metabolism. *Cell Metabolism* (2005) **1**:15–25. doi:10.1016/j.cmet.2004.12.003

88. Brusq J-M, Ancellin N, Grondin P, Guillard R, Martin S, Saintillan Y, et al. Inhibition of lipid synthesis through activation of AMP kinase: an additional mechanism for the hypolipidemic effects of berberine. *J Lipid Res* (2006) **47**: 1281–8. doi:10.1194/jlr.m600020-jlr200

89. Kim SH, Shin E-J, Kim E-D, Bayaraa T, Frost SC, Hyun C-K. Berberine activates GLUT1-mediated glucose uptake in 3T3-L1 adipocytes. *Biol Pharm Bull* (2007) **30**:2120–5. doi:10.1248/bpb.30.2120

90. Lee YS, Kim WS, Kim KH, Yoon MJ, Cho HJ, Shen Y, et al. Berberine, a natural plant product, activates AMP-activated protein kinase with beneficial metabolic effects in diabetic and insulin-resistant states. *Diabetes* (2006) **55**: 2256–64. doi:10.2337/db06-0006

91. Cheng Z, Pang T, Gu M, Gao A-H, Xie C-M, Li J-Y, et al. Berberine-stimulated glucose uptake in L6 myotubes involves both AMPK and p38 MAPK. *Biochim Biophys Acta (BBA)-General Subjects* (2006) **1760**:1682–9. doi:10.1016/j.bbagen.2006.09.007

92. Yin J, Gao Z, Liu D, Liu Z, Ye J. Berberine improves glucose metabolism through induction of glycolysis. *Am J Physiology-Endocrinology Metab* (2008) **294**: E148–E156. doi:10.1152/ajpendo.00211.2007

93. Giugliano D, Ceriello A, Paolisso G. Oxidative stress and diabetic vascular complications. *Diabetes CARE* (1996) **19**:257–67. doi:10.2337/diacare.19.3.257

94. Widowati W. Potensi antioksidan sebagai antidiabetes. *Jkm* (2008) **7**:1–11.

95. Bajaj S, Khan A. Antioxidants and diabetes. *Indian Journal Endocrinol And Metab* (2012) **16**:S267–S71. doi:10.4103/2230-8210.104057

96. Ceriello A, Testa R. Antioxidant anti-inflammatory treatment in type 2 diabetes. *Diabetes Care* (2009) **32**:S232–S236. doi:10.2337/dc09-s316

97. Lockman PR, Oyewumi MO, Koziara JM, Roder KE, Mumper RJ, Allen DD. Brain uptake of thiamine-coated nanoparticles. *J Controlled Release* (2003) **93**: 271–82. doi:10.1016/j.jconrel.2003.08.006

98. Albanese A, Tang PS, Chan WC. The effect of nanoparticle size, shape, and surface chemistry on biological systems. *Annu Rev Biomed Engineering* (2012) **14**: 1–16. doi:10.1146/annurev-bioeng-071811-150124

99. Gratton SE, Ropp PA, Pohlhaus PD, Luft JC, Madden VJ, Napier ME, et al. The effect of particle design on cellular internalization pathways. *Proc Natl Acad Sci* (2008) **105**:11613–18. doi:10.1073/pnas.0801763105

EBM Experimental Biology and Medicine

TYPE Review
PUBLISHED 08 December 2025
DOI 10.3389/ebm.2025.10754

OPEN ACCESS

*CORRESPONDENCE
Tammy R. Dugas,
tammydugas@lsu.edu

RECEIVED 29 July 2025
REVISED 31 October 2025
ACCEPTED 18 November 2025
PUBLISHED 08 December 2025

CITATION
Akers NM and Dugas TR (2025) Peripheral artery disease and local drug delivery: a review of disease pathology and drug delivery systems for therapy below the knee.
Exp. Biol. Med. 250:10754.
doi: 10.3389/ebm.2025.10754

Peripheral artery disease and local drug delivery: a review of disease pathology and drug delivery systems for therapy below the knee

Nicole M. Akers and Tammy R. Dugas*

Department of Comparative Biomedical Sciences, Louisiana State University School of Veterinary Medicine, Baton Rouge, LA, United States

Abstract

Peripheral artery disease (PAD) is a disease of both atherosclerotic and thromboembolic pathology, affecting more than 230 million people globally. PAD patients are at an increased risk of thrombotic events and often require lifelong antithrombotic therapy. Thromboembolism can lead to complete occlusion of affected arteries and put patients at risk for critical limb threatening ischemia (CTLI). PAD blockages are cleared using drug-eluting stents (DES) and drug-coated balloons (DCB). However, PAD treatment below the knee (BTK) presents unique challenges. While DCB are frequently used to treat BTK disease, no DCB has gained FDA approval for this indication. However, innovation in the field has produced drug delivery systems and formulations that may yet enhance the effectiveness of these therapies. In this review, we will provide a brief overview of the pathological mechanisms associated with PAD and review the materials and drugs frequently used in DCBs with an emphasis on excipients and drug carriers. Finally, we will highlight emerging devices undergoing clinical trials to treat BTK disease and how they differ from their predecessors.

KEYWORDS

peripheral artery disease, drug coated balloon, paclitaxel, sirolimus, thrombosis, combination device, biocompatibility

Impact statement

We provide timely updates to the progress being made in combination device development for peripheral artery disease (PAD) therapy. This review article summarizes both basic pathophysiologic information for PAD as well as device development considerations for combination devices. Lesions below the knee have proven challenging to treat. Drug coated balloons are frequently used as a part of PAD lesion treatment below the knee, yet none are approved for use below the knee in the US. Therefore, we discuss the latest updates in the development of several promising

combination and lesion preparation devices for treatment of PAD disease below the knee, a historically recalcitrant area to treat. This information will be useful to both scientists and clinicians who are either developing their own combination devices or looking for cutting edge information on how new devices are different from their predecessors.

Introduction

Peripheral artery disease (PAD) encompasses atherosclerotic and thrombotic pathology outside of the coronary and cerebral vascular systems. The most common presentation of PAD occurs within the lower limbs, with an estimated global prevalence of more than 230 million cases [1]. PAD is associated with significant morbidity, disability, and mortality in affected individuals. These subjects can experience limb weakness and claudication due to decreased tissue perfusion from narrowed, damaged vessels, up to complete occlusion of blood flow, leading to critical limb-threatening ischemia (CLTI) and potential limb amputation. The risk for myocardial infarction (MI) or stroke in PAD patients is on par with patients suffering from coronary artery disease [2]. PAD treatment includes a combination of lifestyle modifications, medical therapy, and when needed, endovascular interventions including surgical approaches and medical device interventions [3, 4]. There are a wide variety of devices available to treat PAD lesions, including the use of bare-metal stents (BMS) and drug-eluting stents (DES), either balloon-expanded or self-expanding, newer woven and covered nitinol stents, dissolvable scaffolds, percutaneous transluminal angioplasty (PTA) with either drug-coated (DCBs) or plain balloons (POBA), intravascular lithotripsy and atherectomy to treat calcified lesions [5]. Treatment approaches are highly dependent on the location, length and number of lesions present, as well as the pattern of disease in the individual and their comorbidities. While both stenting and balloon angioplasty have been successful above the knee, lesions below the knee (BTK) have restenosis rates that approach 70 percent [6]. Additionally, BTK lesions are heavily calcified, cover extensive lengths of the artery, and importantly, possess significant thromboembolic pathology that can lead to adverse outcomes including CLTI and subsequent amputation [7]. Below the knee, DCBs are commonly used to treat lesioned arteries; yet none are FDA approved for use below the knee due to a lack of evidence of long term benefits over POBA. Recent developments in DCB include novel drug formulations and carriers, which may yet improve clinical outcomes in the long term for BTK disease. These carriers include liposomal formulations, polymeric microspheres, and aqueous delivery systems, among others. Before delving into these novel technologies, we will first discuss PAD pathophysiology, drugs commonly used in DCB, the difficulty associated with BTK disease treatment, and how coating formulations can enhance or derail effective DCB treatment.

Pathologic mechanisms of PAD

Endothelial regulation of thrombosis

Healthy endothelial cells express both prostacyclin (PGI_2) and endothelial nitric oxide synthase (eNOS). eNOS provides a source of nitric oxide (NO), which along with PGI_2, synergistically inhibits platelet adhesion and aggregation via binding to receptors expressed on the platelet surface, reducing their activity [8]. NO is additionally a vasodilator that permeates the endothelium, promoting relaxation of the vascular smooth muscle. Vascular endothelial cells are key regulators of coagulation and thrombosis. TV-VIIa (activated factor VII complex) and prothrombinase are key initiators of early clot development; vascular endothelial cells express TFPI-α and TFPI-β (tissue factor pathway inhibitor alpha and beta, respectively) that inhibit the TF-VIIa (activated factor VII) complex and prothrombinase. Therefore, TFPI-α and TFPI-β inhibit clot formation at an early stage [9]. Fibrinolysis is regulated via plasminogen activator inhibitor (PAI-1), endothelial urokinase plasminogen activator (u-PA) and tissue plasminogen activator (t-PA). Thus, under normal circumstances the luminal endothelial surface is antithrombogenic, expressing multiple inhibitors of coagulation, platelet aggregation and adhesion, as well as other factors that promote fibrinolysis. On the other hand, decreased eNOS activity in damaged endothelia promotes platelet aggregation, reactivity, and thrombosis [8].

Invasion of lipids and inflammatory cells

Inflammatory cytokines, reactive oxygen species, and high levels of circulating LDLs behave as endothelial stressors [10, 11]. Under chronic exposure to stressors, endothelia can become dysfunctional. Dysregulated eNOS activity due to endothelial dysfunction reduces NO output. NO is critical for maintaining endothelial barrier function, and NO inhibits NF-κB, a key transcription factor that promotes the expression of ICAM, VCAM-1, E-selectin, and other leukocyte adhesion receptors on the endothelium [12]. As a result of compromised endothelial barrier function, the endothelium becomes permeable to the transmigration of inflammatory cells and lipids via decreased NO production [13]. Monocytes thus

transmigrate through the endothelium and differentiate into macrophages, phagocytizing LDLs. Phagocytosis of LDL transforms macrophages into foam cells. These foam cells become apoptotic and are cleared by M2 macrophages. When these macrophages die, they release TF, lipids, and other inflammatory molecules including matrix metalloproteinases (MMP), further promoting a prothrombotic and inflammatory state [14].

Atheroma development

Transformation of macrophages into foam cells that deposit lipids into the subendothelial matrix marks the initiation of atheroma development. Like coronary artery disease (CAD), atherosclerotic plaques can be found in PAD lesions. Atherogensis can be defined by several stages, beginning with a fatty streak within the artery wall, progressing to a fibrous plaque, to an unstable plaque at risk of rupture, and ultimately, a ruptured plaque. Atherosclerotic plaques contain a mixture of lipids, minerals, inflammatory cells, platelets and cellular degradation products [15]. Additionally, ruptured atherosclerotic plaques release pro-thrombotic factors such as tissue factor (TF) from the necrotic core, which promotes thrombosis [16].

Medial calcification

Calcification associated with CAD and calcified lesions associated with PAD differ. Calcification can be classified as intimal or medial depending on where it is located within the vessel tunics, each with different proposed mechanisms for their pathogenesis. While CAD calcification is primarily intimal and associated with fibrous plaques, PAD calcification can be found in both the intima and media [17]. Importantly, medial calcification is often observed with CTLI [7]. Medial calcification was once considered a benign, aging-associated change in the tunica media; however, it may contribute to thrombotic risk. While atherosclerotic plaque rupture is considered a central mechanism for thromboembolism in the presence of plaques, highly calcified BTK lesions with minimal atherosclerotic involvement also display thromboembolic pathology [7]. This suggests the possibility that there are alternative pro-thrombotic mechanisms outside of atherosclerotic plaque rupture. Chang and coworkers proposed lower leg arterial calcification as a potential risk factor for acute thrombosis independent of atherosclerotic pathology [18]. Accordingly, luminal thrombi in BTK lesions are not routinely associated with atherosclerotic plaques compared to CAD lesions but are commonly associated with heavily calcified arteries [19]. Narula et al., examined 299 arteries collected from 95 patients with CTLI. BTK arteries presented more often with diffuse, chronic, occlusive thromboembolic pathology and significant calcification with minimal atherosclerotic disease when compared to FP lesions, although both BTK and FP segments displayed medial calcification [7].

Additionally, different patterns of calcification present in FP and BTK lesions may complicate patient outcomes. FP segments often have thick, patchy calcifications associated with the tunica intima, whereas BTK lesions frequently present with continuous, annular calcifications which form a circumferential ring of arterial calficiation [20]. Annular calcification patterns have been tied to poor long term survival in patients with CTLI [21]. Lastly, intensely calcified arteries pose a significant physical barrier against the transfer of drugs through the arterial wall.

Mechanisms of vascular remodeling following balloon injury in PAD patients

Balloon angioplasty has become the preferred approach to BTK lesions. However, endothelial damage including complete denudation of the endothelial layer at the site of angioplasty can occur [22]. This damage contributes to IH development, which starts with the recruitment of platelets and inflammatory cells to injured sites and results in the synthetic vascular smooth muscle cells (sVMSC) phenotypic switch that promotes remodeling of the arterial wall. Circulating platelets adhere to exposed subendothelial collagen by binding to vWF and collagen via platelet surface glycoproteins GPVI and GPIb-IX-V [23]. Bound platelets become activated and recruit additional platelets through the release of aggregatory mediators including ADP, thromboxane A_2, and thrombin [24]. Thrombin generated through TF-mediated extrinsic coagulation activity further bolsters platelet aggregation [25]. Importantly, these bound platelets secrete platelet-derived growth factor (PDGF), a potent activator of VSMC migration and proliferation [26, 27]. Additionally, macrophages have been long established as promoters of the sVSMC phenotype. M1 macrophages, which are often found in association with atherosclerotic lesions and in damaged tissues following balloon angioplasty, secrete numerous cytokines including TNF-α, IL-1B and IL-6 [28]. These cytokines have all been implicated in modulating the VSMC phenotype, enhancing proliferation and migration [29, 30]. Under the influence of growth factors PDGF as well as inflammatory cytokines, VSMC behave as sVSMC. These sVSMC migrate from the tunica media to the tunica intima, where they proliferate and secrete extracellular matrix (ECM) components leading to ECM deposition and expansion [31]. Ultimately, the root of the remodeling process is endothelial injury triggering this cascade of events Figure 1.

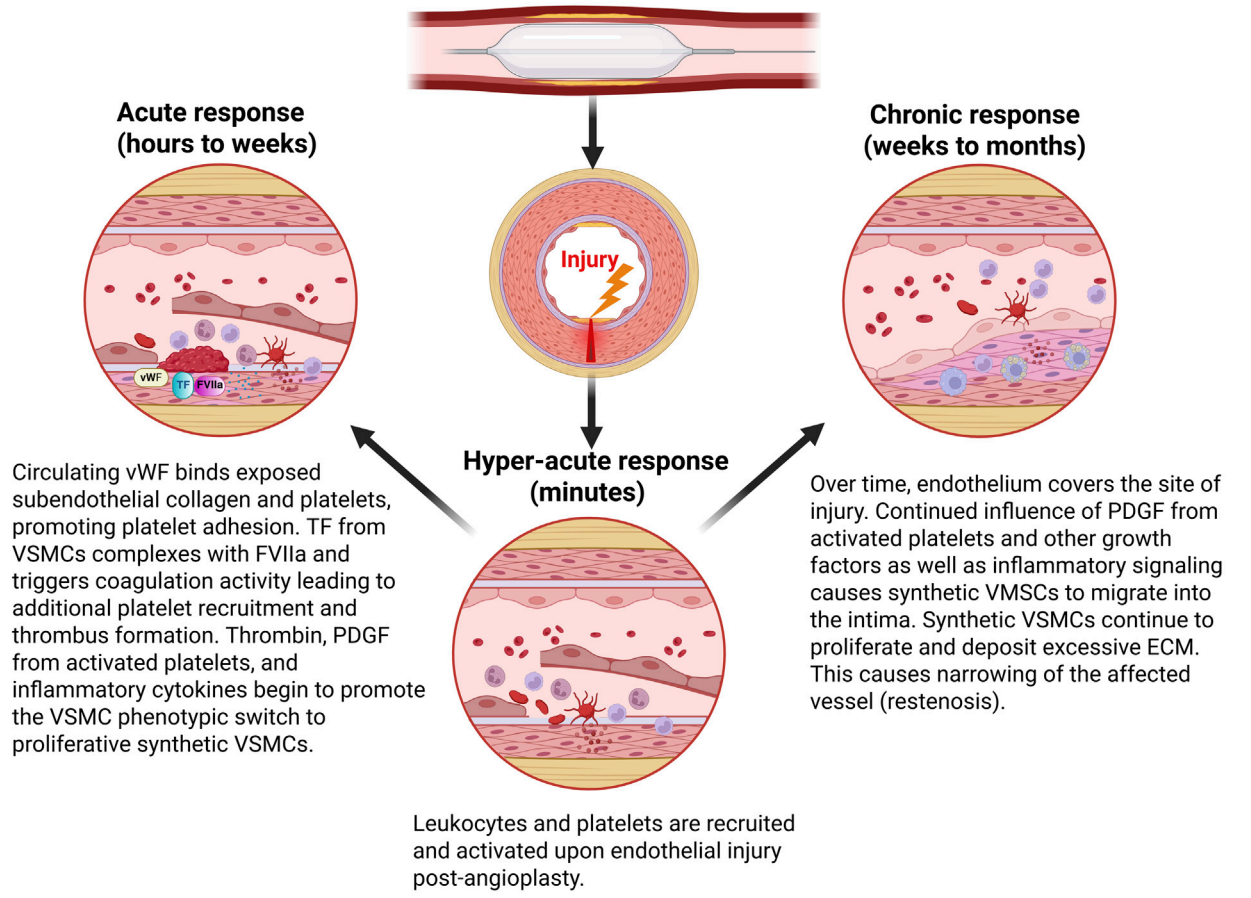

FIGURE 1
Vascular responses to balloon angioplasty leading to intimal hyperplasia. Created in BioRender. Dugas, T. (2025) https://BioRender.com/y22t579.

Challenges in treating PAD below the knee

Drug coated devices targeting vascular smooth muscle cell proliferation have improved vascular patency over bare metal stents and uncoated balloons in femoropopliteal lesions [32, 33]. However, long term benefits from DCBs in BTK segments have yet to be established. Below the knee, the infrapopliteal vessels including the anterior and posterior tibial, fibular, and pedal arteries are smaller, thinner, and are exposed to numerous mechanical forces. Stents run an elevated risk of fracture BTK and are typically used as a bailout option. Balloon angioplasty is considered the primary therapy to treat BTK PAD. However, there are multiple success-limiting factors for BTK lesions which include long lesion length, significant calcification, vascular elastic recoil, flow-limiting dissection, and restenosis [34]. While many DCB have gained FDA approval, none are approved for BTK arteries Table 1.

Drugs used in endovascular device coatings and their cellular targets

Paclitaxel

Paclitaxel, a potent tumoricidal drug, was first isolated in 1967. Paclitaxel has been used extensively as a cancer therapy. However, research performed in the 1990s demonstrated the ability of paclitaxel to inhibit VSMC proliferation [35]. The first paclitaxel-eluting stent was approved by the FDA for use in the

TABLE 1 Endovascular combination devices approved by the FDA in the past 10 years for the treatment of PAD.

Device	Manufacturer	FDA approval status	Lesion indication	Drug (μg/mm^2)	Coating
Esprit™ BTK everolimus eluting resorbable scaffold system	Abbott vascular (IDEF technologies inc.)	Approved 4/26/24	BTK	Everolimus 1 μg/mm^2	Poly (D,L-lactide)
SurVeil drug-coated balloon	Surmodics, inc.	Approved 6/16/23	FP	Paclitaxel 2 μg/mm^2	Polyethyleneimine polymer
Chocolate touch paclitaxel drug-coated PTA balloon catheter	TriReme medical, LLC, (now genesis medtech)	Approved 11/04/22	FP	Paclitaxel 2.95 μg/mm^2	Propyl gallate
Ranger™ paclitaxel-coated PTA balloon catheter	Boston Scientific corporation	Approved 10/30/20	FP	Paclitaxel 2 μg/mm^2	Acetyl tributyl citrate
Eluvia drug-eluting vascular stent system	Boston Scientific corporation	Approved 9/18/18	FP	Paclitaxel 0.167 μg/mm^2	PBMA (poly (n-butylmethacrylate)) and PVDF-HFP (vinylidene fluoride and hexafluoropropylene copolymer)
Stellarex 0.035 OTW drug-coated angioplasty balloon	The spectranetics corp.	Approved 7/26/17	FP	Paclitaxel 2 μg/mm^2	PEG-8000
IN.PACT admiral paclitaxel-coated PTA balloon catheter and IN.PACT 018 paclitax	Medtronic inc.	Approved 05/29/14	FP	Paclitaxel 3.5 μg/mm^2	Urea
Lutonix drug coated balloon PTA catheter	Lutonix	Approved 10/09/14	FP	Paclitaxel 2 μg/mm^2	Polysorbate and sorbitol

coronary arteries in 2004 after promising results from the TAXUS trials [36]. However, concerns regarding permanent stents and their association with IH lead to the development of paclitaxel coated balloons for coronary angioplasty. In the 2010s, paclitaxel-coated balloons underwent clinical trials to evaluate their use in small coronary arteries [37]. In 2015, the first trial using a Paclitaxel-coated DCB in FP arteries followed [38]. Since then, paclitaxel has been used commonly as a DCB coating. Paclitaxel acts as a microtubule stabilizing agent that prevents the tubular migration necessary for mitotic spindle assembly and causes cell cycle arrest in the G2/M phase [39]. Ultimately, these arrested cells undergo apoptosis. Paclitaxel upregulates BCL-2, DAP3, BAX, DAD1, and several other pro-apoptotic genes [40]. Additionally, paclitaxel affects multiple pathways associated with cellular proliferation, including receptor tyrosine kinases (RTK), TGF-B, and upstream regulators of the ERK pathway [40]. The effects of paclitaxel are non-specific; while paclitaxel inhibits VSMC proliferation, it may delay reendothelialization of denuded epithelia [41].

Paclitaxel controversy

With respect to decreased IH and reduced restenosis rates, the use of paclitaxel-coated devices represents a significant improvement over BMS and POBA. However, the use of paclitaxel in DES and DCB has not been without controversy. Katsanos et al. conducted a meta-analysis including 28 research-controlled trials assessing the use of paclitaxel-eluting DES and DCB. Their study demonstrated an increased risk of mortality associated with paclitaxel-coated devices [42]. A follow up meta-analysis demonstrated no significant increase in all-cause mortality between 1 and 2 years, but an increased risk of mortality between year 3 and 5 [43]. In 2019, the FDA issued a letter to healthcare providers to notify them of the increased late mortality signal. Following this, manufacturers of FDA-approved devices submitted deidentified individual patient data to the VIVA Physicians medical research organization, which produced an aggregate meta-analysis published in Circulation in May 2020 stating that no increased mortality signal was found [44]. Further meta-analyses of clinical trial data found no increase in all-cause mortality [45]. The FDA also analyzed data from several trials including the VOYAGER PAD study, the BARMER Health Insurance study, the Medicare Safe-PAD study, the U.S. Veterans Health Administration study, and the SWEDEPAD interim analysis [46]. By July 2023, the FDA issued updated guidance stating there was no increased mortality signal.

Sirolimus

Sirolimus, also known as rapamycin, is a macrolide antibiotic with poor antibacterial capabilities that is used as an immunomodulatory, cytostatic, and antiproliferative agent. Sirolimus acts to inhibit the mTOR pathway by reversibly binding to FK506-binding protein 12 (FKBP12). FKBP12 binds tacrolimus (FK506) as well as rapamycin and

TABLE 2 Paclitaxel versus sirolimus: Reported effects exerted on cellular events that follow endovascular interventions.

Cellular events that follow intervention with stents and balloons	Paclitaxel	Sirolimus
Platelet aggregation	Inhibits collagen-mediated platelet aggregation and TXA_2 synthase [49]; enhances platelet aggregation via increased sensitivity to ADP [50]	Enhanced platelet aggregation via increased platelet sensitivity to ADP [51, 52]
Inflammation	Increased [53, 54]	Reduced [55, 56]
VSMC proliferation	Inhibited [35]	Inhibited [57]
VSMC migration	Inhibited [35]	Inhibited [58]
Cell death	Promotes apoptosis and autophagy [39, 40, 59]	Prolongs the G1 phase prior to the G1/S checkpoint in a reversible manner [47]
Reendothelialization	Inhibited [60]	Inhibited [61]

other rapalogs, creating a complex that inhibits MTORC1 [47]. The downstream result of mTORC1 inhibition is that cells cannot progress through the G1/S transition and are maintained in G1. Sirolimus inhibits VSMC proliferation via this mechanism. Additionally, inhibition of NF-kB by sirolimus has been previously demonstrated [48]. Inhibition of NF-kB has downstream effects on the expression of leukocyte adhesion molecules and chemoattractants, conferring an anti-inflammatory role in addition to its other effects. While sirolimus and paclitaxel are some of the most frequently used drugs in DCBs, there are key differences in how they affect cellular processes Table 2.

Everolimus and other limus drugs

Everolimus, 40-O-(2-hydroxyethyl)-rapamycin, is a sirolimus analog with a hydroxyethyl group at C-40 [62]. Modification of sirolimus in this manner was intended to improve oral bioavailability but resulted in several key differences in the behavior of everolimus [63]. Everolimus is an mTOR inhibitor with a weaker binding affinity for FKBP12 than sirolimus. Unlike sirolimus, which only inhibits MTORC2 with chronic use, everolimus demonstrates activity against both MTORC1 and MTORC2 [64]. Similar to sirolimus, the end result is that cells do not progress past G1 of the cell cycle [65].

Everolimus was initially developed for use in solid organ transplants. Owing to its antiproliferative properties, interest in its use in coronary stents culminated in the FUTURE and SPIRIT FIRST clinical trials [66, 67]. In 2009, the FDA approved the first everolimus-eluting stent for use in the coronary arteries. Since then, everolimus-eluting stents have been designed for use in peripheral arteries, including the XIENCE Prime™ BTK Everolimus Eluting Peripheral Stent by Abbott (currently marketed outside of the US). Most recently, the Esprit™ BTK everolimus eluting resorbable scaffold system by Abbott Vascular was approved by the FDA for use in infrapopliteal arteries.

Zotarolimus is the first limus drug designed specifically for use in drug-eluting stents. Some of these stents include the Medtronic Endeavor stents and now the Medtronic Onyx Frontier stent, which are used in CAD [68, 69]. Zotarolimus exhibits enhanced lipophilicity compared to sirolimus, allowing it to traverse cellular membranes more easily than the less lipophilic drugs sirolimus and paclitaxel [70]. As in sirolimus and everolimus, zotarolimus inhibits smooth muscle cell proliferation via mTOR inhibition [71]. A study assessing reendothelialization rates in an ilio-femoral atherosclerotic rabbit model treated with zotarolimus-compared to everolimus-eluting stents found decreased inflammation and increased expression of CD31, a marker of mature endothelial cells, in the everolimus-treated group compared to the zotarolimus-treated group, suggesting that reendothelialization may occur faster with everolimus than zotarolimus [72]. However, an *in vitro* study examining reendothelialization after inducing an injury in cultured endothelial cells found that regrowth of the injured area occurred more quickly with zotarolimus compared to sirolimus or paclitaxel [73]. While zotarolimus eluting stents have been used in CAD, this technology is not FDA approved for peripheral arteries. Similarly, zotarolimus-coated balloons have been evaluated in pre-clinical studies using the swine femoral artery, however there are no zotarolimus-coated balloons that are FDA approved for treating PAD lesions [74].

Coating technologies and their contributions to efficacy and/or complications

Contributions to efficacy

Unlike DES, which remain in the vessel indefinitely, DCB must be designed such that the coating adheres to the balloon during tracking while also effectively releasing all of their drug/

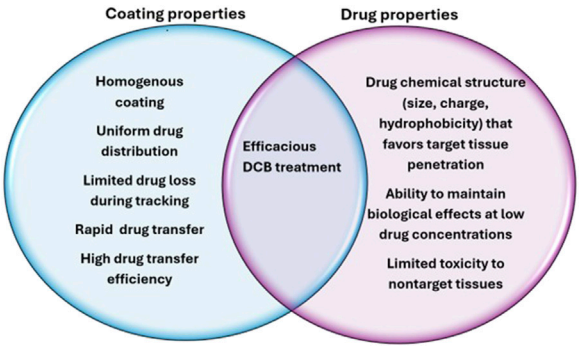

FIGURE 2
Ideal characteristics of DCB coatings and drugs to maximize efficacy.

carrier cargo to the target lesion within a window of 1–3 min. Therefore, the development of effective transfer mechanisms is emphasized in DCB development. Additionally, the coating should have a uniform density and elicit minimal inflammatory responses. The coating should also enhance drug transfer from the device to target tissues with effective tissue penetration and appropriate tissue residence time. Coatings often include excipients, which are defined as ingredients other than the active drug within a formulation. Commonly used excipients in DCBs include urea, polyethylene glycol (PEG), polysorbate and sorbitol, iopromide, and others [75–78]. Excipients can improve drug stability within the vessel environment and modify tissue uptake. Excipients can also act as delivery vehicles, directly transporting drugs to target sites [79–81].

Additional considerations are the hydrophilicity or hydrophobicity of the coating. Hydrophobic coatings create a repellent surface that allows blood to pass over the device. However, hydrophobic coatings may be less hemocompatible than hydrophilic coatings. Multiple studies have associated complement component C3 and fibronectin adsorption as well as monocyte and platelet adhesion with hydrophobic coatings [82–84]. On the other hand, recent investigations into superhydrophobic coatings demonstrate enhanced hemocompatibility. Experimental studies assessing the hemocompatibility of superhydrophobic coatings show reduced protein adsorption and decreased platelet adhesion [85–87].

Polymeric coatings have been used extensively on medical devices. Polymeric hydrophilic coatings exhibit less blood protein adsorption than polymeric hydrophobic coatings, demonstrating enhanced hemocompatibility [82]. Polymeric hydrophilic coatings attract water and tend to be more slippery than hydrophobic coatings, which promotes navigation through tortuous arterial segments during PTA procedures. Additionally, hydrophilic coatings have been shown to promote rapid drug transfer [88]. In DCBs where the drug load needs to be transferred rapidly from the balloon surface to the treatment site, hydrophilic coatings are advantageous. The downside of hydrophilic coatings is that while they promote drug transfer, they are also prone to significant drug loss from the coating surface during catheter tracking [89, 90].

Aside from the physical properties of the coating, the coating method itself is also an important factor that contributes to efficacy. Several methods exist for applying coatings, each with their own benefits and drawbacks. There are many methods including dip coating, air or ultrasonic spray coating, and others. A study conducted by Gandhi and Murthy found that dip coating balloon catheters created a generally smooth surface, but the coating accumulated around pleated regions of the uninflated balloons, which could alter drug release. The same study showed that an ultrasonic spray coating created a balloon surface with microcracks, while airbrushing created the most uniform surface [91]. Ideal properties of coating and drugs used for DCB are summarized below Figure 2.

Coating distribution, dose, composition and their relations to complications

The interactions between active drugs and the coating are critical components of not only drug delivery, but also the biocompatibility of combination devices. While various excipient coatings have markedly improved drug delivery, coating embolization is also a significant concern in endovascular devices. A study performed by Torii and colleagues compared DCB coating embolization in swine arteries using the IN. PACT, Ranger, and Stellarex DCBs. The IN. PACT DCB utilizes a highly hydrophilic urea coating. In contrast, the Ranger DCB uses an acetyl tributyl citrate carrier that is highly hydrophobic. The study concluded that downstream emboli were found more frequently in the IN. PACT DCB treated arteries [92]. While correlations were drawn between increasing paclitaxel concentration and increased incidence of emboli, it is also possible that the hydrophilicity of the IN. PACT DCB urea coating contributed to embolization via loss during tracking or failure to adhere to the vessel wall due to enhanced affinity for the hydrophilic blood compartment compared to hydrophobic cellular membranes [93]. Previous work in porcine models demonstrated distal excipient-crystalline drug emboli present in the coronary band of pigs after femoral artery angioplasty with paclitaxel-coated balloons [94].

Biodegradable polymers were designed to mitigate inflammatory and thrombotic responses associated with early durable stent coatings. However, biodegradable polymers have also been associated with biocompatibility issues. In the multi-center study conducted by van der Giessen and coworkers, coating materials consisting of both durable and

biodegradable polymers were applied to stents that were implanted into pig arteries and left in place for 4 weeks. All of the polymers tested, including biodegradable PLGA, elicited inflammation in the implanted arteries and lumen narrowing was observed [95]. However, the stents themselves could have contributed to the elicited reaction, as the materials were not sterilized prior to implantation. They also observed that the applied polymer coatings did not fully cover the stents after expansion, leaving areas of bare metal in direct apposition to the treated arteries [95]. Other cited drawbacks associated with PLGA are bulk polymer erosion and burst drug release [96]. Additionally, accumulation of glycolic and lactic acid at local sites due to rapid breakdown of PLGA may incite inflammatory responses [97]. Meanwhile, other studies have found PLGA coated stents to be no more inflammatory than BMS [98]. While PLGA is one of the most widely used polymers in medical devices, continued investigations into PLGA biocompatibility are warranted.

Submicron drug coatings including polymeric nanoparticles are being developed for treatment of PAD lesions [32, 99]. While these technologies have been studied in the setting of cancer treatment and have shown promising results, there are points to consider with the use of submicron particles. Adherence of nanoparticles to the balloon surface during delivery is key; otherwise, there is potential for blood flow to cause early deployment of particles to non-target areas. Blood interactions with nanoparticles are important considerations. Nanoparticle composition, size, and charge are determining factors for how the particles interact with cells in the blood compartment. For example, carbon nanoparticles have been shown to promote venous thrombosis and platelet aggregation [100]. Additionally, some nanoparticles can enter cells such as RBCs by direct penetration of the cell membrane [101]. While carbon nanoparticles have been shown to promote thrombosis, other studies have documented a lack of increased platelet aggregation with the use of PLGA nanoparticles, highlighting the importance of particle type selection for use in blood contacting devices [102]. Bakhaidar and coworkers demonstrated that PLGA-PEG nanoparticles ranging from 112 to 576 nm interacted with and bound to platelets; however, this did not increase platelet aggregation [103].

Emerging devices in BTK PAD therapy

Emerging drug coated balloons

While there have been several clinical trials investigating DCBs for use in BTK PAD lesions, none have emerged as FDA-approved. DCB treatment has not yet demonstrated long term benefits over POBA treatment alone in clinical trials. However, several new DCB have been granted breakthrough device designation and are currently in clinical trials. These newer DCB formulations range from microcrystalline polymer-free coatings to liquid delivery systems. These combination devices deliver sirolimus as well as combinations of sirolimus and paclitaxel. A table summarizing these novel devices, what we know about their coating properties, and selected clinical trials is listed below Table 3.

The MagicTouch DCB is used in coronary applications in Europe and Asia; however, it has yet to gain FDA approval in the United States. Recently, Concept Medical's MagicTouch DCB received FDA breakthrough designation for BTK PAD lesions. This DCB utilizes a polymer-free approach with Nanolute technology, proprietary 100–300 nm phospholipid microspheres carrying sirolimus. The coating density of the MagicTouch DCB is 1.27 μg/mm^2 [104]. Three-year results from the XTOSI pilot study published in 2024 demonstrate 77.8% freedom from major amputation for BTK lesions [105]. Several clinical trials are currently investigating the use of MagicTouch DCB in both FP and BTK PAD.

Like the MagicTouch DCB, the Sundance™ DCB by SurModics utilizes a polymer-free formulation. The Sundance formulation is a microcrystalline sirolimus coating with their coating density and proprietary excipient yet to be disclosed. In 2020, they commenced the SWING study, a prospective multi-center single arm study that enrolled 35 patients. The completion date for the study was 30 January 2024. SurModics has yet to publish the results of their study, although they reported 71.4% primary patency maintained at 24 months [106].

The Selution SLR DCB uses sirolimus-loaded PLGA microspheres contained in MicroReservoirs which are coated with Cell Adherent Technology (CAT), a mixture of phospholipids that reportedly protect the microspheres during catheter insertion and tracking. The coating density of the balloon is 1 μg/mm^2 [107]. The PRESTIGE pilot study investigated the performance of the Selution SLR DCB in occlusive tibial disease and showed 81.5% tibial patency at 6 months [108]. In 2023, the prospective, randomized multicenter single blinded study, SELUTION4BTK completed enrollment with 377 subjects. The aim of the study is to assess the safety and effectiveness of the Selution SLR DCB in treating BTK PAD in patients with CTLI. The anticipated completion date is 30 July 2029 [109]. In May 2025, investigators reported 12-month data from SUCCESS PTA study at the 2025 New Cardiovascular Horizons meeting. SUCCESS PTA is a single arm post-market surveillance study conducted out of treatment centers in Europe. They reported 2.2% target limb amputation and greater than 90% freedom from clinically driven target lesion revascularization in the 12 months cohort, with an average lesion length of 12–13 cm [110].

While the use of paclitaxel in DCB products is generally being replaced by sirolimus in new generation products, the SirPlux Duo by Advanced NanoTherapies combines both sirolimus and paclitaxel in a novel dual-agent formulation. Paclitaxel and sirolimus are co-encapsulated at a 1:9 w/w ratio within nanoparticles [32]. The coating density, excipient, and composition of the nanoparticle carrier are unclear, although a patent submitted by Advanced Nanotherapies in 2023 suggests

TABLE 3 Recent DCBs with FDA breakthrough designation for BTK PAD and associated clinical trials.

Device	Drug	Coating	Clinical trials
Sundance™ DCB, surmodics inc	Microcrystalline sirolimus *Coating density undisclosed*	*Undisclosed*	SWING
Selution™ SLR, cordis	Sirolimus 1 μg/mm^2	PLGA (poly (lactic-co-glycolic acid)) microspheres	PRESTIGE PRISTINE SUCCESS SELUTION4BTK
MagicTouch™ DCB, concept medical	Sirolimus 1.27 μg/mm^2	Sub-micron phospholipid carrier	XTOSI FUTURE-BTK LIMES MAGICAL BTK SIRONA
SirPlux duo Advanced NanoTherapies	Co-encapsuled 1:9 paclitaxel:sirolimus w/w *Coating density undisclosed*	Nanoparticle, carrier composition undisclosed	ADVANCE-DCB

TABLE 4 BTK trial data for DCB with FDA breakthrough designation status.

Device	Clinical trial	Trial type	Primary patency	CD-TLR (or freedom from CD-TLR)	Freedom from major amputation
Sundance™ DCB, surmodics inc.	SWING [113] (12 months results)	Single arm feasibility study	80%	8%	Not reported
	SWING [106] (24 months results)	Single arm feasibility study	71.4%	8.3%	Not reported
Selution™ SLR, cordis	PRESTIGE [108] (12 months results)	Single arm pilot study	78%	93% freedom from CD-TLR	87% at 12 months
	PRISTINE [114] (12 months results)	Single arm registry study	59.5%	7.4%	72.6% (amputation free survival)
MagicTouch™ DCB, concept medical	XTOSI [105] (36 months results)	Single arm pilot study	50% (at 24 months)	77.8% freedom from CD-TLR	81% at 36 months
Pending trials, results not yet reported:					
Selution™ SLR, cordis	SELUTION4BTK [115]	Randomized controlled trial vs. POBA			
MagicTouch™ DCB, concept medical	FUTURE-BTK [116]	Randomized controlled trial vs. POBA			
	LIMES [117]	Randomized controlled trial vs. POBA			
	MAGICAL BTK [118]	Randomized controlled trial vs. POBA			

that PLGA may be used to entrap paclitaxel and sirolimus [111]. Preclinical work in porcine coronary and femoral arteries and rabbit iliac arteries demonstrate reduced VSMC proliferation with SirPlux Duo compared to paclitaxel DCB treatment [32]. They also investigated particle embolism in a porcine coronary artery model and found a significant reduction in embolized material with the SirPlux Duo DCB. A first-in-human clinical trial investigating the use of SirPlux Duo in patients with *de novo* CAD lesions is currently ongoing [112]. Listed below are some of the early results and up-and-coming clinical trials for DCBs with breakthrough designation status for BTK disease Table 4.

Other balloon-based therapies and novel lesion preparation devices

Aqueous delivery systems that circumvent concerns surrounding the use of drug-coated surfaces in the blood compartment have also been investigated. Atigh et al., delivered paclitaxel via liquid delivery in saline with iohexol as the excipient in *ex vivo* porcine carotid arteries using the Occlusion Perfusion Catheter system by Advanced Catheter Therapies [119]. They were able to demonstrate that the Occlusion Perfusion Catheter effectively delivered the liquid drug into the arterial wall. Similarly, the Virtue SAB by Orchestra BioMed uses a novel AngioInfusion balloon that delivers lyophilized submicron sirolimus in a polyester

nanoparticle carrier via aqueous delivery. This device received breakthrough designation status for BTK PAD, and most recently, investigational device exemption by the FDA in May 2025. Currently, Orchestra Biomed plans to start the VIRTUE trial, a pivotal clinical trial looking at coronary in-stent restenosis.

While not strictly a balloon device, the novel Spur Retrievable Stent System by Reflow Medical has potential to enhance DCB therapy. This device consists of a self-expanding, balloon-delivered stent covered in radial spikes which penetrate the arterial wall. By creating channels in the arterial wall, the Spur device disrupts calcification and enhances vessel compliance, reducing elastic recoil immediately after treatment [120]. Additionally, these arterial channels may increase DCB drug penetration. Previously completed clinical trials investigating the use of the Spur BTK followed by DCB therapy include the DEEPER [121], DEEPER OUS [120], and most recently, the DEEPER LIMUS [122] trials.

Stents and resorbable scaffolds

While this review focuses primarily on balloon-based therapies, we would be remiss to exclude these devices from discussion. While the "leave nothing behind" approach has favored DCB for BTK disease, stents and resorbable scaffolds have been gaining traction. Several stents and resorbable scaffolds have gained FDA breakthrough designation status, and one resorbable scaffold, the Esprit BTK everolimus-eluting bioresorbable scaffold by Abbott, recently gained FDA approval [123].

Resorbable scaffolds aim to bridge the gap between providing structural support and minimizing permanent implants. In April 2024, Abbott's Esprit BTK everolimus-eluting bioresorbable scaffold received FDA approval [123] for CTLI in BTK disease. According to Abbott, this bioresorbable stent maintains radial strength similar to metal stents for the first 6 months and fully dissolves within two to 3 years. In the LIFE-BTK trial, Abbott reported substantially improved efficacy compared to POBA with respect to primary efficacy endpoints at 1 year [124]. Two-year follow up demonstrated continued superior efficacy over POBA, with respect to a composite of limb salvage and primary patency [125].

In March 2024, the Biotronik Freesolve BTK RMS received breakthrough designation status for CTLI BTK disease. This resorbable metal scaffold consists of a proprietary magnesium alloy utilizing sirolimus to treat lesioned arteries [126]. The first-in-human BIOMAG I trial examined late lumen loss (LLL) as a primary endpoint in coronary artery disease. Between 6 and 12 months, significant increase in in-device LLL was reported, however no scaffold thrombosis was observed [126]. The BIOMAG II RCT trial began enrollment in in May 2024, and will compare safety and efficacy endpoints versus the Xience everolimus-eluting stent [127].

Efemoral medical's Efemoral Vascular Scaffold System also received breakthrough designation status in 2024. This bioresorbable system, like the Freesolve, utilizes sirolimus as an antirestenotic agent. The Efemoral vascular scaffold system focuses on enhancing biomechanical compatibility, utilizing a patented FlexStep system which utilizes interscaffold spaces to enhance device flexibility [128]. The first-in-human EFEMORAL I trial is still ongoing (NCT: 04584632).

Another notable stent to receive FDA breakthrough designation status for BTK indications includes Elixir Medical's DynamX BTK system. The DynamX BTK Bioadaptor represents a hybrid between bioresorbable polymer elements and metallic scaffolding materials which deploy as the polymer dissolves [129]. The bioresorbable coating consists of poly-L-lactide (PLLA) eluting novolimus [129] and is currently undergoing clinical trials for coronary applications, with plans to design a modified version of the device for BTK therapy [130].

Discussion

PAD is a complex and multifactorial disease that leaves patients prone to thrombosis, arterial occlusion, and loss of limb. Endothelial injury and dysfunction play a key role in the pathogenesis of PAD. PAD below the knee is challenging to treat due to the types of lesions, extent of lesions, as well as significant problems with calcification as a barrier to drug penetration and vascular elastic recoil limiting luminal diameter post-treatment. Yet, numerous novel devices are on the horizon. While DCBs for use below the knee have yet to gain FDA approval, lessons learned from previous device iterations pave the way forward for next-generation devices. Further advancement in coating technology and drug delivery systems permit the use of less drug than older generation devices and rely less on large particulate and crystalline coatings. These changes may limit toxicity off target associated with commonly used drugs like paclitaxel and sirolimus. Drug eluting stents and bioresorbable scaffolds have been gaining momentum in BTK disease treatment and provide another promising avenue for interventions. Abbott's Esprit BTK received FDA approval, and several bioresorbable scaffolds and DES received FDA breakthrough designation status in just the past year. As clinical trials progress, we will discover whether these breakthrough therapies can gain FDA approval for BTK disease treatment.

Author contributions

All authors listed have made a substantial, direct, and intellectual contribution to the work and approved it for publication.

Funding

The authors declare that financial support was received for the research and/or publication of this article. Funds for this

work were provided through discretionary funding through the LSU School of Veterinary Medicine (PM20GM130555).

Conflict of interest

The author(s) declared no potential conflicts of interest with respect to the research, authorship, and/or publication of this article.

Generative AI statement

The authors declare that no Generative AI was used in the creation of this manuscript.

Any alternative text (alt text) provided alongside figures in this article has been generated by Frontiers with the support of artificial intelligence and reasonable efforts have been made to ensure accuracy, including review by the authors wherever possible. If you identify any issues, please contact us.

References

1. Criqui MH, Matsushita K, Aboyans V, Hess CN, Hicks CW, Kwan TW, et al. Lower extremity peripheral artery disease: contemporary epidemiology, management gaps, and future directions: a scientific statement from the American heart association. *Circulation* (2021) **144**:e171–e191. doi:10.1161/cir.0000000000001005

2. Agnelli G, Belch JJF, Baumgartner I, Giovas P, Hoffmann U. Morbidity and mortality associated with atherosclerotic peripheral artery disease: a systematic review. *Atherosclerosis* (2020) **293**:94–100. doi:10.1016/j.atherosclerosis.2019.09.012

3. Bevan GH, White Solaru KT. Evidence-based medical management of peripheral artery disease. *Arterioscler Thromb Vasc Biol* (2020) **40**:541–53. doi:10.1161/atvbaha.119.312142

4. Gornik HL, Aronow HD, Goodney PP, Arya S, Brewster LP, Byrd L, et al. 2024 ACC/AHA/AACVPR/APMA/ABC/SCAI/SVM/SVN/SVS/SIR/VESS guideline for the management of lower extremity peripheral artery disease: a report of the American college of cardiology/american heart association joint committee on clinical practice guidelines. *Circulation* (2024) **149**:e1313–e1410. doi:10.1161/CIR.0000000000001251

5. Thukkani AK, Kinlay S. Endovascular intervention for peripheral artery disease. *Circ Res* (2015) **116**:1599–613. doi:10.1161/circresaha.116.303503

6. Liistro F, Angioli P, Ventoruzzo G, Ducci K, Reccia MR, Ricci L, et al. Randomized controlled trial of acotec drug-eluting balloon *versus* plain balloon for below-the-knee angioplasty. *JACC: Cardiovasc Interventions* (2020) **13**:2277–86. doi:10.1016/j.jcin.2020.06.045

7. Narula N, Dannenberg AJ, Olin JW, Bhatt DL, Johnson KW, Nadkarni G, et al. Pathology of peripheral artery disease in patients with critical limb ischemia. *J Am Coll Cardiol* (2018) **72**:2152–63. doi:10.1016/j.jacc.2018.08.002

8. Smolenski A. Novel roles of cAMP/cGMP dependent signaling in platelets. *J Thromb Haemost* (2012) **10**:167–76. doi:10.1111/j.1538-7836.2011.04576.x

9. Wood JP, Bunce MW, Maroney SA, Tracy PB, Camire RM, Mast AE. Tissue factor pathway inhibitor-alpha inhibits prothrombinase during the initiation of blood coagulation. *Proc Natl Acad Sci U S A* (2013) **110**:17838–43. doi:10.1073/pnas.1310444110

10. Rhee M, Lee J, Lee EY, Yoon K-H, Lee S-H. Lipid variability induces endothelial dysfunction by increasing inflammation and oxidative stress. *Endocrinol Metab* (2024) **39**:511–20. doi:10.3803/enm.2023.1915

11. Sellak H, Franzini E, Hakim J, Pasquier C. Reactive oxygen species rapidly increase endothelial ICAM-1 ability to bind neutrophils without detectable upregulation. *Blood* (1994) **83**:2669–77. doi:10.1182/blood.v83.9.2669.bloodjournal8392669

12. De Caterina R, Libby P, Peng HB, Thannickal VJ, Rajavashisth TB, Gimbrone MA, et al. Nitric oxide decreases cytokine-induced endothelial activation. Nitric oxide selectively reduces endothelial expression of adhesion molecules and proinflammatory cytokines. *J Clin Invest* (1995) **96**:60–8. doi:10.1172/jci118074

13. Kubes P, Suzuki M, Granger DN. Nitric oxide: an endogenous modulator of leukocyte adhesion. *Proc Natl Acad Sci* (1991) **88**:4651–5. doi:10.1073/pnas.88.11.4651

14. Badimon L, Vilahur G. Thrombosis formation on atherosclerotic lesions and plaque rupture. *J Intern Med* (2014) **276**:618–32. doi:10.1111/joim.12296

15. Rafieian-Kopaei M, Setorki M, Doudi M, Baradaran A, Nasri H. Atherosclerosis: process, indicators, risk factors and new hopes. *Int J Prev Med* (2014) **5**:927–46.

16. Fernández-Ortiz A, Badimon JJ, Falk E, Fuster V, Meyer B, Mailhac A, et al. Characterization of the relative thrombogenicity of atherosclerotic plaque components: implications for consequences of plaque rupture. *J Am Coll Cardiol* (1994) **23**:1562–9. doi:10.1016/0735-1097(94)90657-2

17. Torii S, Mustapha JA, Narula J, Mori H, Saab F, Jinnouchi H, et al. Histopathologic characterization of peripheral arteries in subjects with abundant risk factors: correlating imaging with pathology. *JACC: Cardiovasc Imaging* (2019) **12**:1501–13. doi:10.1016/j.jcmg.2018.08.039

18. Chang Z, Yan H, Zhen Y, Zheng J, Liu Z. Lower limb arterial calcification and acute thrombosis risk in patients with peripheral artery disease. *Ann Vasc Surg* (2020) **63**:227–33. doi:10.1016/j.avsg.2019.06.043

19. Narula N, Olin JW, Narula N. Pathologic disparities between peripheral artery disease and coronary artery disease. *Arterioscler Thromb Vasc Biol* (2020) **40**:1982–9. doi:10.1161/atvbaha.119.312864

20. Konijn LCD, Takx RAP, Mali WPTM, Veger HTC, van Overhagen H. Different lower extremity arterial calcification patterns in patients with chronic limb-threatening ischemia compared with asymptomatic controls. *J Pers Med* (2021) **11**:493. doi:10.3390/jpm11060493

21. Konijn LCD, Takx RAP, Jong PA, Spreen MI, Veger HTC, Mali WPTM, et al. Arterial calcification and long-term outcome in chronic limb-threatening ischemia patients. *Eur J Radiol* (2025) **132**. doi:10.1016/j.ejrad.2020.109305

22. Block PC, Myler RK, Stertzer S, Fallon JT. Morphology after transluminal angioplasty in human beings. *New Engl J Med* (1981) **305**:382–5. doi:10.1056/nejm198108133050706

23. Bryckaert M, Rosa J-P, Denis CV, Lenting PJ. Of von Willebrand factor and platelets. *Cell Mol Life Sci* (2014) **72**:307–26. doi:10.1007/s00018-014-1743-8

24. Daniel JL, Dangelmaier C, Jin J, Ashby B, Smith JB, Kunapuli SP. Molecular basis for ADP-Induced platelet activation: I. Evidence for three distinct adp receptors on human platelets. *J Biol Chem* (1998) **273**:2024–9. doi:10.1074/jbc.273.4.2024

25. Nakagaki T, Foster DC, Berkner KL, Kisiel W. Initiation of the extrinsic pathway of blood coagulation: evidence for the tissue factor dependent autoactivation of human coagulation factor VII. *Biochemistry* (1991) **30**:10819–24. doi:10.1021/bi00109a001

26. Ha JM, Yun SJ, Kim YW, Jin SY, Lee HS, Song SH, et al. Platelet-derived growth factor regulates vascular smooth muscle phenotype *via* mammalian target of rapamycin complex 1. *Biochem Biophysical Res Commun* (2015) **464**:57–62. doi:10.1016/j.bbrc.2015.05.097

27. Sato Y, Hamanaka R, Ono J, Kuwano M, Rifkin DB, Takaki R. The stimulatory effect of PDGF on vascular smooth muscle cell migration is mediated by the induction of endogenous basic FGF. *Biochem Biophysical Res Commun* (1991) **174**:1260–6. doi:10.1016/0006-291x(91)91557-s

28. Kohno K, Koya-Miyata S, Harashima A, Tsukuda T, Katakami M, Ariyasu T, et al. Inflammatory M1-like macrophages polarized by NK-4 undergo enhanced phenotypic switching to an anti-inflammatory M2-like phenotype upon co-culture with apoptotic cells. *J Inflamm* (2021) **18**:2. doi:10.1186/s12950-020-00267-z

29. Choi S, Park M, Kim J, Park W, Kim S, Lee D-K, et al. TNF-α elicits phenotypic and functional alterations of vascular smooth muscle cells by miR-155-5p–dependent down-regulation of cGMP-dependent kinase 1. *J Biol Chem* (2018) **293**:14812–22. doi:10.1074/jbc.ra118.004220

30. Jovinge S, Hultga˚rdh-Nilsson A, Regnström J, Nilsson J. Tumor necrosis Factor-α activates smooth muscle cell migration in culture and is expressed in the balloon-injured rat aorta. *Arterioscler Thromb Vasc Biol* (1997) **17**:490–7. doi:10.1161/01.atv.17.3.490

31. Rectenwald JE, Moldawer LL, Huber TS, Seeger JM, Ozaki CK. Direct evidence for cytokine involvement in neointimal hyperplasia. *Circulation* (2000) **102**:1697–702. doi:10.1161/01.cir.102.14.1697

32. Kawai K, Rahman MT, Nowicki R, Kolodgie FD, Sakamoto A, Kawakami R, et al. Efficacy and safety of dual paclitaxel and sirolimus nanoparticle-coated balloon. *JACC: Basic Translational Sci* (2024) **9**:774–89. doi:10.1016/j.jacbts.2024.02.002

33. Shishehbor MH, Scheinert D, Jain A, Brodmann M, Tepe G, Ando K, et al. Comparison of drug-coated balloons vs bare-metal stents in patients with femoropopliteal arterial disease. *J Am Coll Cardiol* (2023) **81**:237–49. doi:10.1016/j.jacc.2022.10.016

34. Beckman JA, Schneider PA, Conte MS. Advances in revascularization for peripheral artery disease: revascularization in PAD. *Circ Res* (2021) **128**:1885–912. doi:10.1161/circresaha.121.318261

35. Axel DI, Kunert W, Göggelmann C, Oberhoff M, Herdeg C, Küttner A, et al. Paclitaxel inhibits arterial smooth muscle cell proliferation and migration *in vitro* and *in vivo* using local drug delivery. *Circulation* (1997) **96**:636–45. doi:10.1161/01.cir.96.2.636

36. Grube E, Silber S, Hauptmann KE, Mueller R, Buellesfeld L, Gerckens U, et al. TAXUS I: six- and twelve-month results from a randomized, double-blind trial on a slow-release paclitaxel-eluting stent for *de novo* coronary lesions. *Circulation* (2003) **107**:38–42. doi:10.1161/01.cir.0000047700.58683.a1

37. Unverdorben M, Kleber FX, Heuer H, Figulla H-R, Vallbracht C, Leschke M, et al. Treatment of small coronary arteries with a paclitaxel-coated balloon catheter. *Clin Res Cardiol* (2010) **99**:165–74. doi:10.1007/s00392-009-0101-6

38. Rosenfield K, Jaff MR, White CJ, Rocha-Singh K, Mena-Hurtado C, Metzger DC, et al. Trial of a paclitaxel-coated balloon for femoropopliteal artery disease. *New Engl J Med* (2015) **373**:145–53. doi:10.1056/nejmoa1406235

39. Shu CH, Yang WK, Shih YL, Kuo ML, Huang TS. Cell cycle G2/M arrest and activation of cyclin-dependent kinases associated with low-dose paclitaxel-induced sub-G1 apoptosis. *Apoptosis* (1997) **2**:463–70. doi:10.1023/a:1026422111457

40. Nguyen KT, Shaikh N, Wawro D, Zhang S, Schwade ND, Eberhart RC, et al. Molecular responses of vascular smooth muscle cells to paclitaxel-eluting bioresorbable stent materials. *J Biomed Mater Res A* (2004) **69A**:513–24. doi:10.1002/jbm.a.30020

41. Nakazawa G, Finn AV, Virmani R. Vascular pathology of drug-eluting stents. *Herz* (2007) **32**:274–80. doi:10.1007/s00059-007-2997-9

42. Katsanos K, Spiliopoulos S, Kitrou P, Krokidis M, Karnabatidis D. Risk of death following application of paclitaxel-coated balloons and stents in the femoropopliteal artery of the leg: a systematic review and meta-analysis of randomized controlled trials. *J Am Heart Assoc* (2018) **7**:e011245. doi:10.1161/jaha.118.011245

43. Bittl JA, He Y, Baber U, Feldman RL, von Mering GO, Kaul S. Bayes factor meta-analysis of the mortality claim for peripheral paclitaxel-eluting devices. *JACC: Cardiovasc Interventions* (2019) **12**:2528–37. doi:10.1016/j.jcin.2019.09.028

44. Rocha-Singh KJ, Duval S, Jaff MR, Schneider PA, Ansel GM, Lyden SP, et al. Mortality and paclitaxel-coated devices: an individual patient data meta-analysis. *Circulation* (2020) **141**:1859–69. doi:10.1161/circulationaha.119.044697

45. Dinh K, Limmer AM, Chen AZL, Thomas SD, Holden A, Schneider PA, et al. Mortality rates after paclitaxel-coated device use in patients with occlusive femoropopliteal disease: an updated systematic review and meta-analysis of randomized controlled trials. *J Endovasc Ther* (2021) **28**:755–77. doi:10.1177/15266028211023505

46. Health CD. UPDATE: paclitaxel-coated devices to treat peripheral arterial disease unlikely to increase risk of mortality - letter to health care providers. *FDA* (2023). Available online at: https://www.fda.gov/medical-devices/letters-health-care-providers/update-paclitaxel-coated-devices-treat-peripheral-arterial-disease-unlikely-increase-risk-mortality (Accessed July 9, 2025).

47. Sehgal SN. Sirolimus: its discovery, biological properties, and mechanism of action. *Transplant Proc* (2003) **35**:7S–14S. doi:10.1016/s0041-1345(03)00211-2

48. Liu Y, Li X, Jin A. Rapamycin inhibits Nf-KB activation by autophagy to reduce catabolism in human chondrocytes. *J Invest Surg* (2020) **33**:861–73. doi:10.1080/08941939.2019.1574321

49. Lee J-J, Yu J-Y, Lee J-H, Zhang WY, Kim T-J, Myung C-S, et al. The protective effects of paclitaxel on platelet aggregation through the inhibition of thromboxane A2 synthase. *Arch Pharm Res* (2010) **33**:387–94. doi:10.1007/s12272-010-0307-1

50. Zhang S, Sun C, Hu H, He Y, Yao Y, Cao Y, et al. Effects of paclitaxel on the ability of aspirin and clopidogrel to inhibit platelet aggregation. *Clin Appl Thromb Hemost* (2016) **22**:673–8. doi:10.1177/1076029615576740

51. Wu Q, Huang K-S, Chen M, Huang D-J. Rapamycin enhances platelet aggregation induced by adenosine diphosphate *in vitro*. *Platelets* (2009) **20**:428–31. doi:10.1080/09537100903114552

52. Babinska A, Markell MS, Salifu MO, Akoad M, Ehrlich YH, Kornecki E. Enhancement of human platelet aggregation and secretion induced by rapamycin. *Nephrol Dial Transplant* (1998) **13**:3153–9. doi:10.1093/ndt/13.12.3153

53. Zhang M, Lotfollahzadeh S, Elzinad N, Yang X, Elsadawi M, Gower AC, et al. Alleviating iatrogenic effects of paclitaxel *via* antiinflammatory treatment. *Vasc Med* (2024) **29**:369–80. doi:10.1177/1358863x241231942

54. Farb A, Heller PF, Shroff S, Cheng L, Kolodgie FD, Carter AJ, et al. Pathological analysis of local delivery of paclitaxel *via* a polymer-coated stent. *Circulation* (2001) **104**:473–9. doi:10.1161/hc3001.092037

55. Nührenberg TG, Voisard R, Fahlisch F, Rudelius M, Braun J, Gschwend J, et al. Rapamycin attenuates vascular wall inflammation and progenitor cell promoters after angioplasty. *The FASEB J* (2005) **19**:1–21. doi:10.1096/fj.04-2431fje

56. Kahan BD, Chang JY, Sehgal SN. Preclinical evaluation of a new potent immunosuppressive agent, rapamycin. *Transplantation* (1991) **52**:185–91. doi:10.1097/00007890-199108000-00001

57. Marx SO, Jayaraman T, Go LO, Marks AR. Rapamycin-FKBP inhibits cell cycle regulators of proliferation in vascular smooth muscle cells. *Circ Res* (1995) **76**:412–7. doi:10.1161/01.res.76.3.412

58. Poon M, Marx SO, Gallo R, Badimon JJ, Taubman MB, Marks AR. Rapamycin inhibits vascular smooth muscle cell migration. *J Clin Invest* (1996) **98**:2277–83. doi:10.1172/jci119038

59. Khing TM, Choi WS, Kim DM, Po WW, Thein W, Shin CY, et al. The effect of paclitaxel on apoptosis, autophagy and mitotic catastrophe in AGS cells. *Sci Rep* (2021) **11**:23490. doi:10.1038/s41598-021-02503-9

60. Belotti D, Vergani V, Drudis T, Borsotti P, Pitelli MR, Viale G, et al. The microtubule-affecting drug paclitaxel has antiangiogenic activity. *Clin Cancer Res* (1996) **2**:1843–9.

61. Liu H-T, Li F, Wang W-Y, Li X-J, Liu Y-M, Wang R-A, et al. Rapamycin inhibits Re-Endothelialization after percutaneous coronary intervention by impeding the proliferation and migration of endothelial cells and inducing apoptosis of endothelial progenitor cells. *Tex Heart Inst J* (2010) **37**:194–201.

62. Sedrani R, Cottens S, Kallen J, Schuler W. Chemical modification of rapamycin: the discovery of SDZ RAD. *Transplant Proc* (1998) **30**:2192–4. doi:10.1016/s0041-1345(98)00587-9

63. Schuler W, Sedrani R, Cottens S, Häberlin B, Schulz M, Schuurman HJ, et al. SDZ RAD, a new rapamycin derivative: pharmacological properties *in vitro* and *in vivo*. *Transplantation* (1997) **64**:36–42. doi:10.1097/00007890-199707150-00008

64. Schreiber KH, Ortiz D, Academia EC, Anies AC, Liao C-Y, Kennedy BK. Rapamycin-mediated mTORC2 inhibition is determined by the relative expression of FK506-binding proteins. *Aging Cell* (2015) **14**:265–73. doi:10.1111/acel.12313

65. Chen G, Ding X-F, Bouamar H, Pressley K, Sun L-Z. Everolimus induces G1 cell cycle arrest through autophagy-mediated protein degradation of cyclin D1 in breast cancer cells. *Am J Physiology-Cell Physiol* (2019) **317**:C244–C252. doi:10.1152/ajpcell.00390.2018

66. Tsuchida K, Piek JJ, Neumann F-J, van der Giessen WJ, Wiemer M, Zeiher AM, et al. One-year results of a durable polymer everolimus-eluting stent in *de novo* coronary narrowings (The SPIRIT FIRST Trial). *EuroIntervention* (2005) **1**:266–72.

67. Grube E, Sonoda S, Ikeno F, Honda Y, Kar S, Chan C, et al. Six- and twelve-month results from first human experience using everolimus-eluting stents with bioabsorbable polymer. *Circulation* (2004) **109**:2168–71. doi:10.1161/01.cir.0000128850.84227.fd

68. Leone PP, Assafin M, Scotti A, Gonzalez M, Mignatti A, Dawson K, et al. A technology evaluation of the onyx frontier drug-eluting stent. *Expert Opin Drug Deliv* (2023) **20**:689–701. doi:10.1080/17425247.2023.2216449

69. Kirtane AJ, Leon MB, Ball MW, Bajwa HS, Sketch MH, Coleman PS, et al. The "final" 5-Year Follow-Up from the ENDEAVOR IV trial comparing a zotarolimus-eluting stent with a paclitaxel-eluting stent. *JACC: Cardiovasc Interventions* (2013) **6**:325–33. doi:10.1016/j.jcin.2012.12.123

70. Burke SE, Kuntz RE, Schwartz LB. Zotarolimus (ABT-578) eluting stents. *Adv Drug Deliv Rev* (2006) **58**:437–46. doi:10.1016/j.addr.2006.01.021

71. Chen Y-W, Smith ML, Sheets M, Ballaron S, Trevillyan JM, Burke SE, et al. Zotarolimus, a novel sirolimus analogue with potent anti-proliferative activity on coronary smooth muscle cells and reduced potential for systemic immunosuppression. *J Cardiovasc Pharmacol* (2007) **49**:228–35. doi:10.1097/fjc.0b013e3180325b0a

72. Yazdani SK, Sheehy A, Nakano M, Nakazawa G, Vorpahl M, Otsuka F, et al. Preclinical evaluation of second-generation Everolimus- and zotarolimus-eluting coronary stents. *The J Invasive Cardiology* (2013) **25**:383–90. Available online at: https://www.hmpgloballearningnetwork.com/site/jic/articles/preclinical-evaluation-second-generation-everolimus-and-zotarolimus-eluting-coronary-stents (Accessed August 23, 2024).

73. Miura K, Nakaya H, Kobayashi Y. Experimental assessment of effects of antiproliferative drugs of drug-eluting stents on endothelial cells. *Cardiovasc Revascularization Med* (2015) **16**:344–7. doi:10.1016/j.carrev.2015.07.002

74. Granada JF, Milewski K, Zhao H, Stankus JJ, Tellez A, Aboodi MS, et al. Vascular response to zotarolimus-coated balloons in injured superficial femoral arteries of the familial hypercholesterolemic swine. *Circ Cardiovasc Interventions* (2011) **4**:447–55. doi:10.1161/circinterventions.110.960260

75. Sachar R, Soga Y, Ansari MM, Kozuki A, Lopez L, Brodmann M, et al. 1-Year results from the RANGER II SFA randomized trial of the ranger drug-coated balloon. *JACC: Cardiovasc Interventions* (2021) **14**:1123–33. doi:10.1016/j.jcin.2021.03.021

76. Gruber P, Braun C, Kahles T, Hlavica M, Anon J, Diepers M, et al. Percutaneous transluminal angioplasty using the novel drug-coated balloon catheter SeQuent please NEO for the treatment of symptomatic intracranial severe stenosis: feasibility and safety study. *J NeuroInterventional Surg* (2019) **11**:719–22. doi:10.1136/neurintsurg-2018-014378

77. Chen Z, Guo W, Jiang W, Wang F, Fu W, Zou Y, et al. IN.PACT SFA clinical study using the IN.PACT admiral drug-coated balloon in a Chinese patient population. *J Endovasc Ther* (2019) **26**:471–8. doi:10.1177/1526602819852084

78. Krishnan P, Faries P, Niazi K, Jain A, Sachar R, Bachinsky WB, et al. Stellarex drug-coated balloon for treatment of femoropopliteal disease. *Circulation* (2017) **136**:1102–13. doi:10.1161/circulationaha.117.028893

79. Chen R, Liu E, Fang Y, Gao N, Zhang M, Zhang X, et al. Naturally sourced amphiphilic peptides as paclitaxel vehicles for breast cancer treatment. *Biomater Adv* (2024) **159**:213824. doi:10.1016/j.bioadv.2024.213824

80. Sodha S, Gupta P. PLGA and PEG based porous microparticles as vehicles for pulmonary somatropin delivery. *Eur J Pharmaceutics Biopharmaceutics* (2023) **191**:150–7. doi:10.1016/j.ejpb.2023.08.017

81. Codoni D, Cowan J, Bradley J, McAuley WJ, O'Connell MA, Qi S. Disc-shaped polyoxyethylene glycol glycerides gel nanoparticles as novel protein delivery vehicles. *Int J Pharmaceutics* (2015) **496**:1015–25. doi:10.1016/j.ijpharm.2015.10.067

82. Hezi-Yamit A, Sullivan C, Wong J, David L, Chen M, Cheng P, et al. Impact of polymer hydrophilicity on biocompatibility: implication for DES polymer design. *J Biomed Mater Res Part A* (2009) **90A**:133–41. doi:10.1002/jbm.a.32057

83. Collier TO, Jenney CR, DeFife KM, Anderson JM. Protein adsorption on chemically modified surfaces. *Biomed Sci Instrumentation* (1997) **33**:178–83.

84. Yayapour N, Nygren H. Interactions between whole blood and hydrophilic or hydrophobic glass surfaces: kinetics of cell adhesion. *Colloids Surf B: Biointerfaces* (1999) **15**:127–38. doi:10.1016/s0927-7765(99)00049-1

85. Zhang W, Du J, Zhu T, Wang R. SiO2 nanosphere coated tough catheter with superhydrophobic surface for improving the antibacteria and hemocompatibility. *Front Bioeng Biotechnol* (2023) **10**:1067139. doi:10.3389/fbioe.2022.1067139

86. Zhang J, Li G, Li D, Zhang X, Li Q, Liu Z, et al. *In vivo* blood-repellent performance of a controllable facile-generated superhydrophobic surface. *ACS Appl Mater Inter* (2021) **13**:29021–33. doi:10.1021/acsami.0c21058

87. Movafaghi S, Leszczak V, Wang W, Sorkin JA, Dasi LP, Popat KC, et al. Hemocompatibility of superhemophobic titania surfaces. *Adv Healthc Mater* (2017) **6**:1600717. doi:10.1002/adhm.201600717

88. Shazly T, Eberth JF, Kostelnik CJ, Uline MJ, Chitalia VC, Spinale FG, et al. Hydrophilic coating microstructure mediates acute drug transfer in drug-coated balloon therapy. *ACS Appl Bio Mater* (2024) **7**:3041–9. doi:10.1021/acsabm.4c00080

89. Anbalakan K, Toh HW, Ang HY, Buist ML, Leo HL. How does the nature of an excipient and an atheroma influence drug-coated balloon therapy? *Cardiovasc Eng Tech* (2022) **13**:915–29. doi:10.1007/s13239-022-00626-2

90. Anderson JA, Remund T, Pohlson K, Lamichhane S, Evans C, Evans R, et al. *In vitro* and *in vivo* evaluation of effect of excipients in local delivery of paclitaxel using microporous infusion balloon catheters. *J Biomed Mater Res B: Appl Biomater* (2017) **105**:376–90. doi:10.1002/jbm.b.33564

91. Gandhi PJ, Murthy ZVP. Investigation of different drug deposition techniques on drug releasing properties of cardiovascular drug coated balloons. *Ind Eng Chem Res* (2012) **51**:10800–23. doi:10.1021/ie3006676

92. Torii S, Jinnouchi H, Sakamoto A, Romero ME, Kolodgie FD, Virmani R, et al. Comparison of biologic effect and particulate embolization after femoral artery treatment with three drug-coated balloons in healthy swine model. *J Vasc Interv Radiol* (2019) **30**:103–9. doi:10.1016/j.jvir.2018.07.025

93. Heilmann T, Richter C, Noack H, Post S, Mahnkopf D, Mittag A, et al. Drug release profiles of different drug-coated balloon platforms. *Eur Cardiol Rev* (2010) **6**:40. doi:10.15420/ecr.2010.8.2.40

94. Kolodgie FD, Pacheco E, Yahagi K, Mori H, Ladich E, Virmani R. Comparison of particulate embolization after femoral artery treatment with IN.PACT admiral *versus* lutonix 035 paclitaxel-coated balloons in healthy swine. *J Vasc Interv Radiol* (2016) **27**:1676–85.e2. doi:10.1016/j.jvir.2016.06.036

95. van der Giessen WJ, Lincoff AM, Schwartz RS, van Beusekom HMM, Serruys PW, Holmes DR, et al. Marked inflammatory sequelae to implantation of biodegradable and nonbiodegradable polymers in porcine coronary arteries. *Circulation* (1996) **94**:1690–7. doi:10.1161/01.cir.94.7.1690

96. Bakhrushina EO, Sakharova PS, Konogorova PD, Pyzhov VS, Kosenkova SI, Bardakov AI, et al. Burst release from *in situ* forming PLGA-based implants: 12 effectors and ways of correction. *Pharmaceutics* (2024) **16**:115. doi:10.3390/pharmaceutics16010115

97. Ma S, Feng X, Liu F, Wang B, Zhang H, Niu X. The pro-inflammatory response of macrophages regulated by acid degradation products of poly(lactide-co-glycolide) nanoparticles. *Eng Life Sci* (2021) **21**:709–20. doi:10.1002/elsc.202100040

98. Peng H-Y, Chen M, Zheng B, Wang X-G, Huo Y. Long-term effects of novel biodegradable, polymer-coated, Sirolimus-Eluting stents on neointimal formation in a porcine coronary model. *Int Heart J* (2009) **50**:811–22. doi:10.1536/ihj.50.811

99. Iida O, Soga Y, Saito S, Mano T, Hayakawa N, Ichihashi S, et al. A novel Sirolimus-Coated balloon for the treatment of femoropopliteal lesions. *JACC: Cardiovasc Interventions* (2024) **17**:1547–56. doi:10.1016/j.jcin.2024.03.029

100. Radomski A, Jurasz P, Alonso-Escolano D, Drews M, Morandi M, Malinski T, et al. Nanoparticle-induced platelet aggregation and vascular thrombosis. *Br J Pharmacol* (2005) **146**:882–93. doi:10.1038/sj.bjp.0706386

101. Wang T, Bai J, Jiang X, Nienhaus GU. Cellular uptake of nanoparticles by membrane penetration: a study combining confocal microscopy with FTIR spectroelectrochemistry. *ACS Nano* (2012) **6**:1251–9. doi:10.1021/nn203892h

102. Li X, Radomski A, Corrigan OI, Tajber L, De Sousa Menezes F, Endter S, et al. Platelet compatibility of PLGA, chitosan and PLGA–chitosan nanoparticles. *Nanomedicine* (2009) **4**:735–46. doi:10.2217/nnm.09.65

103. Bakhaidar R, Green J, Alfahad K, Samanani S, Moollan N, O'Neill S, et al. Effect of size and concentration of PLGA-PEG nanoparticles on activation and aggregation of washed human platelets. *Pharmaceutics* (2019) **11**:514. doi:10.3390/pharmaceutics11100514

104. Ninomiya K, Serruys PW, Colombo A, Reimers B, Basavarajaiah S, Sharif F, et al. A Prospective Randomized Trial Comparing Sirolimus-Coated Balloon With Paclitaxel-Coated Balloon in *de novo* Small Vessels. *JACC: Cardiovasc Interventions* (2023) **16**:2884–96. doi:10.1016/j.jcin.2023.09.026

105. Choke ETC, Peh EYL, Tang TY, Cheng SC, Tay JS, Aw DKL, et al. MagicTouch PTA Sirolimus-Coated balloon for femoropopliteal and below-the-knee disease: 3-year outcomes of the XTOSI trial. *Ann Vasc Surg* (2024) **106**:8–15. doi:10.1016/j.avsg.2023.12.096

106. *Surmodics announces 24-Month data from the SWING trial presented at VEITHsymposium surmodics*. Inc. (2025). Available online at: https://surmodics.gcs-web.com/news-releases/news-release-details/surmodics-announces-24-month-data-swing-trial-presented (Accessed 30 January 2025).

107. Tang TY, Chong T-T, Yap CJQ, Soon SXY, Chan SL, Tan RY, et al. Intervention with selution SLR™ agent balloon for endovascular latent limus therapy for failing AV fistulas (ISABELLA) trial: protocol for a pilot clinical study and pre-clinical results. *J Vasc Access* (2023) **24**:289–99. doi:10.1177/11297298211020867

108. Tang TY, Yap C, Soon SXY, Chan SL, Lee QS, Yap HY, et al. World's first experience treating TASC II C and D tibial occlusive disease using the selution SLR Sirolimus-Eluting balloon: six-month results from the PRESTIGE study. *J Endovasc Ther* (2021) **28**:555–66. doi:10.1177/15266028211007457

109. Armstrong E. CRT-300.3 SELUTION4BTK – a randomized clinical trial evaluating selution SLR Sirolimus-Eluting balloon in the treatment of below-the-knee lesions in patients with chronic limb-threatening ischemia. *JACC: Cardiovasc Interventions* (2023) **16**:S50. doi:10.1016/j.jcin.2023.01.162

110. Ncvh 2025 agenda – NCVH (2025). Available online at: https://ncvh.org/ncvh-2025-agenda/ (Accessed 10 July 2025).

111. Berrada-Sounni M, Zuckerman ST. Undulating balloon systems and methods for nanoparticle-based drug delivery. *US20230106928A1* (2023). Available online at: https://patents.google.com/patent/US20230106928A1/de (Accessed February 3, 2025).

112. NanoTherapies A. *ADVANCEd NanoTherapies dual active pharmacological ingredient (Dual-API) drug-coated balloon catheter to treat de-novo lesions in patients with symptomatic stable angina, unstable angina, and NSTEMI*. Clinical trial registration NCT05521542, clinicaltrials.gov (2025). Available online at: https://clinicaltrials.gov/study/NCT05521542 (Accessed July 10, 2024).

113. *Surmodics announces 12-Month data from the SWING trial presented at VEITHsymposium | surmodics*. Inc. (2025) Available online at: https://surmodics.gcs-web.com/news-releases/news-release-details/surmodics-announces-12-month-data-swing-trial-presented (Accessed 29 October 2025).

114. Tang TY, Yap C, Chan SL, Soon SXY, Sivanathan C, Gogna A, et al. The utility of sirolimus eluting balloons in the setting of chronic limb threatening ischaemia in Asian patients from Singapore – 12 months results of the PRISTINE registry. *Cardiovasc Intervent Radiol* (2024) **47**:863–74. doi:10.1007/s00270-024-03756-3

115. M.A. Med Alliance S.A. *SELUTION SLR™ 014 BTK. A prospective randomized multicenter single blinded study to assess the safety and effectiveness of the SELUTION*

SLR™ 014 drug eluting balloon in the treatment of below-the-knee (BTK) atherosclerotic disease in patients with chronic limb threatening ischemia (CLTI). Clinical trial registration NCT05055297, clinicaltrials.gov (2025). Available online at: https://clinicaltrials.gov/study/NCT05055297 (Accessed October 29, 2025).

116. Concept Medical Inc. *FUTURE BTK: randomized controlled trial of first SirolimUs CoaTed balloon versus StandaRd balloon angioplasty in the TrEatment of below the knee arterial disease*. Clinical trial registration NCT04511247, clinicaltrials.gov (2025). Available online at: https://clinicaltrials.gov/study/NCT04511247 (Accessed October 29, 2025).

117. Teichgräber U. *Prospective multi-center randomized controlled trial to evaluate the safety and efficacy of SiroLIMus drug coated balloon versus non-coated standard angioplasty for the treatment of infrapopliteal occlusions in patients with PEripheral arterial DiSease*. Clinical trial registration NCT04772300, clinicaltrials.gov (2024). Available online at: https://clinicaltrials.gov/study/NCT04772300 (Accessed October 29, 2025).

118. Concept Medical Inc. *MAGICAL BTK: randomized controlled trial of MAGIcTouch - sirolimus coated BALloon versus standard balloon angioplasty in the treatment of below the knee arterial disease*. Clinical trial registration NCT06182397, clinicaltrials.gov (2025). Available online at: https://clinicaltrials.gov/study/NCT06182397 (Accessed October 29, 2025).

119. Atigh MK, Turner E, Christians U, Yazdani SK. The use of an occlusion perfusion catheter to deliver paclitaxel to the arterial wall. *Cardiovasc Ther* (2017) **35**:e12269. doi:10.1111/1755-5922.12269

120. Zeller T, Zhang Z, Parise H, Mascho C, Holden A, Schmidt A, et al. *Early tibial vessel recoil following treatment with the bare temporary spur stent system: results from the DEEPER OUS vessel recoil substudy*. J Endovasc Ther (2024).

121. A novel temporary stent for treatment of infrapopliteal arteries in conjunction with drug-coated balloon angioplasty: the DEEPER pilot study | journal of CLI (2025) Available online at: https://www.clijournal.com/article/novel-temporary-stent-treatment-infrapopliteal-arteries-conjunction-drug-coated-balloon (Accessed 15 July 2025).

122. Schweiger L, Gütl K, Rief P, Reiter C, Janisch M, Weinberg I, et al. Retrievable scaffold therapy combined with sirolimus-coated balloon angioplasty for infrapopliteal artery disease: final results from the DEEPER LIMUS trial. *Cardiovasc Intervent Radiol* (2025) **48**:297–303. doi:10.1007/s00270-025-03987-y

123. Health CD. *Esprit BTK everolimus eluting resorbable scaffold system – P230036*. FDA (2024). Available online at: https://www.fda.gov/medical-devices/recently-approved-devices/esprit-btk-everolimus-eluting-resorbable-scaffold-system-p230036 (Accessed October 29, 2025).

124. Varcoe RL, DeRubertis BG, Kolluri R, Krishnan P, Metzger DC, Bonaca MP, et al. Drug-eluting resorbable scaffold *versus* angioplasty for infrapopliteal artery disease. *New Engl J Med* (2024) **390**:9–19. doi:10.1056/nejmoa2305637

125. DeRubertis BG, Varcoe RL, Krishnan P, Bonaca MP, O'Connor DJ, Pin R, et al. Drug-eluting resorbable scaffold *versus* balloon angioplasty for below-the-knee peripheral artery disease: 2-year results from the LIFE-BTK trial. *Circulation* (2025) **152**:1076–86. doi:10.1161/circulationaha.125.075080

126. Haude M, Wlodarczak A, Schaaf Rvan der, Torzewski J, Ferdinande B, Escaned J, et al. A new resorbable magnesium scaffold for *de novo* coronary lesions (DREAMS 3): one-year results of the BIOMAG-I first-in-human study (2025). doi:10.4244/EIJ-D-23-00326

127. Biotronik AG. BIOTRONIK-Safety and Clinical Performance of the Drug Eluting Resorbable Coronary MAGnesium Scaffold System (DREAMS 3G) in the Treatment of Subjects With *de novo* Lesions in Native Coronary Arteries: BIOMAG-II: a Randomized Controlled Trial. *Clin Trial Registration NCT05540223, clinicaltrials.Gov* (2024). Available online at: https://clinicaltrials.gov/study/NCT05540223 (Accessed October 24, 2025).

128. Schwartz LB, Orr G, Santos JD, Haig C. *Multi-element bioresorbable intravascular stent*. US11234844B2 (2022). Available online at: https://patents.google.com/patent/US11234844B2/en?assignee=efemoral+medical&oq=efemoral+medical (Accessed October 25, 2025).

129. Saito S, Nef HM, Webster M, Verheye S. DynamX sirolimus-eluting Bioadaptor *versus* the zotarolimus-eluting Resolute Onyx stent in patients with *de novo* coronary artery lesions: design and rationale of the multi-center, international, randomized BIOADAPTOR-RCT. *Cardiovasc Revascularization Med* (2023) **55**:76–82. doi:10.1016/j.carrev.2023.05.010

130. Elixir Medical Corporation. *DynamX bioadaptor global post-market registry: clinical trial of the elixir medical DynamX coronary bioadaptor system (Bio-RESTORE)*. Clinical trial registration NCT06074549, clinicaltrials.gov (2025). Available online at: https://clinicaltrials.gov/study/NCT06074549 (Accessed October 25, 2025).

EBM Experimental Biology and Medicine

TYPE Original Research
PUBLISHED 18 December 2025
DOI 10.3389/ebm.2025.10824

OPEN ACCESS

*CORRESPONDENCE
Wan Chen,
wanchen_yuhuan@outlook.com

†These authors have contributed equally to this work

RECEIVED 15 September 2025
REVISED 21 November 2025
ACCEPTED 25 November 2025
PUBLISHED 18 December 2025

CITATION
Shi W, Zhao Y, Park J and Chen W (2025) Diet–lifestyle oxidative balance in relation to cardiometabolic multimorbidity: findings from the national health and nutrition examination survey.
Exp. Biol. Med. 250:10824.
doi: 10.3389/ebm.2025.10824

Diet–lifestyle oxidative balance in relation to cardiometabolic multimorbidity: findings from the national health and nutrition examination survey

Wenrui Shi[1†], Yu Zhao[1†], Jieun Park[2] and Wan Chen[3*]

[1]Department of Cardiology, Shanghai Chest Hospital, Shanghai Jiao Tong University School of Medicine, Shanghai, China, [2]School of Medicine, Shanghai Jiao Tong University, Shanghai, China, [3]Department of Endocrinology, Yuhuan Second People's Hospital, Yuhuan, Zhejiang, China

Abstract

Oxidative stress is a critical factor in the development of cardiometabolic diseases. The Oxidative Balance Score (OBS), integrating dietary and lifestyle factors, has been proposed as a measure of the balance between pro-oxidants and antioxidants. This study aims to explore the relationship between OBS and prevalent cardiometabolic multimorbidity (CMM), and to evaluate whether adding OBS into clinical practice is associated with better CMM identification in the general population. A total of 26,191 participants were selected from the National Health and Nutrition Examination Survey. CMM was defined as having a history of two or more conditions: diabetes mellitus, stroke, or coronary heart disease. The prevalence of CMM was 2.95%. After adjusting for demographic, anthropometric, laboratory, and medical history data, each standard deviation increase in OBS was associated with a 26.1% reduction in the risk of prevalent CMM. Participants in the highest quartile of OBS had a 0.530-fold risk of prevalent CMM compared to those in the lowest quartile. Smooth curve fitting indicated a proportional reduction in CMM risk with increasing OBS. Sensitivity analysis confirmed significant associations between both dietary and lifestyle OBS with prevalent CMM. ROC analysis revealed that incorporating OBS into conventional cardiometabolic risk factors was associated with a slight improvement in CMM identification (AUC: 0.912 vs. 0.916, P = 0.001). Reclassification analysis further indicated the incremental value of OBS. This study revealed a negative, linear, and robust association between OBS and prevalent CMM in the general population. However, reverse causation cannot be ruled out. Future studies should use longitudinal or Mendelian randomization approaches to establish causality.

KEYWORDS

oxidative stress, diet, oxidative balance score, cardiometabolic multimorbidity, NHANES

Impact statement

Cardiometabolic multimorbidity (CMM) is an increasing health challenge with limited tools for early detection. This study shows that the Oxidative Balance Score (OBS), reflecting dietary and lifestyle factors, is strongly and inversely associated with CMM in a large national population. Importantly, incorporating OBS into conventional risk models was associated with improved CMM identification, highlighting its potential value for CMM identification. These findings advance the field by supporting OBS as a practical, quantifiable, and supplemental marker to assist the identification of CMM. The study highlights OBS as a potentially useful tool for guiding personalized lifestyle interventions, supporting prevention strategies, and helping to monitoring the burden of cardiometabolic diseases at the population level.

Introduction

As global population aging and urbanization accelerate, the risk of individuals developing multiple chronic diseases—particularly cardiovascular disease (CVD) and its associated complications—continues to grow, leading to steadily increasing morbidity and mortality rates [1, 2]. Multimorbidity has emerged as a significant public health challenge due to its links to diminished quality of life, increased disability, and higher mortality rates [3–5]. Among the various forms of multimorbidity, cardiometabolic multimorbidity (CMM)—characterized by the presence of two or more conditions such as diabetes mellitus, stroke, and coronary heart disease (CHD)—is both the most prevalent and the most severe. Research indicated that individuals with CMM experience a reduction in life expectancy of 12–15 years by age 60 and face a 3.7–6.9 times higher risk of all-cause mortality compared to those without cardiometabolic conditions, with a significantly greater risk increase than those with only one such disease [3]. Given this serious situation, there is an urgent need to explore and expand the risk factor profile for CMM to facilitate its early detection and intervention.

Oxidative stress plays a pivotal role in endothelial dysfunction, atherosclerosis, and other pathogenic mechanisms contributing to the development of atherosclerotic CVD and diabetes [6, 7]. While substantial evidence links individual antioxidant or pro-oxidant exposure to CVD [8–10], few observational studies have explored the relationship between overall oxidative balance status and CVD. This gap may be due to the complexity of measuring oxidative balance-related exposures and the potential biological interactions between multiple pro-oxidants and antioxidants. Research indicates that lifestyle and dietary patterns can influence the body's oxidative stress state [11]. In this context, the Oxidative Balance Score (OBS)—a metric assessing lifestyle and dietary factors—can be used to calculate behavioral scores and gauge antioxidant exposure levels [12]. Evidence strongly suggests a negative correlation between OBS and conditions such as diabetes [13], hypertension [14], chronic kidney disease [11], and CHD [15]. However, the relationship between OBS and the risk of CMM remains unclear.

Therefore, this study aimed to assess the relationship between OBS and the prevalence of CMM, and to evaluate whether adding OBS into clinical practice is associated with better CMM identification in the general population.

Materials and methods

Study design and population

The datasets for this study were derived from the National Health and Nutrition Examination Survey (NHANES) website, covering the years 1999–2018. NHANES is an ongoing program conducted by the National Center for Health Statistics that consists of a series of independent, nationally representative surveys. Using a cross-sectional design, NHANES has been conducted biennially in the United States for over 20 years. It employs a multistage, stratified, and clustered probability sampling strategy to ensure representativeness of the data. Data from different survey cycles are designed to be combinable for integrated analysis. Comprehensive details about NHANES, including its recruitment strategies, population coverage, and methodological design, are accessible on the Centers for Disease Control and Prevention (CDC) website.[1]

For this analysis, we included subjects who participated in NHANES between 2003 and 2018 (N = 80,312). Exclusion criteria included individuals under 20 years of age and those with missing data on OBS, CMM, or other covariates. After applying these criteria, a total of 26,191 participants were included in the study (Figure 1). The NHANES protocol was approved by the NCHS Institutional Ethics Review Board, and as our study utilized de-identified data, no additional ethical review was required. All data used in this study are publicly available through the official NHANES website.

Outcome ascertainment

CMM was defined as the presence of at least two of the following conditions: CHD, stroke, and diabetes [16, 17]. CHD was identified by a "yes" response to any of the questions: "Ever

1 https://www.cdc.gov/nchs/nhanes/index.htm

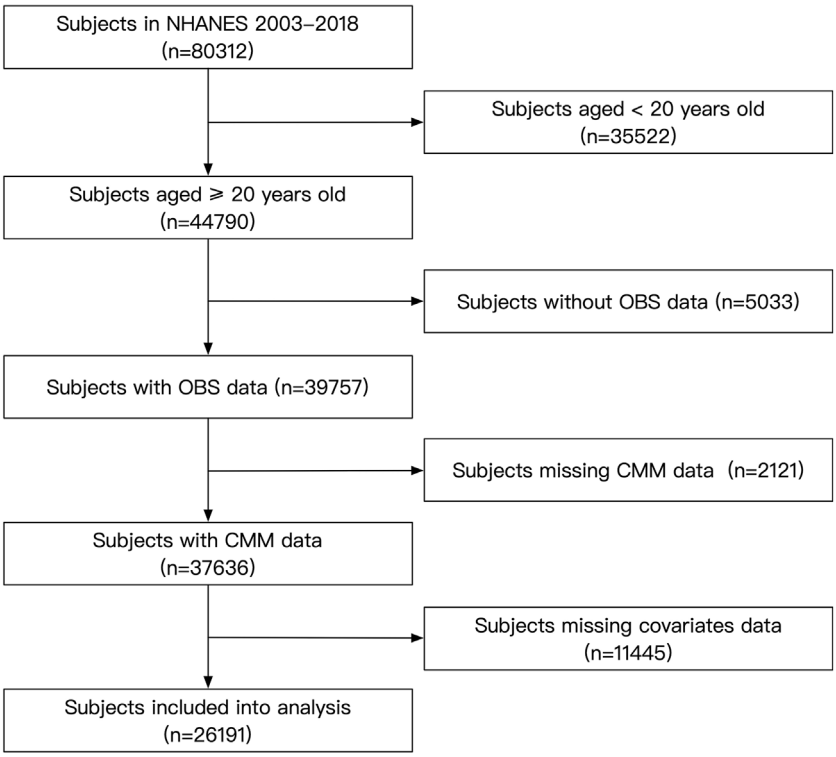

FIGURE 1
Flow chart of the subject's enrollment.

told you had coronary heart disease," "Ever told you had angina," or "Ever told you had a heart attack." Stroke was determined by a "yes" response to the question "Ever told you had a stroke." Receiving anti-diabetic therapy was indicated by a "yes" response to either "Take diabetic pills to lower blood sugar" or "Taking insulin now." Diagnosed diabetes was defined as a "yes" response to "Doctor told you have diabetes." Diabetes was classified based on fasting plasma glucose ≥7 mmol/L, receiving anti-diabetic therapy, or a diagnosis of diabetes [18].

Exposure definition

The OBS was derived from 20 components, including 16 dietary and 4 lifestyle factors. Each factor was assigned a score between 0 and 2 based on predefined cut-offs. The classification of components as pro-oxidants (total fat, iron, alcohol, BMI, cotinine) or antioxidants (dietary fiber, carotene, riboflavin, niacin, vitamin B6, total folate, vitamin B12, vitamin C, vitamin E, calcium, magnesium, zinc, copper, selenium, and physical activity) was based on extensive prior literature. For pro-oxidants, higher values were associated with lower scores, while for antioxidants, higher values corresponded to higher scores. A higher OBS indicates a greater balance toward antioxidant behaviors, whereas a lower score reflects a pro-oxidant balance [19]. Detailed information about OBS score distribution and cut-off values was presented in Supplementary Table S1.

BMI, physical activity, smoking, and alcohol consumption were included as indicators in the Lifestyle OBS. BMI was calculated by dividing weight (kg) by height squared (m^2). Physical activity data were collected using the NHANES Physical Activity Questionnaire, administered in participants' homes by trained interviewers through the Computer-Assisted Personal Interview system. The questionnaire captured both work-related activities (vigorous and moderate intensity) and leisure-time physical activities (such as walking, cycling, and other moderate to vigorous activities). Physical activity levels were calculated based on established methodologies, using the product of activity frequency per week, activity duration, and the Metabolic Equivalent score [20]. Cotinine, the primary metabolite of nicotine, was used as a marker for active smoking and exposure to environmental tobacco smoke or passive smoking, due to its longer half-life in the bloodstream compared to nicotine [21]. Plasma cotinine levels have also been widely utilized in quantitative exposure assessment studies. Alcohol consumption was defined as the average number of alcoholic drinks consumed per day over the past 12 months on days when alcohol was consumed, encompassing all types of alcoholic beverages.

To provide a detailed analysis of dietary intake in the US population, trained dietary interviewers conducted face-to-face 24-hour dietary recall interviews with participants using data from NHANES. The interviews were conducted in private rooms at the NHANES Mobile Examination Center (MEC). Each dietary interview room at the MEC was equipped with a standardized set of measurement guides to help respondents accurately report the quantity of food consumed. These guides, explicitly developed for the NHANES setting, were designed to facilitate accurate dietary assessment for the non-institutionalized US civilian population. The National Center for Health Statistics (NCHS) oversaw sample design and data collection, while the United States Department of Agriculture Food Survey Research Group provided expertise on dietary survey methodology, data processing, and review.

Covariates

Answering "Yes" to the question "Now taking prescribed medicine for hypertension" was determined as anti-hypertensive therapy; A mean systolic blood pressure (SBP) ≥ 140 mmHg, and/or a mean diastolic blood pressure (DBP) ≥ 90 mmHg, and/or anti-hypertensive therapy were indicated as hypertension [22]. Estimated glomerular filtration rate (eGFR) was calculated according to the Chronic Kidney Disease Epidemiology Collaboration (CKD-EPI) equation [23].

Laboratory tests were performed in CDC-certified laboratories. FPG was measured using the oxygen rate method on the Beckman DxC800 modular chemistry analyzer. Scr was assessed using the Jaffe rate method on the DxC800 modular chemistry platform. Blood lipid levels were quantified via enzymatic assays conducted on the Roche Modular P and Roche Cobas 6000 chemistry analyzers.

Statistical analysis

This study employed statistical weighting to account for the complex design of the NHANES survey. Categorical variables were summarized as frequencies with 95% confidence intervals (CIs), while continuous variables were presented as means with 95% CIs. Group comparisons were conducted using Chi-square tests for categorical variables and t-tests for continuous variables. The analysis was divided into two main components. First, the association between OBS and the risk of prevalent CMM was investigated using multivariate logistic regression, with results expressed as odds ratios (ORs) and 95% CIs. OBS was analyzed both as a continuous variable, with effects reported per standard deviation (SD) change, and as a categorical variable divided into quartiles, with a P-for-trend analysis to examine whether ORs decreased significantly from quartile 1 to quartile 4. A generalized additive model with a spline smooth-fitting function was applied to explore the linearity of the association across the full OBS range. Sensitivity analyses were conducted to assess the associations of dietary and lifestyle OBS with CMM prevalence, and subgroup analyses tested the robustness of the logistic regression results across conventional subpopulations. Another sensitive analysis was used to evaluate the impact of including hypertension and obesity in the definition of CMM. This analysis aimed to assess the robustness of the observed associations between the OBS and CMM under an extended definition of CMM. Second, receiver operating characteristic (ROC) analysis and reclassification analysis, including the continuous net reclassification index (NRI) and integrated discrimination index (IDI), were performed to assess the association between OBS and the identification of prevalent CMM. To evaluate the clinical utility of OBS, decision curve analysis (DCA) was performed. DCA was used to assess the net benefit of the predictive models with and without the inclusion of OBS across a range of clinically relevant risk thresholds (0–0.4). Net benefit was calculated by considering the trade-off between true positives and false positives, with threshold values set at clinically relevant levels (5%–10% risk). The analysis was conducted to assess the incremental value of adding OBS to the clinical risk factor model. All statistical analyses were conducted using Stata (version 15.0), R (The R Foundation), and EmpowerStats (X&Y Solutions, Inc., Boston, MA, USA), with statistical significance defined as a two-tailed P-value less than 0.05.

Results

Characteristics of subjects

Characteristic data were summarized in Table 1. 772 of the 26,191 subjects were diagnosed with CMM. The overall mean age was 44.60 years, with significant differences across subgroups ($P = 0.016$). The proportion of males was 51.53%, with no significant variation between groups ($P = 0.549$). Racial distribution showed significant variation across OBS quartile groups ($P < 0.001$), with the proportion of non-Hispanic whites continuously increasing and that of non-Hispanic blacks steadily decreasing from quartile 1 to quartile 4. PIR also continuously rose from 2.70 in quartile 1 to 3.41 in quartile 4 ($P < 0.001$). For anthropometric parameters, height gradually increased, whereas weight, BMI, WC, SBP, and DBP consistently decreased from the lowest to the highest quartile. Regarding laboratory data, FPG, glycohemoglobin, LDL-C, and Scr decreased while HDL-C increased from the bottom quartile to the top quartile. The differences in TC, triglycerides, and eGFR among the quartile groups were significant but did not exhibit a clear trend. Regarding the medical history data, the percentages of individuals receiving anti-hypertensive therapy, anti-diabetic therapy, and those with diagnosed diabetes gradually decreased

TABLE 1 Characteristic profile of the enrolled subjects classified by OBS quartiles.

Variables	Total (26,191)	OBS quartile 1 (n = 6644)	OBS quartile 2 (n = 6593)	OBS quartile 3 (n = 7,005)	OBS quartile 4 (n = 5,949)	P value[a]
Age (years)	44.60 (44.10–45.09)	44.07 (43.42–44.72)	44.99 (44.32–45.67)	44.95 (44.33–45.57)	44.27 (43.56–44.98)	0.016
Male (%)	51.53 (50.88–52.17)	52.51 (51.03–53.99)	50.87 (49.45–52.29)	51.47 (49.98–52.96)	51.36 (49.73–52.99)	0.549
Race (%)						<0.001
Mexican American	7.69 (6.62–8.91)	7.16 (5.96–8.59)	7.97 (6.79–9.35)	7.62 (6.46–8.96)	7.96 (6.78–9.32)	
Other hispanic	4.73 (4.14–5.41)	4.98 (4.07–6.07)	4.90 (4.22–5.67)	4.43 (3.76–5.20)	4.69 (3.97–5.53)	
Non-hispanic white	71.15 (68.86–73.34)	66.16 (63.06–69.13)	70.61 (67.95–73.13)	72.78 (70.41–75.03)	74.31 (71.94–76.55)	
Non-hispanic black	9.67 (8.55–10.92)	15.31 (13.44–17.38)	10.20 (8.91–11.65)	8.07 (7.09–9.17)	5.92 (5.13–6.84)	
Others	6.76 (6.14–7.42)	6.39 (5.59–7.29)	6.32 (5.50–7.26)	7.10 (6.28–8.03)	7.12 (6.21–8.14)	
PIR	3.12 (3.05–3.18)	2.70 (2.63–2.77)	3.07 (3.00–3.14)	3.23 (3.16–3.30)	3.41 (3.32–3.49)	<0.001
Height (cm)	169.69 (169.51–169.86)	168.75 (168.45–169.05)	169.14 (168.83–169.45)	170.01 (169.69–170.33)	170.69 (170.34–171.04)	<0.001
Weight (kg)	82.17 (81.72–82.61)	84.30 (83.56–85.04)	82.94 (82.30–83.57)	82.39 (81.75–83.04)	79.24 (78.44–80.04)	<0.001
BMI (kg/m^2)	28.45 (28.29–28.61)	29.52 (29.26–29.79)	28.91 (28.70–29.12)	28.41 (28.20–28.61)	27.09 (26.84–27.34)	<0.001
WC (cm)	97.76 (97.35–98.18)	100.31 (99.67–100.94)	98.81 (98.27–99.34)	97.78 (97.22–98.33)	94.45 (93.76–95.13)	<0.001
SBP (mmHg)	121.02 (120.66–121.37)	122.40 (121.75–123.04)	121.85 (121.32–122.39)	120.97 (120.42–121.51)	119.02 (118.49–119.54)	<0.001
DBP (mmHg)	70.98 (70.63–71.33)	71.32 (70.82–71.81)	70.94 (70.45–71.43)	71.23 (70.79–71.67)	70.45 (70.01–70.89)	0.003
FPG (mmol/L)	5.36 (5.34–5.39)	5.45 (5.40–5.50)	5.40 (5.36–5.45)	5.37 (5.32–5.43)	5.23 (5.19–5.28)	<0.001
Glycohemoglobin (%)	5.51 (5.50–5.53)	5.57 (5.54–5.60)	5.54 (5.51–5.56)	5.52 (5.49–5.54)	5.44 (5.41–5.47)	<0.001
TC (mmol/L)	5.02 (5.00–5.05)	5.04 (4.99–5.08)	5.04 (5.00–5.08)	5.04 (5.00–5.08)	4.98 (4.94–5.01)	0.010
Triglycerides (mmol/L)	1.66 (1.64–1.69)	1.69 (1.65–1.73)	1.68 (1.63–1.72)	1.71 (1.65–1.77)	1.57 (1.52–1.62)	0.001
LDL-C (mmol/L)	3.30 (3.28–3.32)	3.37 (3.33–3.42)	3.33 (3.30–3.36)	3.29 (3.26–3.32)	3.21 (3.18–3.24)	<0.001
HDL-C (mmol/L)	1.39 (1.38–1.40)	1.33 (1.31–1.34)	1.38 (1.36–1.39)	1.41 (1.39–1.42)	1.45 (1.43–1.47)	<0.001
Scr (μmol/L)	78.16 (77.72–78.60)	80.35 (79.40–81.29)	78.27 (77.60–78.94)	77.83 (77.17–78.48)	76.47 (75.83–77.11)	<0.001
eGFR (ml/min/1.73 m^2)	96.04 (95.41–96.68)	96.06 (95.10–97.03)	95.60 (94.70–96.50)	95.71 (94.96–96.46)	96.85 (95.98–97.71)	0.028
Anti-hypertension therapy (%)	22.24 (21.36–23.15)	26.19 (24.73–27.71)	23.18 (21.54–24.90)	22.39 (20.96–23.88)	17.63 (16.36–18.97)	<0.001
Anti-diabetic therapy (%)	5.36 (5.01–5.72)	6.35 (5.59–7.21)	5.53 (4.85–6.30)	5.44 (4.81–6.15)	4.19 (3.58–4.90)	<0.001
Diagnosed diabetes (%)	6.91 (6.50–7.35)	8.43 (7.63–9.31)	7.19 (6.40–8.07)	6.85 (6.10–7.68)	5.36 (4.67–6.14)	<0.001
Hypertension (%)	29.16 (28.16–30.17)	33.04 (31.19–34.94)	30.74 (29.22–32.30)	29.31 (27.68–30.99)	23.94 (22.53–25.41)	<0.001
Diabetes (%)	10.78 (10.31–11.27)	12.55 (11.50–13.67)	11.79 (10.85–12.80)	10.56 (9.69–11.49)	8.46 (7.63–9.35)	<0.001

(Continued on following page)

TABLE 1 (*Continued*) Characteristic profile of the enrolled subjects classified by OBS quartiles.

Variables	Total (26,191)	OBS quartile 1 (n = 6644)	OBS quartile 2 (n = 6593)	OBS quartile 3 (n = 7,005)	OBS quartile 4 (n = 5,949)	P value[a]
CHD (%)	4.53 (4.18–4.90)	6.62 (5.88–7.45)	4.64 (4.04–5.32)	3.96 (3.45–4.56)	3.18 (2.63–3.84)	<0.001
Stroke (%)	1.78 (1.59–2.00)	2.62 (2.18–3.14)	1.79 (1.45–2.21)	1.76 (1.41–2.19)	1.05 (0.78–1.41)	<0.001
CMM (%)	2.09 (1.88–2.33)	3.43 (2.94–3.99)	2.30 (1.87–2.83)	1.63 (1.38–1.93)	1.21 (0.92–1.59)	<0.001

Data were displayed as mean (95% confidence intervals) or numbers (95% confidence intervals) according to their data type.
[a]Comparison of categorical variables was performed by Chi-square test. ANOVA was used for the comparison of continuous variables.
Abbreviations: OBS, oxidative balance score; PIR, poverty-to-income ratio; BMI, body mass index; WC, waist circumference; SBP, systolic blood pressure; DBP, diastolic blood pressure; FPG, fasting plasma glucose; TC, total cholesterol; LDL-C, low density lipoprotein cholesterol; HDL-C, high density lipoprotein cholesterol; Scr, serum cholesterol; eGFR, estimated glomerular filtration rate; CHD, coronary heart disease; CMM, cardiometabolic multimorbidity.

TABLE 2 Association between OBS and the prevalent CMM.

Variables	Odds ratio (95% CI)					
	Crude	P value	Model 1	P value	Model 2	P value
OBS (per SD increase)	0.649 (0.587–0.718)	<0.001	0.685 (0.612–0.767)	<0.001	0.739 (0.654–0.835)	<0.001
Quartiles of OBS						
Quartile 1	Reference		Reference		Reference	
Quartile 2	0.663 (0.520–0.846)	0.001	0.687 (0.533–0.887)	0.004	0.741 (0.565–0.973)	0.031
Quartile 3	0.468 (0.370–0.592)	<0.001	0.509 (0.399–0.649)	<0.001	0.544 (0.418–0.707)	0.001
Quartile 4	0.345 (0.251–0.474)	<0.001	0.417 (0.298–0.582)	<0.001	0.530 (0.372–0.754)	<0.001
P for trend		<0.001		<0.001		<0.001

Crude: no adjustment.
Model 1: adjusted for demographic covariates (age sex race PIR).
Model 2: further adjusted for anthropometric, laboratory, and medical history data (BMI, WC, SBP, FPG, TC, LDL-C, HDL-C, eGFR, anti-hypertensive therapy, anti-diabetic therapy).
Abbreviations: OBS, oxidative balance score; CMM, cardiometabolic multimorbidity; OR, odds ratio; CI, confidence interval; SD, standard deviation; PIR, poverty-to-income ratio; BMI, body mass index; WC, waist circumference; SBP, systolic blood pressure; FPG, fasting plasma glucose; TC, total cholesterol; LDL-C, low density lipoprotein cholesterol; eGFR, estimated glomerular filtration rate.

from quartile 1 to quartile 4, along with the prevalence rates of hypertension and diabetes. Meanwhile, the rates of diagnosed CHD and stroke followed the same pattern. Finally, the estimated prevalence of CMM decreased from 3.43% in quartile 1–1.21% in quartile 4 ($P < 0.001$).

Linear association between OBS and the prevalent CMM

The results of the logistic regression analysis were presented in Table 2. Analyzing OBS as a continuous variable revealed that each SD increase was associated with a 35.1% reduction in CMM risk. After adjusting for age, sex, race, and PIR status, the risk reduction decreased to 31.5% per SD increase. Further adjustments for BMI, WC, mSBP, FPG, TC, HDL-C, eGFR, anti-hypertensive therapy, and anti-diabetic therapy reduced the risk reduction to 26.1%. When OBS was categorized into quartiles, the highest quartile showed a 0.530-fold risk of prevalent CMM compared to the lowest quartile in Model 2, with a clear trend of decreasing risk from quartile 1 to quartile 4 (P for trend <0.001). To validate this observed trend in the logistic regression analysis, a smooth curve fitting analysis was performed (Figure 2), which demonstrated a linear decrease in CMM risk across the entire range of OBS values.

Sensitivity analysis for the association between OBS and the prevalent CMM

We further explored the associations between dietary OBS, lifestyle OBS, and prevalent CMM (Table 3), using the same adjustment strategy as in Table 2. Consistent with the findings for OBS, each SD increase in dietary OBS was associated with a 24.5% reduction in the risk of prevalent CMM. Additionally, individuals in the highest quartile of dietary OBS had a 0.513-fold risk of prevalent CMM compared to those in the lowest quartile, with a clear linear trend of decreasing risk from quartile 1 to quartile 4 (P for trend <0.001). In contrast, while higher lifestyle OBS was also linked to a reduced risk of CMM, the risk reduction did not follow a linear pattern across the quartiles.

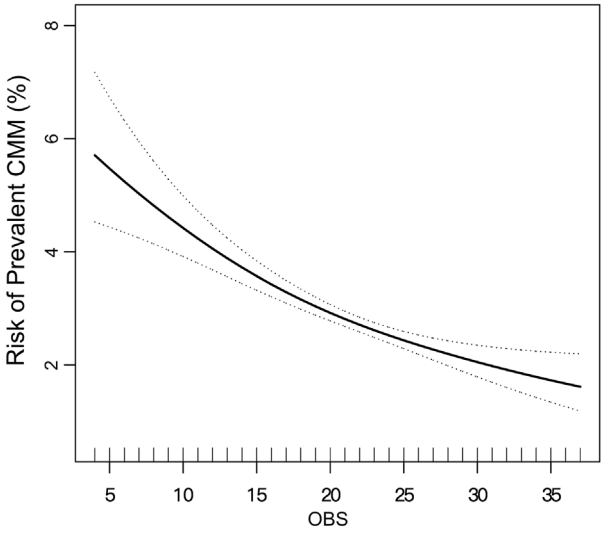

FIGURE 2
Smooth curve fitting illustrating the linear relationship between OBS and prevalent CMM. The model was adjusted for age, sex, race, PIR, BMI, WC, SBP, FPG, TC, HDL-C, eGFR, anti-hypertensive therapy, and anti-diabetic therapy, consistent with Model 2 in Table 2. The solid line represents the estimated risk of prevalent CMM, while the dotted lines indicate the pointwise 95% confidence intervals. The association remained linear across the entire range of OBS.

Subgroup analysis was further performed to evaluate the effectiveness of the results observed in the overall population across various conventional subpopulations (Figure 3). Logistic regression models were adjusted for all covariates included in Model 2, excluding those used to define the subgroups. The findings confirmed that the association between OBS and prevalent CMM remained robust across subgroups defined by sex, age, race, PIR, diabetes, hypertension, and obesity (all P values for interaction >0.05). In Supplementary Table S2, we added hypertension and obesity to the definition of CMM. Similar results were observed under the same adjusting strategy. In model 2, each SD increase in OBS was associated with a 12.3% decrease in the risk of prevalent CMM.

Association of OBS with the identification of prevalent CMM

ROC and reclassification analyses were conducted to assess the association between OBS and the identification of prevalent CMM (Table 4). In the ROC analysis, the AUC for OBS alone was 0.622 (95% CI: 0.616–0.628). Adding OBS to the clinical risk factors (covariates from Model 2 in Table 2) was associated with a slight increase in the AUC from 0.912 to 0.916 (P = 0.001). Reclassification analysis further indicated this association, with a

TABLE 3 Association between dietary and lifestyle OBS and the prevalent CMM.

Variables	Odds ratio (95% CI)					
	Crude	P value	Model 1	P value	Model 2	P value
Dietary OBS (per SD increase)	0.672 (0.609–0.741)	<0.001	0.730 (0.656–0.813)	<0.001	0.755 (0.670–0.850)	<0.001
Quartiles of dietary OBS						
Quartile 1	Reference		Reference		Reference	
Quartile 2	0.677 (0.536–0.855)	0.001	0.722 (0.561–0.929)	0.012	0.732 (0.556–0.963)	0.026
Quartile 3	0.481 (0.368–0.630)	<0.001	0.556 (0.423–0.731)	<0.001	0.567 (0.424–0.758)	0.001
Quartile 4	0.339 (0.238–0.483)	<0.001	0.447 (0.308–0.648)	<0.001	0.513 (0.351–0.749)	<0.001
P for trend		<0.001		<0.001		<0.001
Lifestyle OBS (per SD increase)	0.782 (0.716–0.854)	<0.001	0.696 (0.633–0.765)	<0.001	0.840 (0.744–0.949)	0.005
Quartiles of lifestyle OBS						
Quartile 1	Reference		Reference		Reference	
Quartile 2	0.711 (0.546–0.925)	0.012	0.588 (0.449–0.769)	<0.001	0.658 (0.500–0.866)	0.003
Quartile 3	0.836 (0.649–1.076)	0.162	0.672 (0.518–0.872)	0.003	0.844 (0.643–1.107)	0.219
Quartile 4	0.409 (0.299–0.559)	<0.001	0.315 (0.229–0.432)	<0.001	0.635 (0.442–0.912)	0.014
P for trend		<0.001		<0.001		0.048

Crude: no adjustment.
Model 1: adjusted for demographic covariates (age sex race PIR).
Model 2: further adjusted for anthropometric, laboratory, and medical history data (BMI, WC, SBP, FPG, TC, LDL-C, HDL-C, eGFR, anti-hypertensive therapy, anti-diabetic therapy).
Abbreviations: OBS, oxidative balance score; CMM, cardiometabolic multimorbidity; OR, odds ratio; CI, confidence interval; SD, standard deviation; PIR, poverty-to-income ratio; BMI, body mass index; WC: waist circumference; SBP, systolic blood pressure; FPG, fasting plasma glucose; TC, total cholesterol; LDL-C, low density lipoprotein cholesterol; eGFR, estimated glomerular filtration rate.

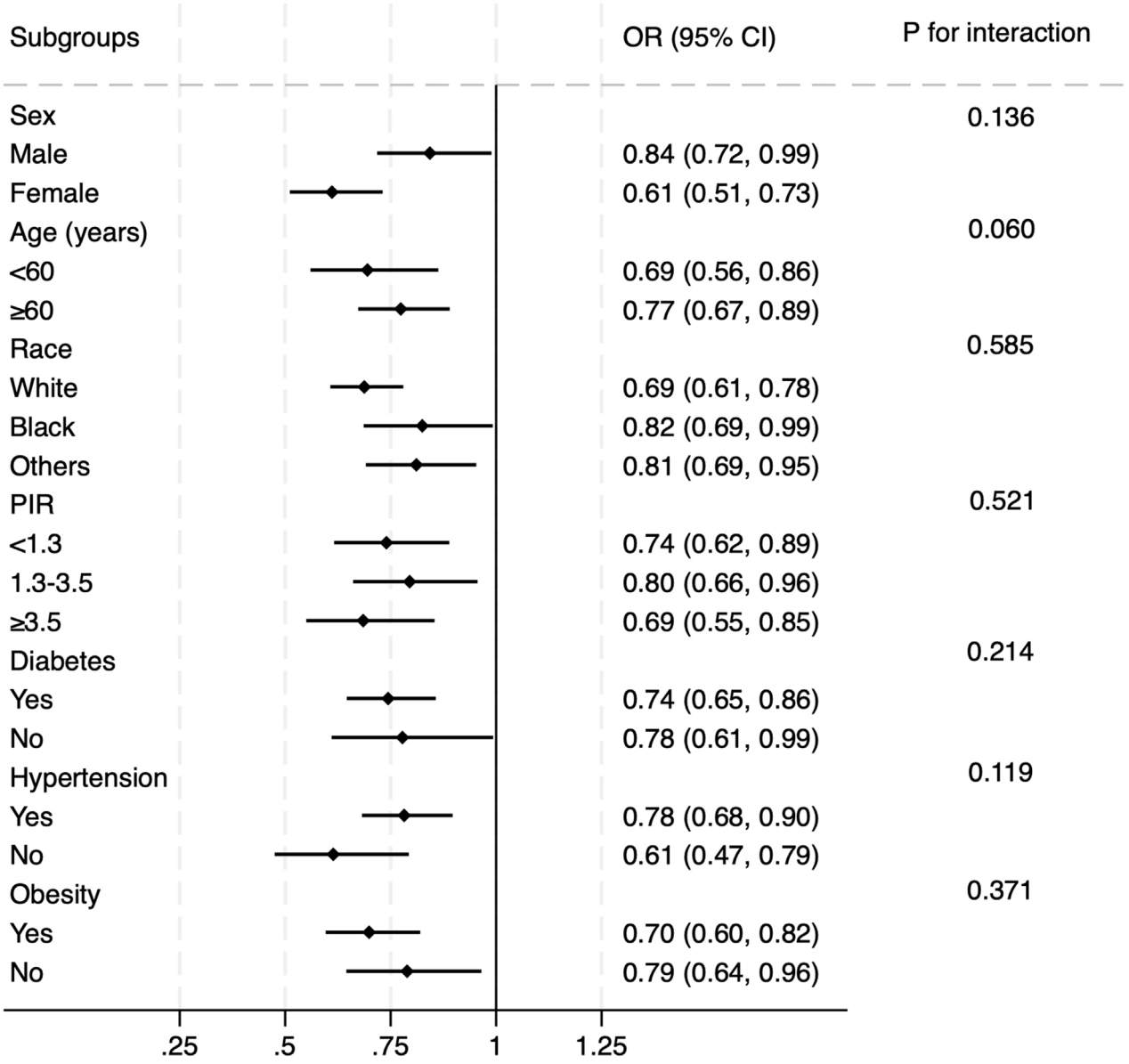

FIGURE 3
Subgroup analysis of the correlation between OBS and prevalent CMM. The multivariate logistic model was adjusted for all variables included in Model 2 of Table 2, except the variable used to define each subgroup. The association remained consistent across subgroups defined by sex, age, race, diabetes, hypertension, and obesity.

continuous NRI of 0.243 (95% CI: 0.172–0.314, P < 0.001) and an IDI of 0.007 (95% CI: 0.004–0.010, P < 0.001), suggesting that OBS may be associated with improved identification of prevalent CMM. DCA also showed a significant improvement when OBS was added to clinical risk factors (Supplementary Figure S1). The results showed that adding OBS to the clinical risk factors model was associated with an increase in net benefit across a range of clinically relevant risk thresholds (0–0.4).

Discussion

In the current analysis, our findings revealed a significant association between OBS and prevalent CMM in the general population. This relationship was negatively linear across the entire range of OBS, indicating that the risk of prevalent CMM increased proportionally with higher OBS values. The association remained consistent after adjusting for common cardiovascular

TABLE 4 Assessment of the value of OBS for detecting prevalent CMM.

Model	AUC (95% CI)	P value	P for comparison	NRI (continuous)	P value	IDI	P value
OBS	0.622 (0.616–0.628)	<0.001	-	-	-	-	-
Clinical risk factors[a]	0.912 (0.908–0.915)	<0.001	-	-	-	-	-
Clinical risk factors + OBS	0.916 (0.913–0.920)	<0.001	0.001	0.243 (0.172–0.314)	<0.001	0.007 (0.004–0.010)	<0.001

[a]Clinical risk factors: age, sex, race, PIR, BMI, WC, SBP, FPG, TC, HDL-C, eGFR, anti-hypertensive therapy, and anti-diabetic therapy.
Abbreviations: OBS, oxidative balance score; CMM, cardiometabolic multimorbidity; AUC, area under the curve; NRI, net reclassification index; IDI, integrated discrimination index; PIR, poverty-to-income ratio; BMI, body mass index; WC, waist circumference; SBP, systolic blood pressure; FPG, fasting plasma glucose; TC, total cholesterol; LDL-C, low density lipoprotein cholesterol; eGFR, estimated glomerular filtration rate.

risk factors, demonstrating its robustness across various subpopulations. Furthermore, the addition of OBS to conventional cardiovascular risk factors achieved significance improvement in ROC and reclassification analysis, suggesting that applying OBS into clinical practice may be associated with improved identification of prevalent CMM in the general population.

The linear association between OBS and the risk of prevalent CMM

The findings from this analysis supported the hypothesis of a significant association between OBS and prevalent CMM, highlighting the potential utility of OBS in detecting CMM in the general population. The first part of the analysis focused on this association, using multivariate logistic regression adjusted for demographic, laboratory, anthropometric, and medical history variables. The results demonstrated a significant and independent relationship between OBS and prevalent CMM, unaffected by conventional cardiovascular risk factors. Assuming a linear association, a smooth curve-fitting analysis was performed, confirming that the relationship between OBS and prevalent CMM was linearly negative across the entire OBS range. This indicated that the risk of prevalent CMM increased proportionally with higher OBS values, without evidence of a threshold or saturation effect.

The analysis also explored the individual contributions of dietary and lifestyle OBS to prevalent CMM. Dietary OBS exhibited a significant and linear association with CMM, with a slightly higher effect size (OR) compared to total OBS. In contrast, lifestyle OBS, while significantly associated with CMM, did not show a linear relationship. This discrepancy may be due to the limited number of elements in the lifestyle OBS (physical activity, alcohol, BMI, cotinine), with scores ranging only from 0 to 8, which could potentially affect the linearity due to score distribution and sample size. Further research is needed to determine whether the association between lifestyle OBS and CMM follows a non-linear pattern.

Finally, a subgroup analysis was conducted to evaluate whether the findings were consistent across key cardiovascular subpopulations defined by age, gender, race, socioeconomic status, diabetes, hypertension, and obesity. The results showed that the main findings from the overall population were robust and applicable across these subpopulations, reinforcing the generalizability of the observed association between OBS and prevalent CMM.

In the current study, we defined CMM as the coexistence of two or more conditions: diabetes mellitus, stroke, or coronary heart disease. This definition was based on prior literature [16, 17], which identified these conditions as key components of CMM. While hypertension and obesity are also major cardiometabolic conditions, they were not included in the primary definition due to their potential impact on the event prevalence. Including hypertension and obesity would have led to a dramatic increase in CMM prevalence from 2.95% to 23.70%, violating a key assumption of logistic regression that event prevalence should remain below 15%. This change could result in inflated odds ratios and distorted estimates. Nevertheless, we still conducted a sensitivity analysis that included hypertension and obesity in the CMM definition. The results of this analysis, presented in Supplementary Table S2, were consistent with our primary findings, indicating that the associations between OBS and CMM remained robust. These findings suggest that our conclusions are not influenced by the exclusion of hypertension and obesity.

Association of OBS with the identification of prevalent CMM

In the second part of our statistical analysis, we shifted focus to evaluating the association between OBS and improved identification of prevalent CMM in the general population. To this end, both ROC, reclassification, and DCA analyses were employed to assess the supplemental value of OBS from a different perspective. While the AUC for OBS alone in identifying prevalent CMM was modest, incorporating OBS into conventional cardiovascular risk factors significantly improved the model's ability to identify prevalent CMM. The increase in AUC is also limited, suggesting that OBS functions primarily as an additional and supplemental tool, rather than a

replacement, for traditional risk factors. By assessing dietary and lifestyle factors, OBS helps identify individuals who may not be captured by conventional cardiovascular risk factors alone. This highlights OBS's potential to identify individuals who might otherwise be overlooked by traditional models, offering a more comprehensive approach to CMM, particularly in relation to dietary and lifestyle habits.

However, it is important to note that ROC analysis evaluates the overall performance of the combined model (cardiovascular risk factors + OBS) rather than isolating the specific contribution of OBS to improving detection. As such, ROC analysis may overestimate or underestimate the individual value of OBS, providing limited insight into whether adding OBS to conventional cardiovascular risk factors meaningfully refines the detection of prevalent CMM [24, 25]. To address this limitation, reclassification analysis—using metrics such as NRI and IDI—has been proposed as an alternative approach to assess the added value of novel markers [26–28].

In our study, introducing OBS into the cardiovascular risk factors model resulted in significant improvements in both continuous NRI and IDI. While these values (NRI: 0.243 and IDI: 0.007) represent modest changes, they suggest better refinement in identifying prevalent CMM and demonstrate that OBS contributes incremental value to the existing model. The NRI suggests that OBS facilitates more accurate reclassification of individuals into categories, potentially enabling more targeted interventions. Similarly, while the IDI value was small, it reflects a refinement in the model's discriminatory power, which may have important practical implications for clinical decision-making. These results, supported by both ROC and reclassification analyses, implicate OBS's potential as a supplementary marker capable of identifying CMM patients who might otherwise be overlooked by traditional models, offering a more comprehensive approach to CMM identification.

As highlighted in the literature, even small increases in AUC are often considered meaningful in clinical practice, as they can lead to better model discrimination between high and low-risk individuals. Baker et al. noted that even a slight AUC improvement could substantially impact clinical decision-making by enhancing the model's ability to identify at-risk patients with greater accuracy [29]. To better assess the practical value of this slight increase in AUC, we further conducted DCA (Supplementary Figure S1). In our results, we observed that adding OBS to the clinical risk factor model improved the net benefit across a range of thresholds. This phenomenon demonstrated that OBS could still provide some valuable information to the model and function as a supplemental tool. In conclusion, the slight increase in AUC is clinically relevant, as supported by the DCA. Applying OBS in clinical practice could be associated with improved clinical decision-making. This finding underscores the potential value of OBS as a supplemental marker to identify prevalent CMM in clinical practice.

Mechanisms underlying the association between OBS and CMM

Both dietary components of OBS play their role in the development and progression of cardiometabolic diseases. Vitamin C intake is significantly associated with a reduced risk of CHD and heart failure [30]. A high intake of vitamin E may lower the risk of CHD by preventing the formation of oxidized LDL-C, which can trigger endothelial cells to produce inflammatory markers, exert cytotoxic effects on these cells, and impair nitric oxide-mediated vasodilation [31]. Additionally, combining vitamin C with other antioxidants, such as vitamin E, leads to improved antioxidant effectiveness. Selenium, a vital component of glutathione peroxidase, plays a crucial role in protecting aerobic tissues from oxidative damage caused by free radicals during myocardial ischemia [32]. Magnesium deficiency, linked to the onset and progression of atherosclerotic injury, can trigger oxidative stress in the body. Magnesium intake enhances the vasodilatory effects of both endogenous and exogenous vasodilators and reduces cardiovascular risk by inhibiting platelet function [32]. Antioxidants also play a vital role in mitigating oxidative stress induced by reactive oxygen species, which are primarily triggered by uncontrolled high blood sugar levels in diabetes. Supplements such as vitamin C, vitamin E, selenium, and alpha-lipoic acid have demonstrated potential in reducing oxidative stress markers and enhancing antioxidant status in laboratory studies, animal models, and diabetic patients. Antioxidant supplementation has also been shown to improve endothelial function, insulin sensitivity, and glucose metabolism, contributing to better glycemic control and overall management of diabetes [7].

Clinical implications

The primary clinical implication of this study is the detailed characterization of the association between OBS and prevalent CMM, which reinforces the link between oxidative balance and CMM. OBS, as a measure of oxidative stress balance, was found to have a linear association with the risk of prevalent CMM, suggesting that managing oxidative stress may be associated with a lower likelihood of CMM. Another key implication is that applying OBS in clinical practice could be associated with improved identification of prevalent CMM, particularly in primary care settings. CMM is one of the most prevalent and hazardous forms of multimorbidity, associated with reduced life expectancy and increased mortality, making it a significant cardiovascular risk factor, especially in older populations. However, CMM is often overlooked, particularly in primary care, where its identification is critical for cardiovascular prevention. This issue is more pronounced in rural areas of developing countries, where many individuals with cardiometabolic diseases remain undiagnosed, and essential

treatment is lacking. The identification rate of CMM is notably low in these populations.

Our findings suggest that OBS could be associated with improved identification of prevalent CMM in the general population. Given its cost-effectiveness, integrating OBS into clinical practice could improve the identification of CMM in primary care settings. This, in turn, would enable general practitioners to deliver more personalized medical care for patients with CMM, addressing an unmet need in managing this high-risk condition.

Limitations

Our study has some limitations. First, a major limitation of this study is the cross-sectional design, which prevents us from establishing causality. Individuals with existing cardiometabolic conditions could have altered their diet or lifestyle in response to their health status, potentially influencing their OBS. Therefore, while we observe an association between OBS and CMM, future studies utilizing longitudinal data or Mendelian randomization approaches are needed to better establish causal relationships. These methods would help to confirm whether OBS directly influences the risk of CMM or if the relationship is due to reverse causation. Second, as shown in Figure 1. 18,599 participants were excluded due to missing data related to key variables, including OBS, CMM, and other covariates. While we focused on complete cases to maintain the integrity of the analysis, the excluded participants may differ systematically from those included in the study, potentially leading to selection bias. For instance, those excluded due to missing OBS data, CMM data, or covariate data might represent different demographic or clinical groups, which could affect the generalizability of our results. This selection bias could lead to over- or underestimation of the association between the OBS and CMM, particularly in the underrepresented groups. Although multiple imputation is a standard method for handling missing data, it was not applied in this study due to the complexity of imputing OBS data, which involves a combination of dietary, lifestyle, and clinical factors that may not be easily modeled with the available data. Additionally, the assumptions required for multiple imputation, such as missing data being missing at random, were difficult to verify given the nature of the missing data in our dataset. Given these challenges, we chose to exclude participants with missing data to ensure the validity and robustness of our analysis. However, the potential impact of this exclusion on the overall findings remains an important consideration. Therefore, our findings still require future studies with more complete data collection to verify.

Third, the reliance on self-reported data in NHANES raises concerns about recall bias and subjectivity, potentially compromising data accuracy. Further studies using more reliable and objective definitions are required to validate our conclusions. Fourth, while we adjusted for a range of covariates, unmeasured confounders may still have influenced our results. Therefore, studies with more comprehensive data collection are needed to confirm our findings. Last, as NHANES was conducted exclusively in the United States, the generalizability of our results to other populations remains uncertain. Additional research involving diverse populations is essential to verify the applicability of our findings.

Author contributions

WS: Conceptualization, Data curation, Formal analysis, Writing – original draft. YZ: Data curation, Formal analysis, Writing – original draft. JP: Writing – original draft. WC: Conceptualization, Writing – review and editing. All authors contributed to the article and approved the submitted version.

Data availability

The datasets presented in this study can be found in online repositories. The names of the repository/repositories and accession number(s) can be found below: The data used in the current study could be acquired from WC with a reasonable request. The data could also be downloaded from the NHANES official website (https://www.cdc.gov/nchs/nhanes/index.htm).

Ethics statement

The studies involving humans were approved by Every subject in the NHANES study provided a written consent for participating the survey. The NCHS institutional Ethics Review Board approved the study design of NHANES. Therefore, additional Ethics Review is unnecessary for the current analysis. The studies were conducted in accordance with the local legislation and institutional requirements. The participants provided their written informed consent to participate in this study.

Funding

The authors declare that no financial support was received for the research and/or publication of this article.

Conflict of interest

The author(s) declared no potential conflicts of interest with respect to the research, authorship, and/or publication of this article.

Generative AI statement

The authors declare that Generative AI was used in the creation of this manuscript. AI-assisted technology was only used in the writing process to improve the readability and language of the manuscript.

Any alternative text (alt text) provided alongside figures in this article has been generated by Frontiers with the support of artificial intelligence and reasonable efforts have been made to ensure accuracy, including review by the authors wherever possible. If you identify any issues, please contact us.

Supplementary material

The Supplementary Material for this article can be found online at: https://www.ebm-journal.org/articles/10.3389/ebm.2025.10824/full#supplementary-material

References

1. GBD 2019 Diseases and Injuries Collaborators. Global burden of 369 diseases and injuries in 204 countries and territories, 1990-2019: a systematic analysis for the global burden of disease study 2019. *Lancet* (2020) **396**:1204–22. doi:10.1016/S0140-6736(20)30925-9

2. Roth GA, Mensah GA, Johnson CO, Addolorato G, Ammirati E, Baddour LM, et al. Global burden of cardiovascular diseases and risk factors, 1990-2019: update from the GBD 2019 study. *J Am Coll Cardiol* (2020) **76**:2982–3021. doi:10.1016/j.jacc.2020.11.010

3. Di Angelantonio E, Kaptoge S, Wormser D, Willeit P, Butterworth AS, Bansal N, et al. Association of cardiometabolic multimorbidity with mortality. *Jama* (2015) **314**:52–60. doi:10.1001/jama.2015.7008

4. Feng L, Jehan I, de Silva HA, Naheed A, Farazdaq H, Hirani S, et al. Prevalence and correlates of cardiometabolic multimorbidity among hypertensive individuals: a cross-sectional study in rural south asia-Bangladesh, Pakistan and Sri Lanka. *BMJ Open* (2019) **9**:e030584. doi:10.1136/bmjopen-2019-030584

5. Canoy D, Tran J, Zottoli M, Ramakrishnan R, Hassaine A, Rao S, et al. Association between cardiometabolic disease multimorbidity and all-cause mortality in 2 million women and men registered in UK general practices. *BMC Med* (2021) **19**:258. doi:10.1186/s12916-021-02126-x

6. Yan Q, Liu S, Sun Y, Chen C, Yang S, Lin M, et al. Targeting oxidative stress as a preventive and therapeutic approach for cardiovascular disease. *J Transl Med* (2023) **21**:519. doi:10.1186/s12967-023-04361-7

7. Dilworth L, Stennett D, Facey A, Omoruyi F, Mohansingh S, Omoruyi FO. Diabetes and the associated complications: the role of antioxidants in diabetes therapy and care. *Biomed and Pharmacother* (2024) **181**:117641. doi:10.1016/j.biopha.2024.117641

8. Degerud E, Høiseth G, Mørland J, Ariansen I, Graff-Iversen S, Ystrom E, et al. Associations of binge drinking with the risks of ischemic heart disease and stroke: a study of pooled Norwegian health surveys. *Am J Epidemiol* (2021) **190**:1592–603. doi:10.1093/aje/kwab063

9. Kodali HP, Pavilonis BT, Schooling CM. Effects of copper and zinc on ischemic heart disease and myocardial infarction: a Mendelian randomization study. *The Am J Clin Nutr* (2018) **108**:237–42. doi:10.1093/ajcn/nqy129

10. Arabshomali A, Bazzazzadehgan S, Mahdi F, Shariat-Madar Z. Potential benefits of antioxidant phytochemicals in type 2 diabetes. *Molecules* (2023) **28**:7209. doi:10.3390/molecules28207209

11. Ilori TO, Sun Ro Y, Kong SY, Gutierrez OM, Ojo AO, Judd SE, et al. Oxidative balance score and chronic kidney disease. *Am J Nephrol* (2015) **42**:320–7. doi:10.1159/000441623

12. Van Hoydonck PG, Temme EH, Schouten EG. A dietary oxidative balance score of vitamin C, beta-carotene and iron intakes and mortality risk in male smoking Belgians. *The J Nutr* (2002) **132**:756–61. doi:10.1093/jn/132.4.756

13. Wu C, Ren C, Song Y, Gao H, Pang X, Zhang L. Gender-specific effects of oxidative balance score on the prevalence of diabetes in the US population from NHANES. *Front Endocrinol (Lausanne)* (2023) **14**:1148417. doi:10.3389/fendo.2023.1148417

14. Lee JH, Son DH, Kwon YJ. Association between oxidative balance score and new-onset hypertension in adults: a community-based prospective cohort study. *Front Nutr* (2022) **9**:1066159. doi:10.3389/fnut.2022.1066159

15. Cheng S, Han Y, Jiang L, Lan Z, Liao H, Guo J. Associations of oxidative balance score and visceral adiposity index with risk of ischaemic heart disease: a cross-sectional study of NHANES, 2005-2018. *BMJ Open* (2023) **13**:e072334. doi:10.1136/bmjopen-2023-072334

16. Xie H, Li J, Zhu X, Li J, Yin J, Ma T, et al. Association between healthy lifestyle and the occurrence of cardiometabolic multimorbidity in hypertensive patients: a prospective cohort study of UK biobank. *Cardiovasc Diabetol* (2022) **21**:199. doi:10.1186/s12933-022-01632-3

17. Luo H, Zhang Q, Yu K, Meng X, Kan H, Chen R. Long-term exposure to ambient air pollution is a risk factor for trajectory of cardiometabolic multimorbidity: a prospective study in the UK Biobank. *EBioMedicine* (2022) **84**:104282. doi:10.1016/j.ebiom.2022.104282

18. ElSayed NA, Aleppo G, Aroda VR, Bannuru RR, Brown FM, Bruemmer D, et al. 2. Classification and diagnosis of diabetes: standards of care in Diabetes-2023. *Diabetes Care* (2023) **46**:S19–40. doi:10.2337/dc23-S002

19. Liu F, You F, Yang L, Du X, Li C, Chen G, et al. Nonlinear relationship between oxidative balance score and hyperuricemia: analyses of NHANES 2007-2018. *Nutr J* (2024) **23**:48. doi:10.1186/s12937-024-00953-1

20. Tian X, Xue B, Wang B, Lei R, Shan X, Niu J, et al. Physical activity reduces the role of blood cadmium on depression: a cross-sectional analysis with NHANES data. *Environ Pollut* (2022) **304**:119211. doi:10.1016/j.envpol.2022.119211

21. Gorber SC, Schofield-Hurwitz S, Hardt J, Levasseur G, Tremblay M. The accuracy of self-reported smoking: a systematic review of the relationship between self-reported and cotinine-assessed smoking status. *Nicotine and Tob Res* (2009) **11**:12–24. doi:10.1093/ntr/ntn010

22. McEvoy JW, McCarthy CP, Bruno RM, Brouwers S, Canavan MD, Ceconi C, et al. 2024 ESC guidelines for the management of elevated blood pressure and hypertension. *Eur Heart J* (2024) **45**:3912–4018. doi:10.1093/eurheartj/ehae178

23. Levey AS, Stevens LA, Schmid CH, Zhang YL, Castro AF, 3rd, Feldman HI, et al. A new equation to estimate glomerular filtration rate. *Ann Intern Med* (2009) **150**:604–12. doi:10.7326/0003-4819-150-9-200905050-00006

24. Cook NR. Use and misuse of the receiver operating characteristic curve in risk prediction. *Circulation* (2007) **115**:928–35. doi:10.1161/circulationaha.106.672402

25. Pickering JW, Endre ZH. New metrics for assessing diagnostic potential of candidate biomarkers. *Clin J Am Soc Nephrol* (2012) **7**:1355–64. doi:10.2215/cjn.09590911

26. Pencina MJ, D'Agostino RB, D'Agostino RB, Jr, Vasan RS. Evaluating the added predictive ability of a new marker: from area under the ROC curve to reclassification and beyond. *Stat Med* (2008) **27**:157–72. doi:10.1002/sim.2929

27. Pencina MJ, D'Agostino RB, Steyerberg EW. Extensions of net reclassification improvement calculations to measure usefulness of new biomarkers. *Stat Med* (2011) **30**:11–21. doi:10.1002/sim.4085

28. Grunkemeier GL, Jin R. Net reclassification index: measuring the incremental value of adding a new risk factor to an existing risk model. *The Ann Thorac Surg* (2015) **99**:388–92. doi:10.1016/j.athoracsur.2014.10.084

29. Baker SG, Schuit E, Steyerberg EW, Pencina MJ, Vickers A, Moons KG, et al. How to interpret a small increase in AUC with an additional risk prediction marker: decision analysis comes through. *Stat Med* (2014) **33**:3946–59. doi:10.1002/sim.6195

30. Morelli MB, Gambardella J, Castellanos V, Trimarco V, Santulli G. Vitamin C and cardiovascular disease: an update. *Antioxidants (Basel)* (2020) **9**:1227. doi:10.3390/antiox9121227

31. Violi F, Nocella C, Loffredo L, Carnevale R, Pignatelli P. Interventional study with vitamin E in cardiovascular disease and meta-analysis. *Free Radic Biol Med* (2022) **178**:26–41. doi:10.1016/j.freeradbiomed.2021.11.027

32. Benstoem C, Goetzenich A, Kraemer S, Borosch S, Manzanares W, Hardy G, et al. Selenium and its supplementation in cardiovascular disease--what do we know? *Nutrients* (2015) **7**:3094–118. doi:10.3390/nu7053094

EBM Experimental Biology and Medicine

TYPE Original Research
PUBLISHED 13 January 2026
DOI 10.3389/ebm.2025.10815

OPEN ACCESS

*CORRESPONDENCE
Yu Wang,
uygnaw0@126.com
Lei Fan,
fanl1006@163.com
Hao Xie,
hao_xie2018@163.com
Xiaolong Hu,
503342422@qq.com

†These authors have contributed equally to this work

RECEIVED 09 September 2025
REVISED 26 November 2025
ACCEPTED 10 December 2025
PUBLISHED 13 January 2026

CITATION
Ye Z, Zhao T, Huang X, Song Y, Cheng L, Liu Y, Qiu M, Long R, Chen W, Wang Y, Xie H, Fan L and Hu X (2026) Inflammatory indicators derived from complete blood counts in relation to osteoarthritis prevalence: findings from the NHANES 2007–2020 cross-sectional survey.
Exp. Biol. Med. 250:10815.
doi: 10.3389/ebm.2025.10815

Inflammatory indicators derived from complete blood counts in relation to osteoarthritis prevalence: findings from the NHANES 2007–2020 cross-sectional survey

Zimo Ye[1,2†], Tianran Zhao[2†], Xinlin Huang[2], Yingxue Song[2], Luyi Cheng[3], Yunyi Liu[3], Mingde Qiu[3], Ruke Long[3], Weihao Chen[1,2], Yu Wang[4*], Hao Xie[5*], Lei Fan[5*] and Xiaolong Hu[1*]

[1]Huiqiao Medical Center, Nanfang Hospital, Southern Medical University, Guangzhou, Guangdong, China, [2]The Second School of Clinical Medicine, Southern Medical University, Guangzhou, Guangdong, China, [3]The School of Public Health, Southern Medical University, Guangzhou, Guangdong, China, [4]Department of Orthopedics, Affiliated Hospital of Jilin Medical College, Jilin City, Jilin Province, China, [5]Department of Orthopedic Surgery, Nanfang Hospital, Southern Medical University, Guangzhou, Guangdong, China

Abstract

Although multiple studies have confirmed the importance of chronic low-grade inflammation in the development of osteoarthritis (OA), the association between complete blood count (CBC)-derived inflammatory indicators and osteoarthritis prevalence remains unclear. The present study aims to explore the association between CBC-derived inflammatory indicators and OA prevalence. We used NHANES data from 2007 to 2020 for a cross-sectional analysis. Multivariate logistic regression models were used to evaluate the association between CBC-derived inflammatory indicators and OA prevalence. Restricted cubic spline function (RCS) and threshold analysis were used to assess potential nonlinear associations. In addition, subgroup and sensitivity analyses were performed to assess the stability of the results. Finally, we used LASSO regression to identify the variables most associated with OA outcomes to construct a prediction model, and the model's validity was verified. Among the 24,112 patients in this study, 3,195 were diagnosed with OA. In the adjusted model, multivariate logistic regression analysis showed that 5 inflammatory indicators (SII, SIRI, MLR, NMLR, NLR) were positively associated with OA prevalence. RCS and threshold analysis showed nonlinear associations between (SII, NMLR, NLR) and OA prevalence. After variable screening, we established an OA risk prediction model with an area under the curve (AUC) of 0.735 (95% CI: 0.726–0.744). Both the decision and calibration curve showed that the model had good clinical significance. The Present study suggests that CBC-derived

inflammatory indicators are statistically associated with OA prevalence. Furthermore, MLR and NMLR could be valuable predictors of OA and offer novel perspectives on its assessment and treatment.

KEYWORDS

epidemiology, inflammation, leukocyte, orthopaedics, osteoarthritis

Impact statement

This study challenges the traditional view of osteoarthritis as merely a consequence of joint wear by demonstrating significant associations between systemic inflammation (measured through widely available CBC indicators) and OA prevalence in a major U.S. cohort. It identifies novel nonlinear associations of SII, NMLR, and NLR with OA prevalence, suggesting complex dynamic relationships between cellular inflammation and OA that merit further mechanistic investigation. By integrating MLR and NMLR into a clinically applicable prediction model with strong discriminatory power (AUC = 0.735), this work provides an accessible tool for early OA risk assessment using routine blood parameters. These findings underscore the role of immune-inflammatory processes in OA and may inform future strategies for prevention, early intervention, and mechanistic research.

Introduction

Osteoarthritis (OA) is a common chronic joint disease characterized by pathological changes in articular cartilage, subchondral bone remodeling, and synovial abnormalities, which eventually lead to clinically significant pain and functional impairment [1]. According to Hunter et al, more than 500 million people are affected by OA worldwide [2]. A recent study by Sun et al. [3] found that nearly 14 million people in the United States suffer from knee OA, which has led to a heavy public health burden. Currently, drug therapy is the main treatment for early and middle-stage OA, while joint replacement surgery remains the only effective treatment for end-stage disease [4]. However, postoperative joint function may be unsatisfactory, and patients face the problem of limited lifespan of the replacement joint, which, in addition to pain, leads to reoperation and increased costs. Therefore, identifying modifiable factors is crucial to developing feasible strategies to delay the progression of OA and reduce the associated social and economic burden and negative impact on patients [5]. Currently, there is no recognized risk predictor for OA. To address this gap, we conducted the present study to examine whether CBC-derived inflammatory indicators are associated with OA risk and to identify predictors that may be clinically useful. In addition, the findings may provide useful perspectives and references for future mechanistic research.

OA is a multifactorial disease influenced by aging, genetic susceptibility, obesity, and, in particular, inflammatory processes [6, 7], with specific inflammatory biomarkers being key indicators of disease progression. Emerging evidence indicates that TNF-α and IL-1β are key inflammatory mediators in OA. These cytokines interact with multiple signaling pathways to promote further cytokine release and are involved in the pathogenesis of OA [8]. Systemic inflammatory responses can be assessed using complete blood count (CBC)-derived inflammatory indicators, which are calculated from routine blood count parameters and include systemic immune inflammatory index (SII), systemic inflammatory response index (SIRI), monocyte-to-lymphocyte ratio (MLR), (neutrophil + monocyte)-to-lymphocyte ratio (NMLR), neutrophil-to-lymphocyte ratio (NLR), and derived NLR (dNLR). Peripheral platelets, lymphocytes, and neutrophils together comprise these inflammatory markers, which constitute a comprehensive set of parameters used for prognosis. Compared with a single inflammatory signal, they can more comprehensively reflect the host's immune-inflammatory status [9, 10], highlighting their potential as key indicators of the body's inflammatory and immune status. In addition, since CBC-derived inflammatory indicators are readily obtained from routine complete blood counts, they are easy to use in clinical applications.

It is noteworthy that multiple complete blood count (CBC)-derived inflammatory indicators are crucial for diagnosing and treating various diseases [11–13]. A study by Ke et al. [14] found that elevated NLR and SII levels in asthma patients were associated with an increased likelihood of respiratory disease-related death. In addition, studies have found that NLR and PLR are closely associated with PASI scores in patients with psoriasis, suggesting that they can reflect systemic inflammation [15].

Abbreviations: SII, Systemic immune-inflammation index; SIRI, Systemic Inflammation Response Index; MLR, Monocyte - to - Lymphocyte Ratio; NMLR, (Neutrophil + Monocyte) - to - Lymphocyte Ratio; NLR, Neutrophil - to - Lymphocyte Ratio; dNLR, derived Neutrophil - to - Lymphocyte Ratio; PLR, Platelet - to - Lymphocyte Ratio; OA, osteoarthritis; BMI, Body mass index; NHANES, National Health and Nutrition Examination Survey; RCS, Restricted Cubic Splines; OR, Odd Ratio; IL, Interleukin; TNF, Tumour necrosis factor; MAPK, Mitogen-activated protein kinase; JNKs, c-Jun N-terminal kinases; EPKs, Extracellular signal-regulated kinases; ECM, Extracellular matrix.

Previous studies on OA have mainly focused on the association between individual inflammatory indicators [16–18] and disease status. However, this approach focuses on a limited date range and specific indices [19], which may lead to false findings. Therefore, we comprehensively investigated the association between CBC-derived inflammatory indicators and OA prevalence and tested their predictive performance. We hypothesized that the OA patients have a higher level of CBC-derived inflammatory indicators.

Materials and methods

Study design and population

The present study used publicly available datasets obtained from the NHANES[1] platform. All procedures were approved by the institutional review board of the National Center for Health Statistics, and participants were requested to submit informed consent [20].

Of the NHANES 2007–2020 data, 66,148 individuals were recognized. The exclusion criteria were as follows: (1) individuals younger than 18 years or pregnant; (n = 26,069); (2) participants with missing covariate data (n = 10,895); (3) participants without osteoarthritis information (n = 5,039); (4) participants without CBC data (n = 73). In the end, 24,112 individuals participated in the present research. Figure 1 depicts the complete data selection procedure. Every piece of statistical data used in the present study is publicly accessible and demographically weighted for further study.

Definition of CBC-derived inflammatory indicators

The NHANES mobile examination center (MEC) used the Beckman Coulter DxH 800 device to analyze CBCs on blood samples and report blood cell distribution for each individual. The procedure was overseen by qualified medical staff. Subsequently, using certain mathematical formulae based on the complete counts of various blood cell subpopulations, we computed the following inflammatory indicators: SII, SIRI, MLR, NMLR, NLR, and dNLR. SII = neutrophil counts × platelet counts/lymphocyte counts, SIRI = neutrophil counts × monocyte counts/lymphocyte counts, MLR = monocyte counts/lymphocyte counts, NMLR = (neutrophil counts + monocyte counts)/lymphocyte counts, NLR = neutrophil counts/lymphocyte counts, dNLR = neutrophil counts/(white blood cell counts-lymphocyte counts).

1 https://www.cdc.gov/nchs/nhanes

Definition of osteoarthritis

A questionnaire survey was used to determine whether a subject had OA. "Did a doctor or other healthcare professional ever tell you that you have arthritis?" is the first question that participants would be asked. The question of "What type of arthritis was it?" would be required if the response to the first question was "yes." Each individual was assigned to an OA or non-OA subgroup based on their responses to the two questions. The individuals were placed in the non-OA subgroup if they answered "no" to the first question. The OA group was assigned to the participant if they answered "yes" to the first question and "OA" to the second. In comparison, participants were placed in the non-OA group if they answered "no" to the first question.

Definition of covariates

Covariates for statistical analysis included demographic statistics (age, gender, race, marital status, educational level), life behavior traits (energy intake, smoking status, and drinking status), body mass index (BMI), concurrent illnesses (diabetes and hypertension), and laboratory indicators that could influence the results (albumin, urine acid, and urine creatinine). From the demographic statistics, the age of each participant was gathered. The individuals were then further divided into two subgroups: Age <60 and 60 ≤ Age [21]. Every individual involved in the present research was older than 18. The participants were stratified by race into five subgroups: non-Hispanic White, non-Hispanic Black, other Hispanic, Mexican American, and other race. Marital status was categorized into three states: never married, married/living with partner, and widowed/divorced/separated. Education level was further classified into five subgroups: less than 9th grade, 9–11th grade, high school graduate/GED or equivalent, some college or AA degree, and college graduate or above. The initial 24-h recall questionnaire enabled the collection of data on energy intake. Using a smoking questionnaire, participants' smoking status was categorized as never smoking (no more than 100 tobacco products), previous smoking (greater than 100 tobacco products, not smoking at the moment), and present smoking (greater than 100 tobacco products, currently smoking). Each participant's BMI, calculated as weight divided by height squared (kg/m2), was derived from the examination statistics. According to the drinking questionnaire, the drinking status was classified as no drinking (less than one time a week), mild (one to three times a week), and intense (more than three times a week) [22]. Diagnosis of diabetes was based on antidiabetic medication use, questionnaire results, or a fasting plasma glucose level >7.0 mmol/L. Once systolic pressure was greater than 140 mmHg or diastolic pressure was greater than 90 mmHg, the diagnosis of hypertension was established. The NHANES program's laboratory test data included statistics on albumin, creatinine, and calcium.

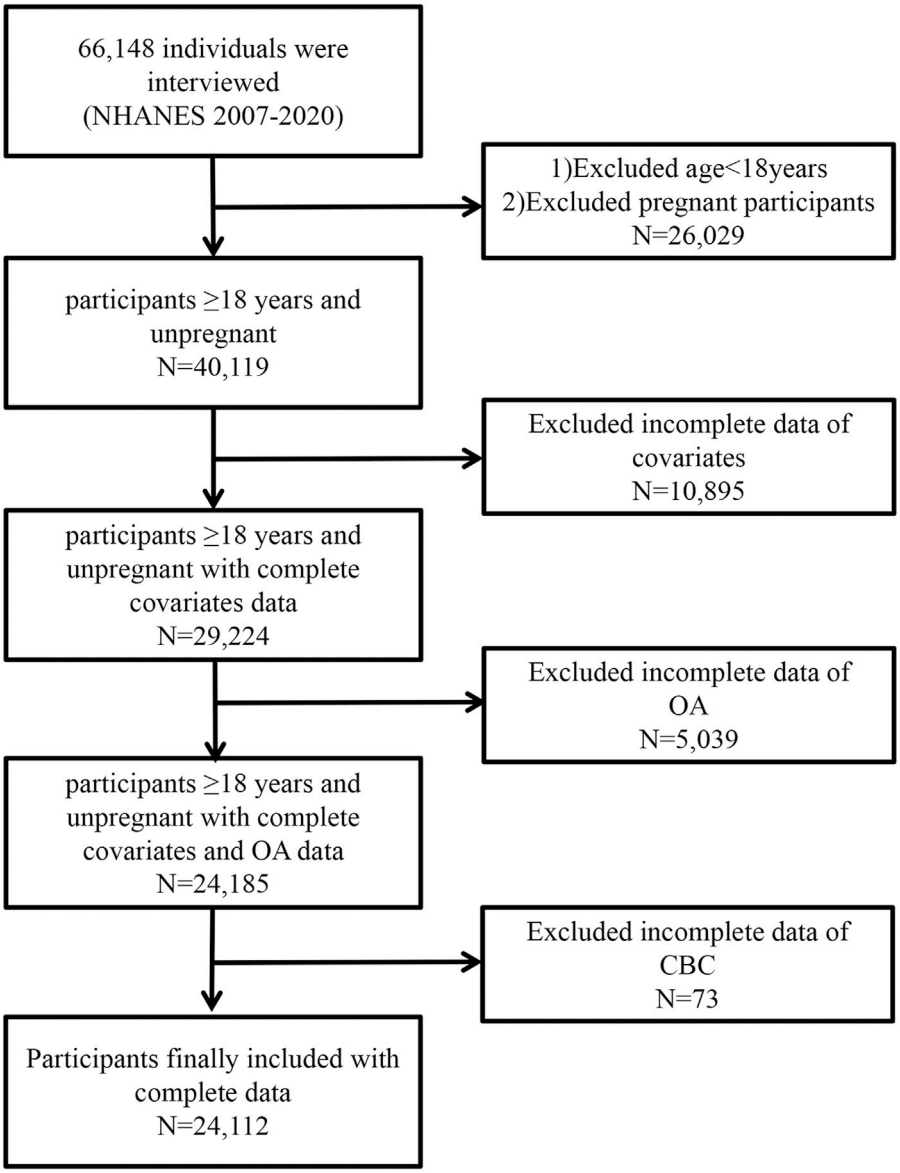

FIGURE 1
Flow diagram of the selection of eligible participants.

Statistical analysis

Weighted analyses were conducted in accordance with NHANES guidelines due to the complex sample survey. To examine baseline differences between normal and OA groups, a weighted chi-square test (categoric variables) and the weighted Wilcoxon Rank Sum Test (continuous variables) were employed. The association between CBC-derived inflammatory indicators and the OA prevalence was examined using weighted multivariate logistic regression: no variables were adjusted for in the crude model. Model 1 was adjusted for age, gender, race, marital status, and education level; Model 2 was adjusted for age, gender, race, marital status, education level, smoking status, drinking status, energy intake, BMI, diabetes, and hypertension; and Model 3 was adjusted for age, gender, race, marital status, education level, smoking status, drinking status, energy intake, BMI, diabetes, hypertension, albumin, creatinine, and calcium. CBC-derived inflammatory indicators were considered both continuous and categorical (trichotomies). To assess whether the logistic regression model was affected by multicollinearity, we examined pairwise correlations among the continuous variables included in the fully adjusted model

by constructing correlation matrices (Supplementary Figure S1). In addition, we calculated the variance inflation factor (VIF) for all variables in the fully adjusted model, as shown in Supplementary Table S1.

To explore nonlinear associations, our study also uses restricted cubic splines (RCS). We evaluated spline specifications with 3, 4, and 5 knots and selected the 3-knot structure based on the lowest Akaike Information Criterion (AIC) together with model parsimony. The AIC values for the fully adjusted models under the 3-, 4-, and 5-knot specifications are provided in Supplementary Table S2. The log-likelihood ratio test was used to compare two-segment linear regression models (segmented regression models) with a single linear model (nonsegmented model) for indicators with nonlinear relationships. Threshold effects were then computed. The association between CBC-derived inflammatory indicators and OA across subgroups was subsequently investigated using subgroup analysis. Age, gender, race, marital status, education level, diabetes, and hypertension were among the stratification variables. Then, sensitivity analyses were conducted to evaluate the reliability of our studies. To reconfirm the correlation between CBC inflammatory indicators and OA prevalence and eliminate the influence of confounding factors, we performed multiple imputation for missing data using the mice package in R. We applied the default settings of the defaultMethod parameter, which imputes continuous variables, binary variables, unordered categorical variables, and ordered categorical variables using the package's corresponding default methods. Density plots comparing the distributions of observed and imputed values are provided in Supplementary Figure S2.

Subsequently, a predictive model was constructed and validated. First, variables were screened and regressed using LASSO regression, and the optimal lambda was selected via cross-validation to determine the best prediction model. The risk prediction model was visually represented as a nomogram that quantifies the overall likelihood of developing OA by assigning weighted scores to various factors based on their risk contributions. To construct the nomogram, the VIFs for each predictor (Supplementary Table S3) were also computed to assess potential multicollinearity further. Finally, the specificity and sensitivity of the model were evaluated by ROC curve analysis and the corresponding AUC. Internal validation was also performed using the bootstrap resampling method, with 1,000 bootstrap samples generated to estimate the model's accuracy and stability. In addition, decision curve analysis and calibration curves were performed to evaluate the model's clinical utility and the accuracy of its predicted probability.

All analyses were conducted using R software (version 4.4.2), and a two-sided P value <0.05 was considered statistically significant. Moreover, we completed this checklist (Supplementary Material) in accordance with the STROBE statement to ensure completeness of reporting of our cross-sectional study.

Results

Baseline characteristics of the study population

The present data set included 24,112 participants (23.8% were older than 60 years, and 50.2% were male), of whom 3,195 had OA, yielding a weighted prevalence of 14.28%. The median values of CBC-derived inflammatory indicators [Q1, Q3] were calculated as follows: SII 462.68 [336.54, 640.64], SIRI 1.04 [0.73, 1.50], MLR 0.26 [0.21, 0.33], NMLR 2.22 [1.73, 2.87], NLR 1.95 [1.50, 2.55], dNLR 0.84 [0.80, 0.87]. CBC-derived inflammatory indicators (except dNLR) were significantly increased in OA patients compared with non-OA patients ($p < 0.001$). The body mass index (BMI) and age of OA patients were considerably greater than those of the non-OA group. Additionally, there were substantially more women in the OA group than in the non-OA group. Baseline characteristics such as race, marital status, education level, smoking and drinking status, diabetes, hypertension, energy intake, and albumin showed significant statistical differences among different OA statuses (Table 1).

Association between CBC-derived inflammatory indicators and OA

Multivariate logistic regression analysis showed (Table 2) that after full adjustment for covariates in model 3, the five inflammatory indicators SII, SIRI, MLR, NMLR, and NLR were all positively associated with OA, with the following odds ratio (OR) values: SII: OR = 1.000, 95% CI: 1.000–1.000; SIRI: OR = 1.068, 95% CI: 1.107–1.121; MLR: OR = 1.703, 95% CI: 1.161–2.499; NMLR: OR = 1.064, 95% CI: 1.022–1.108; NLR: OR = 1.066, 95% CI: 1.021–1.114. However, no significant association was found between dNLR and OA. Then, we divided the continuous inflammatory indicators into three groups. Participants in the highest tertile of MLR and SIRI had a considerably higher likelihood of having OA than those in the lowest tertile, indicating a strong positive association, according to the fully adjusted model. No positive association was found between the remaining inflammatory indicators in the other tertile models (T2-T3) and the lowest tertile (T1), suggesting that there may be nonlinear associations between these three CBC-derived inflammatory indicators and OA prevalence. We then performed RCS analysis and threshold analysis to test the nonlinear association between these CBC-derived inflammatory indices and OA prevalence.

Nonlinear relationship between CBC-derived inflammatory indicators and OA

As shown in Figure 2, we ultilized three nodes (10th, 50th, and 90th) and drew the RCS curve with the median as the

TABLE 1 Baseline characteristics of participants according to osteoarthritis.

Characteristic	Overall	Osteoarthritis		p-value[a]
		No	Yes	
Unweighted number	24,122	20,927	3,195	
Weighted number	161,493,424	138,427,174	23,066,250	
Demographic data				
Age,mean (SD)	46.08 (16.77)	43.44 (15.87)	61.92 (12.78)	<0.001
Age,%				<0.001
<60 years	76.2	82.4	38.9	
>60 years	23.8	17.6	61.1	
Gender,%				<0.001
Male	50.2	52.8	34.7	
Female	49.8	47.2	65.3	
Race,%				<0.001
Mexican American	8.8	9.8	2.6	
Non-hispanic white	67.6	64.9	83.3	
Non-hispanic black	9.9	10.6	6.0	
Other hispanic	6.0	6.6	2.8	
Other race	7.7	8.1	5.2	
Educational level,%				
Less than 9th grade	4.2	4.3	3.2	0.063
9–11th grade	9.4	9.5	8.3	
High school graduate/GED or equivalent	23	22.9	23.6	
Some college or AA degree	31.3	31.0	33.2	
College graduate or above	32.2	32.3	31.6	
Marital status,%				<0.001
Married/Living with partner	63.5	63.3	65.3	
Widowed/Divorced/Separated	16.6	14.6	28.2	
Never married	19.9	22.1	6.5	
Concurrent disease				
Diabetes,%				<0.001
Yes	10.4	8.9	19.6	
No	89.6	91.1	80.4	
Hypertension,%				<0.001
Yes	32.4	28.0	59.2	
No	67.6	72.0	40.8	

(Continued on following page)

TABLE 1 (*Continued*) Baseline characteristics of participants according to osteoarthritis.

Characteristic	Overall	Osteoarthritis		p-value[a]
		No	Yes	
Life behavior characteristics				
BMI, median [IQR]	27.77 [24.13, 32.30]	27.50 [23.96, 31.90]	29.49 [25.60, 34.10]	<0.001
Energy intake, median [IQR]	2034.00 [1,521.00, 2,692.00]	2061.00 [1,546.00, 2,730.04]	1854.72 [1,387.91, 2,419.98]	<0.001
Smoking status,%				<0.001
Never smoking	57.2	58.8	47.4	
Previous smoking	24.2	22.1	36.8	
Present smoking	18.7	19.2	15.8	
Drinking status,%				0.449
No	89.5	89.5	89.3	
Mild	5.9	6.0	89.3	
Intense	4.6	4.5	5.2	
Laboratory data				
Uric acid, median [IQR]	5.30 [4.40, 6.30]	5.30 [4.40, 6.30]	5.30 [4.40, 6.20]	0.842
Albumin, median [IQR]	43.00 [41.00, 45.00]	43.00 [41.00, 45.00]	42.00 [40.00, 44.00]	<0.001
Creatinine, median [IQR]	75.14 [63.65, 87.52]	75.14 [63.65, 87.52]	74.26 [63.65, 88.40]	0.111
Calcium, median [IQR]	2.35 [2.30, 2.40]	2.35 [2.30, 2.40]	2.35 [2.28, 2.40]	0.485
Neutrophil count, median [IQR]	4.00 [3.10, 5.10]	4.00 [3.10, 5.10]	4.00 [3.20, 5.20]	0.002
Monocyte count, median [IQR]	0.50 [0.40, 0.70]	0.50 [0.40, 0.70]	0.60 [0.40, 0.70]	<0.001
Lymphocyte count, median [IQR]	2.00 [1.70, 2.50]	2.10 [1.70, 2.50]	1.90 [1.60, 2.40]	<0.001
White blood cell count, median [IQR]	6.90 [5.70, 8.30]	6.90 [5.70, 8.30]	6.90 [5.70, 8.40]	0.511
Platelet count, median [IQR]	237.00 [203.00, 279.00]	238.00 [204.00, 279.00]	233.00 [196.00, 277.00]	0.004
Inflammatory indicators				
NLR,median [IQR]	1.95 [1.50, 2.55]	1.93 [1.48, 2.51]	2.10 [1.59, 2.80]	<0.001
dNLR, median [IQR]	0.84 [0.80, 0.87]	0.84 [0.80, 0.87]	0.84 [0.80, 0.87]	0.087
MLR, median [IQR]	0.26 [0.21, 0.33]	0.26 [0.21, 0.33]	0.29 [0.23, 0.36]	<0.001
NMLR, median [IQR]	2.22 [1.73, 2.87]	2.20 [1.71, 2.81]	2.40 [1.84, 3.15]	<0.001
SIRI, median [IQR]	1.04 [0.73, 1.50]	1.02 [0.72, 1.47]	1.15 [0.82, 1.68]	<0.001
SII, median [IQR]	462.68 [336.54, 640.64]	458.18 [334.80, 633.32]	492.57 [349.96, 688.03]	<0.001
Monocyte count, median [IQR]	116.67 [93.16, 144.81]	116.11 [92.86, 144.00]	120.53 [95.26, 151.87]	<0.001

[a]Wilcoxon rank-sum teat for complex survey samples; chi-squared test with Rao & Scott's second-order correction.
BMI, body mass index; SII, Systemic Immune - Inflammation Index; SIRI, Systemic Inflammation Response Index; MLR, Monocyte - to - Lymphocyte Ratio; NMLR, (Neutrophil + Monocyte) - to - Lymphocyte Ratio; NLR, Neutrophil - to - Lymphocyte Ratio; dNLR, Derived Neutrophil - to - Lymphocyte Ratio; PLR, Platelet - to - Lymphocyte Ratio.

reference value The RCS image showed that, except for dNLR, there was a significant overall trend between the other CBC-derived inflammatory indicators and the prevalence of OA (p for overall <0.05), among which SII, NLR, and NMLR showed significant nonlinear associations (p for nonlinear <0.05). Consistent with the results of the weighted logistic regression analysis, MLR and SIRI showed significant linear associations (p for nonlinear >0.05).

It is worth noting that when we performed threshold analysis of the five CBC-derived inflammatory indicators associated with

OA prevalence (Table 3), the nonlinear association pattern of SII differed from those of NLR and NMLR. Specifically, the dose-response pattern between SII and the prevalence of OA was "U"-shaped, while the dose-response pattern between NLR and NMLR and the prevalence of OA was "J"-shaped, and the log-likelihood ratio test $p < 0.05$. For SII, the estimated threshold was 402.857. When SII exceeded this level, OA prevalence increased significantly, whereas values below the threshold showed a decreasing trend. Similarly, a threshold of 2.522 was identified for NLR. Below this threshold, the association between NLR and OA was not statistically significant, whereas above it the risk of OA increased markedly, with an adjusted OR of 1.093 (1.047–1.141) per unit increase. NMLR also showed a comparable J-shaped pattern, with a threshold of 1.538. Beyond this threshold, the risk of OA rose significantly, with an adjusted OR of 1.070 (1.036–1.104).

In the threshold analysis, the log-likelihood ratio test of the two-segment linear regression model of MLR and SIRI was $p > 0.05$, which once again verified the strong positive association between MLR and SIRI and the prevalence of OA.

Subgroup and sensitivity analyses between CBC-derived inflammatory indicators and OA

In certain categories, there was inconsistent evidence of a correlation between elevated CBC-derived inflammatory indicators and OA incidence (Figure 3). The findings demonstrated that most subgroups did not exhibit a substantially distinct association between CBC-derived inflammatory indicators and OA incidence, and all interaction p-values were greater than 0.05. However, we found that increased MLR and NMLR were associated with increased OA prevalence in non-diabetic and non-hypertensive populations after adjusting for all covariates, but not in diabetic and hypertensive populations.

To test the robustness of the study results, we performed sensitivity analyses (Table 4). Multiple imputation was performed for variables with missing values. Then, the association between CBC-derived inflammatory indicators and OA prevalence was repeatedly verified in 10 imputed complete data sets. The impact of missing data on the results was somewhat mitigated by the consistent association between OA prevalence and CBC-derived inflammatory indicators throughout the 10 imputed data sets.

Establishment of OA prediction model

A total of 25 potential predictor variables, identified from the literature and clinical experience, were incorporated into the LASSO regression analysis. After 10-fold cross-validation, we obtained the minimum lambda value ($\lambda_{min} = 0.000392$) and the lambda value under 1 standard error ($\lambda_{1se} = 0.010160$). To simplify the prediction model as much as possible, we selected λ_{1se} as the optimal penalty parameter. According to the minimum criterion of non-zero coefficients, 12 variables were ultimately retained (Figure 4). These 12 variables included sex, education level, marital status, diabetes, hypertension, smoking status, BMI, daily energy intake, albumin, platelet count, MLR, and NMLR. Results from the univariable and multivariable logistic regression analyses indicated that all osteoarthritis-related risk factors were statistically significant ($p < 0.05$). Detailed regression results are provided in Supplementary Table S4.

Subsequently, considering the feasibility of data collection in primary healthcare settings, we excluded albumin, daily energy intake, and smoking status, as these factors are not routinely accessible through standard physical examinations, brief patient interviews, or complete blood count testing. To protect patient privacy, we also removed education level and marital status.

To provide doctors with a simple, understandable, and easy-to-use visual scoring tool, seven predictors—sex, diabetes, hypertension, BMI, platelet count, MLR, and NMLR—were selected and incorporated into the final nomogram (Figure 5). In this nomogram, each predictor is assigned a corresponding number of points, reflecting its relative contribution to OA risk. The total score obtained by summing these points provides an overall risk estimate, from which the probability of OA can be directly calculated.

To evaluate the predictive performance of the CBC-derived inflammatory indicators model and the OA prediction model, the respective receiver operating characteristic (ROC), decision curve (DCA), and calibration curves were plotted (Figure 6). The AUC of the whole prediction model was 0.735 (95% CI: 0.726–0.744), with a sensitivity of 73.4% and a specificity of 67.5%. The AUCs of MLR and NMLR were 0.580 (95% CI: 0.569–0.591) and 0.565 (95% CI: 0.554–0.576), respectively. To further evaluate the model's robustness, we performed internal validation using bootstrap resampling. After 1,000 resamplings, the model showed an accuracy of 0.867 and a kappa of 0.317, indicating good accuracy and moderate agreement. We also generated ROC curves based on the bootstrap samples (Supplementary Figure S3), which illustrate both the model's predictive performance and the stability of the internal validation results. Additionally, the DCA curve demonstrated that the model's net benefit outperformed the "all-cure" and "no-cure" approaches across a broad range of threshold probabilities and had substantial clinical relevance. Although the calibration curve was somewhat below the optimal value at high risks, it was frequently around the reference line, particularly with the best match at low and medium risks.

Discussion

Utilizing data from the National Health and Nutrition Examination Survey (NHANES) from 2007 to 2020, the

TABLE 2 Weighted multivariable logistic regression analyses for inflammatory indicators and osteoarthritis.

Index	Characteristic	Crude model[a]		Model 1[b]		Model 2[c]		Model 3[d]	
		OR (95% CI)	P value	OR (95% CI)	P value	OR (95% CI)	P value	OR (95% CI)	P value
NLR	Continuous	1.190 (1.144, 1.237)	<0.001***	1.095 (1.053, 1.138)	<0.001***	1.069 (1.024, 1.116)	0.003**	1.066 (1.021, 1.114)	0.004**
	Tertile 1 (1.29 [<1.64])	Reference		Reference		Reference		Reference	
	Tertile 2 (1.95 [1.64–2.32])	1.202 (1.066, 1.354)	0.003**	1.115 (0.995, 1.250)	0.060	1.052 (0.937, 1.181)	0.389	1.046 (0.932, 1.174)	0.437
	Tertile 3 (2.93 [>2.32])	1.641 (1.446, 1.861)	<0.001***	1.274 (1.101, 1.475)	0.001**	1.146 (0.983, 1.336)	0.081	1.136 (0.975, 1.324)	0.100
	p for trend		<0.001***		0.002**		0.082		0.100
dNLR	Continuous	0.622 (0.272, 1.425)	0.259	1.172 (0.463, 2.965)	0.735	0.694 (0.259, 1.864)	0.465	0.643 (0.243, 1.703)	0.369
	Tertile 1 (0.78 [<0.82])	Reference		Reference		Reference		Reference	
	Tertile 2 (0.84 [0.82–0.86])	0.908 (0.806, 1.022)	0.107	0.911 (0.794, 1.045)	0.180	0.877 (0.761, 1.011)	0.070	0.873 (0.757, 1.006)	0.061
	Tertile 3 (0.88 [>0.86])	0.896 (0.800, 1.004)	0.058	0.962 (0.847, 1.093)	0.549	0.891 (0.781, 1.018)	0.088	0.884 (0.775, 1.008)	0.065
	p for trend		0.050		0.478		0.076		0.056
MLR	Continuous	5.777 (3.819, 8.740)	<0.001***	1.797 (1.261, 2.560)	0.001**	1.697 (1.150, 2.504)	0.008**	1.703 (1.161, 2.499)	0.007**
	Tertile 1 (0.18 [<0.23])	Reference		Reference		Reference		Reference	
	Tertile 2 (0.26 [0.23–0.31])	1.406 (1.231, 1.605)	<0.001***	1.265 (1.086, 1.474)	0.003**	1.284 (1.094, 1.506)	0.003**	1.295 (1.105, 1.517)	0.002**
	Tertile 3 (0.38 [>0.31])	1.897 (1.664, 2.162)	<0.001***	1.340 (1.164, 1.542)	<0.001***	1.350 (1.161, 1.568)	<0.001***	1.353 (1.167, 1.569)	<0.001***
	p for trend		<0.001***		<0.001***		<0.001***		<0.001***
NMLR	Continuous	1.186 (1.142, 1.231)	<0.001***	1.090 (1.051, 1.130)	<0.001***	1.066 (1.024, 1.109)	0.002**	1.064 (1.022, 1.108)	0.003**
	Tertile 1 (1.51 [<1.89])	Reference		Reference		Reference		Reference	
	Tertile 2 (2.22 [1.89–2.61])	1.188 (1.060, 1.331)	0.003**	1.107 (0.994, 1.232)	0.064	1.045 (0.938, 1.164)	0.421	1.039 (0.933, 1.158)	0.479
	Tertile 3 (3.26 [>2.61])	1.677 (1.484, 1.895)	<0.001***	1.278 (1.112, 1.467)	<0.001***	1.154 (0.999, 1.332)	0.052	1.145 (0.993, 1.321)	0.061
	p for trend		<0.001***		<0.001***		0.051		0.059
SII	Continuous	1.000 (1.000, 1.001)	<0.001***	1.000 (1.000, 1.000)	<0.001***	1.000 (1.000, 1.000)	0.031**	1.000 (1.000, 1.000)	0.038**
	Tertile 1 (289.25 [<375.66])	Reference		Reference		Reference		Reference	
	Tertile 2 (469.93 [375.66–573.00])	1.130 (1.011, 1.262)	0.031**	1.006 (0.893, 1.134)	0.916	0.933 (0.820, 1.061)	0.284	0.928 (0.816, 1.056)	0.252
	Tertile 3 (766.11 [>573.00])	1.386 (1.249, 1.538)	<0.001***	1.165 (1.035, 1.312)	0.012	1.013 (0.891, 1.152)	0.844	0.999 (0.880, 1.135)	0.991
	p for trend		<0.001***		0.007**		0.626		0.782

(Continued on following page)

TABLE 2 (*Continued*) Weighted multivariable logistic regression analyses for inflammatory indicators and osteoarthritis.

Index	Characteristic	Crude model[a]		Model 1[b]		Model 2[c]		Model 3[d]	
		OR (95% CI)	P value	OR (95% CI)	P value	OR (95% CI)	P value	OR (95% CI)	P value
SIRI	Continuous	1.242 (1.187, 1.300)	<0.001***	1.139 (1.091, 1.189)	<0.001***	1.068 (1.018, 1.120)	0.007**	1.068 (1.017, 1.121)	0.009**
	Tertile 1 (0.60 [<0.83])	Reference		Reference		Reference		Reference	
	Tertile 2 (1.04 [0.83–1.31])	1.403 (1.243, 1.584)	<0.001***	1.296 (1.130, 1.486)	<0.001***	1.171 (1.018, 1.347)	0.027**	1.164 (1.011, 1.341)	0.035**
	Tertile 3 (1.80 [>1.31])	1.713 (1.526, 1.922)	<0.001***	1.398 (1.227, 1.592)	<0.001***	1.164 (1.016, 1.334)	0.029**	1.156 (1.010, 1.323)	0.036**
	p for trend		<0.001***		<0.001***		0.076		0.089

[a]No variables were adjusted for the crude model.
[b]Model 1 was adjusted for age, gender, race, marital status, and education level.
[c]Model 2 was adjusted for age, gender, race, marital status, education level, smoking status, drinking status, energy intake, BMI, diabetes, and hypertension.
[d]Model 3 was adjusted for age, gender, race, marital status, education level, smoking status, drinking status, energy intake, BMI, diabetes, hypertension, urine acid, urine creatinine, albumin, and calcium.

current study investigated the association between the prevalence of OA in Americans and CBC-derived inflammatory indicators. 3,195 (13.25%) of the 24,112 individuals in the final sample had an OA diagnosis. Weighted multivariate logistic regression models found that increased OA incidence was associated with increased levels of SII, SIRI, MLR, NMLR, and NLR. The crude model and the modified models 1, 2, and 3 all showed this connection to be consistent. Stratifying CBC-derived inflammatory indicators into tertiles, we found a strong linear association between SIRI and MLR and the prevalence of OA. This strong linear association was further confirmed by RCS and threshold analyses, which also revealed potential nonlinear associations between SII, NMLR, and NLR and OA prevalence. Subgroup analyses and interaction tests showed stratification by diabetes status and hypertension.

SIRI and MLR are comprehensive indicators closely related to systemic inflammation and the immune response. These ratios have been widely studied in various inflammatory-related diseases, including psoriasis, cardiovascular disease, and cancer [23–25]. In a previous study, He et al. found that the risk of OA increased by 15% for each unit increase in log 2 (SIRI). However, in a sensitivity analysis that changed log 2 (SIRI) from a continuous variable to a categorical variable (quartiles), no positive correlation was found between the other quartile models (Q2-Q4) and the lowest quartile (Q1) [17]. In contrast, Yan et al. demonstrated that SIRI was significantly positively correlated with OA. In all adjusted models, the prevalence of OA gradually increased with increasing SIRI, especially in Q3 and Q4 [26]. In the present study, we found a strong linear association between MLR (OR = 1.35 [1.17, 1.57] T3 vs. T1; OR = 1.30 [1.11, 1.52] T2 vs. T1) and SIRI (OR = 1.16 [1.01, 1.52] T3 vs. T1; OR = 1.16 [1.01, 1.34] T2 vs. T1) and the prevalence of OA, supporting their findings.

Our study also explored the association between OA and other inflammatory indices, SII, NLR, and NMLR. Although the logistic regression model with SII, NLR, and NMLR as continuous variables showed a significant association between higher levels of these indices and increased OA prevalence, we found no significant association between the other tertiles (T2–T3) and the lowest tertile (T1) after transforming them into tertiles. Therefore, we inferred that there might be nonlinear associations between SII, NLR, and NMLR and OA prevalence. The subsequent RCS models confirmed this nonlinear pattern, and the threshold analysis further identified their risk thresholds.

These risk thresholds are not intended to serve as diagnostic cut-off values. Instead, they offer practical reference points for understanding how inflammatory indicators, even within the range observed in healthy adults, may indicate varying risk trends. The 95% reference interval for SII reported by Liu et al. is 162–811 [27], and the risk threshold identified in this study (SII = 402.857) falls within this range for healthy populations. Clinically, this may prompt physicians to exercise greater vigilance in identifying patients in subclinical or early stages of OA. When an individual's SII level deviates significantly from the lowest-risk point, clinicians may consider more cautious evaluations, such as follow-up or imaging assessments, even if the value remains within the normal range. NLR has been extensively studied in cardiovascular diseases, infections, inflammatory disorders, and various cancers. The NLR threshold (2.522) identified in our study for OA risk also lies within the established normal range of 0.78–3.53 [28]. When a patient's NLR exceeds this threshold, clinicians may be prompted to pay closer attention to subtle joint symptoms, medical history, obesity, and other OA-related risk factors, enabling earlier intervention when appropriate. As for NMLR, a relatively novel inflammatory indicator, its reference interval has yet to be determined.

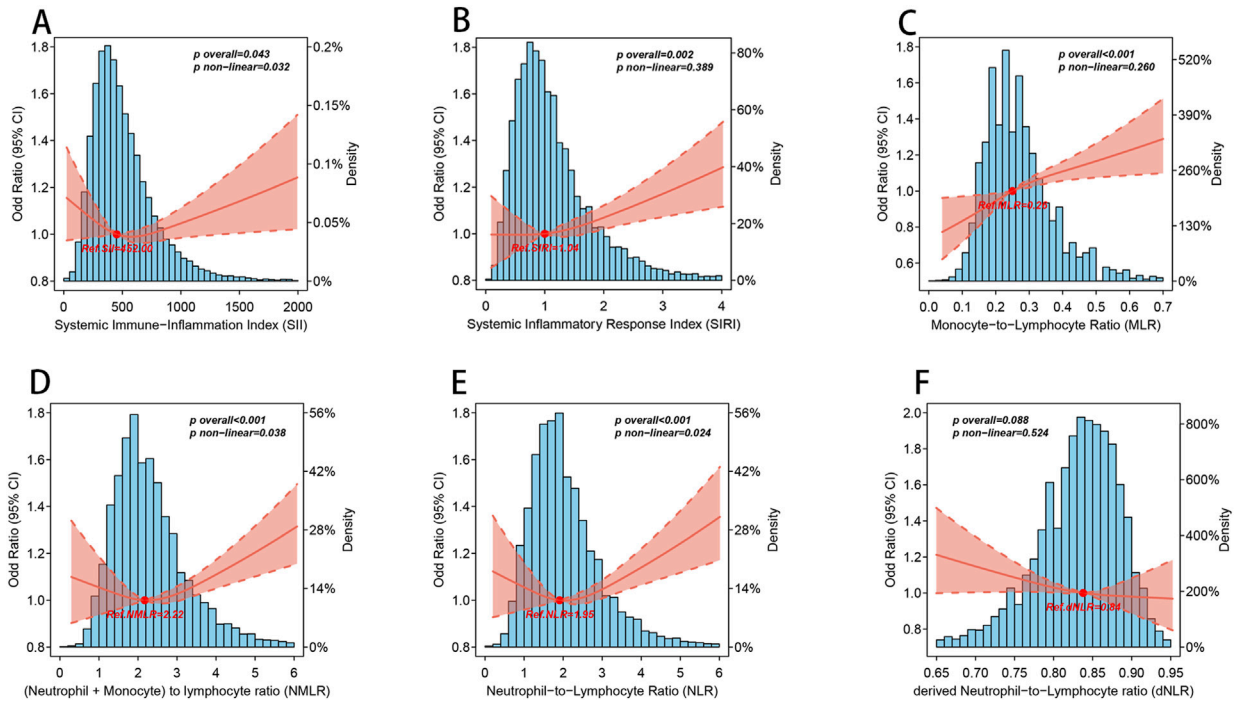

FIGURE 2
The nonlinear association between CBC-derived inflammatory indicators and OA. Blue histogram bars represent probability density estimates. Solid rad line represents the smooth curve fit between CBC-derived inflammatory indicators and OA. Pale red bands between dashed lines represent the 95% of confidence interval from the fit. The above models were adjusted for age, gender, race, marital status, education level, smoking status, drinking status, energy intake, BMI, diabetes, hypertension, urine acid, urine creatinine, albumin, and calcium. **(A)** SII and OA; **(B)** SIRI and OA; **(C)** MLR and OA; **(D)** NMLR and OA; **(E)** NLR and OA; **(F)** dNLR and OA.

TABLE 3 Analysis of the threshold effect between inflammatory indicators and osteoarthritis.

Outcome:OA	NLR	MLR	NMLR	SII	SIRI
	OR (95%CI)	OR (95%CI)	OR (95%CI)	OR (95%CI)	OR (95%CI)
Fitting by standard linear model					
OR	1.058 (1.024–1.093)	1.930 (1.407–2.639)	1.057 (1.026–1.09)	1.000 (1.000–1.000)	1.079 (1.032–1.127)
P-value	0.001	<0.001	<0.001	0.053	0.001
Fitting by two-piecewise linear model					
Breakpoint(K)	2.522	0.143	1.538	402.857	0.632
OR1 < K	0.968 (0.891–1.052)	0.017 (0.000–4.789)	0.777 (0.586–1.038)	0.999 (0.999–1.000)	0.656 (0.385–1.131)
	0.447	0.144	0.084	0.019	0.126
OR2 > K	1.093 (1.047–1.141)	2.042 (1.48–2.811)	1.07 (1.036–1.104)	1.000 (1.000–1.000)	1.092 (1.043–1.143)
	<0.001	<0.001	<0.001	0.012	<0.001
Logarithmic likelihood ratio test P-value	0.023	0.098	0.036	0.008	0.072

Age, gender, race, marital status, education level, smoking status, drinking status, energy intake, BMI, diabetes, hypertension, urine acid, urine creatinine, albumin,and calcium were adjusted.

Nevertheless, we hypothesize that its risk pattern may resemble that of NLR. In summary, these risk thresholds can assist clinicians in understanding how different levels of inflammatory indicators correspond to changes in OA risk among otherwise healthy individuals, thereby supporting earlier identification and timely clinical management.

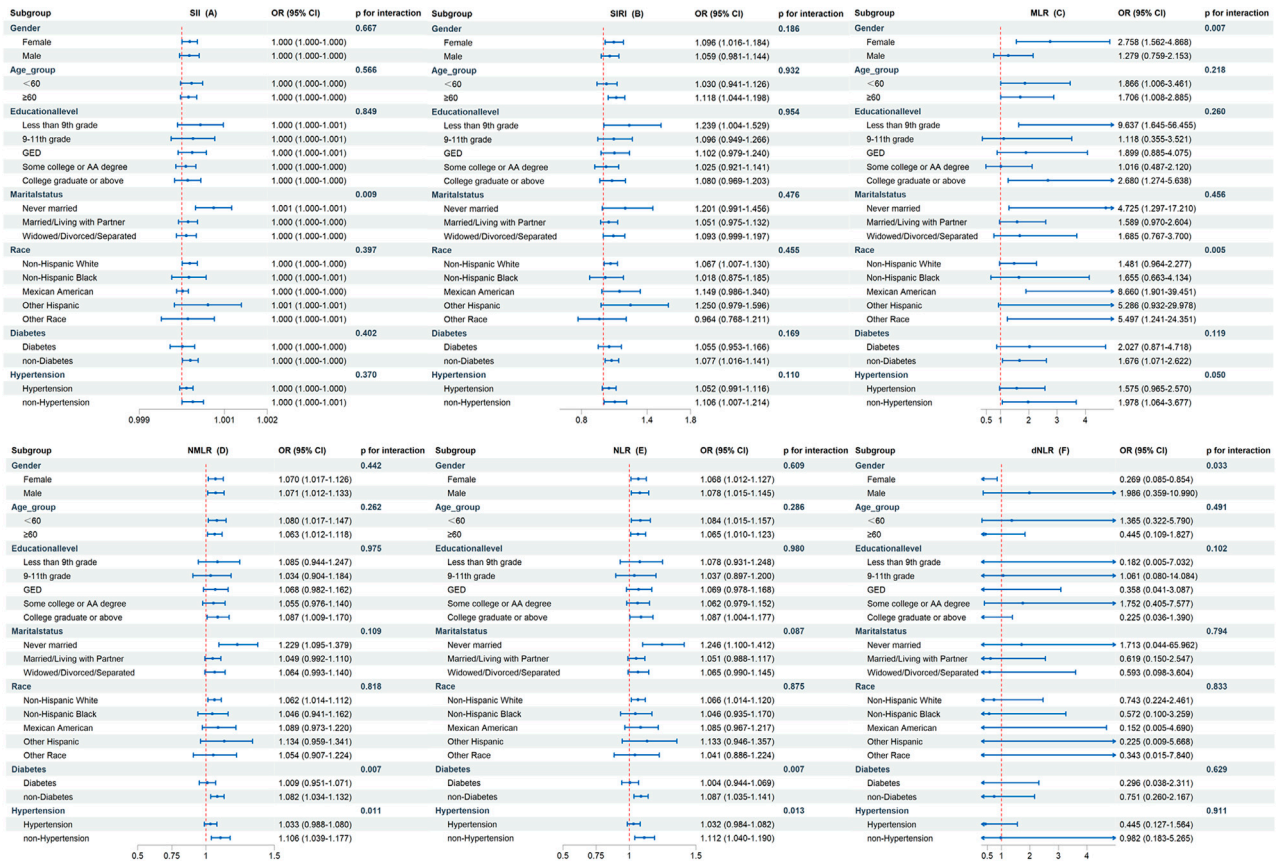

FIGURE 3
Subgroup analysis of the association between CBC-derived inflammatory indicators and OA prevalence. The above models were adjusted for age, gender, race, marital status, education level, smoking status, drinking status, energy intake, BMI, diabetes, hypertension, urine acid, urine creatinine, albumin, and calcium. In each case, the models were not adjusted for stratification variables. **(A)** SII and OA; **(B)** SIRI and OA; **(C)** MLR and OA; **(D)** NMLR and OA; **(E)** NLR and OA; **(F)** dNLR and OA.

For the first time, we studied the association between NMLR and dNLR and OA prevalence. NMLR and dNLR are considered novel indicators of cellular immune activation and have attracted the attention of many researchers [29, 30]. These two indices reflect interactions among neutrophils, monocytes/macrophages, and lymphocytes. They may offer fresh perspectives on the intricate association between inflammatory processes and osteoarthritis. In this study, both the continuous and tertile models showed that the association between dNLR and OA was not statistically significant.

Subgroup analyses revealed a consistent pattern that higher MLR/NMLR levels were significantly associated with increased OA risk among individuals without diabetes or hypertension. In contrast, this association did not reach statistical significance among those with either condition. One possible explanation is that, in individuals with diabetes or hypertension, systemic inflammation may contribute to OA development primarily through these comorbidities rather than acting independently. Insulin resistance—a common feature of both diabetes and hypertension—has recently been recognized as a key risk factor underlying these disorders [31]. Under systemic inflammatory conditions, elevated cytokine production by circulating immune cells can impair insulin signaling through multiple intermediate pathways [32]. For example, tumor necrosis factor-α (TNF-α) activates the IKKβ, SOCS1/3, PKC, and ERK pathways, leading to serine phosphorylation of insulin receptor substrates (IRS) in insulin-responsive tissues. These pathways suppress Akt activity, a critical mediator of the insulin signaling cascade [33–35]. The resulting impairment of insulin signaling may further amplify systemic inflammation and contribute to OA pathogenesis among individuals with diabetes or hypertension. Consequently, the independent associations between these inflammatory indices and OA risk may be attenuated in these subgroups.

Our findings show that MLR, SIRI, and the threshold-based increases in NLR, MLR, and NMLR are positively associated with OA risk. These composite inflammatory indices integrate circulating counts of platelets, neutrophils, monocytes, and

TABLE 4 Weighted multivariable logistic regression analyses for inflammatory indicators and osteoarthritis after multiple imputation.

Index	Characteristic	Crude model[a]		Model 1[b]		Model 2[c]		Model 3[d]	
		OR (95% CI)	P value	OR (95% CI)	P value	OR (95% CI)	P value	OR (95% CI)	P value
NLR	Continuous	1.190 (1.156, 1.225)	<0.001***	1.082 (1.050, 1.116)	<0.001***	1.058 (1.024, 1.093)	<0.001***	1.060 (1.026, 1.095)	<0.001***
	Tertile 1 (1.32 [<1.65])	Reference		Reference		Reference		Reference	
	Tertile 2 (1.95 [1.65–2.32])	1.188 (1.092, 1.292)	<0.001***	1.078 (0.992, 1.171)	0.076	1.014 (0.930, 1.105)	0.755	1.014 (0.930, 1.105)	0.752
	Tertile 3 (2.91 [>2.32])	1.660 (1.511, 1.823)	<0.001***	1.268 (1.141, 1.410)	0.001**	1.129 (1.011, 1.260)	0.031*	1.131 (1.013, 1.264)	0.029*
	p for trend		<0.001***		<0.001***		0.023*		0.021*
dNLR	Continuous	0.818 (0.465, 1.438)	0.483	1.559 (0.806, 3.013)	0.185	0.944 (0.469, 1.900)	0.870	0.907 (0.452, 1.818)	0.781
	Tertile 1 (0.78 [<0.82])	Reference		Reference		Reference		Reference	
	Tertile 2 (0.84 [0.82–0.86])	0.990 (0.910, 1.078)	0.820	1.011 (0.915, 1.117)	0.825	0.979 (0.884, 1.084)	0.676	0.976 (0.881, 1.082)	0.644
	Tertile 3 (0.88 [>0.86])	0.932 (0.857, 1.013)	0.097	1.018 (0.924, 1.121)	0.721	0.946 (0.857, 1.044)	0.264	0.941 (0.852, 1.038)	0.223
	p for trend		0.113		0.721		0.278		0.236
MLR	Continuous	5.920 (4.452, 7.872)	<0.001***	1.655 (1.248, 2.194)	<0.001***	1.611 (1.192, 2.177)	0.002**	1.677 (1.241, 2.267)	<0.001***
	Tertile 1 (0.18 [<0.22])	Reference		Reference		Reference		Reference	
	Tertile 2 (0.26 [0.22–0.30])	1.296 (1.163, 1.444)	<0.001***	1.133 (1.011, 1.271)	0.032*	1.147 (1.021, 1.290)	0.022*	1.153 (1.027, 1.295)	0.017*
	Tertile 3 (0.38 [>0.30])	1.832 (1.679, 1.999)	<0.001***	1.235 (1.123, 1.357)	<0.001***	1.247 (1.130, 1.378)	<0.001***	1.257 (1.139, 1.388)	<0.001***
	p for trend		<0.001***		<0.001***		<0.001***		<0.001***
NMLR	Continuous	1.187 (1.155, 1.221)	<0.001***	1.078 (1.048, 1.109)	<0.001***	1.056 (1.024, 1.088)	<0.001***	1.058 (1.027, 1.091)	<0.001***
	Tertile 1 (1.53 [<1.90])	Reference		Reference		Reference		Reference	
	Tertile 2 (2.22 [1.90–2.60])	1.187 (1.091, 1.291)	<0.001***	1.077 (0.990, 1.171)	0.083	1.024 (0.937, 1.119)	0.599	1.025 (0.938, 1.119)	0.585
	Tertile 3 (3.25 [>2.60])	1.695 (1.548, 1.857)	<0.001***	1.257 (1.136, 1.390)	<0.001***	1.130 (1.018, 1.255)	0.022*	1.134 (1.021, 1.259)	0.019*
	p for trend		<0.001***		<0.001***		0.018*		0.015*
SII	Continuous	1.000 (1.000, 1.000)	<0.001***	1.000 (1.000, 1.000)	0.001**	1.000 (1.000, 1.000)	0.188	1.000 (1.000, 1.000)	0.157
	Tertile 1 (289.25 [<380.16])	Reference		Reference		Reference		Reference	
	Tertile 2 (469.93 [380.16–585.57])	1.163 (1.064, 1.270)	<0.001***	1.063 (0.974, 1.160)	0.171	1.000 (0.914, 1.094)	0.995	0.999 (0.914, 1.093)	0.986
	Tertile 3 (766.11 [>585.57])	1.350 (1.238, 1.472)	<0.001***	1.149 (1.046, 1.262)	0.004**	1.004 (0.909, 1.109)	0.937	1.005 (0.911, 1.108)	0.927
	p for trend		<0.001***		0.005**		0.931		0.916

(Continued on following page)

TABLE 4 (*Continued*) Weighted multivariable logistic regression analyses for inflammatory indicators and osteoarthritis after multiple imputation.

Index	Characteristic	Crude model[a]		Model 1[b]		Model 2[c]		Model 3[d]	
		OR (95% CI)	P value	OR (95% CI)	P value	OR (95% CI)	P value	OR (95% CI)	P value
SIRI	Continuous	1.237 (1.196, 1.280)	<0.001***	1.117 (1.077, 1.159)	<0.001***	1.060 (1.019, 1.102)	0.004**	1.064 (1.022, 1.107)	0.003**
	Tertile 1 (0.65 [<0.83])	Reference		Reference		Reference		Reference	
	Tertile 2 (1.03 [0.83–1.31])	1.188 (1.092, 1.292)	<0.001***	1.078 (0.992, 1.171)	0.076	1.014 (0.930, 1.105)	0.755	1.014 (0.930, 1.105)	0.752
	Tertile 3 (1.68 [>1.31])	1.660 (1.511, 1.823)	<0.001***	1.268 (1.141, 1.410)	<0.001***	1.129 (1.011, 1.260)	0.031*	1.131 (1.013, 1.264)	0.029*
	p for trend		<0.001***		<0.001***		0.022*		0.020*

[a]No variables were adjusted for the crude model.
[b]Model 1 was adjusted for age, gender, race, marital status, and education level.
[c]Model 2 was adjusted for age, gender, race, marital status, education level, smoking status, drinking status, energy intake, BMI, diabetes, and hypertension.
[d]Model 3 was adjusted for age, gender, race, marital status, education level, smoking status, drinking status, energy intake, BMI, diabetes, hypertension, urine acid, urine creatinine, albumin, and calcium.

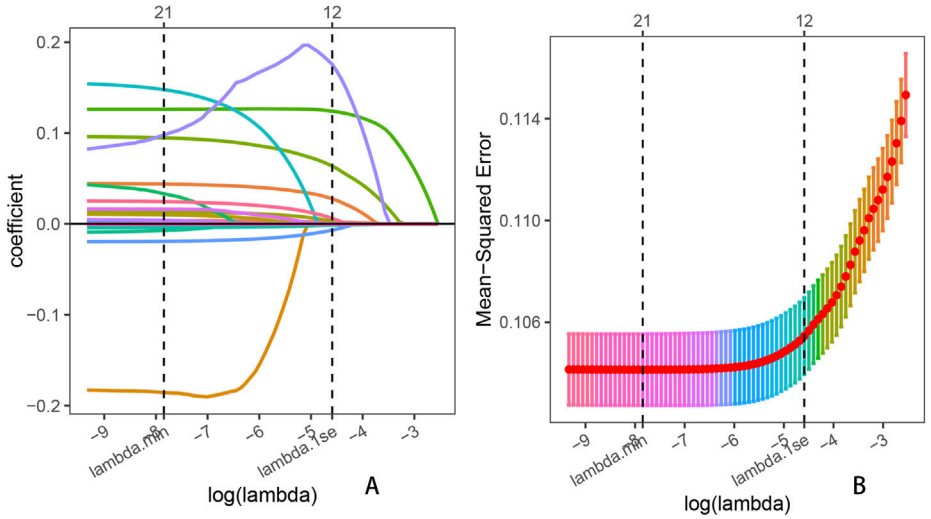

FIGURE 4
Lasso penalized regression analysis was used to identify key predictors of OA prevalence. **(A)** Coefficient shrinkage for all 25 variables, including age, sex, race, education level, marital status, diabetes, hypertension, BMI, smoking status, drinking status, daily energy intake, uric acid, albumin, total calcium, neutrophil count, lymphocyte count, leukocyte count, monocyte count, platelet count, NLR, dNLR, MLR, NMLR, SIRI, and SII; **(B)** Ten-fold cross-validation for the LASSO regression.

lymphocytes, collectively reflecting the overall level of systemic inflammation. Systemic inflammatory states associated with obesity, aging, or chronic diseases may promote local joint inflammation [36, 37]. Elevated systemic inflammation leads to increased recruitment of immune cells, including neutrophils and monocytes/macrophages, into the joint cavity [38, 39]. These infiltrating cells release large amounts of pro-inflammatory cytokines, such as IL-1β, IL-6, and TNF-α [8], thereby directly contributing to and amplifying intra-articular inflammation.

By activating the mitogen-activated protein kinase (MAPK) signaling pathway, IL-1β induces catabolic processes, including cartilage degradation, which are key mechanisms in OA progression [40]. IL-1β activates MAPK signaling, which upregulates catabolic enzymes, including MMP-1, MMP-3, MMP-13, ADAMTS-4, and ADAMTS-5. These enzymes then directly degrade components of the extracellular matrix. These processes lead to chondrocyte hypertrophy, dedifferentiation, and ultimately apoptosis [41]. Another major pathway in IL-

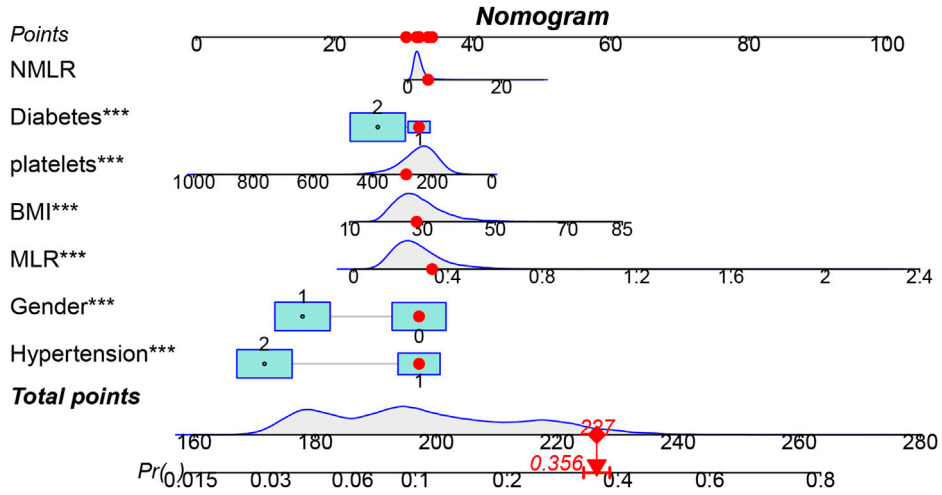

FIGURE 5
Visualization of OA prevalence risk model. The top horizontal line of the column bar is the score bar, and the sum of the scores is the risk of osteoarthritis. A total of 7 indicators were included in the risk prediction table.

1β–mediated OA progression is NF-κB. Once activated, NF-κB suppresses type II collagen synthesis and increases the production of matrix metalloproteinases, aggrecanases, and various chemokines—including IL-8, monocyte chemoattractant protein-1 (MCP-1/CCL2), CCL5, and macrophage inflammatory protein-1α (MIP-1α)—which further attract inflammatory cells and intensify joint inflammation [42].

An important finding of our study is that, compared with indices incorporating only monocytes/macrophages (MLR), those incorporating neutrophils (NLR, NMLR) showed clear nonlinear relationships and threshold effects. This pattern suggests that different immune cell populations may have distinct associations with OA risk. One possible explanation is that neutrophils may exert certain protective effects against cartilage damage under conditions of low-grade systemic inflammation [43]. Previous studies have shown that neutrophil-derived extracellular vesicles (EVs) can act in an anti-inflammatory manner [44] and protect cartilage by increasing type II collagen and reducing type X collagen within the joint. Further evidence indicates that neutrophil EVs enhance cartilage protection by inducing transforming growth factor-β (TGF-β) production, a key mediator of chondrocyte homeostasis. This process promotes the deposition of type II collagen (COL2) and glycosaminoglycans (GAGs), while downregulating cartilage-degrading enzymes (MMPs) [45].

We also observed a similar nonlinear pattern when comparing indices involving neutrophils and platelets (SII) with those involving neutrophils and monocytes/macrophages (SIRI). Platelet-rich plasma (PRP) has been shown to have beneficial effects in OA [46], yet the specific role of platelets and their underlying mechanisms remains incompletely understood. In rodent models of OA, platelet-derived ADP has been shown to increase bone morphogenetic protein 7 (BMP7) levels markedly. Through autocrine and paracrine actions, BMP7 promotes chondrocyte proliferation via the ERK/CDK1/cyclin B1 signaling pathway [47]. The protective effects of platelets on cartilage may help explain the inverse association observed between SII and OA risk below the identified threshold.

This study comprehensively explored the association between CBC-derived inflammatory indicators and OA prevalence. After observational analysis, we developed and validated a prediction model incorporating the CBC-derived inflammatory indicators and demonstrated its clinical utility. After LASSO regression analysis, we identified seven independent risk factors with the best predictive power for OA, including MLR and NMLR, and demonstrated their clinical utility. In addition, it should be clarified that the proposed model is particularly applicable to OA screening in primary healthcare settings, where access to advanced imaging modalities may be limited and CBC-derived inflammatory indicators are readily available.

The present research has several significant advantages. Firstly, to fully examine the association between exposure and outcomes, we have used large samples and long-term tracking data from NHANES. Secondly, there is little evidence from earlier research linking CBC-derived inflammatory indicators to OA. Novel quantitative associations between CBC-derived inflammatory indicators and the prevalence of OA among the United States general population are revealed in the present study. Finally, utilizing complete blood counts, one of the most widely used assays in clinical practice, we assessed the association between various inflammatory indicators and the prevalence of OA. These indicators, however, have not been thoroughly examined in earlier

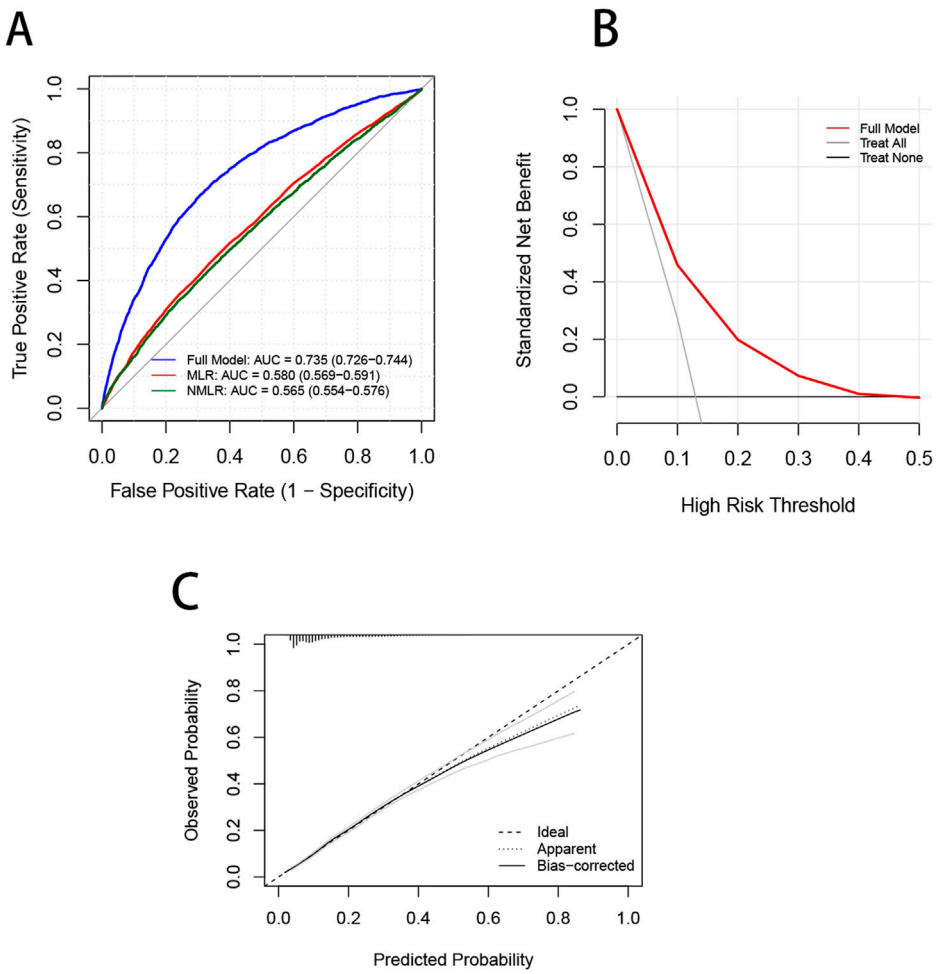

FIGURE 6
Validation of the OA prevalence risk model. **(A)** ROC curves are used to evaluate the ability of the Nomagram model and CBC inflammation-derived indicators to predict OA prevalence. **(B)** The red curve in the DCA curve represents the net benefit of the model, and the black lines represent the benefits of "no intervention" and "full intervention", respectively. **(C)** The dotted line in the calibration curve represents that the model's predicted probability is completely consistent with the actual observed probability, the dotted line reflects the model's prediction performance without bias correction, and the actual line represents the model's prediction performance after bias correction using bootstrap resampling.

research and are often examined as individual indicators. In the present study, we analyzed the indicators in greater detail and comprehensively examined their association with OA prevalence.

However, we must acknowledge some limitations of the present study. Firstly, we could not establish a causal association between CBC-derived inflammatory indicators and OA prevalence due to the cross-sectional design of NHANES. Future population-based prospective cohort studies should be conducted to verify the causal relationship between CBC-derived inflammatory indicators and OA and to clarify their influence on OA development and progression. Secondly, residual confounding persists even after we carefully account for several factors associated with the outcome. It is impossible to completely rule out the possibility that unmeasured variables might influence our findings, and residual confounding could introduce some bias. Thirdly, the NHANES statistics, which are representative of the United States population, served as the basis for the research population. It's possible that the results won't apply to groups with distinct healthcare or demographic systems. Additionally, the NHANES database lacks information on OA anatomical sites, longitudinal CBC data, and joint fluid biomarkers that reflect local inflammatory activity. Future studies could focus on addressing these data gaps to explore whether CBC-derived inflammatory indicators exhibit different associations across specific OA sites. Additionally, prospective cohort studies could be conducted, or investigations into the relationship between systemic inflammation and local intra-articular inflammation could

be pursued, providing deeper mechanistic insights into how systemic inflammation influences OA progression.

The reliance on self-reported OA diagnoses may introduce several types of information bias. Previous studies have shown that differences in survey methods, question wording, and sample composition can lead to variations of 2–3 percentage points in the prevalence of arthritis based on self-reports [48]. The agreement between large surveys can be as low as 70% [49, 50]. In this context, the self-reported OA prevalence in NHANES is also lower than that in other databases (such as CCS and NADW) that rely on ICD-9-CM diagnostic codes [51]. This suggests that self-reporting may lead to under-ascertainment and affect prevalence estimates. In addition, self-reports are influenced by the intermittent nature of OA symptoms. Individuals are more likely to recall and report a diagnosis when symptoms are pronounced or when they have recently sought medical care. This recall bias may either inflate or attenuate the observed associations between inflammatory indices and OA. Overall, recall bias in self-reported OA may weaken true associations. Therefore, our findings should be interpreted with caution, and future studies using imaging findings or clinical diagnoses are needed to improve the accuracy of outcome definitions.

Conclusion

In conclusion, in this nationally representative US sample, CBC-derived inflammatory indicators (SII, SIRI, MLR, NMLR, NLR) were significantly associated with OA prevalence. Further investigation revealed that NLR, NMLR, and SII were nonlinearly associated with OA prevalence. Our study reinforces the view that inflammation promotes the pathological process of OA. In addition, we constructed a prediction model for OA risk, emphasizing the predictive power of MLR and NMLR.

Author contributions

YW, LF, and XaH designed the study; XnH, XoH, YL, and YS contribute to data collection; ZY, TZ, RL, LC, MQ, and WC analyzed the data; ZY and TZ wrote the manuscript. All authors contributed to the article and approved the submitted version.

Data availability

The original contributions presented in the study are included in the article/Supplementary Material, further inquiries can be directed to the corresponding authors. Online repositories include the datasets used in this investigation. Publicly accessible datasets used in the present research are available here: https://www.cdc.gov/nchs/nhanes/.

Ethics statement

The studies involving humans were approved by National Center for Health Statistics. The studies were conducted in accordance with the local legislation and institutional requirements. The participants provided their written informed consent to participate in this study.

Funding

The author(s) declared that financial support was received for this work and/or its publication. This work was supported by Jilin Provincial Department of Education “Thirteenth Five-Year Plan” Science and Technology Project (JJKH20200458KJ), Jilin Province Health Science and Technology Capacity Improvement Project (2024A092), National Natural Science Foundation of China Youth Fund (grant number 82202662, 2022), the China Postdoctoral Science Foundation (grant number 2024T170380, 2024), the Natural Science Foundation of Guangdong Province of China (grant number 2024A1515012767, 2024) and the Guangzhou Science and Technology Planning Project (grant number 2023A04J2314, 2023).

Acknowledgements

The National Center for Environmental Health and all National Health and Nutrition Examination Survey participants and staff are greatly appreciated by the authors for their significant contributions.

Conflict of interest

The author(s) declared no potential conflicts of interest with respect to the research, authorship, and/or publication of this article.

Generative AI statement

The author(s) declared that generative AI was not used in the creation of this manuscript.

Any alternative text (alt text) provided alongside figures in this article has been generated by Frontiers with the support of artificial intelligence and reasonable efforts have been made to ensure accuracy, including review by the authors wherever possible. If you identify any issues, please contact us.

Supplementary material

The Supplementary Material for this article can be found online at: https://www.ebm-journal.org/articles/10.3389/ebm.2025.10815/full#supplementary-material

References

1. Glyn-Jones S, Palmer AJR, Agricola R, Price AJ, Vincent TL, Weinans H, et al. Osteoarthritis. *Lancet* (2015) **386**(9991):376–87. doi:10.1016/s0140-6736(14)60802-3

2. Hunter DJ, March L, Chew M. Osteoarthritis in 2020 and beyond: a *lancet* commission. Editorial material. *Lancet* (2020) **396**(10264):1711–2. doi:10.1016/s0140-6736(20)32230-3

3. Vina ER, Kwoh CK. Epidemiology of osteoarthritis: literature update. Review. *Curr Opin Rheumatol* (2018) **30**(2):160–7. doi:10.1097/bor.0000000000000479

4. Damsted C, Thorlund JB, Hölmich P, Lind M, Varnum C, Villumsen MD, et al. Effect of exercise therapy *versus* surgery on mechanical symptoms in young patients with a meniscal tear: a secondary analysis of the DREAM trial. *Br J Sports Med* (2023) **57**(9):521. doi:10.1136/bjsports-2022-106207

5. Hiligsmann M, Cooper C, Arden N, Boers M, Branco JC, Luisa Brandi M, et al. Health economics in the field of osteoarthritis: an Expert's consensus paper from the european Society for clinical and economic aspects of osteoporosis and osteoarthritis (ESCEO). Review. *Semin Arthritis Rheum* (2013) **43**(3):303–13. doi:10.1016/j.semarthrit.2013.07.003

6. Felson DT, Lawrence RC, Dieppe PA, Hirsch R, Helmick CG, Jordan JM, et al. Osteoarthritis: new insights. Part 1: the disease and its risk factors. Consensus development conference; consensus development conference, NIH; research support, non-U.S. Gov't; research support, U.S. Gov't, P.H.S.; review. *Ann Internal Medicine* (2000) **133**(8):635–46. doi:10.7326/0003-4819-133-8-200010170-00016

7. Jinfeng Wen YY, Gao P, Liu S, Man Q, Huang Y, et al. Hemoglobin-to-red blood cell distribution width ratio as a predictor of cardiovascular and all-cause mortality in osteoarthritis patients. *Orthopedics Tissue Eng* (2025). doi:10.36922/ote.7109

8. Molnar V, Matišić V, Kodvanj I, Bjelica R, Jeleč Ž, Hudetz D, et al. Cytokines and chemokines involved in osteoarthritis pathogenesis. Review. *Int J Mol Sci* (2021) **22**(17):23–9208. doi:10.3390/ijms22179208

9. Li QX, Ma XT, Shao QY, Yang Z, Wang Y, Gao F, et al. Prognostic impact of multiple lymphocyte-based inflammatory indices in acute coronary syndrome patients. *Front Cardiovasc Med* (2022) **9**:811790. doi:10.3389/fcvm.2022.811790

10. Xing YY, Tian ZB, Jiang YP, Guan G, Niu Q, Sun X, et al. A practical nomogram based on systemic inflammatory markers for predicting portal vein thrombosis in patients with liver cirrhosis. *Ann Med* (2022) **54**(1):302–9. doi:10.1080/07853890.2022.2028893

11. Haybar H, Pezeshki SMS, Saki N. Evaluation of complete blood count parameters in cardiovascular diseases: an early indicator of prognosis? Review. *Exp Mol Pathol* (2019) **110**:104267. doi:10.1016/j.yexmp.2019.104267

12. El-Gazzar AG, Kamel MH, Elbahnasy OKM, El-Naggar ME. Prognostic value of platelet and neutrophil to lymphocyte ratio in COPD patients. *Expert Rev Respir Med* (2020) **14**(1):111–6. doi:10.1080/17476348.2019.1675517

13. Zorlu D, Ozyurt S, Bircan HA, Erturk A. Do complete blood count parameters predict diagnosis and disease severity in obstructive sleep apnea syndrome?. *Eur Rev Med Pharmacol Sci* (2021) **25**(11):4027–36. doi:10.26355/eurrev_202106_26044

14. Ke JH, Qiu FS, Fan WX, Wei SQ. Associations of complete blood cell count-derived inflammatory biomarkers with asthma and mortality in adults: a population-based study. *Front Immunol* (2023) **14**:1205687. doi:10.3389/fimmu.2023.1205687

15. Asahina A, Kubo N, Umezawa Y, Honda H, Yanaba K, Nakagawa H. Neutrophil-lymphocyte ratio, platelet-lymphocyte ratio and mean platelet volume in Japanese patients with psoriasis and psoriatic arthritis: response to therapy with biologics. *J Dermatol* (2017) **44**(10):1112–21. doi:10.1111/1346-8138.13875

16. Fugaru O-F, Şerbanescu M-S, Traistaru MR. The role of neutrophil to lymphocyte ratio in the assessment and rehabilitation of knee osteoarthritis patients. *Curr Health Sciences Journal* (2023) **49**(4):546–54. doi:10.12865/chsj.49.04.10

17. He Q, Wang Z, Mei J, Xie CX, Sun X. Relationship between systemic immune-inflammation index and osteoarthritis: a cross-sectional study from the NHANES 2005-2018. *Front Med* (2024) **11**:1433846. doi:10.3389/fmed.2024.1433846

18. Zhang S, Zhong Y, Wang X, Jiang W, Chen X, Kang Y, et al. Association of peripheral inflammatory indicators with osteoarthritis risk. *Osteoarthritis and Cartilage Open* (2024) **6**(3):100496. doi:10.1016/j.ocarto.2024.100496

19. Suchak T, Aliu AE, Harrison C, Zwiggelaar R, Geifman N, Spick M. Explosion of formulaic research articles, including inappropriate study designs and false discoveries, based on the NHANES US national health database. *Plos Biol* (2025) **23**(5):e3003152. doi:10.1371/journal.pbio.3003152

20. Curtin LR, Mohadjer LK, Dohrmann SM, Kruszon-Moran D, Mirel LB, Carroll MD, et al. National health and nutrition examination survey: sample design, 2007-2010. *Vital Health Statistics Ser 2, Data Evaluation Methods Research* (2013) **160**:1–23.

21. Liu B, Wang J, Li YY, Li KP, Zhang Q. The association between systemic immune-inflammation index and rheumatoid arthritis: evidence from NHANES 1999-2018. *Arthritis Res Ther* (2023) **25**(1):10–34. doi:10.1186/s13075-023-03018-6

22. Di XP, Liu SZ, Xiang LY, Jin X. Association between the systemic immune-inflammation index and kidney stone: a cross-sectional study of NHANES 2007-2018. *Front Immunol* (2023) **14**:1116224. doi:10.3389/fimmu.2023.1116224

23. Liu JX, Liu XG, Li YP, Quan J, Wei S, An S, et al. The association of neutrophil to lymphocyte ratio, mean platelet volume, and platelet distribution width with diabetic retinopathy and nephropathy: a meta-analysis. *Biosci Rep* (2018) **38**:18. doi:10.1042/bsr20180172

24. Pinheiro Machado G, Araujo GN, Carpes CK, Lech MC, Mariani S, Valle FH, et al. Elevated neutrophil-to-lymphocyte ratio can predict procedural adverse events in patients with ST-elevation myocardial infarction undergoing primary percutaneous coronary intervention. *Coron Artery Dis* (2019) **30**(1):20–5. doi:10.1097/mca.0000000000000671

25. Mayito J, Meya DB, Miriam A, Dhikusooka F, Rhein J, Sekaggya-Wiltshire C. Monocyte to lymphocyte ratio is highly specific in diagnosing latent tuberculosis and declines significantly following tuberculosis preventive therapy: *a cross-sectional and nested prospective observational study*. *PLoS One* (2023) **18**(11):e0291834. doi:10.1371/journal.pone.0291834

26. Xue Y, Chang C, Chen Y, Jia L, Wang H, Liu Z, et al. Association between the immune-inflammation indicators and osteoarthritis - NHANES 1999-2018. *Osteoarthritis and Cartilage Open* (2025) **7**(1):100453. doi:10.1016/j.ocarto.2024.100453

27. Liu Q, Xu AG, Hang H, Chen X, Dai Y, Wang M, et al. Establishment of reference intervals for SII, NLR, PLR, and LMR in healthy adults in Jiangsu region in eastern China. *Clin Lab* (2023) **69**(5):966–74. doi:10.7754/Clin.Lab.2022.220837

28. Forget P, Khalifa C, Defour JP, Latinne D, Van Pel MC, De Kock M. What is the normal value of the neutrophil-to-lymphocyte ratio? *BMC Res Notes* (2017) **10**(1):12. doi:10.1186/s13104-016-2335-5

29. Wang J, Li H, Xu R, Lu T, Zhao J, Zhang P, et al. The MLR, NLR, PLR and D-dimer are associated with clinical outcome in lung cancer patients treated with surgery. *BMC Pulm Med* (2022) **22**(1):7. doi:10.1186/s12890-022-01901-7

30. Wang LY, Li XW, Liu M, Zhou HY, Shao JF. Association between monocyte-to-lymphocyte ratio and prostate cancer in the US population: a population-based study. *Front Cell Dev Biol* (2024) **12**:1372731. doi:10.3389/fcell.2024.1372731

31. Tsao PS, Niebauer J, Buitrago R, Lin PS, Wang BY, Cooke JP, et al. Interaction of diabetes and hypertension on determinants of endothelial adhesiveness.; research support, non-U.S. Gov't; research support, U.S. Gov't, P.H.S. *Arteriosclerosis, Thrombosis, Vascular Biology* (1998) **18**(6):947–53. doi:10.1161/01.Atv.18.6.947

32. Khodabandehloo H, Gorgani-Firuzjaee S, Panahi G, Meshkani R. Molecular and cellular mechanisms linking inflammation to insulin resistance and β-cell dysfunction. Review. *Transl Res* (2016) **167**(1):228–56. doi:10.1016/j.trsl.2015.08.011

33. Bjornholm M, Kawano Y, Lehtihet M, Zierath JR. Insulin receptor substrate-1 phosphorylation and phosphatidylinositol 3-kinase activity in skeletal muscle from NIDDM subjects after *in vivo* insulin stimulation.; research support, non-U.S. gov't. *Diabetes* (1997) **46**(3):524–7. doi:10.2337/diabetes.46.3.524

34. Moeschel K, Beck A, Weigert C, Lammers R, Kalbacher H, Voelter W, et al. Protein kinase C-ζ-induced phosphorylation of Ser^{318} in insulin receptor substrate-1 (IRS-1) attenuates the interaction with the insulin receptor and the tyrosine phosphorylation of IRS-1. *J Biol Chem* (2004) **279**(24):25157–63. doi:10.1074/jbc.M402477200

35. Yu C, Chen Y, Cline GW, Zhang D, Zong H, Wang Y, et al. Mechanism by which fatty acids inhibit insulin activation of insulin receptor substrate-1 (IRS-1)-associated phosphatidylinositol 3-kinase activity in muscle.; research support, non-U.S. Gov't; research support, U.S. Gov't, P.H.S. *The J Biological Chemistry* (2002) **277**(52):50230–6. doi:10.1074/jbc.M200958200

36. Robinson WH, Lepus CM, Wang Q, Raghu H, Mao R, Lindstrom TM, et al. Low-grade inflammation as a key mediator of the pathogenesis of osteoarthritis. Review. *Nat Rev Rheumatol* (2016) **12**(10):580–92. doi:10.1038/nrrheum.2016.136

37. Babaei M, Javadian Y, Narimani H, Ranaei M, Heidari B, Basereh H, et al. Correlation between systemic markers of inflammation and local synovitis in knee osteoarthritis. *Caspian Journal Internal Medicine* (2019) **10**(4):383–7. doi:10.22088/cjim.10.4.383

38. Loukov D, Karampatos S, Maly MR, Bowdish DME. Monocyte activation is elevated in women with knee-osteoarthritis and associated with inflammation, BMI and pain. *Osteoarthritis Cartilage* (2018) **26**(2):255–63. doi:10.1016/j.joca.2017.10.018

39. Nicolai L, Schiefelbein K, Lipsky S, Leunig A, Hoffknecht M, Pekayvaz K, et al. Vascular surveillance by haptotactic blood platelets in inflammation and infection. *Nat Commun* (2020) **11**(1):16–5778. doi:10.1038/s41467-020-19515-0

40. Jenei-Lanzl Z, Meurer A, Zaucke F. Interleukin-1β signaling in osteoarthritis - chondrocytes in focus. Review. *Cell Signal* (2019) **53**:212–23. doi:10.1016/j.cellsig.2018.10.005

41. Hwang HS, Kim HA. Chondrocyte apoptosis in the pathogenesis of osteoarthritis. Review. *Int J Mol Sci* (2015) **16**(11):26035–54. doi:10.3390/ijms161125943

42. Kapoor M, Martel-Pelletier J, Lajeunesse D, Pelletier JP, Fahmi H. Role of proinflammatory cytokines in the pathophysiology of osteoarthritis. Review. *Nat Rev Rheumatol* (2011) **7**(1):33–42. doi:10.1038/nrrheum.2010.196

43. Liu MX, Wu CQ, Wu CF, Zhou Z, Fang R, Liu C, et al. Immune cells differentiation in osteoarthritic cartilage damage: friends or foes? Review. *Front Immunol* (2025) **16**:1545284. doi:10.3389/fimmu.2025.1545284

44. Hsu AY, Huang Q, Pi X, Fu J, Raghunathan K, Ghimire L, et al. Neutrophil-derived vesicles control complement activation to facilitate inflammation resolution. *Cell* (2025) **188**(6):1623–41 e26. doi:10.1016/j.cell.2025.01.021

45. Thomas BL, Montero-Melendez T, Oggero S, Kaneva MK, Chambers D, Pinto AL, et al. Molecular determinants of neutrophil extracellular vesicles that drive cartilage regeneration in inflammatory arthritis. *Arthritis Rheumatol* (2024) **76**(12):1705–18. doi:10.1002/art.42958

46. Costa LAV, Lenza M, Irrgang JJ, Fu FH, Ferretti M. How does platelet-rich plasma compare clinically to other therapies in the treatment of knee osteoarthritis? A systematic review and meta-analysis. Review. *Am J Sports Med* (2023) **51**(4):1074–86. doi:10.1177/03635465211062243

47. Zhou Q, Xu CH, Cheng XY, Liu Y, Yue M, Hu M, et al. Platelets promote cartilage repair and chondrocyte proliferation *via* ADP in a rodent model of osteoarthritis. *Platelets* (2016) **27**(3):212–22. doi:10.3109/09537104.2015.1075493

48. Li CY, Balluz LS, Ford ES, Okoro CA, Zhao GX, Pierannunzi C. A comparison of prevalence estimates for selected health indicators and chronic diseases or conditions from the behavioral risk factor surveillance system, the national health interview survey, and the national health and nutrition examination survey, 2007-2008. *Prev Med* (2012) **54**(6):381–7. doi:10.1016/j.ypmed.2012.04.003

49. Sacks JJ, Harrold LR, Helmick CG, Gurwitz JH, Emani S, Yood RA. Validation of a surveillance case definition for arthritis. *J Rheumatol* (2005) **32**(2):340–7.

50. Lix LYM, Burchill C, Metge C, McKeen N, Moore D. Defining and validating chronic diseases: an administrative data approach. (2006).

51. Murphy LB, Cisternas MG, Greenlund KJ, Giles W, Hannan C, Helmick CG. Defining arthritis for public health surveillance: methods and estimates in four US population health surveys. *Arthritis Care Res* (2017) **69**(3):356–67. doi:10.1002/acr.22943

EBM Experimental Biology and Medicine

EBM is the official journal of the Society for Experimental Biology and Medicine

Experimental Biology and Medicine (EBM) is a global, peer-reviewed journal dedicated to the publication of multidisciplinary and interdisciplinary research in the biomedical sciences.

Discover more of our Special Issues

See more →

Contact

development@ebm-journal.org

See more

ebm-journal.org

publishingpartnerships.frontiersin.org/our-partners